FUGRO

Geophysical Results Report

Energinet Denmark Hesselø Geophysical Survey | Denmark, Inner Danish Sea, *Kattegat*

F172145-REP-GEOP-001 02 | 13 August 2021
Final
Energinet Eltransmission A/S

ENERGINET

Document Control

Document Information

Project Title	Energinet Denmark Hesselø Geophysical Survey
Document Title	Geophysical Results Report
Fugro Project No.	F172145
Fugro Document No.	F172145-REP-GEOP-001
Issue Number	02
Issue Status	Final
Fugro Legal Entity	Fugro Netherlands Marine
Issuing Office Address	Prismastraat 4, Nootdorp, 2631RT, The Netherlands

Client Information

Client	Energinet Eltransmission A/S
Client Address	Tonne Kjærsvej 65, DK-7000 Fredericia, Denmark
Client Contact	Søren Stricker Mathiasen
Client Document No.	N/A

Document History

Issue	Date	Status	Comments on Content	Prepared By	Checked By	Approved By
01	2 July 2021	Complete		JS/MH/PSC	MvL/BBK/CIW	AP
02	13 Aug 2021	Final		JS/MH/PSC	MvL/BBK/CIW	AP

Project Team

Initials	Name	Role
AP	A. Padwalkar	Project Manager
JS	Julia Szudzinska	Geophysicist
MH	Menno Hofstra	Geologist
PSC	Peter Schilder	Geologist
BBK	Bogusia Klosowska	Principal Geologist
MvL	Martine van der Linde	Geophysics Group Leader
CIW	Chris Wright	Project Reporting and Deliverables Manager

FUGRO
Fugro Netherlands Marine Limited
Prismastraat 4
Nootdorp
2631 RT
The Netherlands

Energinet Eltransmission A/S
Tonne Kjærsvej 65
DK-7000 Fredericia
Denmark Bldg

13 August 2021

Dear Sir/Madam,

We have the pleasure of submitting the 'Geophysical Results Report' for the Energinet Denmark Hesselø Geophysical Survey. This report presents the results of the Geophysical Survey.

This report was prepared by Julia Szudzinska, Peter Schilder and Menno Hofstra under the supervision of Chris Wright (Project Reporting and Deliverables Manager)

We hope that you find this report to your satisfaction; should you have any queries, please do not hesitate to contact us.

Yours faithfully,

Chris Wright
Project Reporting and Deliverables Manager

Executive Summary

Interpretative Site Investigation – Hesselø		
Survey Dates	Geophysical	14 October to 30 December 2020
	Environmental	24 October to 26 October 2020 5 December 2020
Equipment	Geophysical	Multibeam echo sounder (MBES), side scan sonar (SSS), magnetometer (MAG), sub-bottom profiler (SBP), 2D ultra high resolution seismic (2D UHR)
	Environmental	Seafloor grab samples were acquired using a Dual Van Veen grab sampler
Coordinate System		Datum: European Terrestrial Reference System 1989 (ETRS89) Projection: UTM Zone 32N, CM 3°E
Bathymetry		
Water depths range from 24.7 m to 33.5 m. The site is characterised by gentle seafloor slopes, on average ranging between approximately 0˚ and 3˚. Localised gradients exceeding 10° were observed in areas of seafloor scour and areas of potential debris.		
Seafloor Morphology		
Several morphological features were observed on the seafloor within the site, including: area of circular seafloor depressions, area with occasional boulders, erosional escarpment, gullies, ice-sculpted area, shoals, area of debris and trawl marks, which are evidence of an extensive fishing activity and are present across the whole site.		
Substrate Type		
Following the classification presented in the Danish Råstofbekendtgørelsen (BEK no. 1680 of 17/12/2018, Phase IB), there were two substrate types identified within the HOWF site: 1a – silty soft bottom and 1b – solid sandy bottom.		
Seafloor Sediments		
Based on the results on the backscatter data and grab sampling campaign, the dominant seafloor sediment type in the HOWF site is muddy sand. Areas of gravel and coarse sand were identified in the north-east part of the site and within the erosional escarpment observed in the west.		
Seabed Targets and Potential Site-Specific Hazards		
Wrecks		One target was interpreted as potential wreck and classified as a potential archaeological finding (HAJ_SSS_00023). It was observed in the central part of the HOWF site and surrounded by scattered debris items.
Cables		No telecommunication cables are crossing the HOWF site.
Debris		75 targets were identified as man-made objects.
Boulders and coarse materials		In total 1534 targets were picked and classified as (possible) boulders. The highest boulder density was observed in the north-east part of the site where approximately 90% of the boulders exceeding 1 m in height/length/width were identified.
Other targets		The seafloor targets were identified from SSS, MBES and MAG datasets. In total, 4221 magnetic anomalies and 1627 side-scan sonar targets were observed across the site. SSS targets were rationalised to the MBES position. No targets were noted on the MBES that were not also seen on other sensor(s).
Mobile seafloor sediments		There was no evidence of seafloor sediments mobility observed within the HOWF site.
Geological Features		

Late Glacial anomalies	These anomalies occur sporadically in Late Glacial units (i.e. below Horizon H10, mainly in the northern and eastern part of the site. They appear as vertically stacked enhanced amplitude point reflections and/or diffraction hyperbolas.
Postglacial anomalies	These anomalies occur as enhanced amplitude parallel reflectors, with a varying spatial extent. Occasionally acoustic blanking and/or signal distortion was observed below. They are mainly observed in Unit A and Unit B and locally appear to extend below into Late Glacial units, e.g. Unit D. The anomalies are most abundant in the central part of the HOWF site, in the area of the pre-Quaternary depression and locally in the western limits of the site.
Shallow gas	Acoustic blanking was observed locally, and is thought to indicate the presence of shallow gas in the soil. The main area where acoustic blanking occurs is in the large pre-Quaternary depression.
Peat pockets	An area containing abundant discontinuous high negative amplitude reflectors was observed. These seismic events occur in Unit B and most likely represent small pockets of peat or organic-rich clays.
Boulders, cobbles and gravel	Diffraction hyperbolas were observed in the SBP data and possibly represent gravel to cobble-sized shells and rock fragments. They were frequently observed in Unit A. Point anomalies were observed in the 2D-UUHR data and may indicate the presence of individual boulders, cobbles or coarse gravel. They are most abundant in Unit D and may represent ice-rafted debris.
Mass-transport deposits (MTDs)	Unit D bears evidence for multiple stages of mass wasting processes, resulting in a variety of seismic characters. The MTDs may exhibit different geotechnical properties compared to surrounding undeformed material.
Glacial deformation	Ice movement may have deformed the Weichselian deposits, resulting in folding and/or thrusting of soil units. The degree of deformation increases towards the south of the site.
Areas of debris	Irregular seafloor was identified in 17 areas with a diameter size ranging from 100 m to 200 m. Numerous diffraction hyperbolas were observed just below the irregular seafloor. These areas may have a man-made origin and could represent debris dropped on the seafloor.
Shallow Geology	
Unit A	Unit A is present across the entire site, except for small areas in the western part of the site, where erosional escarpments were observed on the seafloor. The acoustically transparent material forms thin sheets of marine clayey SAND or sandy GYTTJA and drapes over older units.
Unit B	Unit B is present in the central and western part of the site. The seismic character changes laterally from high amplitude stratification where it is thickest to low amplitude reflectors where it thins. It consists of CLAY and SILT deposited in a deltaic environment.
Unit C	Unit C is present in the south-western part of the site and is distinctive for its chaotic seismic character. It represents sandy spits or barrier islands that were formed during the early Holocene marine transgression.
Unit D	Unit D appears as dominantly low to medium amplitude bedding-style reflectors, which become increasingly distorted towards the south. Three internal horizons discriminate between different acoustic facies. Unit C comprises Late Glacial CLAYS deposited in a glaciomarine, glaciolacustrine and/or fluvial environment.
Unit E	Unit E is present across a large part of the site, except in the north. The internal seismic character of Unit E is semi-transparent to chaotic. The unit comprises glacially deformed glaciomarine and glaciolacustrine CLAY.

FUGRO

Unit F	Unit F forms medium to high amplitude, closely spaced parallel reflectors and is present in the northern and western part of the site. Lithology is expected to comprise glaciomarine CLAY with laminae of SILT and SAND of Pleistocene age.
Unit G	The extent of Unit G is mainly confined to the large pre-Quaternary depression, where it cuts into Unit H and Unit I. The infilling material appears semi-transparent to chaotic in the seismic data.
Unit H	Unit H has a very variable seismic character and consists of early Pleistocene glacial, periglacial and/or glaciomarine TILL.
Unit I	The seismic character of Unit I displays low to medium amplitude, low-frequency parallel reflectors. It comprises pre-Quaternary bedrock and is composed of Jurassic sandy MUDSTONE to Lower Cretaceous LIMESTONE and glauconitic SANDSTONE deposited in a marine environment.

Document Arrangement

Document Number	Document Title
F172145-REP-MOB-001	Mobilisation Report - Pioneer
F172145-REP-MOB-002	Mobilisation Report - Frontier
F172145-REP-OPS-001	Operations Report - Pioneer
F172145-REP-OPS-002	Operations Report - Frontier
F172145-REP-GEOP-001	**Geophysical Survey Report (WPA scope)**
F172145-REP-HYD-001	Hydrographical Report (WPB scope)
F172145-REP-MAG-001	Magnetometer Box Survey Report (WPC scope)
F172145-REP-UHR-001	3D UHR Survey Results Report (WPD scope)

fUGRO

Contents

Appendices

Figures in the Main Text

Tables in the Main Text

Abbreviations

ALARP	As low as reasonably practicable
BEK	Danish Råstofbekendtgørelsen
BH	Borehole
BSF	Below seafloor
CM	Central meridian
COG	Centre of gravity
CPT	Cone penetrometer test
CRP	Central reference point
CUBE	Combined Uncertainty and Bathymetric Estimator
DGPS	Differential global positioning system
DTM	Digital terrain model
DTU	Technical University of Denmark
ETRS	European Terrestrial Reference System
GEUS	Danish GEologiske (Geological) UnderSøgelse (Survey).
GIS	Geographic information system
(H)OWF	(Hesselo) Offshore Wind Farm
HVF	HIPS vessel file
IODP	International Ocean Discovery Program
IHO	International Hydrographic
ka BP	Kilo annum before present
LAT	Lowest Astronomical Tide
MAG	Magnetometer
MBES	Multibeam echosounder
MDAC	Methane-derived authigenic carbonates
MMO	Man made objects
MOB	Mobilisation
MSL	Mean Sea Level
MSS	Mean sea surface
MTD	Mass-transport deposits
OCR	Offshore Client Representative
OPS	Operations
OSS	Offshore sub-station
QC	Quality control
QHD	Qinhuangdao
REP	Report
SBP	Sub-bottom profiler
SEM	Scanning electron microscopy

FUGRO

SSS	Side scan sonar
SVP	Sound velocity probe
TQ	Technical query
TSG	Template Survey Geodatabase
TVU/THU	Total vertical uncertainty / total horizontal uncertainty
UUHR/UHR	(Ultra) Ultra high resolution
USBL	Ultra short baseline
UTM	Universal Transverse Mercator
WPA/B/C/D	Work package A/B/C/D

1. Introduction

1.1 General

Energinet Eltransmission A/S (Energinet) is developing a new offshore wind farm in the inner Danish Sea, Kattegat, the Hesselø Offshore Wind Farm (HOWF). The project survey site, henceforth referred to as 'the HOWF site' and 'the site' is located between Denmark and Sweden, approximately 30 km north of Sjælland. Figure 1.1 presents the location of the site.

This report details the results of the geophysical survey covering the HOWF site.

Guidelines on the use of this report are provided in Appendix A.
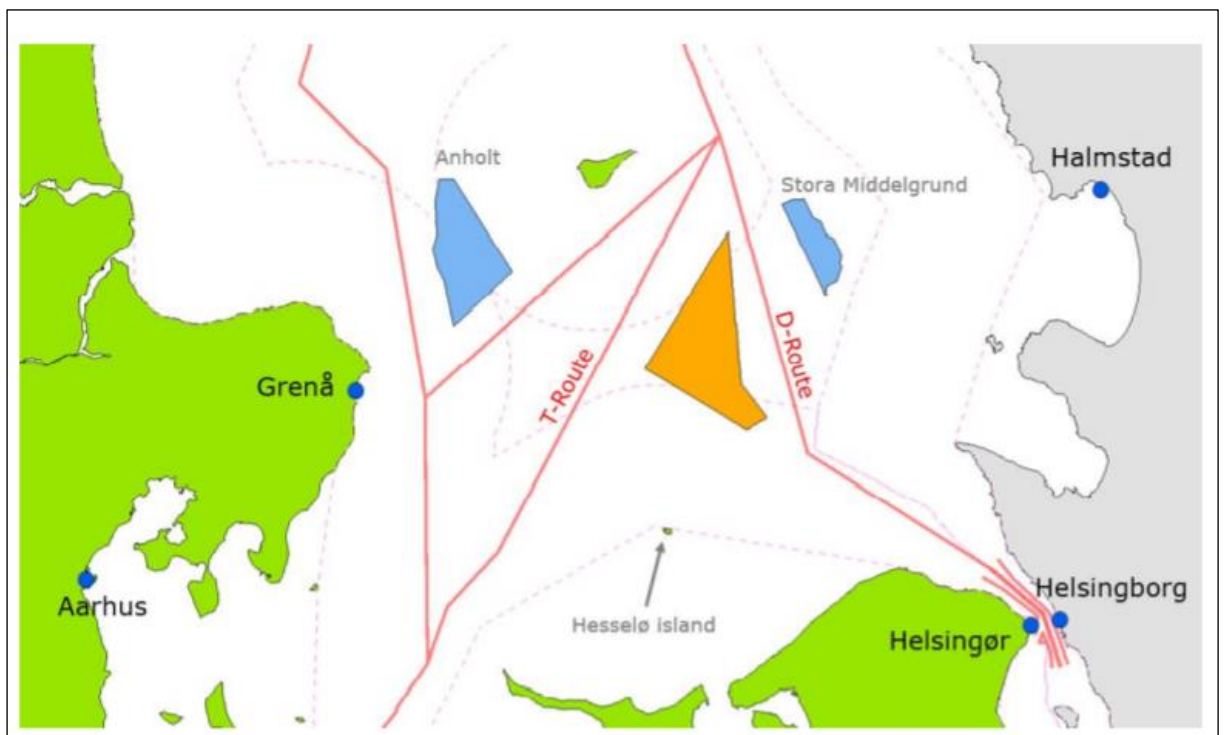
Figure 1.1: Location of the HOWF site (marked in orange).

1.2 Survey Aims and Overview

The following sub-sections provide details about the main survey requirements and the scope of work for the Client's Work Package A (WPA); the Energinet Denmark Hesselø Geophysical Survey.

1.2.1 Survey Aims

The aim of the offshore geophysical survey is to map the bathymetry, the static and dynamic elements of the seafloor and the sub-seafloor geological soil layers to at least 100 m below seafloor (BSF). The survey was required to commence in 2020 and be completed as soon as possible with the acquired data having full coverage of the HOWF site.

The acquired data will be used as the basis for:

- Initial marine archaeological site assessment;
- Planning of environmental investigations;
- Planning of initial geotechnical investigations;
- Decision of foundation concept and preliminary foundation design;
- Assessment of subsea inter-array cable burial design;
- Assessment of installation conditions for foundations and subsea cables;
- Site information enclosed in the tender for the offshore wind farm concession.

To achieve these objectives Fugro:

- Acquired accurate site-wide bathymetric data in order to determine water depths, topography, gradients etc. using multibeam echosounder (MBES);
- Acquired site-wide, high-resolution side scan sonar (SSS) data to determine seabed features and the possible presence of boulders, seafloor sediments, debris and items that may impact foundation and cable installation;
- Acquired magnetometer data across the site (along the planned survey lines) to support the ALARP principle of UXO risk reduction prior to grab and geotechnical operations and any other metallic debris or uncharted wrecks;
- Acquired high-resolution sub-bottom profiler (SBP) data to determine the shallow sub-seafloor soil conditions that may influence foundation and cable installation, such as boulders and shallow geological features;
- Acquired multichannel 2D-UUHR (ultra ultra high resolution) seismic data with penetration to 100 m BSF to determine deeper sub-seafloor soil conditions that may influence foundation design below the effective penetration of the SBP.

1.2.2 Survey Overview

A summary of the main survey requirements for the geophysical survey operations is presented in Table 1.1.

Table 1.1: Survey requirements overview – geophysical survey operations (Work Package A).

Equipment Method	Survey Requirements
Vessels	■ Fugro Frontier and Fugro Pioneer
Line spacing	■ Geophysical lines were run at 62 m (50 m) spacing[1] ■ 2D-UUHR main lines and cross lines were run at 250 m and 1 km spacing, respectively
Maximum vessel speed	■ Maximum of 4.0 knots (±10%)
Surface positioning	■ Dynamic heading accuracy of ± 0.2° or better ■ Static heading accuracy of ± 0.05° or better ■ Horizontal uncertainty of the vessel of ± 0.5 m or better
USBL	■ USBL accuracy. Fugro was able to repeatedly achieve +/- 1 m accuracy for USBL calibration and +/-2 m accuracy for data acquired from towed sensors. i.e. a processed target accuracy of +/-2 m
2D-UUHR	■ Vertical resolution of 0.3 m to 1.0 m in the first 100 m below seafloor

Equipment Method	Survey Requirements
	■ Main lines and cross lines spaced at 0.25 km and 1 km, respectively
Multibeam echosounder/backscatter	■ 100% coverage ■ 0.25 m x 0.25 m bin size / 16 x pings per 1.0 m x 1.0 m *(Refer TQ-016)* ■ THU is < 0.5 m ■ TVU is compliant with IHO Special Order ■ Grid standard deviation (95% confidence interval) is less than 0.2 m
Innomar SBP	■ Transmit and receive frequency: 8 to 12 kHz (adjustable) ■ Minimum penetration: 10 m dependent on geology ■ Vertical resolution: better than 0.3 m ■ Compensated for vessel motion ■ Infill requirement: data gaps > 20 m
Side scan sonar	■ 0.5 m x 0.5 m x 0.1 m minimum target size sonification *(Refer TQ-003)* ■ 200% coverage including nadir *(Refer TQ-013)* [3] ■ Altitude set to 8% to 12% of range[2] ■ Survey speed below 4.0 knots (±10%) ■ Infill required where USBL gaps of more than 10 s
Magnetometer	■ 5 m maximum altitude (gaps if more than 10 m along track above 5.0 m altitude) ■ Sampling frequency: 10 Hz ■ Maximum noise level: 2 nT (minimum layback: 110 m)[6] *(Refer TQ-012)* ■ Lateral blanking distance of 5 m ■ Infill requirement: USBL gaps > 10 s
SVP	■ The speed of sound in water was measured in the HOWF site using a sound velocity profiler (SVP) ■ The vertical SVP measurements were undertaken with a resolution of 0.1 m/s and an accuracy of ±0.15 m/s ■ SVP was able to measure within the range of 1350 m/s to 1600 m/s

Grab Sampler	■ Day or Dual Van Veen Grab Sampler
	■ Precise positioning of the grab sample location *(Refer TQ-011)*[5]
	■ Proper and clear communication with vessel navigators and survey personnel
	■ Safe winch operation and deployment of the grab
	■ Monitoring of the tension of the winch wire
	■ Upon recovery of the soil sample:
	  • Visual analysis of the sample (According to Danish Standard; Larsen et al., 1995)
	  • Sample photography
	■ Safe storage of the sample (at least 3 kg) for onshore delivery with proper labelling *(Refer TQ-009)*[4]

Notes:	

Equipment Method	Survey Requirements
1)	Original line spacing for geophysical lines was set to 62 m with SSS range of 75 m. However due to a strong pycnocline i.e. combination of thermocline and halocline, affecting the SSS & MBES data, the SSS range was reduced to 60 m and the line spacing was changed to 50 m.
2)	SSS towfish flying height was also reduced from 8 m to 6 m to adhere with proper data quality. *Refer TQ-013 and TQ-022 for more details.*
3)	The 200% coverage of SSS data was not achievable due to the existing adverse pycnocline effect within the survey site. *Refer TQ-013 for more details.*
4)	Weight of collected grab samples was revised to 3 kg. *Refer TQ-009 for more details.*
5)	Grab sample locations were finalised and adjusted upon the scouting line survey results. *Refer TQ-011 for more details.*
6)	Due to safety reasons it was agreed to tow the magnetometer piggy-backed from the SSS fish which resulted in a decrease in distance of the layback. *Refer TQ-012 for more details.*

1.3   Geodetic Parameters

The project geodetic and projection parameters are summarised in Table 1.2.

Table 1.2: Project geodetic and projection parameters.

Project Global Positioning System Geodetic Parameters	
Datum	ETRS89
EPSG code	25832
Semi major axis	6 378 137.000 m
Semi minor axis	6 356 752.314 m
Inverse flattening	298.257222101
Project Projection Parameters	
Grid Projection	Universal Transverse Mercator, Northern Hemisphere
UTM Zone	32 N
Central Meridian	009° 00' 00.000" East
Latitude of Origin	00° 00' 00.000" North
False Easting	500 000 m
False Northing	0 m
Scale Factor at Central Meridian	0.9996
Units	Metres

1.4   Vertical Datum

The vertical datum for Energinet Hesselø project is reduced to Mean Sea Level (MSL) utilising the DTU18 MSS Tide Model as a vertical offshore reference frame supplied by the Technical University of Denmark (DTU).

2. Mobilisation and Operations

The data was acquired using the survey vessels Fugro Pioneer and Fugro Frontier.

Fugro Frontier mobilisation and calibrations for survey operations were undertaken between 10 October and 12 October 2020 in the port of IJmuiden, The Netherlands; 23 October 2020 and 04 November 2020 near the survey site (see report F172145-REP-MOB-002).

Fugro Pioneer mobilisation and calibrations for survey operations were undertaken between 11 to 20 November 2020 in the port of Great Yarmouth, UK and at an offshore calibration site close to the survey site (see report F172145-REP-MOB-001).

Operations on the Fugro Frontier occurred between 14 October and 26 December 2020. Details are provided in report F172145-REP-OPS-002.

Operations on the Fugro Pioneer occurred between 20 November and 30 December 2020. Details are provided in report F172145-REP-OPS-001.

3. Vessel Details and Instrument Spread

3.1 Vessel Details Fugro Pioneer

The Fugro Pioneer (Figure 3.1) is a 53 m vessel built at Damen Shipyards in 2014. Being purpose designed for the demanding environments in which Fugro's coastal fleet operate, the Fugro Pioneer has excellent weather capabilities and is an ideal platform for 2D UHRS and geophysical surveys.

Figure 3.1: Fugro Pioneer

The Fugro Pioneer is equipped for 24-hour operations with space for a maximum of 31 persons.

3.2 Instrument Spread Fugro Pioneer

The equipment used for the survey is presented in Table 3.1.

Table 3.1: Instrument Spread Fugro Pioneer

Requirement	Equipment
Primary GNSS	Fugro StarPack GNSS receiver with StarFix.G2+ (dual frequency) corrections
Secondary GNSS	Fugro StarPack GNSS receiver with StarFix.G2+ (dual frequency) corrections
MRU and heading sensor	IXSEA Hydrins, IXBLUE Octans
USBL	Kongsberg HiPAP 501 with C-Node beacons
Multibeam echosounder	Dual Head Kongsberg EM2040
Side scan sonar	Edgetech 4200 (300/600 kHz)
Magnetometer	Geometrics G-882 fitted with a depth sensor and altimeter, towed behind the side scan sonar fish with a 20 m soft-tow cable (changed to 8,9 m on the 1st of December 2020)

Requirement	Equipment
Parametric Sub-bottom Profiler	Innomar Medium SES-2000
Sound velocity probe	2x SAIV CTD
Sound velocity sensor	1x Valeport Mini SVS installed near MBES head with 1x spare
Tidal heights	Fugro StarPack GNSS receiver with Starfix.G2+ corrections
2D UHRS Source	Fugro Multi-Level Stacked Sparker (160, 120 and 80 tips, at depths of 0.52 m, 0.67 m and 1.12m)
2D UHRS Receiver	Geometrics 48 channel hydrophone streamer with 2x Digi birds

For full details of the Fugro Pioneer including weather limitations, vessel offsets and field procedures refer to Fugro report F145225-REP-OPS-001.

3.3 Vessel Details Fugro Frontier

Fugro Frontier (Figure 3.1) is a 53m vessel built at Damen Shipyards Galati, Romania in 2014. Being purpose designed for the demanding environments in which Fugro's coastal fleet operate, with a minimum draught of 3.1m, Fugro Frontier is able to conduct geophysical survey operations in water depths greater than 10m. Fugro Frontier has excellent weather capabilities and is an ideal platform for 2DUHR and geophysical surveys.

Figure 3.2: Fugro Frontier

Fugro Frontier has space for a maximum of 31 persons and is equipped for 24-hour operations.

3.4   Instrument Spread Fugro Frontier

The equipment used for the survey is presented in Table 3.1.

Table 3.2: Instrument Spread Fugro Frontier

Requirement	Equipment
Primary GNSS	Fugro StarPack GNSS receiver with StarFix.G2+ (dual frequency) corrections
Secondary GNSS	Fugro StarPack GNSS receiver with StarFix.G2+ (dual frequency) corrections
MRU and heading sensor	IXSEA Hydrins, IXBLUE Octans
USBL	Kongsberg HiPAP 501 with C-Node beacons including Cymbal
Multibeam echosounder	Dual Head Kongsberg EM2040
Side scan sonar	Edgetech 4205 Side Scan towfish with Ixblue Micro Octans (300/600 kHz)
Magnetometer	Geometrics G-882 fitted with a depth sensor and altimeter, towed behind the side scan sonar fish
Parametric Sub-bottom Profiler	Innomar Medium SES-2000
Grab Sampler	Dual Van Veen Grab Sampler with accessories
Sound velocity probe	1x Valeport fast SVS & 1x Valeport Fast CTD
Sound velocity sensor	1x Valeport Mini SVS installed near MBES head with 1x spare
Tidal heights	Fugro StarPack GNSS receiver with Starfix.G2+ corrections
2DUHR Source	Fugro Multi-Level Stacked Sparker with 360 tips on three levels, at depths of 0.52 m, 0.67 m and 1.12m
2DUHR Receiver	Geometrics 48 channel hydrophone streamer with 2x Digibirds, 1x Head Buoy & 1 Tail Buoy

For full details of the Fugro Pioneer including weather limitations, vessel offsets and field procedures refer to Fugro report F145225-REP-OPS-002.

4. Results

4.1 Regional Geological Setting

The geological record at the HOWF site has been heavily influenced by the Sorgenfrei–Tornquist Zone. This is a fault system with a south-east to north-west orientation, located between Skåne in southern Sweden, the Kattegat and northern Jutland (Figure 4.1). It forms the south-western boundary of the Baltic Shield (Erlström and Sivhed, 2001). The fault system has been active since the Palaeozoic and has been re-activated multiple times, most recently during the Quaternary (Jensen et al., 2002), as result of isostatic (re)adjustments following ice sheet advances and retreats. One of the major faults of the Sorgenfrei–Tornquist Zone, the Børglum Fault, is located in the northern part of the HOWF site, and has a south-east to north-west orientation (Figure 4.1). The Børglum Fault is associated with a large pre-Quaternary depression (Figure 4.2), which influenced the depositional patterns during the Quaternary.

The bedrock at the HOWF site consists of Jurassic sandy mudstone and Upper Cretaceous limestones and glauconitic sandstones (Erlström and Sivhed, 2001).

During the Pleistocene, the Scandinavian Ice Sheet advanced and retreated several times in northern Jutland and the Kattegat. This resulted in the accumulation of a series of glacial tills and interglacial lacustrine and marine deposits (Jensen et al., 2002; Larsen et al., 2009). In addition, the repeated ice sheet advance and retreat also formed a complex series of ice-terminal ridges (terminal moraines or push-moraines). These can still be recognised in the geomorphology of the islands and bathymetry of the southern Kattegat. During the relative sea level rise in the Late Glacial period (Late Weichselian; 16.0 to 12.6 ka BP), a thick package of glaciomarine clay was deposited (Jensen et al., 2002; Houmark-Nielsen and Kjær, 2003). Figure 4.3 illustrates paleogeography and depositional environments during the Weichselian in the wider Kattegat area.

In the early Holocene or Postglacial period (~10.5 to 12.6 ka BP) the relative sea level dropped due to isostatic rebound. This resulted in erosion of Late Weichselian deposits and is evidenced by an unconformity in the larger Hesselø area (Jensen et al., 2002; Bendixen et al., 2015, 2017; GEUS 2020). Due to the ongoing eustatic sea level rise, the area was once again inundated, and sediment was deposited in a transgressive, shallow marine environment between 11.7 to 10.8 ka BP. During this time a freshwater lake (Ancylus Lake) was present in the Baltic Sea. Between 11.9 and 9.1 ka BP, the Ancylus Lake drained via the Dana river system through the Storebælt in the south-east, into the Kattegat and resulted in the deposition of coastal sediments in the Hesselø area. From 9.1 ka BP the Holocene marine transgression continued, and a thin layer of marine sediment was deposited (Bendixen et al., 2015, 2017).

Figure 4.4 presents interpretative profiles of the shallow geology at and in close proximity of the HOWF site, based on information available in public domain (Jensen et al., 2002; Bendixen et al., 2015).
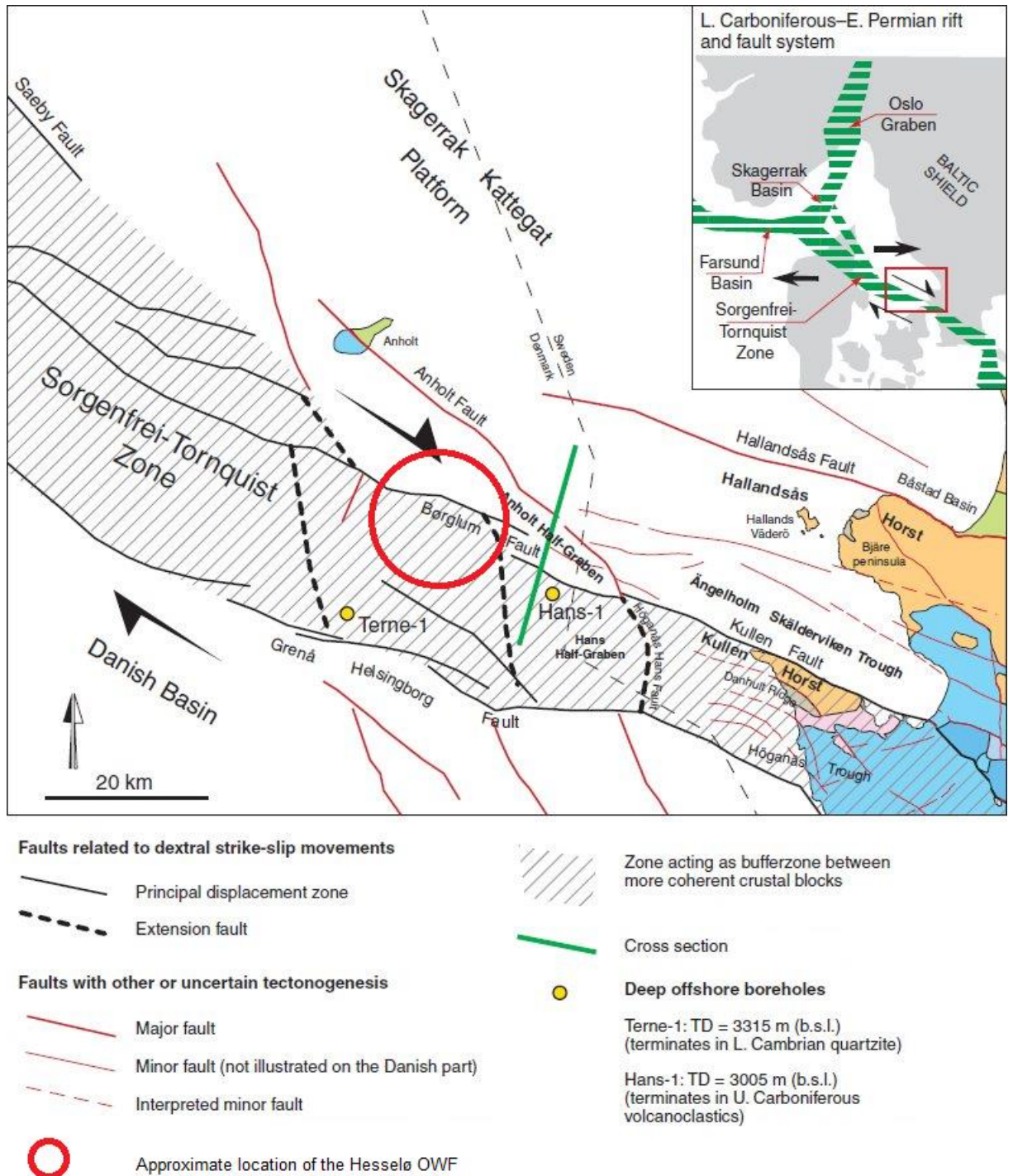
Figure 4.1: Structural setting of the southern Kattegat and the Sorgenfrei–Tornquist Zone (after GEUS, 2020).
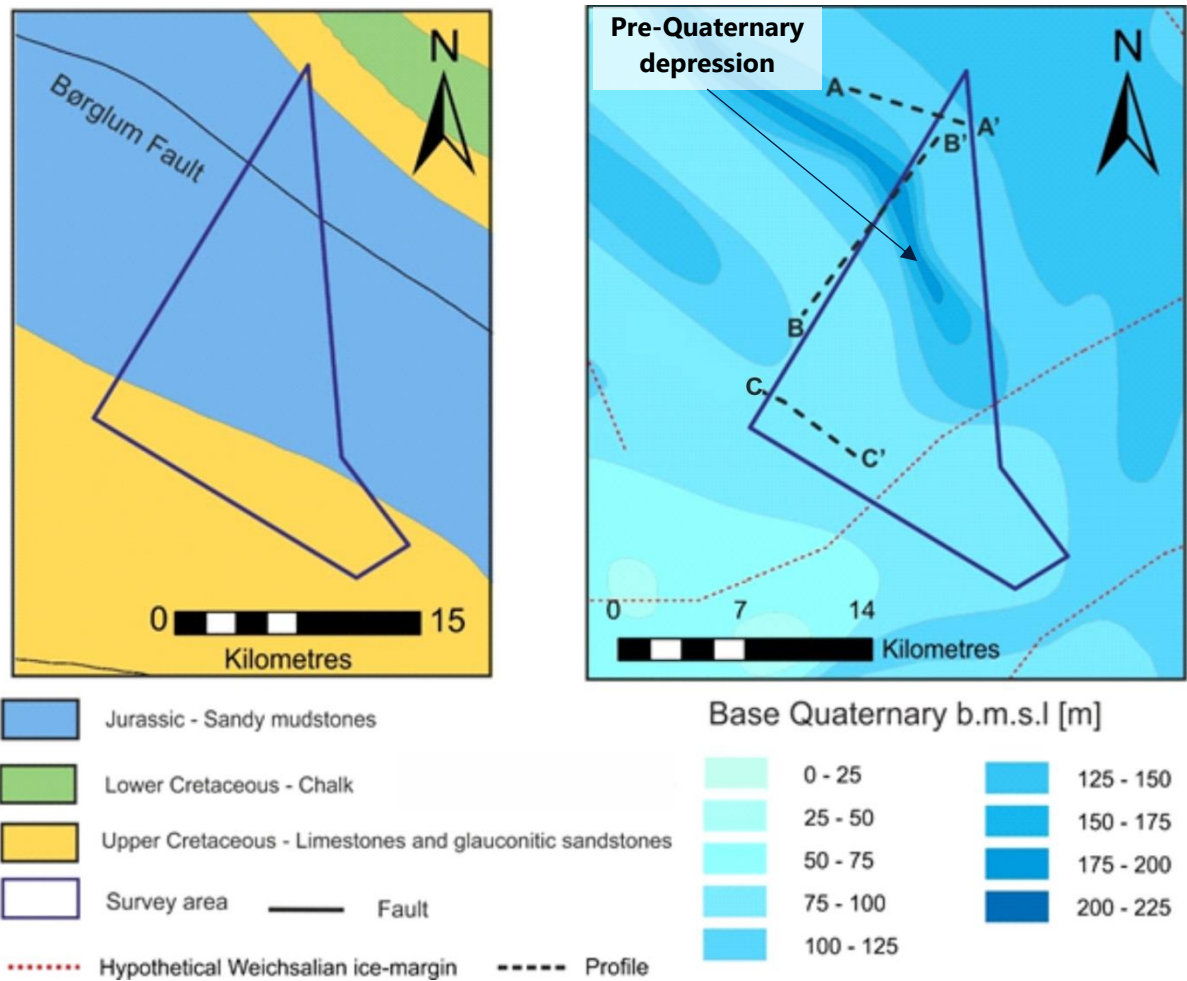
Figure 4.2: Bedrock geology (left image) and depth to the base of Quaternary (right image) at the HOWF site (modified after GEUS, 2020). Profiles are presented in Figure 4.4.
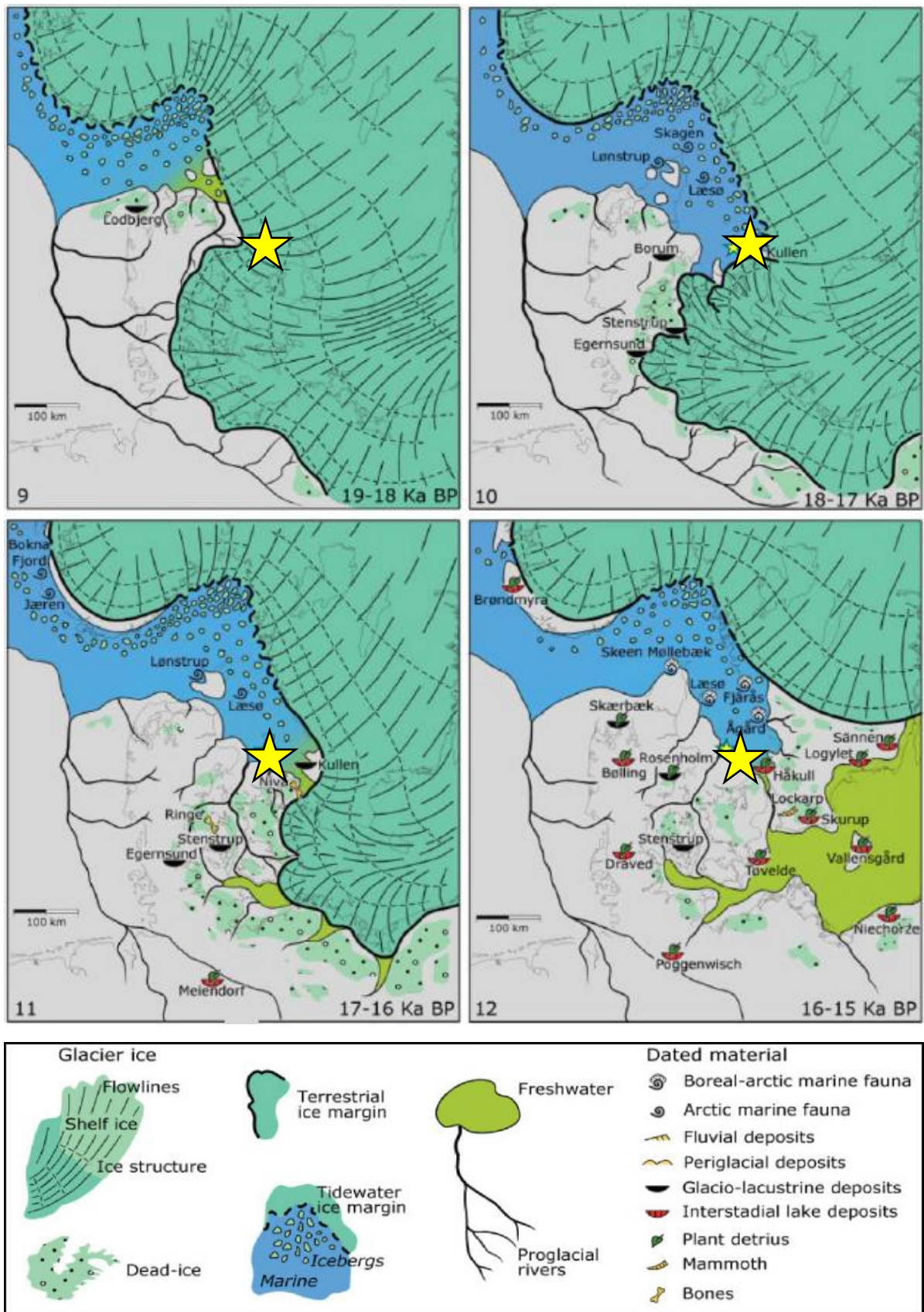
Figure 4.3: Palaeogeographies during the Weichselian in the Kattegat area (after Houmark-Nielsen and Kjær, 2003). The yellow star indicates the approximate location of the HOWF site.
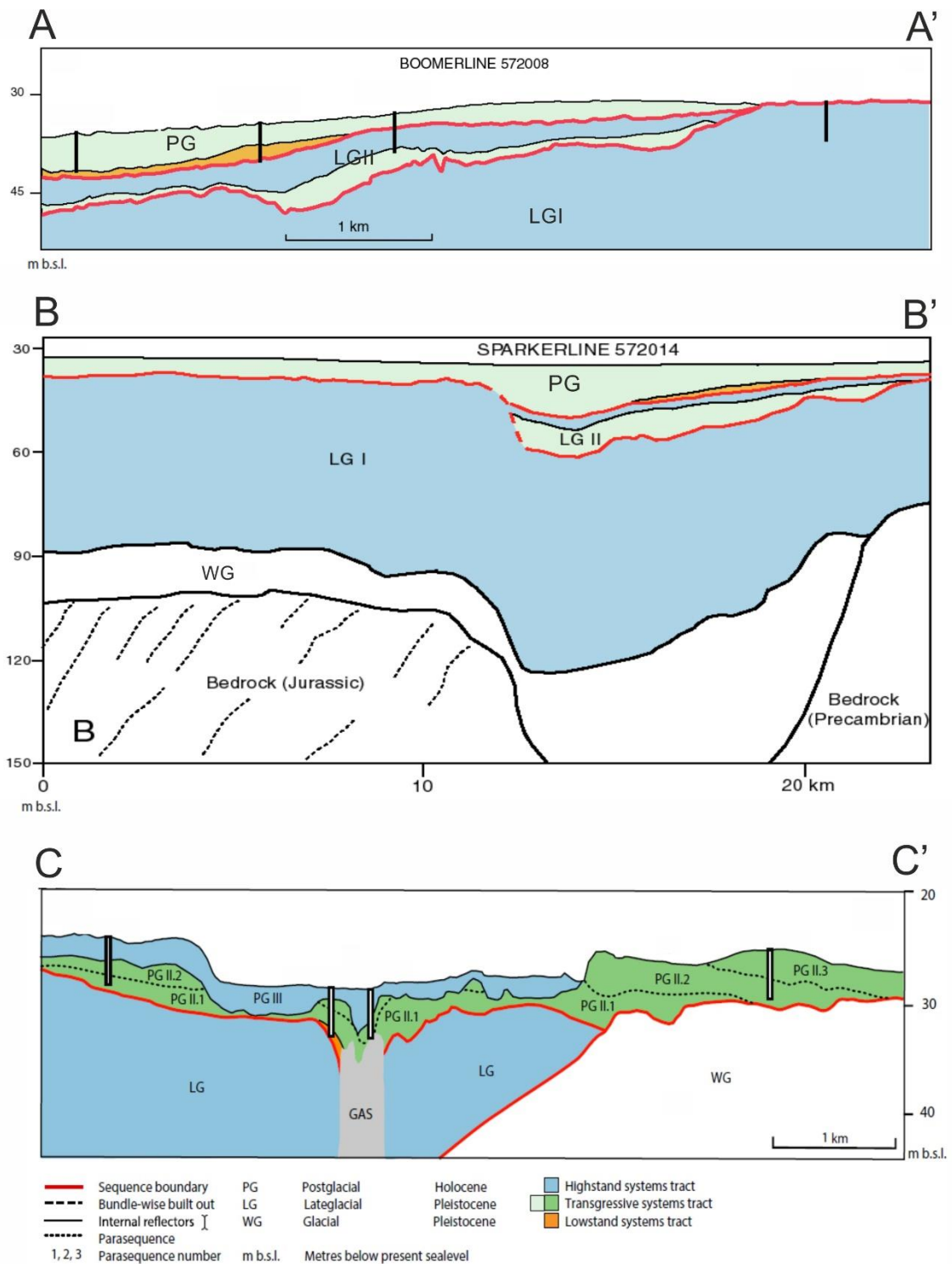
Figure 4.4 Interpretative profiles of the shallow geology at/near the HOWF site; profiles A-A' and B-B' from Jensen et al. (2002), profile C-C' from Bendixen et al. (2015). See Figure 4.2 for the location of the profiles.

4.2 Seafloor Conditions

4.2.1 Bathymetry

An overview of the bathymetry within the HOWF site is shown in Figure 4.5 and charts provided in a separate PDF file (see Appendix B). Seafloor gradient is illustrated in Figure 4.6.

In the HOWF site water depths range from 24.7 m to 33.5 m MSL. The minimum water depth was observed in the south-western part of the site and the maximum depth was recorded in the east.

The HOWF site is characterised by gentle seafloor slopes, on average between approximately 0˚ and 3˚. Seafloor gradients locally exceed 10˚, in areas of seafloor scour and potential areas of debris.
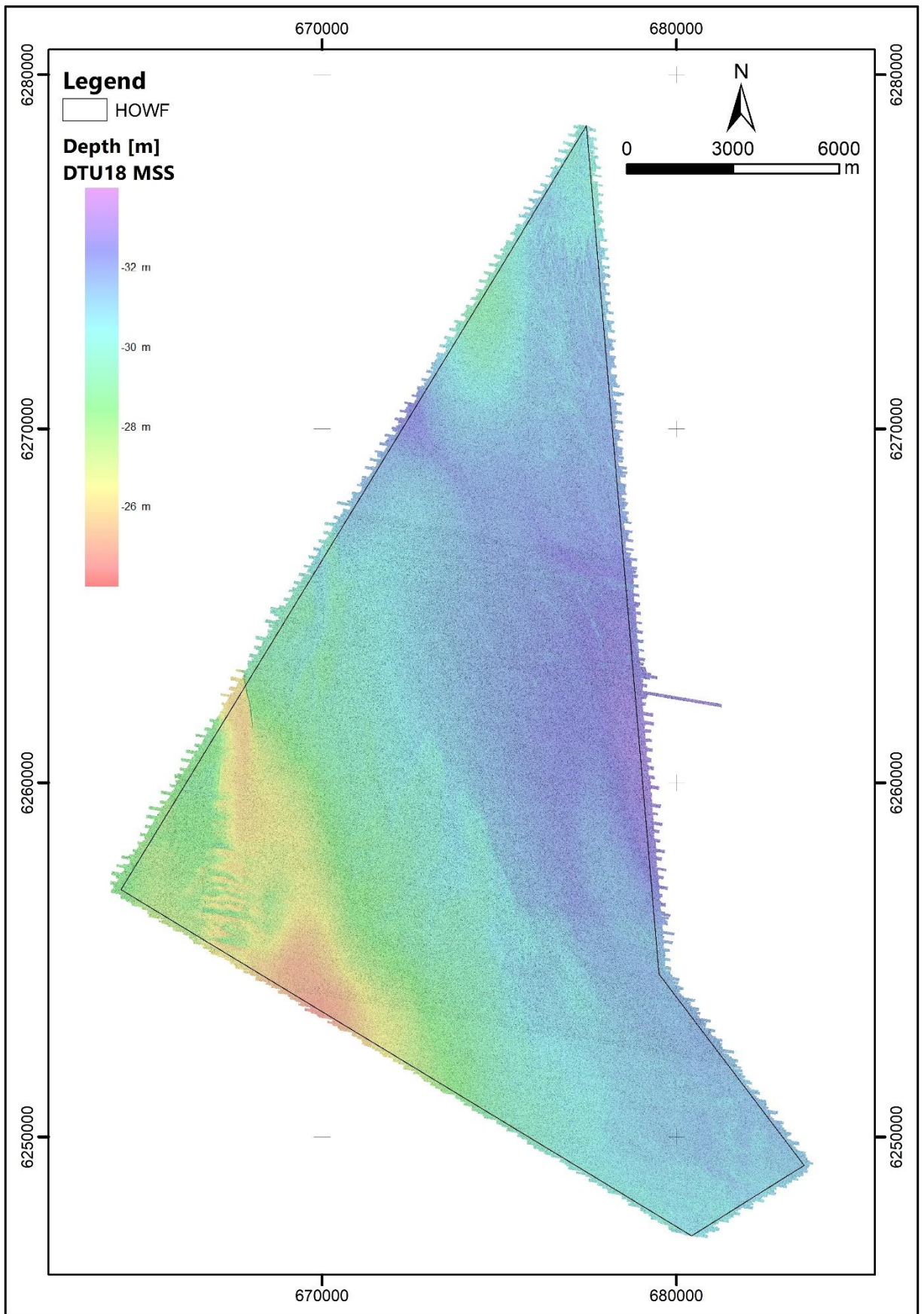
Figure 4.5: Bathymetry overview of the HOWF site.
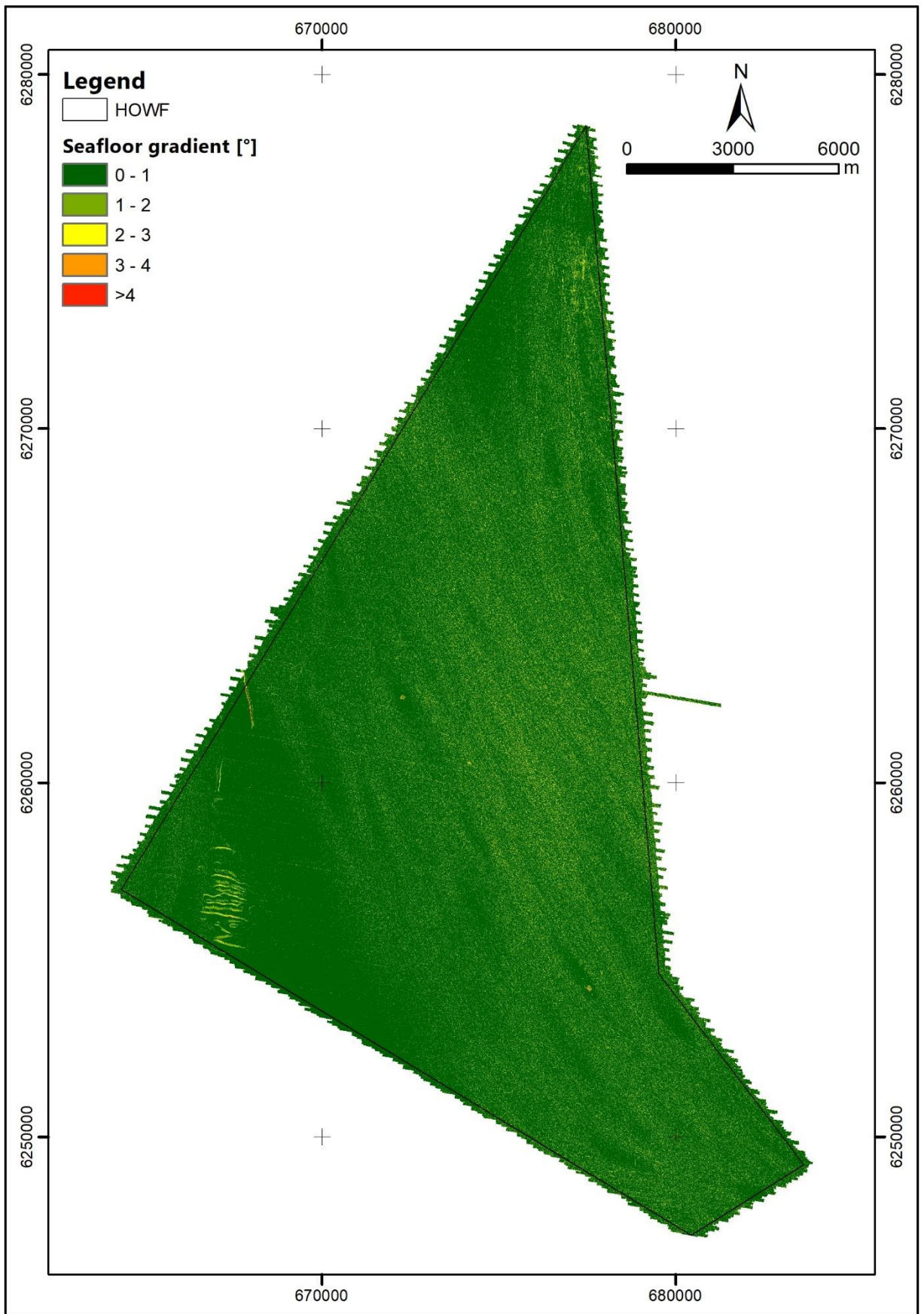
Figure 4.6: Seafloor gradient overview in the HOWF site.

4.2.2   Seafloor Morphology

Various morphological features of different dimensions were identified at the seafloor. These morphological features are a result of the interplay of variable (sub-seafloor) geological conditions and past and present hydrodynamic conditions (e.g. tides, currents) under the influence of changes in sea level.

An overview of the seafloor morphology is shown in Figure 4.7 and presented in charts provided in a separate PDF file (see Appendix B).

Seafloor morphology interpretation was based on the combination of MBES, backscatter and SBP datasets. The data analysis was carried out using acoustic characteristics such as overall pattern, roughness, reflectivity and backscatter strength.

The following natural morphological features were identified in the HOWF site:
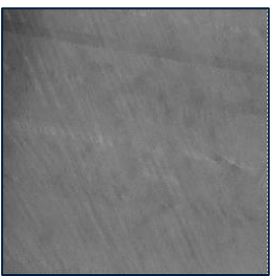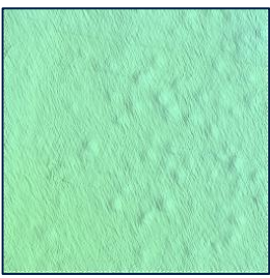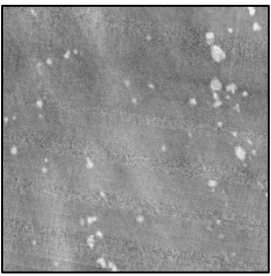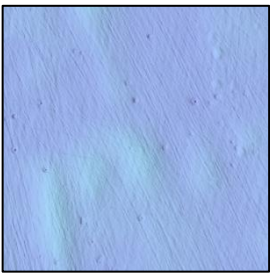
- Areas of circular seafloor depressions
- Areas with occasional boulders
- Erosional escarpments
- Gullies
- Ice-sculpted areas
- Shoals
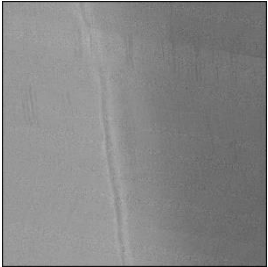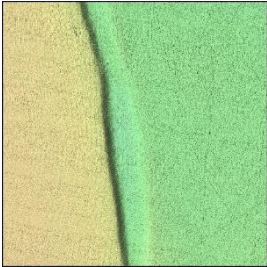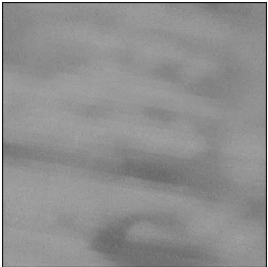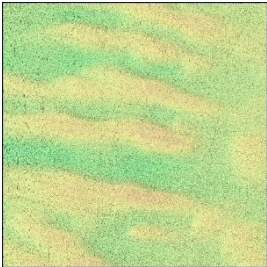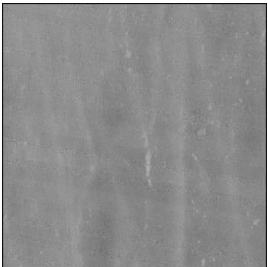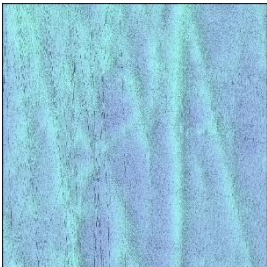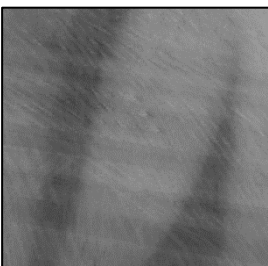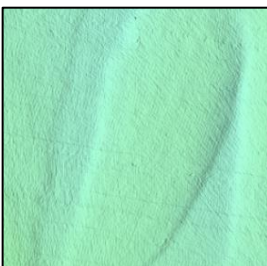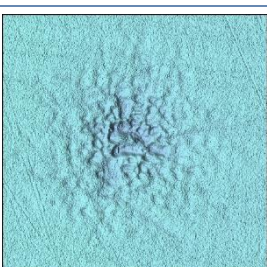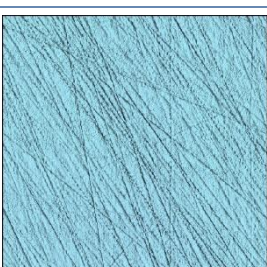
Additionally, the following morphological features of anthropogenic origin were identified:

- Areas of debris
- Trawl marks

The acoustic characteristics of the types of morphology identified are summarised in Table 4.1.

Table 4.1: Acoustic characteristics of the morphological features identified in the HOWF site.

Backscatter Image	MBES Image	Acoustic Description	Morphological Interpretation
		Medium reflectivity	Area of circular seafloor depressions
		Very high to medium reflectivity	Area with occasional boulders

Backscatter Image	MBES Image	Acoustic Description	Morphological Interpretation
		High to low reflectivity	Erosional escarpment
		High to medium reflectivity	Gullies
		Very high to high reflectivity	Ice-sculpted area
		High to low reflectivity	Shoal
		Medium reflectivity	Area of debris
		Low reflectivity	Trawl marks

Notes: For the MBES images high shadow strength was applied to better visualise elevation differences. Scale varies between the examples of the features.
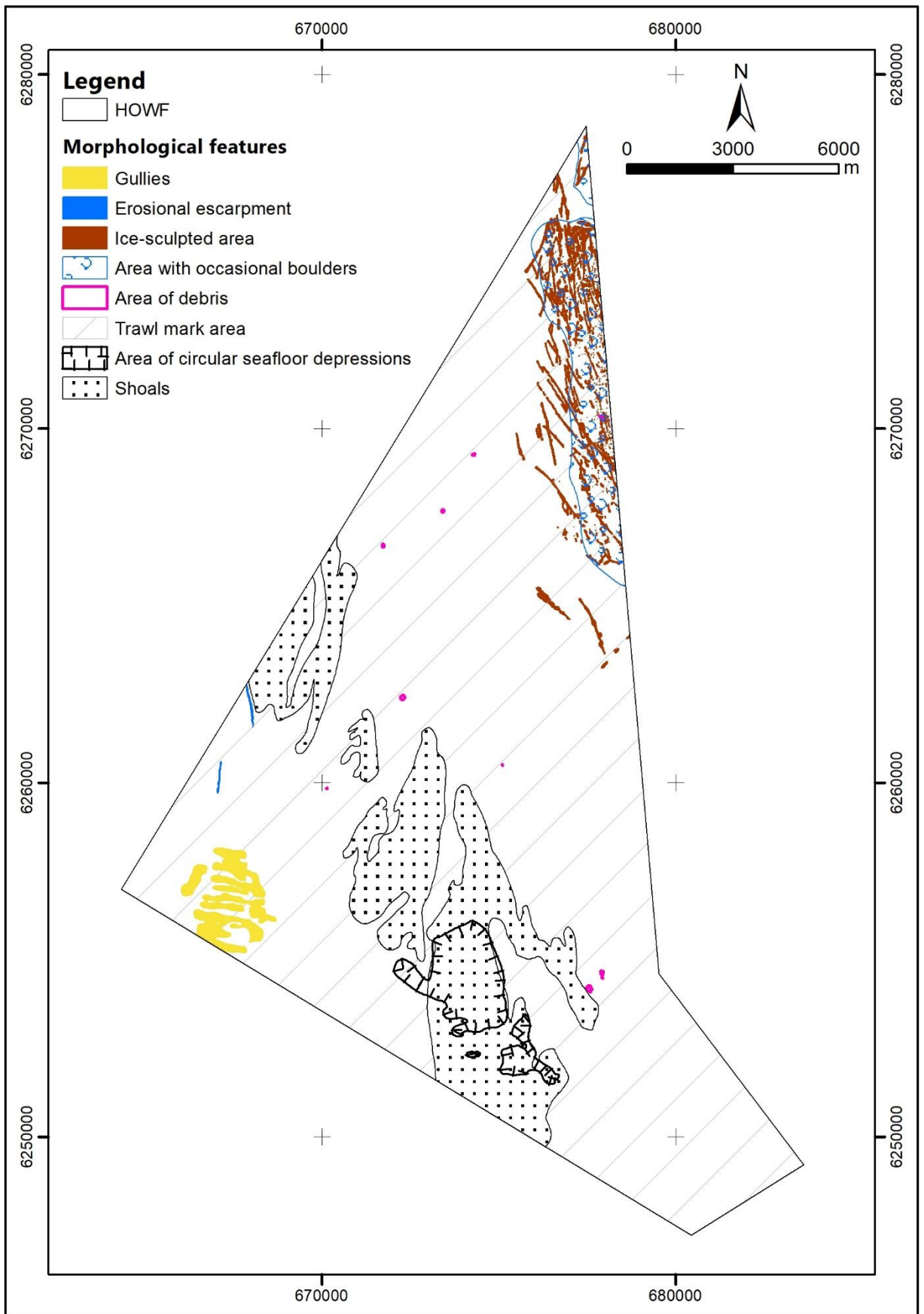
Figure 4.7: Overview of the morphological features in the HOWF site.

4.2.2.1   Area of Circular Seafloor Depressions

An area of numerous circular seafloor depressions was observed in the southern part of the site. The depth of these depressions does not exceed 0.1 m to 0.2 m and the slope angles are below 1°.

The depressions locally correspond to high-amplitude anomalies (Postglacial anomalies) observed in SBP and 2D-UUHR data in Unit A and Unit B. Further description of these anomalies is provided in Section 4.3.3.1.

Figure 4.8 presents an example of circular seafloor depressions.
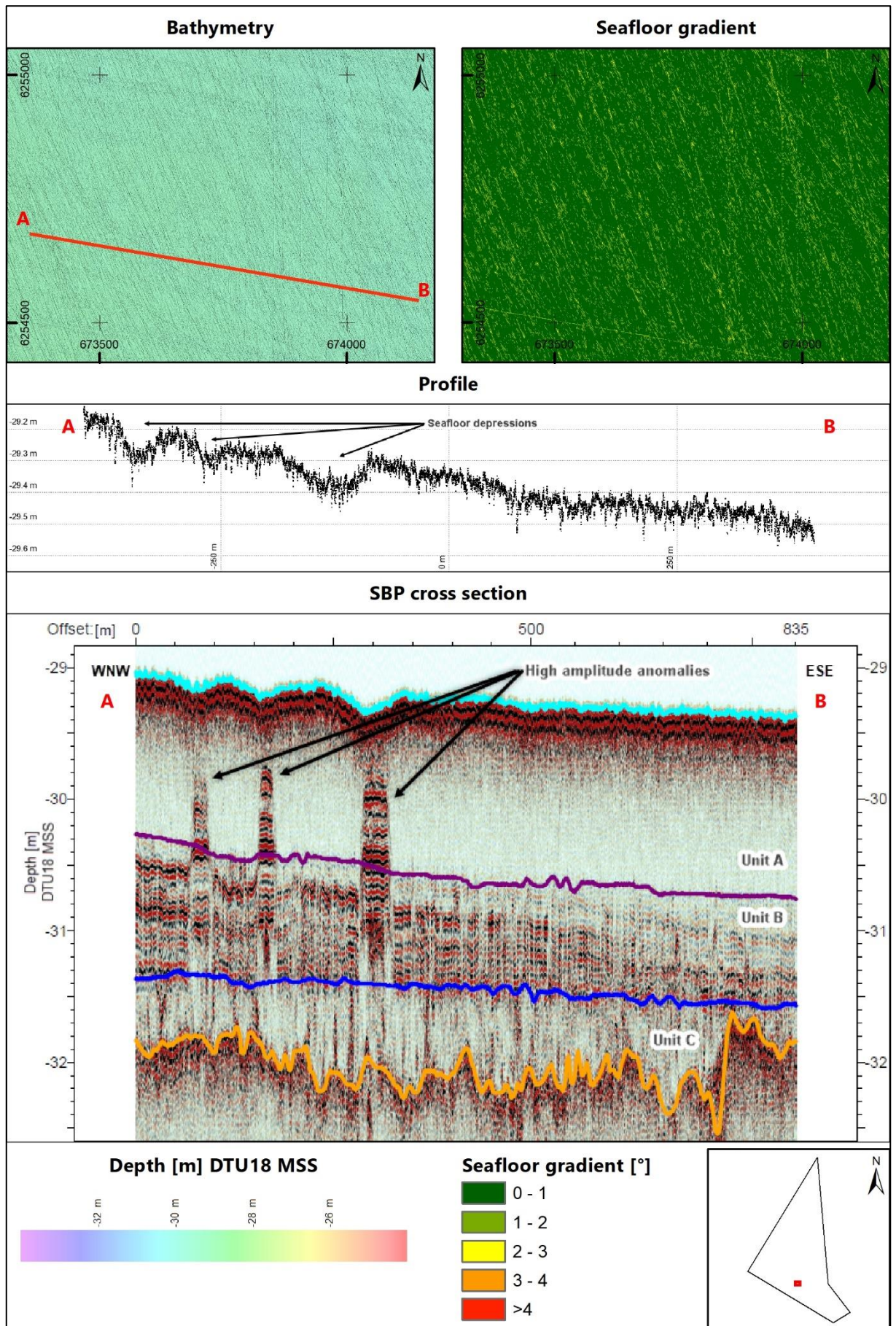
Figure 4.8: Example of an area of circular seafloor depressions in the HOWF site.

4.2.2.2 Area of Occasional Boulders

Most of the targets observed in SSS and MBES datasets in the HOWF site are interpreted as boulders (refer to Section 4.3.3.4). Over 80% of them were observed in the north-eastern part of the site. This part was classified as an area of occasional boulders and it coincides with the ice-sculpted area and where the Holocene is thin (Section 4.3.2).

Boulders vary in size, ranging from below 1.0 m in any dimension to over 3.0 m in length and over 1.0 m in height. Many of the observed boulders are in small depressions, due to scouring of the surrounding seabed, which consists of soft sediments. Figure 4.9 presents an example of an area of occasional boulders.
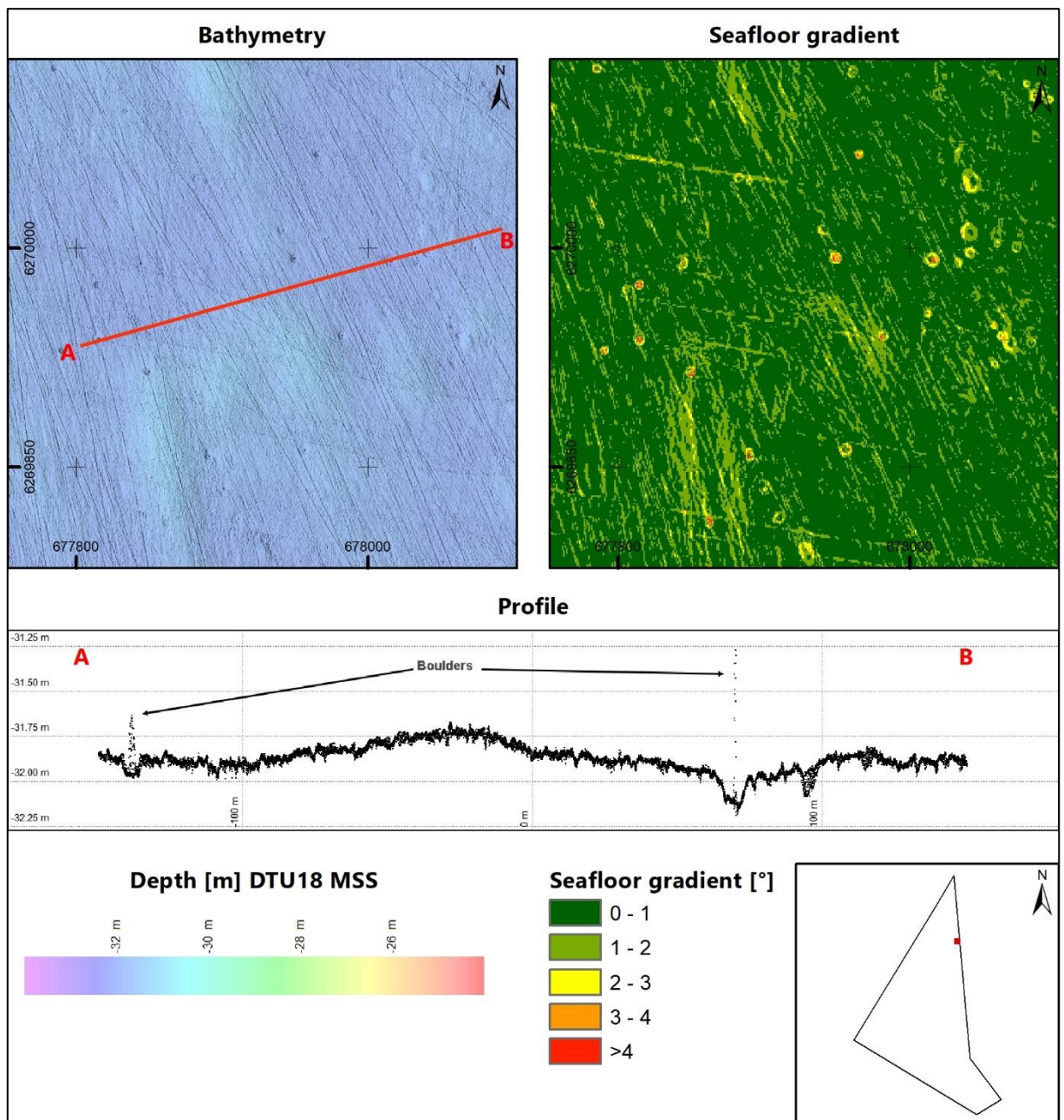
Figure 4.9: Example of an area of occasional boulders in the HOWF site.

4.2.2.3 Erosional Escarpment

Two erosional escarpments were observed in the western part of the HOWF site. The escarpments form elongated depressions stretching in roughly north–south direction on both west and east sides of an elongated seafloor elevation. Their lengths are approximately 1200 m and 900 m, respectively. These features are characterised by high seafloor gradients and correspond to the very few areas where Unit A is absent (see Section 4.3.2.1). Figure 4.10 presents an example of an erosional escarpment.
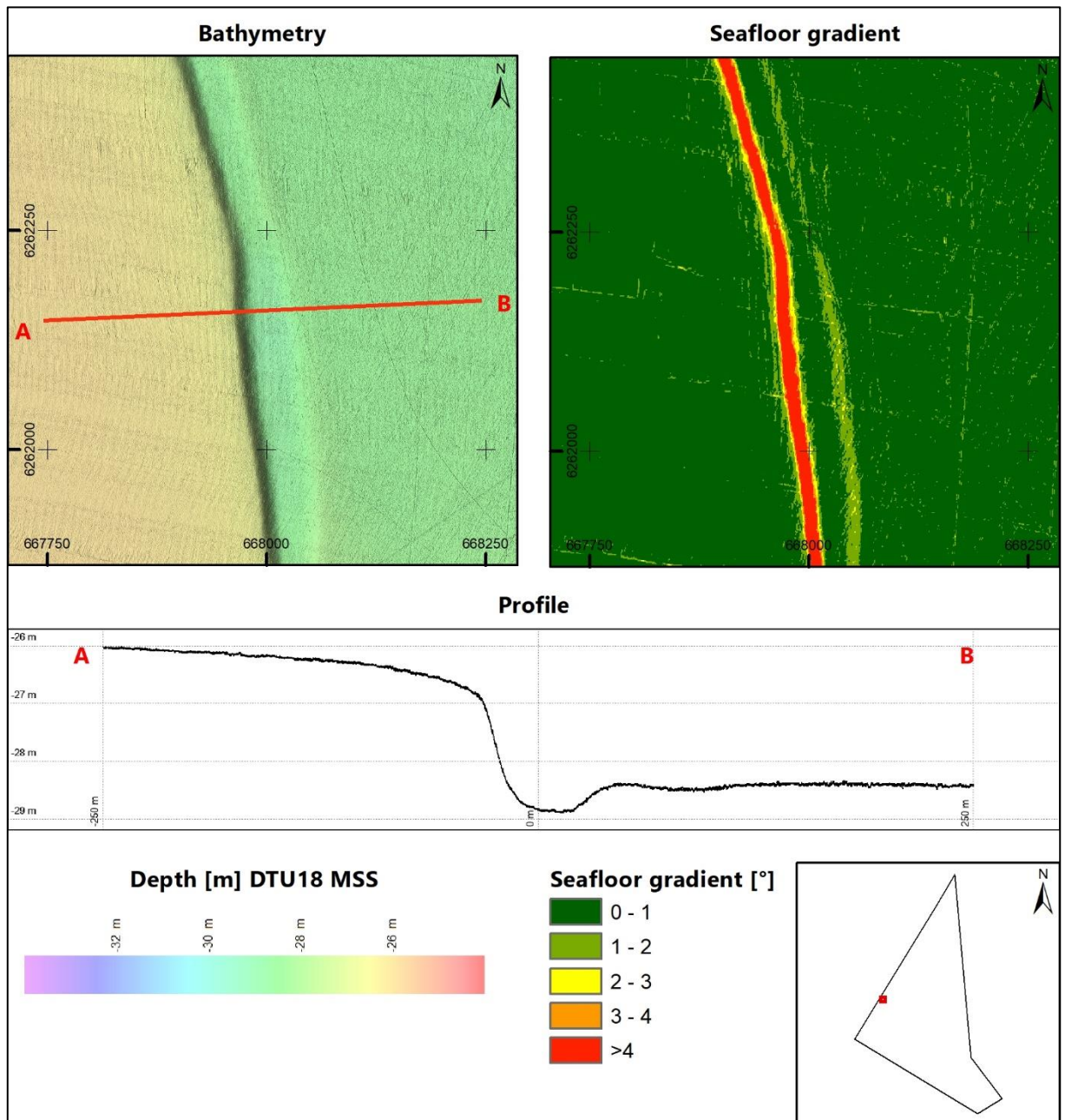
Figure 4.10: Example of an erosional escarpment in the HOWF site.

4.2.2.4 Gullies

Erosional features interpreted as gullies were observed in the south-western part of the HOWF site. These features have a west to east orientation, nearly exactly perpendicular to the coast of Jutland. Depths of the gullies range between 1.0 m and 3.0 m.

The SBP data show that these gullies were formed within the Holocene Unit B (see Section 4.3.2.2) and that the overlying Unit A drapes this paleo-topography. These features may have been created by erosive outwash during the drainage of the Ancylus lake. Figure 4.11 and Figure 4.12 present examples of seafloor gullies.
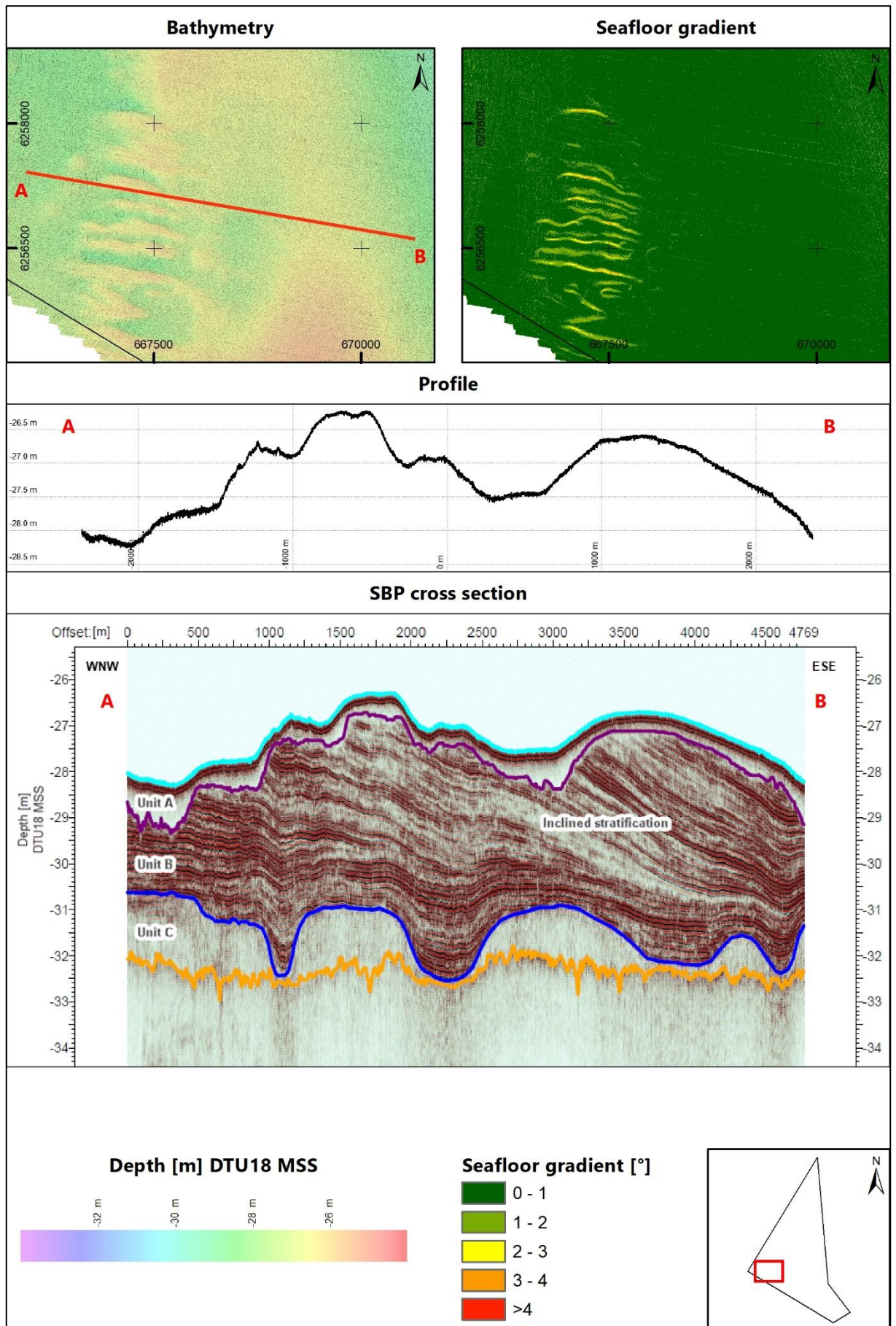
Figure 4.11: Example of gullies in the HOWF site (main line).
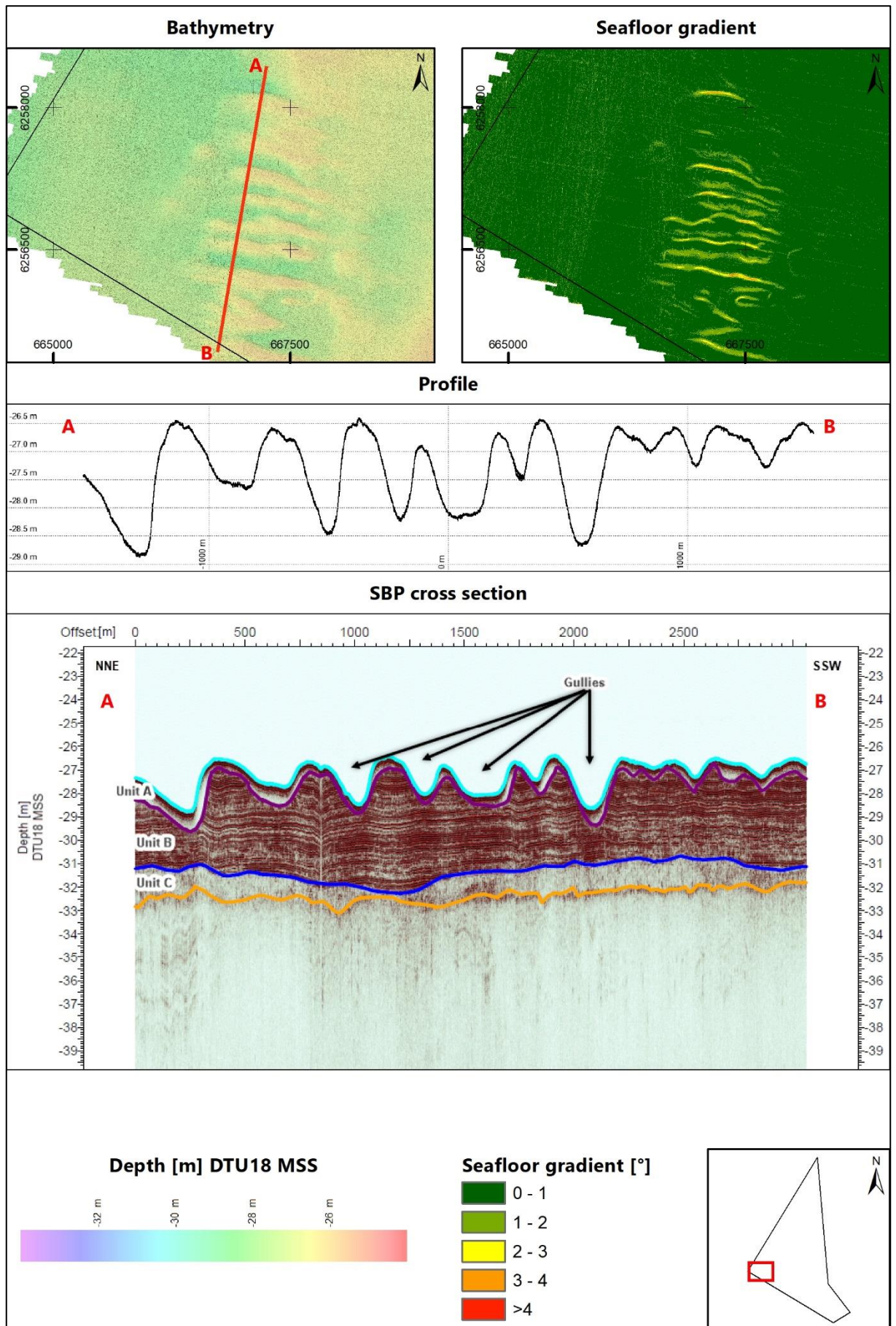
Figure 4.12: Example of gullies in the HOWF site (cross line).

4.2.2.5   Ice-sculpted Area

The north-eastern part of the HOWF site was interpreted as a possible ice-sculpted area, where Pleistocene sediments are covered only by a thin layer of Holocene deposits.

In the north-eastern part of the HOWF site, elongated features of predominantly north–south orientation were observed (Figure 4.13 and Figure 4.14). The observed elevations do not exceed 1.0 m above the surrounding seafloor and gradually decrease from north to south. Seafloor gradients on the slopes of the features vary from 1° to 3°. Locally, the Holocene sediments are only centimetres thick or even absent. Here, patches of outcropping Pleistocene sediment (Unit D; see Section 4.3.2.4) were identified and mapped. These patches are also evident in backscatter data as areas of very high reflectivity.

Bathymetry

Seafloor gradient

Profile

SBP cross section

Depth [m] DTU18 MSS

Seafloor gradient [°]

- 0 - 1
- 1 - 2
- 2 - 3
- 3 - 4
- >4
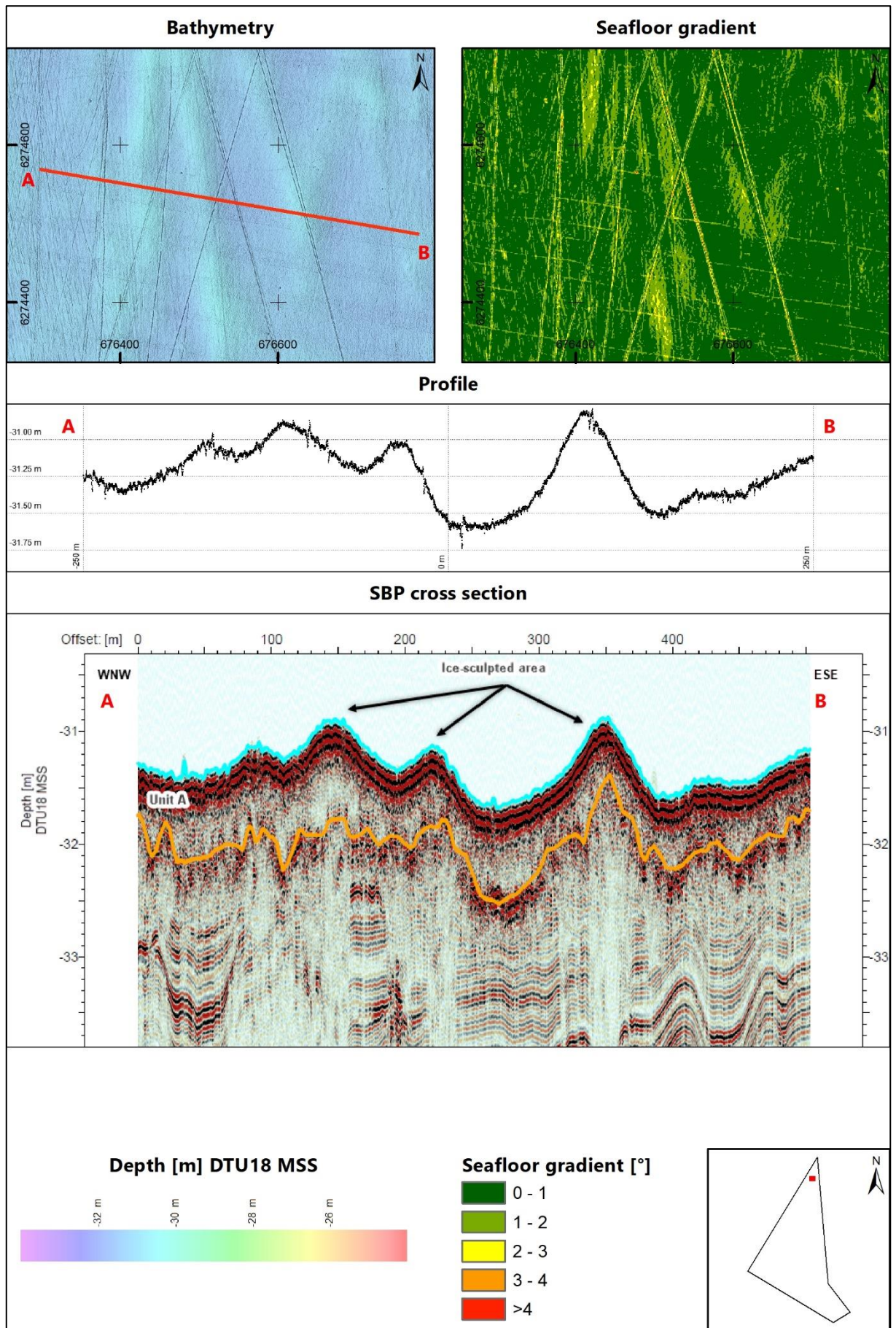
Figure 4.13: Example of ice-sculpted area in the HOWF site - thick Holocene cover.
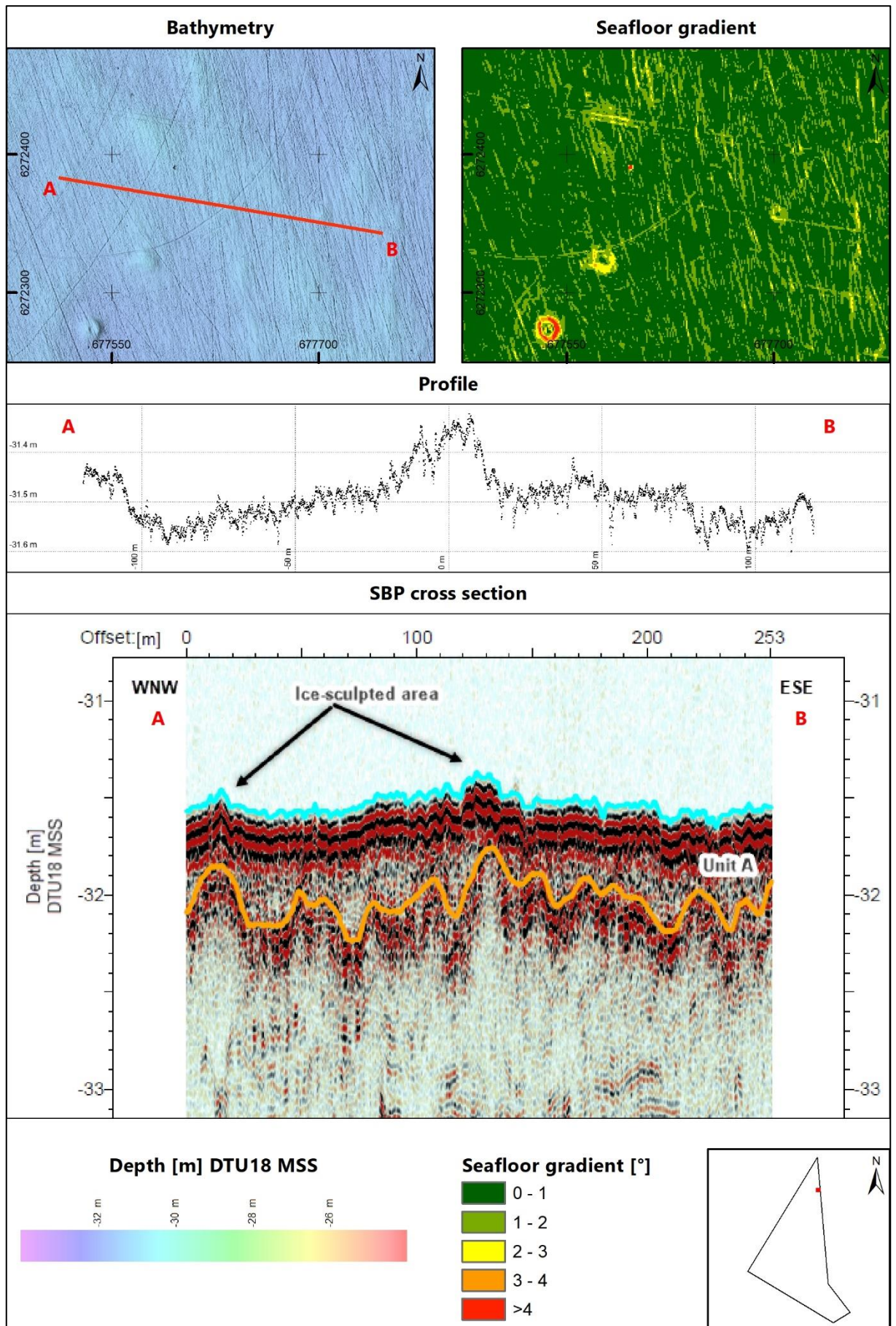
Figure 4.14: Example of ice-sculpted area in the HOWF site - thin Holocene cover.

These features are interpreted as the side berms of iceberg plough marks. Floating icebergs may have been present in this area during the Late Pleistocene to Early Holocene during climatic amelioration. These positive relief structures were later (i.e. after iceberg ploughing) draped with clayey sediments during the Holocene, revealing the underlying palaeotopography.

Figure 4.15 illustrates the possible process that formed the features observed in the north-eastern part of the HOWF site.
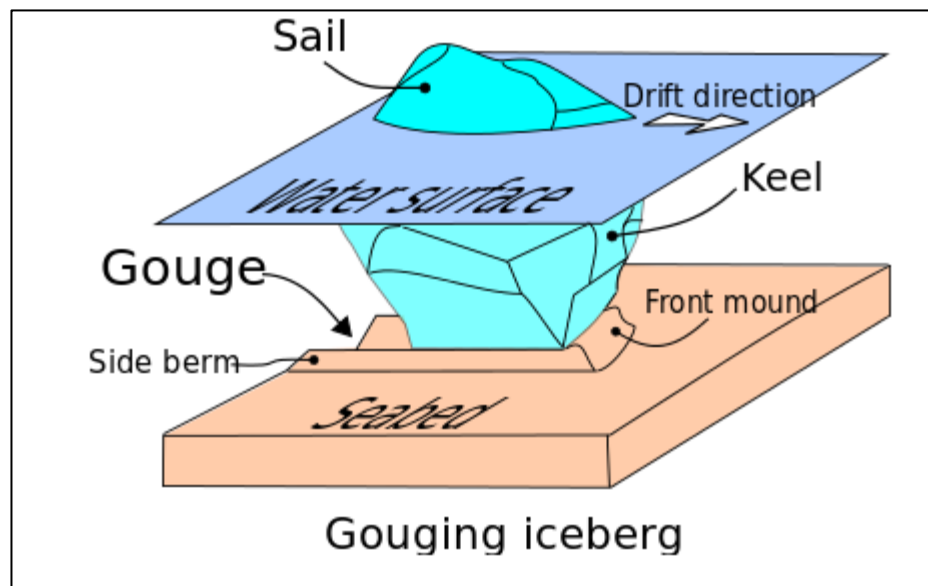
Figure 4.15: Possible process that formed the features observed in the north-eastern part of the HOWF site (https://en.wikipedia.org/wiki/Seabed_gouging_by_ice).

4.2.2.6 Shoals

In the central and southwestern parts of the HOWF site, morphological features resembling shoals were observed. These features have elevations ranging from 0.2 m to 1.0 m above the surrounding seafloor. These features are thought to be remnants of sand spits and/or barrier islands that were formed during the Holocene in the central and south-western part of the site (Unit C, see Section 4.3.2.3).

In the south-western corner of the site, the morphology of these features was later obscured by the accumulation of Unit B. In the central part of the site, however, Unit B is thin, and these palaeotopographic features can be seen at seafloor as shoals. Figure 4.16 presents an example of a shoal.
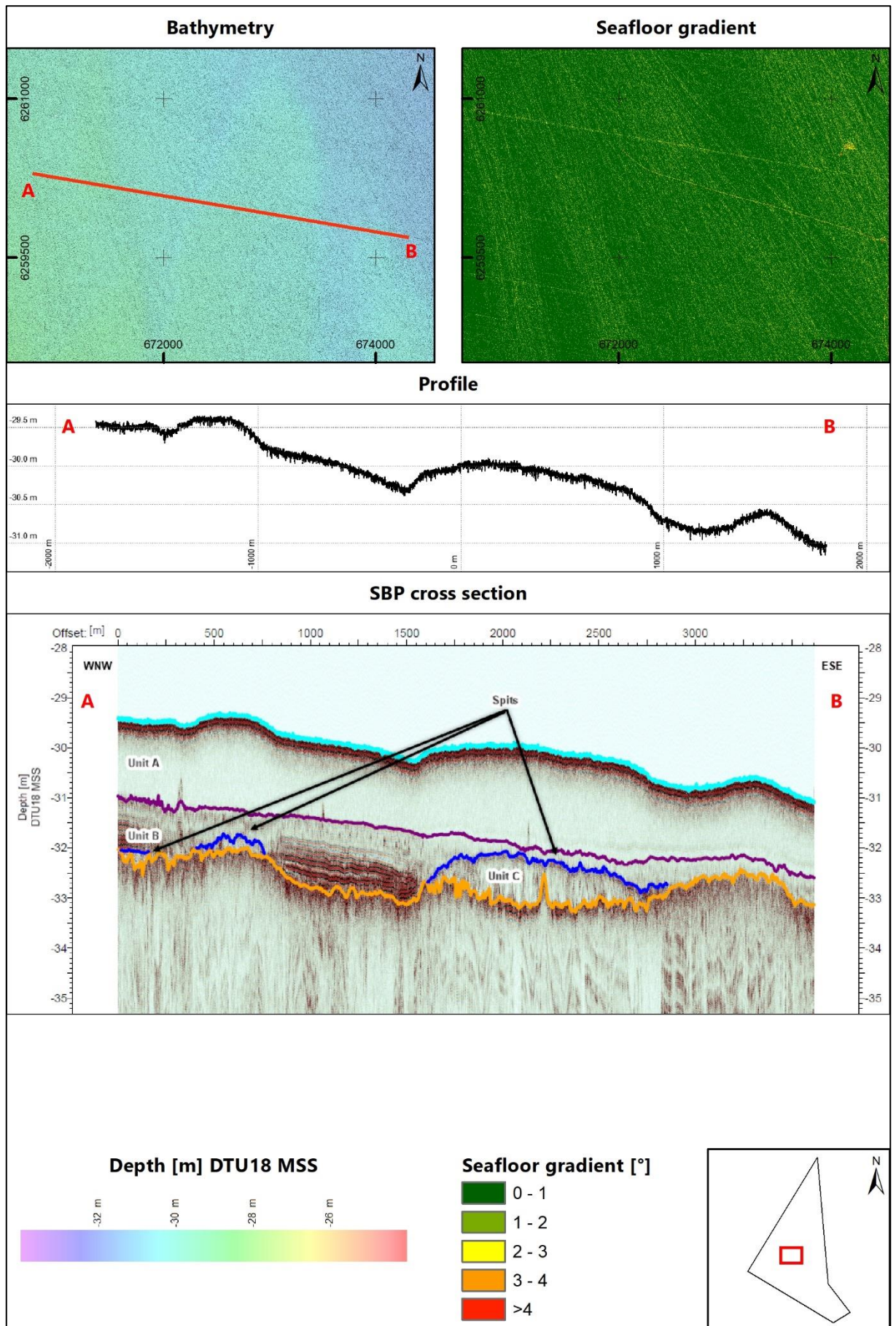
Figure 4.16: Example of shoals in the HOWF site.

4.2.2.7   Area of Debris

Areas of disturbed seafloor were observed in several parts of the HOWF site. These areas vary in depth but generally do not exceed 0.75 m below surrounding seafloor. In the direct vicinity of the more significant areas of debris, the trawl mark density was lower which may indicate these features are known to local fishermen operating in the HOWF site.

in the SBP data, diffraction hyperbolas were observed in these areas below the seafloor within Unit A (see Section 4.3.3.9). Twelve (12) areas of debris were mapped and within six (6) of them magnetic anomalies > 5 nT were observed. However, due to the scarce magnetometer coverage resulting from single magnetometer survey, no clear correlation between the observed magnetic anomalies and the identified areas of debris can be established. The cause of the disturbed seafloor is unknown, however it is believed to be of possible anthropogenic origin. Figure 4.17 presents an example of the largest area of debris identified in the HOWF site.
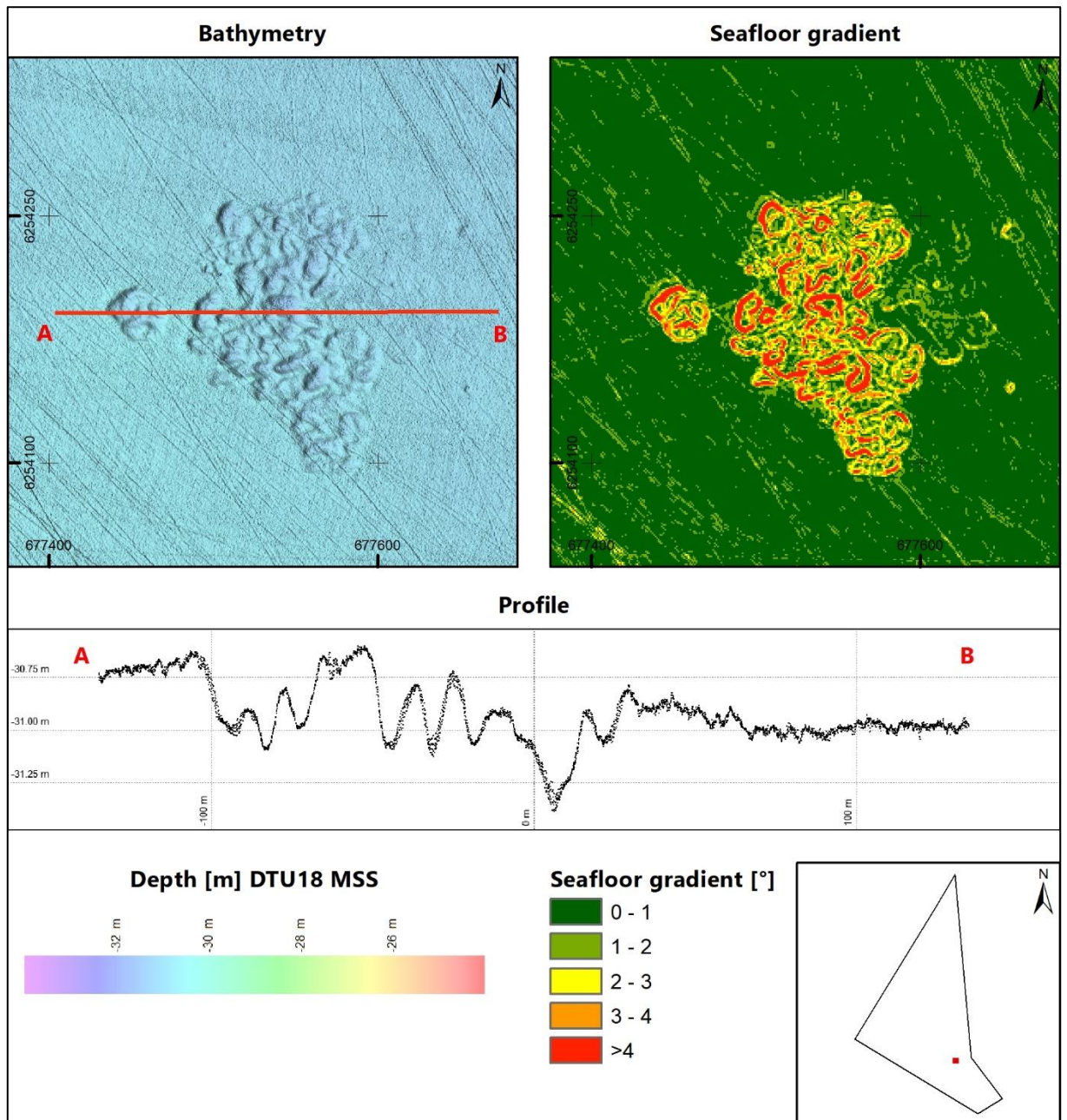
Figure 4.17: Example of an area of debris in the HOWF site.

4.2.2.8 Trawl marks

The entire HOWF site shows evidence of extensive fishing activity. Numerous well-preserved trawl marks of various orientations and depths (up to 0.3 m below surrounding seafloor) were observed in both the SSS and MBES data. The density of trawl scars is lower in the south-western part of the site compared to the density observed elsewhere. Figure 4.18 presents an example of trawl marks.
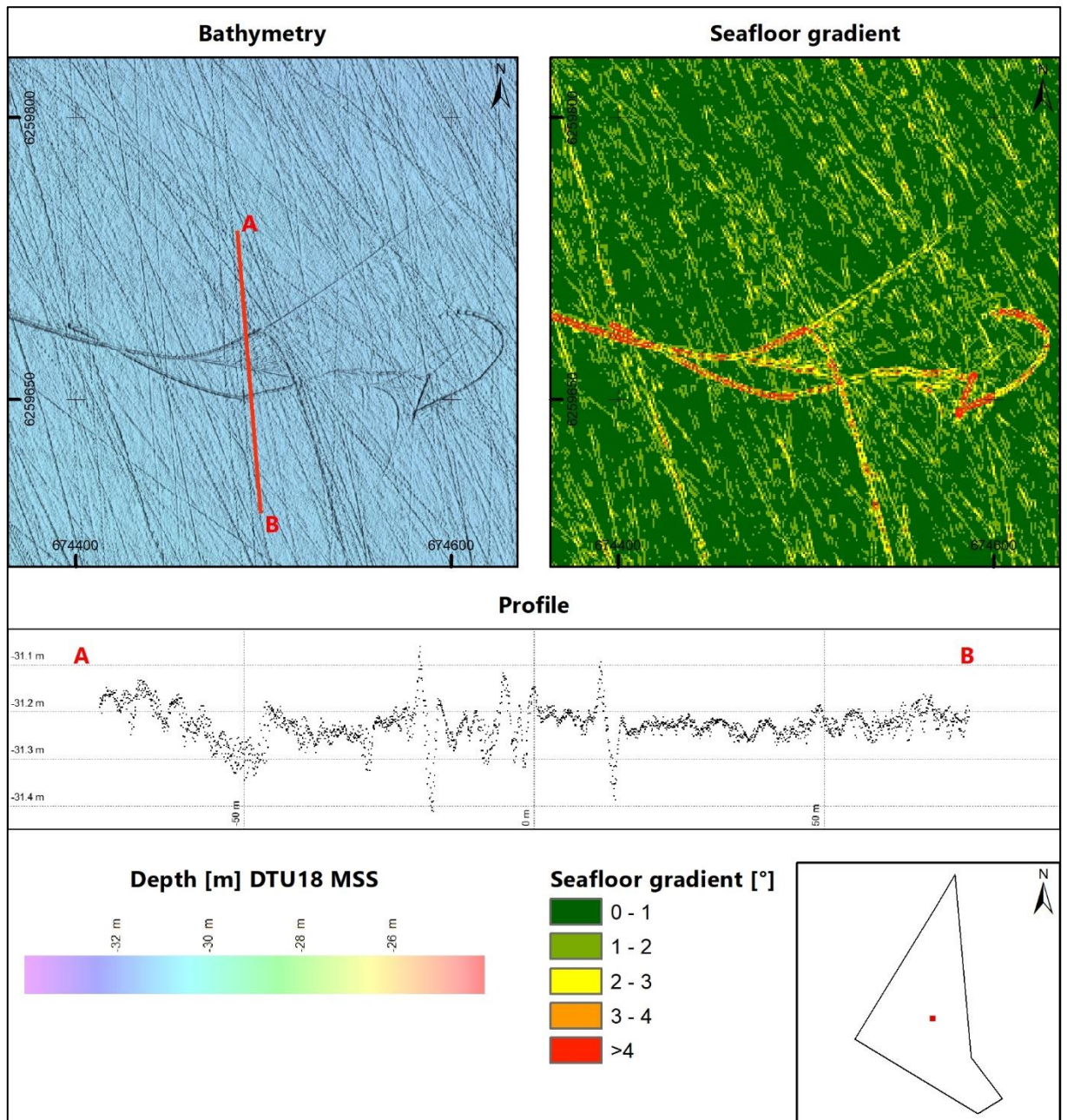
Figure 4.18: Example of an area with trawl marks in the HOWF site.

In addition to trawl marks, several scour patterns are preserved on the seafloor across the site even though no debris items were observed. Figure 4.19 shows a dragging pattern created by a linear object. At the time of the survey no such object was observed on the available data in the surrounding area.
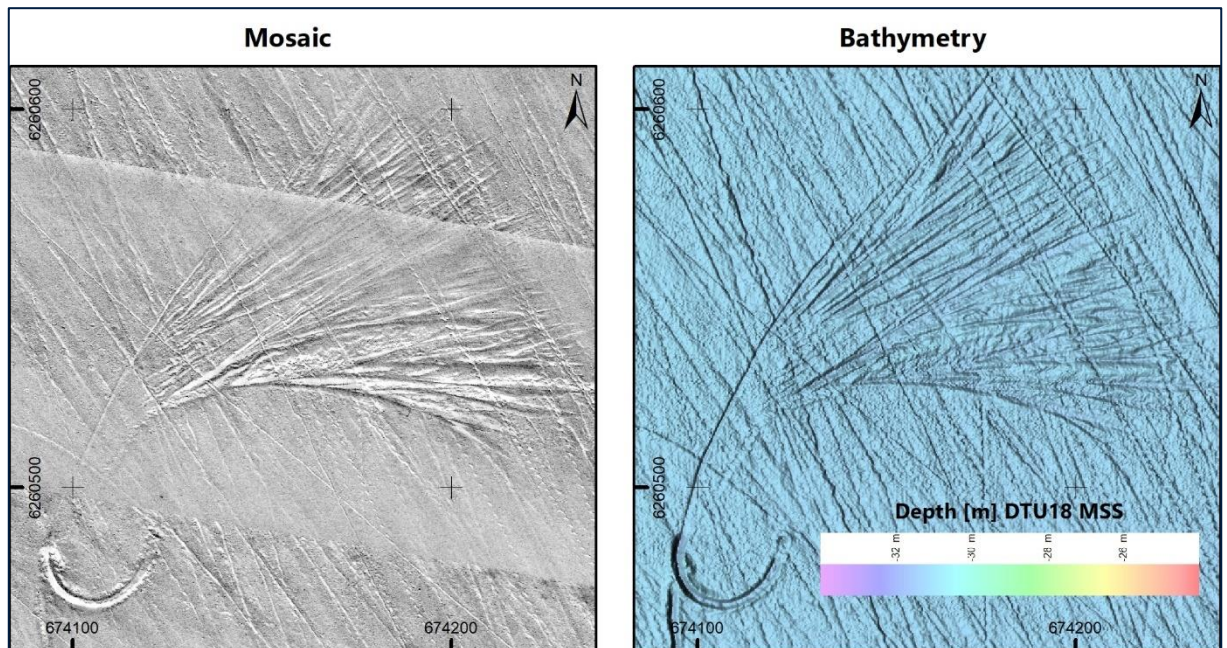
Figure 4.19: Example of the scour pattern created by a linear object.

4.2.3 Substrate Type

An overview of the substrate type interpretation and classification is shown in Figure 4.20 and presented in the charts provided in a separate PDF file (see Appendix B).

Substrate type interpretation and classification was based on a combination of MBES and a backscatter dataset supported by grab sample descriptions derived from laboratory analysis. The substrate type classification followed Danish Råstofbekendtgørelsen (BEK no. 1680 of 17/12/2018, Phase IB).

Initial analysis of the available datasets determined that only the substrate type 1 is present in the HOWF site. As the Danish Råstofbekendtgørelsen (BEK no. 1680 of 17/12/2018, Phase IB) presents no quantitative ranges for classification, the interpretation remains very subjective. To remove the subjective interpretation process Fugro proposed and applied the following ranges:

- Samples containing ≥65% of sand, were classified as 1b – Sand, solid sandy bottom
- Samples containing <65% sand were classified as:
    - 1a – Sand, silty, soft bottom when % silt > % clay
    - 1c – Clay bottom when % clay > % silt

The data analysis was carried out using acoustic characteristics such as overall pattern, roughness, reflectivity and backscatter strength. An overview of the backscatter data is presented in Figure 4.21.

The substrate type polygon boundaries were derived from seafloor sediment interpretation. Several polygons were grouped and adjusted where necessary based on the grab sample analysis following the classification specified above. An overview of the grab samples collected in the HOWF site is presented in Figure 4.22.

The substrate types identified in the HOWF site were as follows:

- 1a – silty soft bottom; comprising mainly mud and sandy mud and muddy sand;
- 1b – solid sandy bottom; comprising mainly gravel and coarse sand, muddy sand, Quaternary sand and silt and sand.
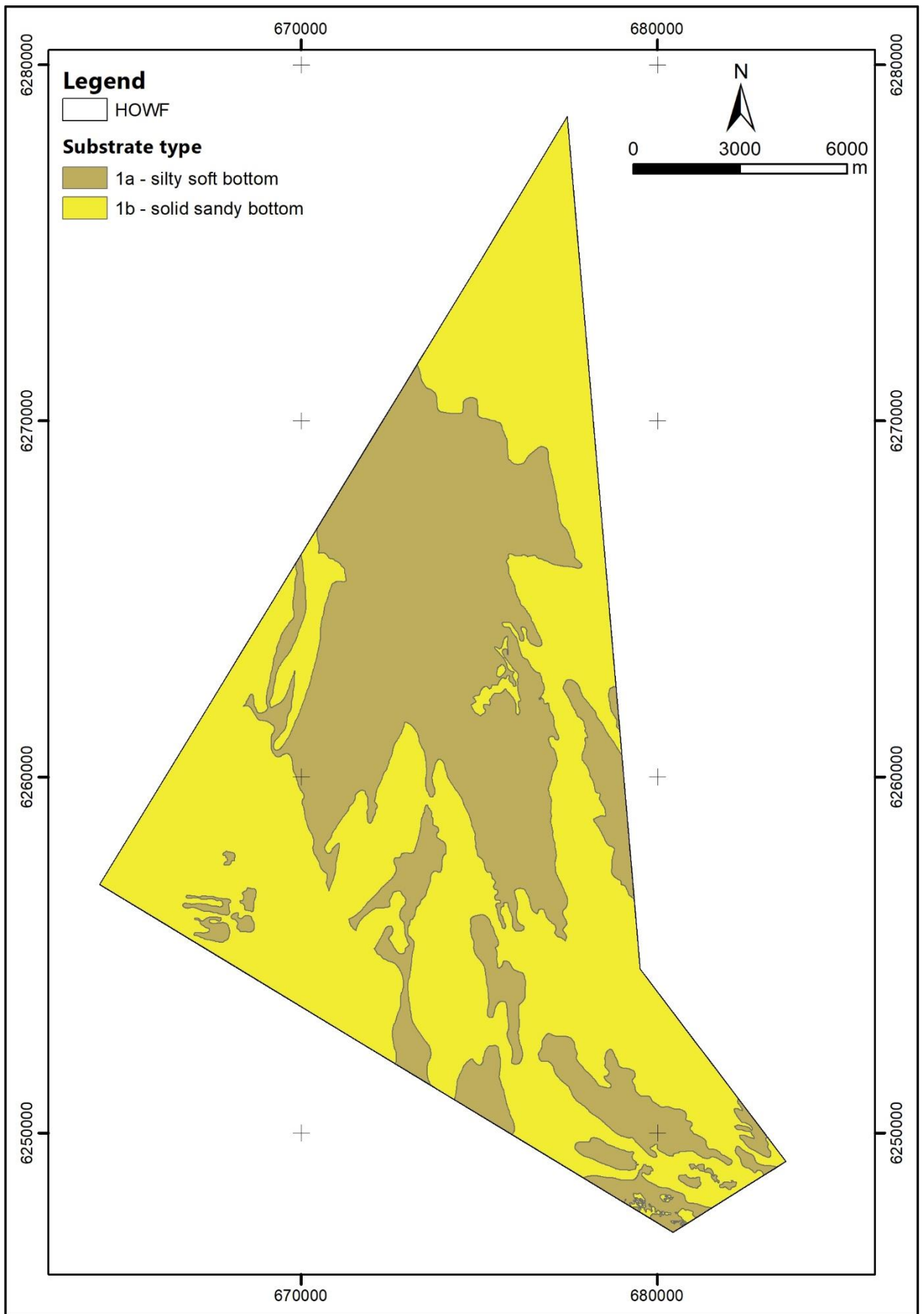
Figure 4.20: Overview of the substrate types in the HOWF site.
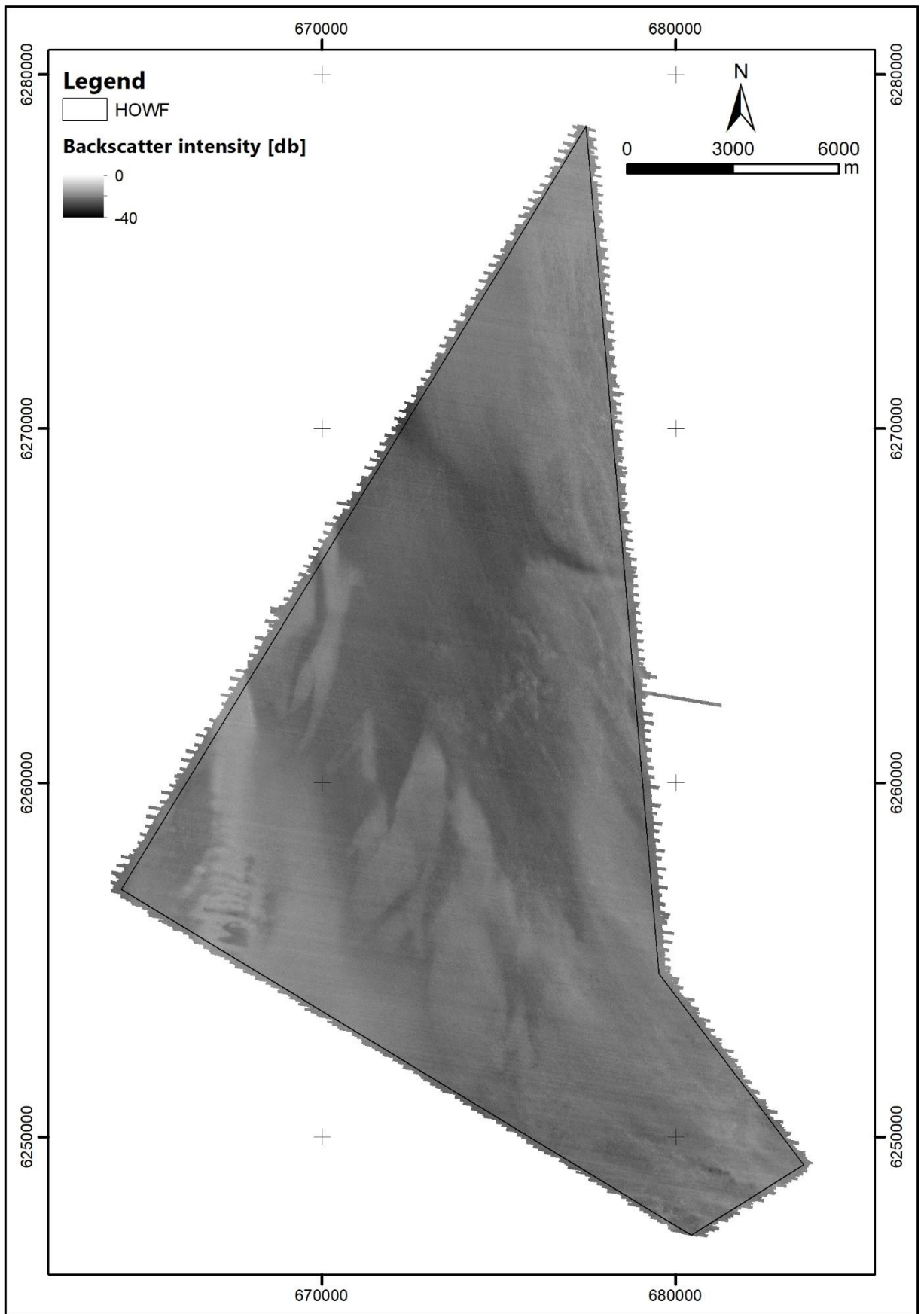
Figure 4.21: Overview of the backscatter data in the HOWF site.
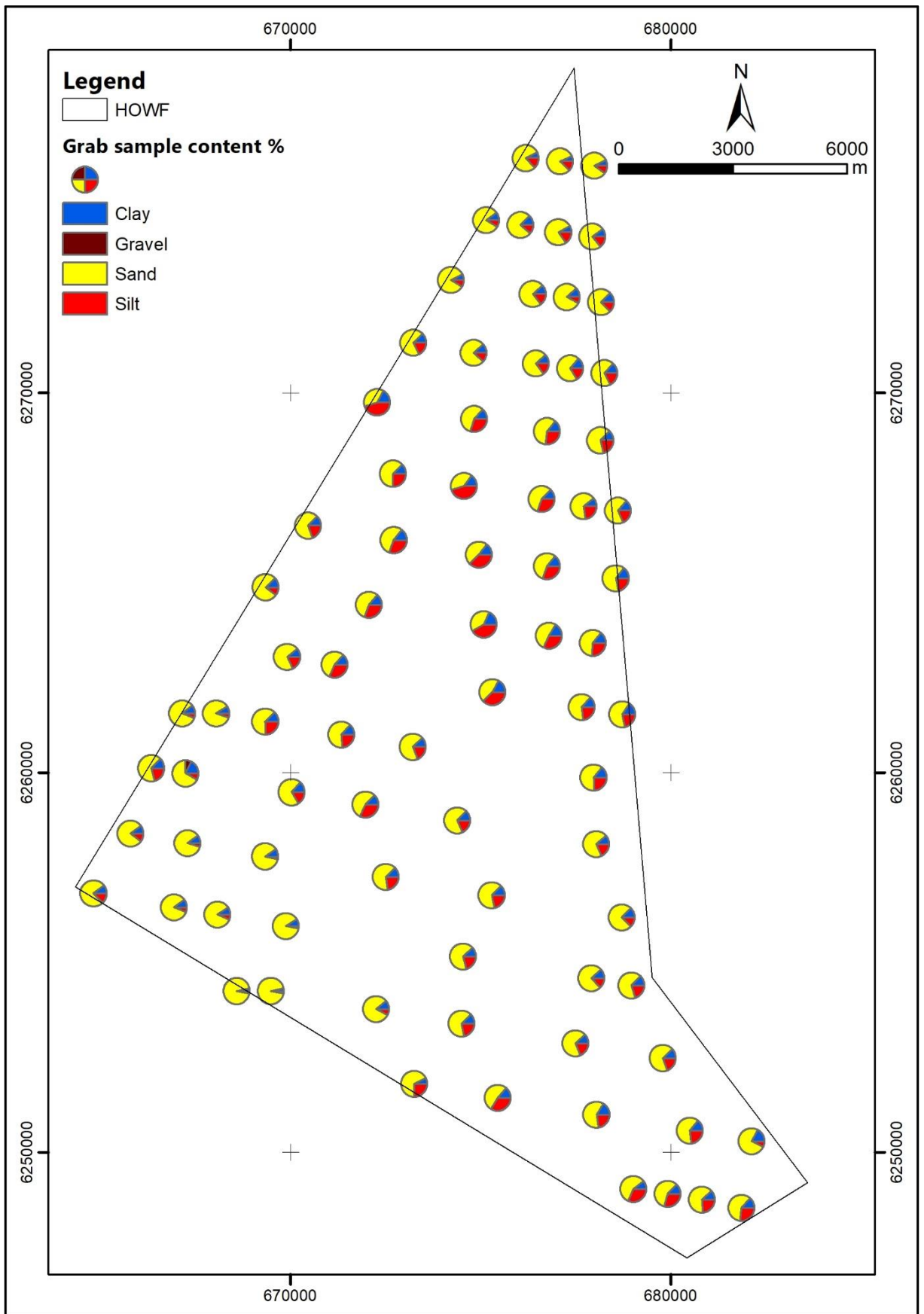
Figure 4.22: Overview of the grab samples collected in the HOWF site.

4.2.4 Seafloor Sediments

An overview of the seafloor sediment interpretation and classification is shown in Figure 4.23 and presented in the charts provided in a separate PDF file (see Appendix B).

Seafloor sediment interpretation and classification was based on a combination of MBES and backscatter datasets and correlated with the sub-surface geology interpreted in the SBP data. The data analysis was carried out using acoustic characteristics such as overall pattern, roughness, reflectivity and backscatter strength.

In addition, seafloor sediment interpretation incorporated soil description of grab samples following from onshore laboratory analysis. The grab sample soil descriptions are based on Danish standard (Larsen et al., 1995) and GEUS terminology was used to define mapped sediment classes. Detailed laboratory analyses of the collected grab samples are supplied as a part of the final deliverables.
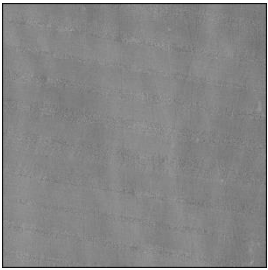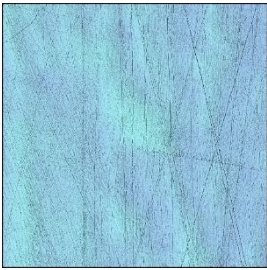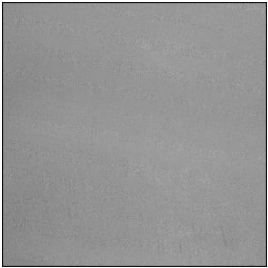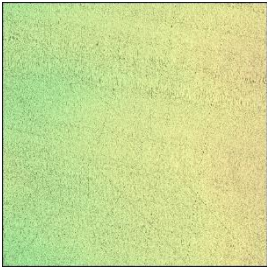
An overview of the backscatter data is presented in Figure 4.21, followed by an overview of the grab sampling results shown in Figure 4.22.
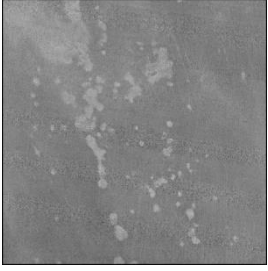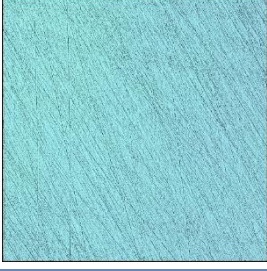
The seafloor sediments identified in the HOWF site comprise the following:

- Gravel and coarse sand
- Sand
- Muddy sand
- Mud and sandy mud
- Quaternary clay and silt

The acoustic characteristics of the identified sediment types are summarised in Table 4.2.

Table 4.2: Acoustic characteristics of the sediment types identified in the HOWF site.

Backscatter Image	MBES Image	Acoustic Characteristics	Geological Interpretation
		High to medium reflectivity	Gravel and coarse sand
		High reflectivity	Sand

Backscatter Image	MBES Image	Acoustic Characteristics	Geological Interpretation
		Low reflectivity	Muddy sand
		Medium to low reflectivity	Mud and sandy mud
		Very high reflectivity	Mud and sandy mud (localised patches in the north-east part of the HOWF site)
		Medium reflectivity	Quaternary clay and silt

Notes: Scale varies between the examples of sediment classes.

The dominant sediment type in the HOWF site is muddy sand. Areas of gravel and coarse sand were identified in the north-eastern part of the site and within the erosional escarpment observed in the west. Sand was mostly found within the gullies in the south-western part of the site.

Distinct patches of mud and sandy mud were interpreted in the north-eastern part of the HOWF site. These are characterised by very high backscatter intensities which distinguishes them from areas of mud and sandy mud observed elsewhere in the site. Based on the correlation of surface (MBES and backscatter) and sub-surface datasets (SBP and grab samples), these patches most likely occur where Pleistocene sediments are covered by a thin layer of Holocene sediments. The lab analysis results of the grab samples collected in the proximity of these patches match other locations where mud and sandy mud were identified. The presence of very shallow Pleistocene sediments might contribute to the observed increase of the backscatter intensity.
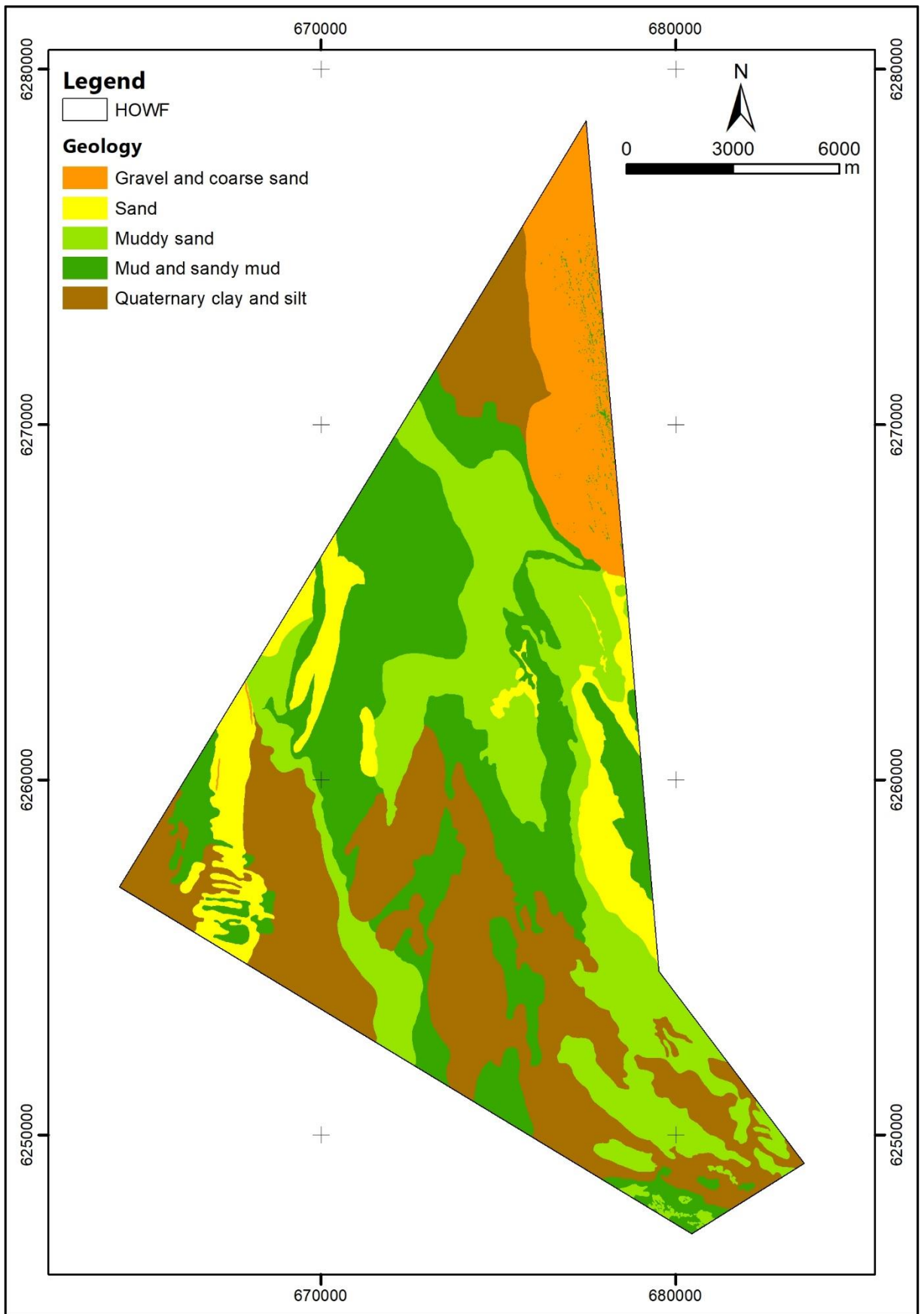
Figure 4.23: Overview of the seafloor sediment interpretation in the HOWF site.

4.2.5 Seafloor Features and Targets

Seafloor features and targets were identified in the SSS, MBES and MAG data and cross-correlated where possible. The identified targets are shown on charts provided in a separate PDF file (see Appendix B).

Table 4.3 summarises the quantities of targets picked.

Table 4.3: Summary of seafloor targets identified in the HOWF site.

Sensor	Target Classification	Quantity
SSS/MBES	Anchor chain	1
	Boulder	1534
	Cable/wire	1
	Debris/suspected debris	72
	Isolated depression/pockmark	14
	Seafloor mound	1
	Soft	2
	Soft rope	1
	Unidentified	1
MAG	Unidentified	4221

4.2.5.1 Side-scan Sonar and MBES Targets

A total of 1627 targets measuring at least 1.0 m in any dimension were identified. Out of 1627 targets, 1569 were observed in both the SSS and MBES datasets.

Target dimensions were measured in the SSS data. A limited number of targets had no observed shadow and their dimensions were subsequently marked with 'non-measurable height'. For these targets, as well as for the depressions, height column lists 0 m.

Details of all the identified SSS targets are presented in the target list supplied in the GIS database as part of the final deliverables and catalogues including SSS images (Appendix D). An overview of the SSS targets is presented in charts provided in a separate PDF file (see Appendix B).

Boulders

Most of the identified targets observed in the SSS and MBES datasets were boulders of varying dimensions. The highest boulder density was observed in the north-eastern part of the site where approximately 90% of the boulders exceeding 1.0 m in height/length/width were identified.

The areas where boulders were observed never reached a density of at least 40 boulders in a seafloor area measuring 100 m x 100 m. As a result, no boulder polygons were mapped.

Figure 4.24 presents a data example of boulders picked in the HOWF site (HAM_SSS_00271: L=1.2 m, W=0.65 m, H=0.36 m; HAM_SSS_00575: L=1.4 m, W=0.35 m, H=0.34 m).
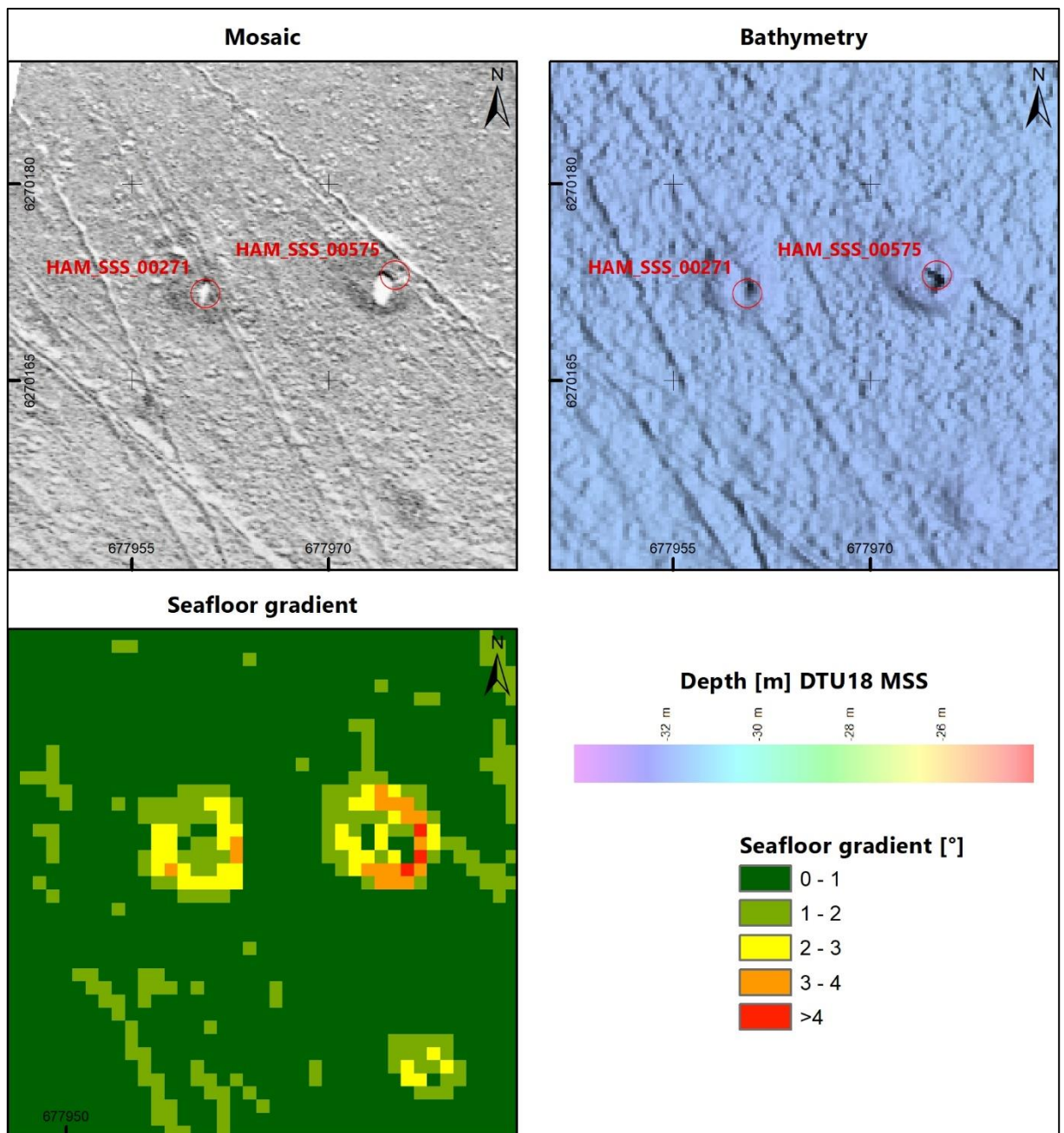
Figure 4.24: Example of boulders observed in the HOWF site.

Suspected Debris

The second most numerous group of identified targets was suspected debris. Items interpreted as potential debris are generally characterised by more angular or elongated shape and relatively high reflectivity compared to the targets described as boulders. It should be noted that certain ambiguity of the interpretation is to be expected and some of the targets interpreted as debris might in fact be of geological origin.

Figure 4.25 presents a data example of debris (HAN_SSS_00567: L=2.4 m, W=1.71 m, H=0.87 m).

Seafloor Mounds

Figure 4.25 presents another type of target found on the seafloor which is interpreted as seafloor mound (HAN_SSS_01466: L=7.47 m, W=6.5 m, H=0.29 m). SSS reflectivity of a seafloor mound is medium to low which indicates geological origin. This target was found in the north-eastern part of the site where ice-sculpted features are present.
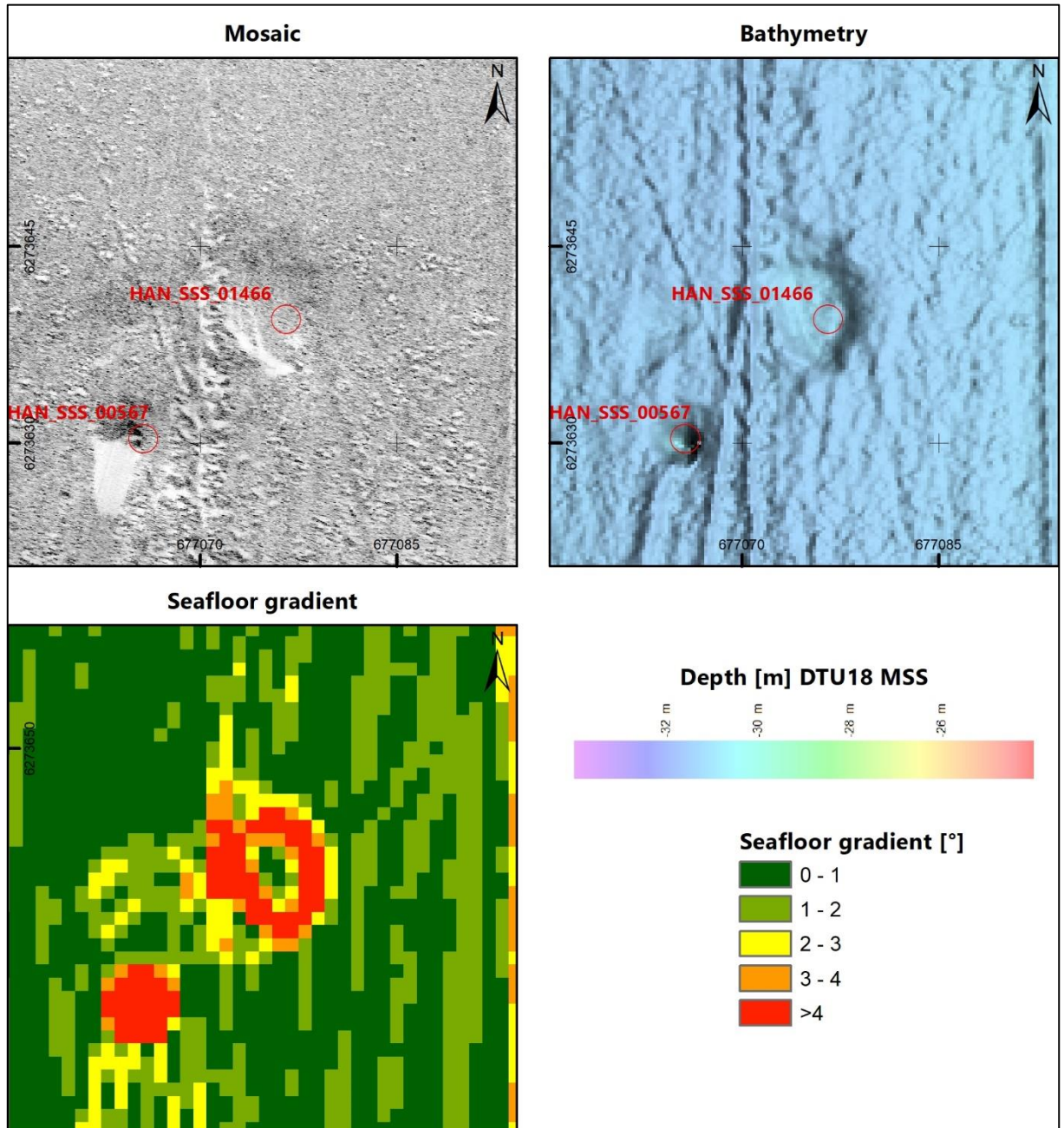
Figure 4.25: Seafloor mound and an example of suspected debris observed in the HOWF site.

Depressions

SSS targets classified as isolated depressions were observed in the northern part of the HOWF site. These depressions measure approximately 2 m to 3 m in diameter while their depths do not exceed 0.4 m below the surrounding seafloor. In size and shape they resemble scoured seafloor around boulders found in the same area (refer to Section 4.2.5.1). Some of them coincide with trawl marks, and observed drag marks extending from the depressions suggest that once they might have contained boulders, which were later removed as a result of fishing activity in the area.

Figure 4.26 presents a data example of a depression (HAM_SSS_00611: L=3.29 m, W=2.83 m).
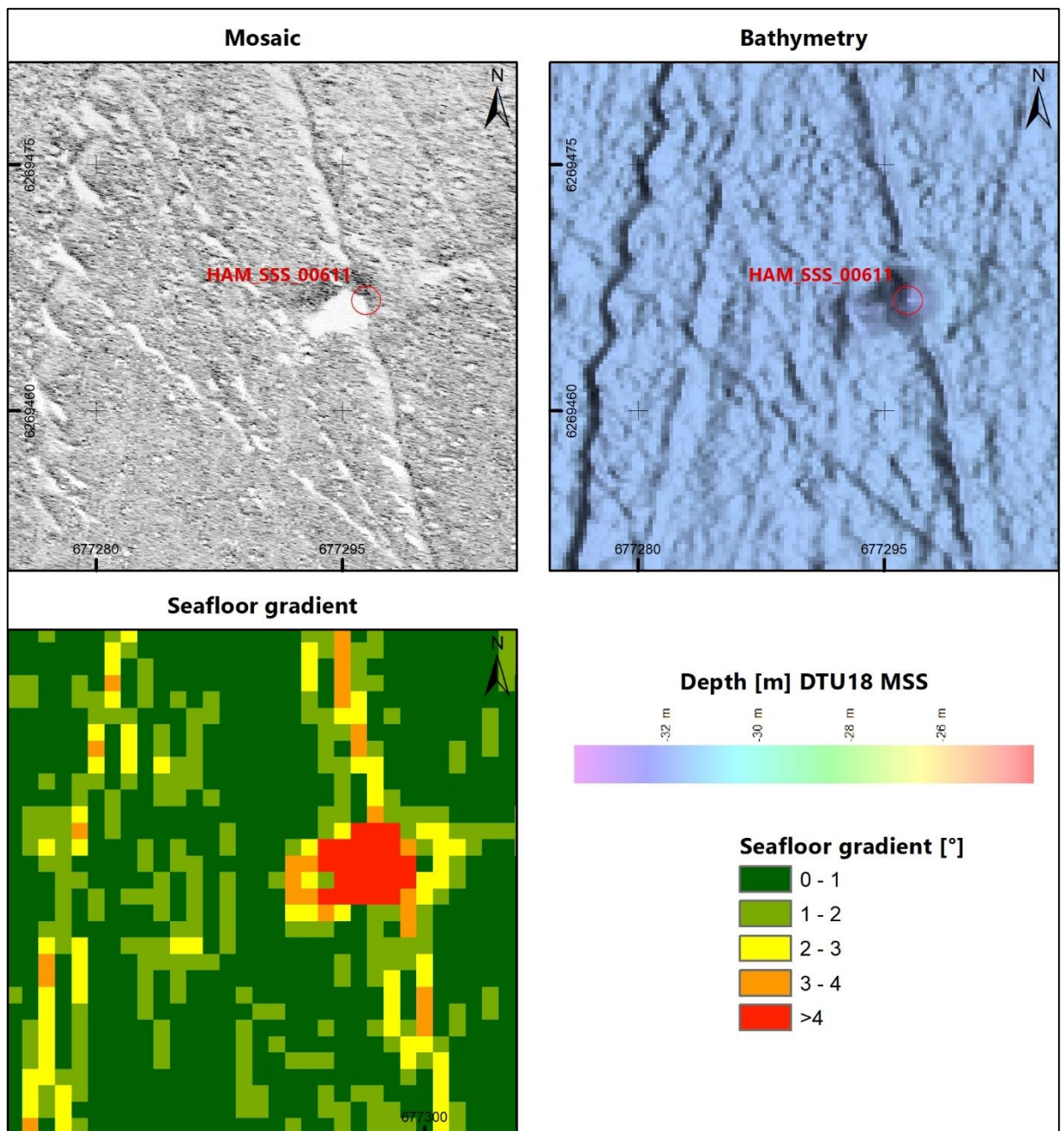
Figure 4.26: Example of a depression observed in the HOWF site.

Soft targets

One of the 1627 SSS targets observed in the site was primarily identified on MBES rather than SSS. As this target was characterised by very low reflectivity, it was classified as soft. Figure 4.27 presents a data example of the soft target (HAE_SSS_00198: L=1.75 m, W=1.48 m, H=0.2 m).
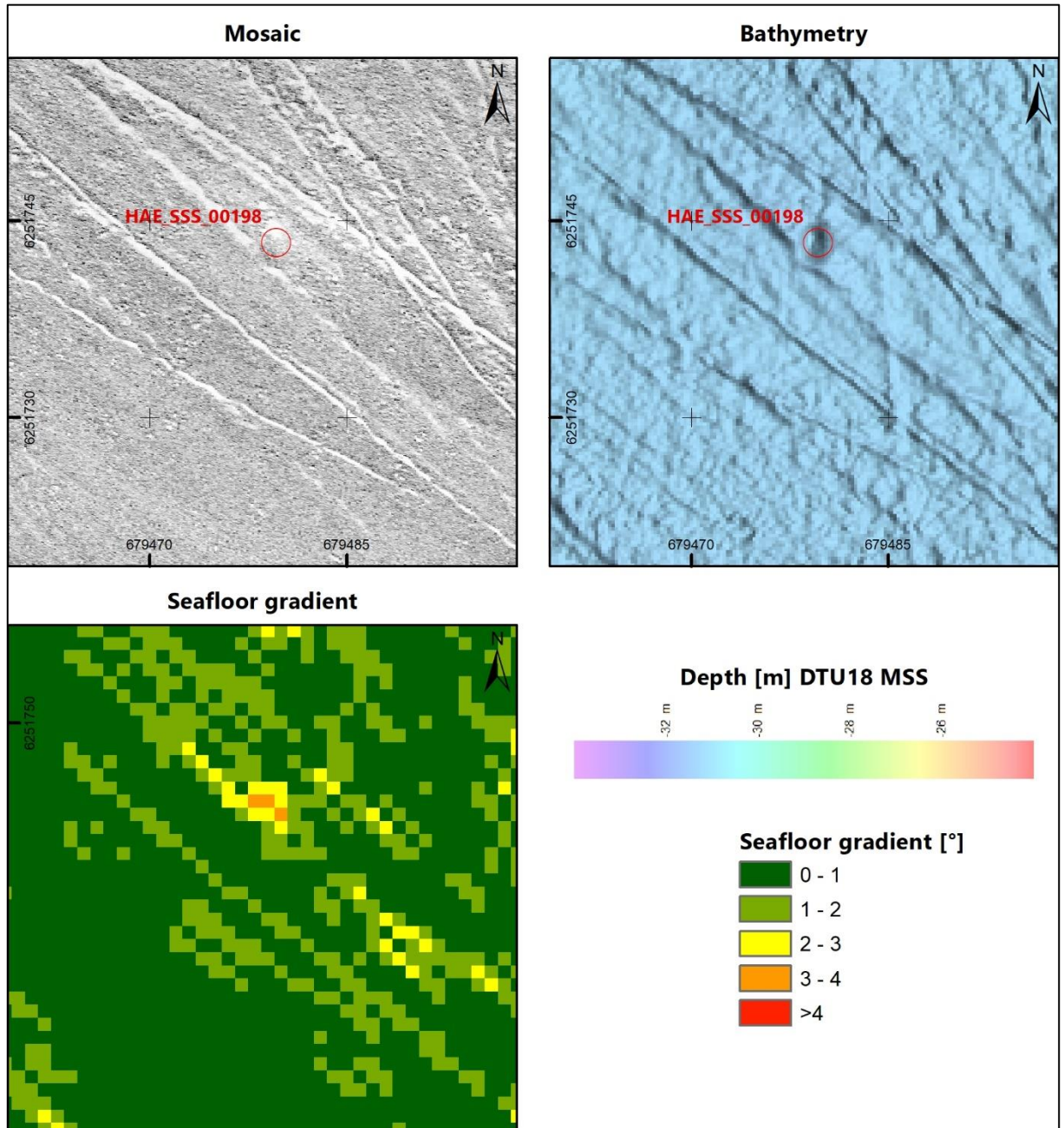
Figure 4.27: Example of a soft target observed in the HOWF site.

4.2.5.2 Magnetometer Anomalies

For the purpose of target picking and data interpretation, a residual grid was created assuming a blanking distance of 5 m and cell size of 1 m. A cluster of relatively high-amplitude anomalies was observed in the southern part of the site. In the western and

northern parts of the site significantly fewer anomalies were identified. Refer to Figure 4.30 for data examples of the magnetic residual grid in the HOWF site.

A total of 4221 anomalies of peak to peak amplitudes ranging from 5.0 nT to 444.26 nT were identified in the HOWF site. All the identified magnetic anomalies were manually measured on the magnetic residual field profiles and classified as monopole (positive or negative), dipole or complex. Additionally, each anomaly was interpreted as non-discrete or discrete. Non-discrete anomalies are those observed very close to each other; defining the exact start and end of the anomaly is not possible (Figure 4.28). Discrete anomalies are observed in separation from other anomalies; start and end of the anomaly is clearly defined (Figure 4.29). Both classifications were based on the single magnetometer data which do not provide full information about the size and shape of the anomaly and should be treated as approximations.
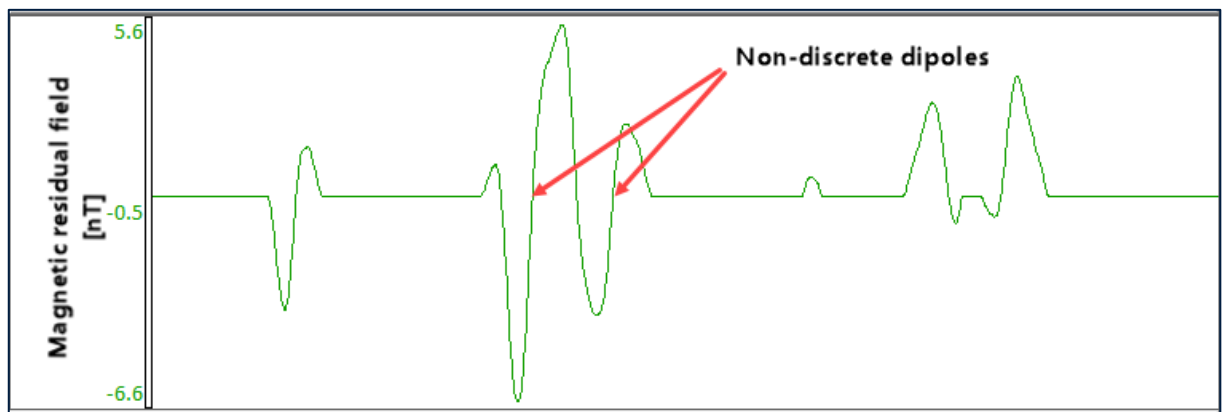
Figure 4.28: Example of two non-discrete magnetic anomalies observed in the HOWF site.
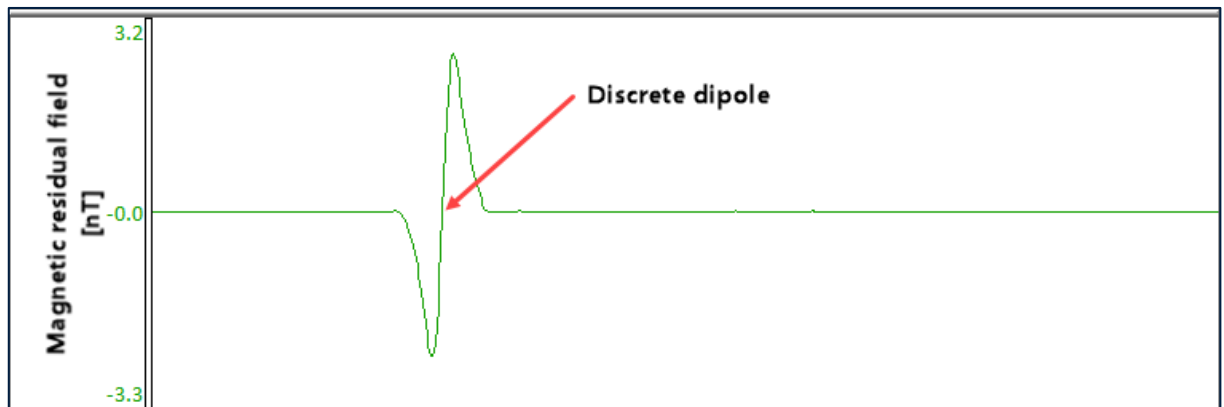
Figure 4.29: Example of a discrete magnetic anomaly observed in the HOWF site.

Details of all the identified magnetometer targets are presented in the target list supplied in the GIS database as part of the final deliverables. An overview of the magnetometer targets is presented in charts provided in a separate PDF file (see Appendix B).

The magnetic residual grid shows evidence of anomalies caused by the geological conditions present across the site. Some of these anomalies can be related to buried structures. A north-west to south-east oriented cluster of low-amplitude magnetic anomalies (< 5 nT) was observed in the north of the site, measuring approximately 2500 m in length and 450 m in

width. This area corresponds to the centre of the large pre-Quaternary depression with an abundance of Postglacial anomalies and a large blanking zone within the Holocene units (see Section 4.3.3.2).

Refer to Figure 4.31 for a data example of the correlation between the magnetic residual field and sub-surface features interpreted in the SBP data. Further description of this sub-surface feature is presented in Section 4.3.3.1.
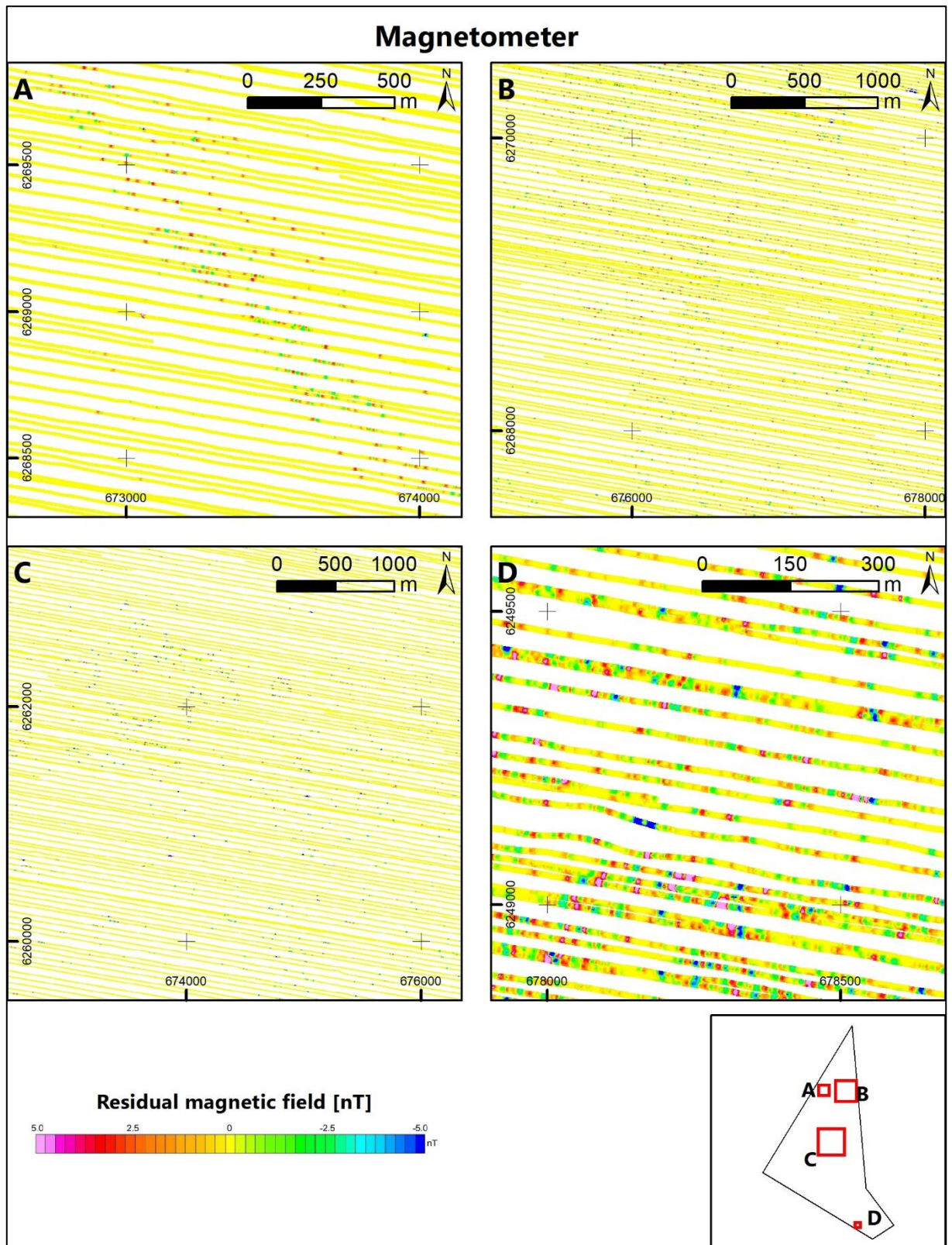
Figure 4.30: Examples of the magnetic residual grid in the HOWF site.
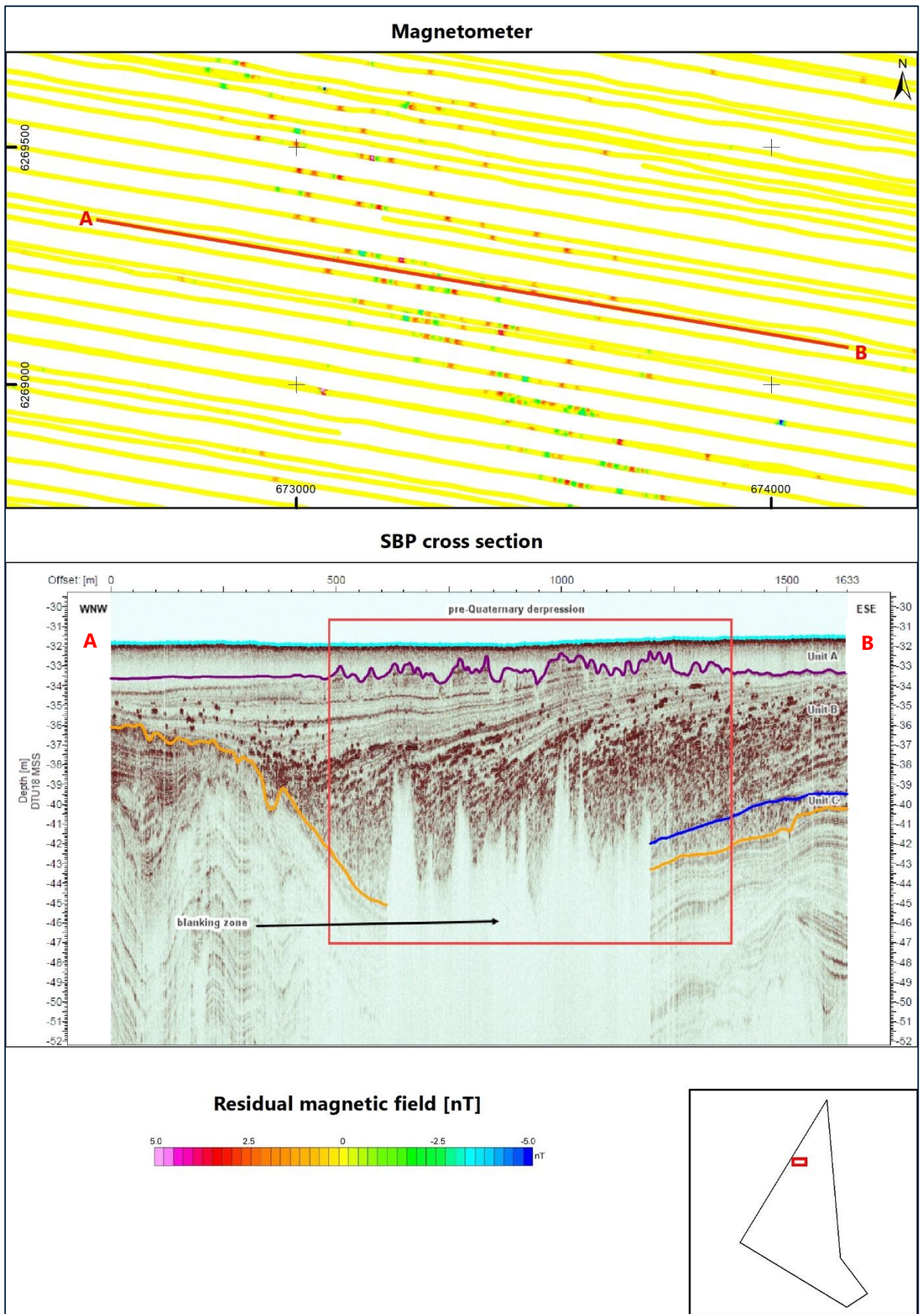
Figure 4.31: Example of correlation between the magnetic residual field and subsurface geology in the HOWF site.

4.2.5.3   Target Cross-correlation

Automatic and manual cross-correlations of all seafloor and SBP targets and anomalies were performed based on the criteria presented in Table 4.4 with the following results.

Table 4.4: Cross-correlation between targets identified on SSS, MBES, MAG and SBP datasets.

Correlated Sensors	Correlation Criteria	Total Correlated Targets
SSS and MBES	■ Manual cross-correlation ■ SSS targets observed on the MBES 0.25 m grid were moved to MBES position ■ No cross-correlation radius was used	1569
SSS and MAG	■ Automatic spatial cross-correlation followed by manual cross-correlation where relevant ■ One to multiple method: all the targets within a 2-m radius were correlated	41 MAG anomalies correlated with 43 SSS targets
SBP and MAG	■ Automatic spatial cross-correlation ■ Only SBP anomalies found within 2 m below the seafloor were used for cross-correlation with the magnetometer anomalies ■ One to multiple method: all the anomalies within a 2-m radius were correlated	4

In addition to the automatic spatial cross-correlation between SSS and MAG targets, both datasets were reviewed and in several cases the targets falling outside the correlation radius of 2 m were cross-correlated manually. Manual cross-correlation was carried out for point targets identified within 2 m to 4 m distance between the SSS and MAG datasets. For linear targets no fixed radius was assumed and the cross-correlation was based on individual interpretation of the available datasets.

The seafloor targets correlating with magnetic anomalies included an anchor chain, boulders, cable or wire, and several debris items. Observed targets were interpreted and classified based on the SSS and MBES datasets.

Refer to Figure 4.32 and Figure 4.33 for data examples of the cross-correlated targets between SSS and MAG datasets.

The SBP anomalies correlating with magnetometer anomalies were identified as Postglacial anomalies observed within Unit A and Unit B. Further description of these sub-surface anomalies is provided in Section 4.3.3.1.
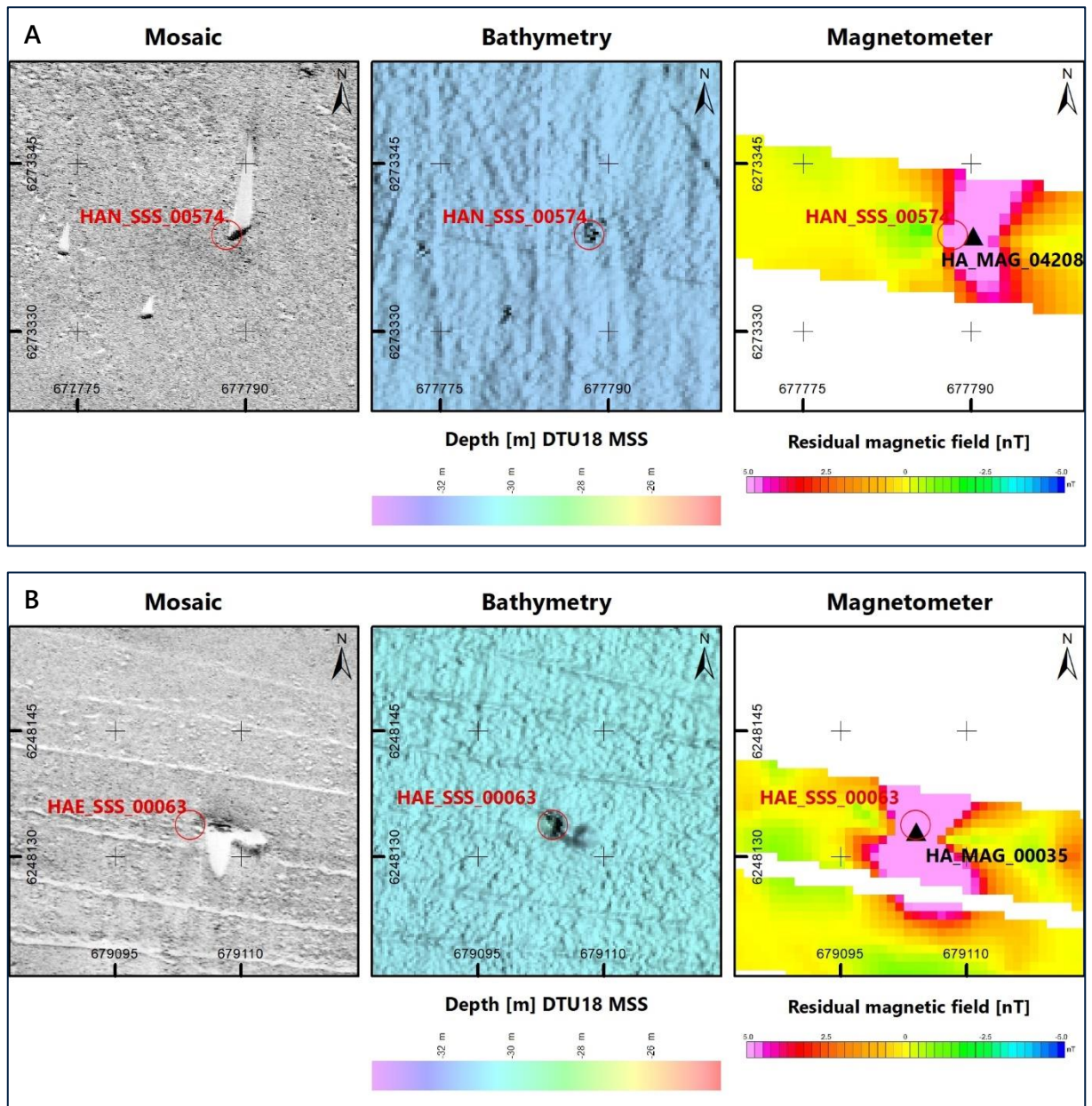
Figure 4.32: Example of the automatic target cross-correlation between the SSS targets and magnetic anomalies observed in the HOWF site: (A) boulder, (B) suspected debris.
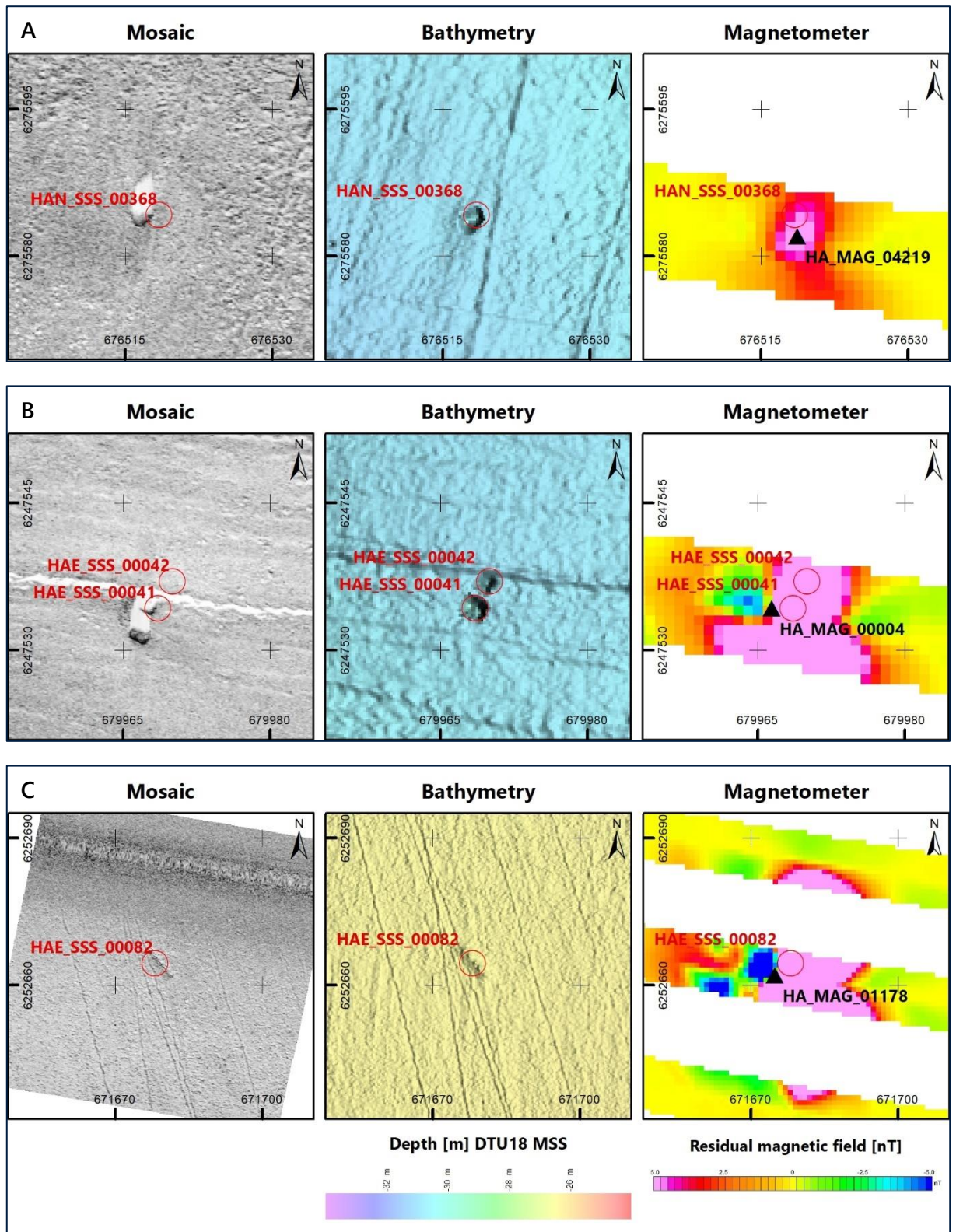
Figure 4.33: Example of the manual target cross-correlation between the SSS targets and magnetic anomalies observed in the HOWF site: (A) boulder, (B) suspected debris items, (C) linear debris.

4.2.6   Seafloor Man-Made Objects

Several targets observed in the SSS, MAG, MBES and SBP datasets and included in respective target lists were further classified as potential man-made objects (MMOs). Each target interpreted as potential MMO was assigned a type as specified in a document provided by Energinet (Template Survey Geodatabase (TSG): Requirements to TSG).

Identified MMOs include:

- Point features classified as wire (1), soft rope (1) and other (73) – subset of the SSS target list;
- Linear features (10) including all targets of elongated shape and potentially anthropogenic origin which length exceeds 5 m – subset of the SSS target list;
- Potential areas of debris (12) identified during the morphological classification.

Selected items of the observed MMOs are presented in Table 4.5 with corresponding data examples shown in Figure 4.34, Figure 4.35 and Figure 4.36.

Detailed information on all the MMOs identified in the HOWF site is supplied in the GIS database as part of the final deliverables.

Table 4.5: Examples of man-made objects observed in the HOWF site.

SSS ID	Measurements* L x W x H [m]	MAG ID	Peak to Peak Amplitude* [nT]	Classification (MMO Type)
HAF_SSS_00048	52.1 x 0.5 x 0.8	HA_MAG_02560	27.0	Anchor Chain (Other)
HAF_SSS_00050	38.0 x 1.4 x 0.4	HA_MAG_02559	11.8	Suspected debris (Other)
HAF_SSS_00036	20.3 x 0.8 x nmh[†]	HA_MAG_02735	18.6	Cable-Wire (Wire)
HAE_SSS_00041	2.2 x 1.4 x 0.7	HA_MAG_00004	45.4	Suspected debris (Other)
HAE_SSS_00042	1.9 x 1.4 x 0.6	HA_MAG_00004	45.4	Suspected debris (Other)
HAE_SSS_00043	3.0 x 1.8 x 0.8	HA_MAG_01419	17.5	Suspected debris (Other)
Notes: *Measurements are rounded to one decimal point [†]nmh = non-measurable height				
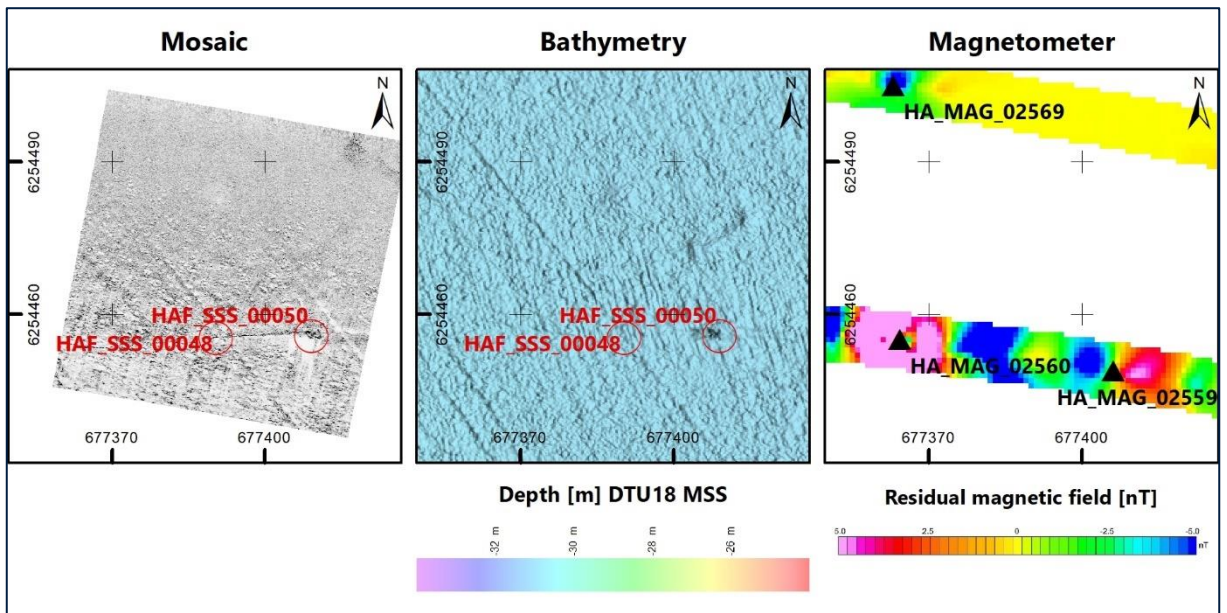
Figure 4.34: Example of linear MMO type 'Other' observed in the HOWF site (SSS-MAG targets correlated manually).
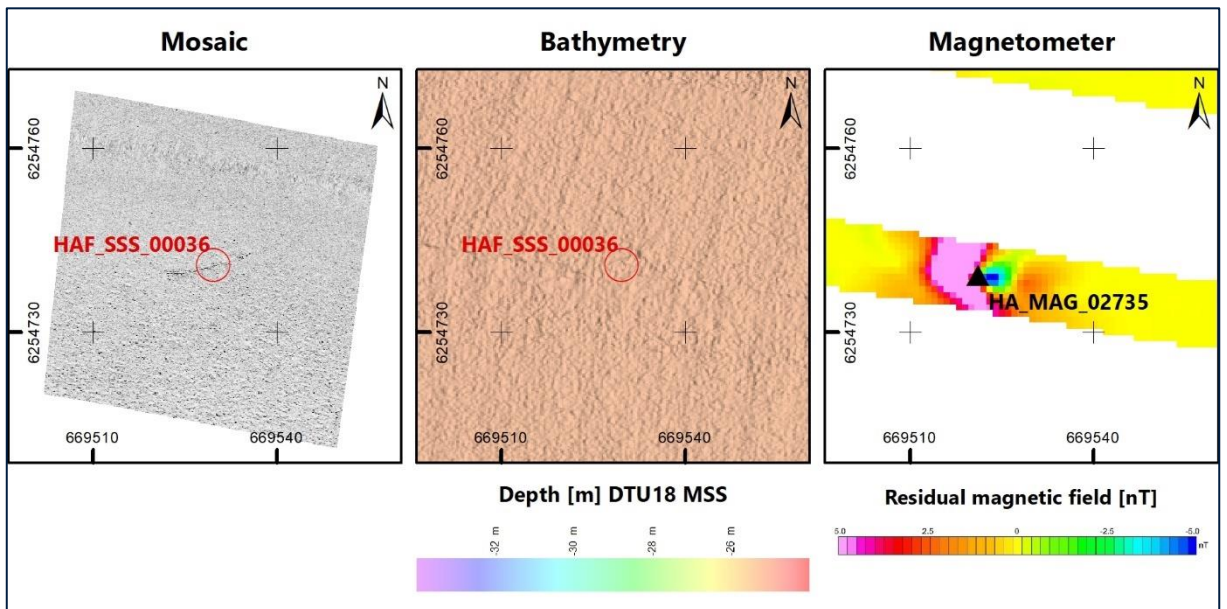
Figure 4.35: Example of linear MMO type 'Wire' observed in the HOWF site (SSS-MAG targets correlated manually).
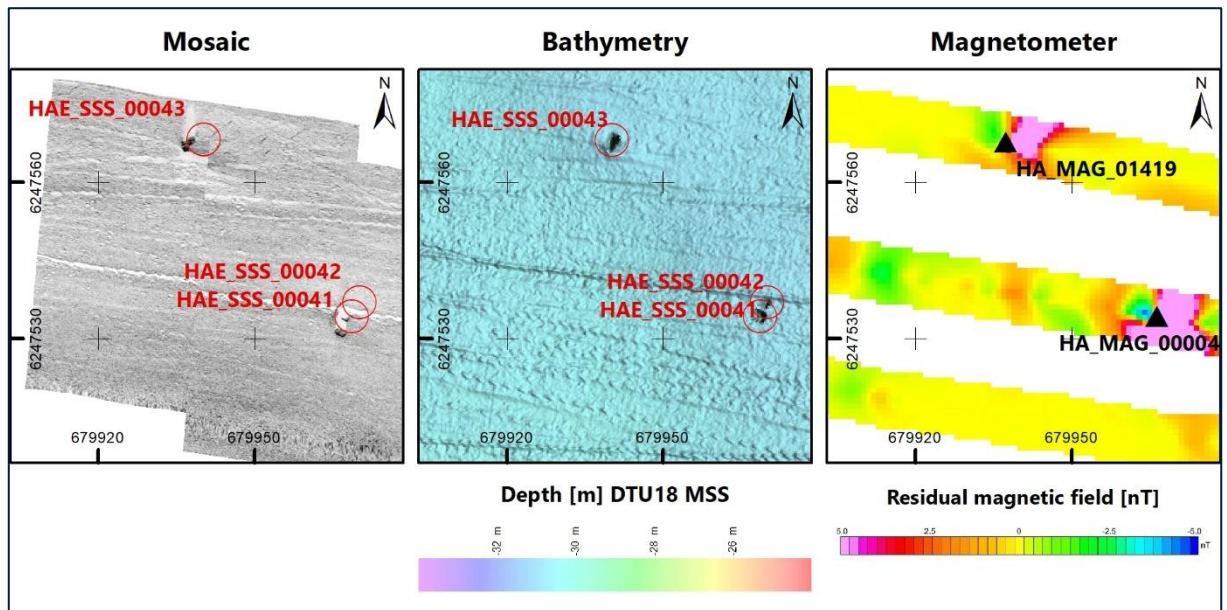
Figure 4.36: Example of MMO type 'Other' observed in the HOWF site (SSS-MAG targets correlated manually).

4.3   Sub-seafloor Geology

4.3.1   Overview

Table 4.6 presents an overview of the interpreted horizons and seismostratigraphic units in the HOWF site. Arbitrary cross sections through the site are given in Figure 4.37 and Figure 4.38.

Nine (9) seismostratigraphic units were interpreted in the SBP and 2D-UUHR data of which some are present across the whole site (Unit A and Unit I), some are present across a large part of the site (Unit B, Unit D, Unit E, Unit G and Unit I) and some occur only locally (Unit C, Unit F and Unit H).

The large pre-Quaternary depression is present within the central part of the site (Figure 4.2). Where the depression is deepest it is generally parallel to the orientation of the Børglum Fault and appears to be split into two smaller depressions towards the east, each with a north to south and east to west orientation.

The depression has had substantial influence on the distribution of the interpreted units. Several units display an increased thickness within this depression (Unit B, Unit D and Unit E) and the distribution of Unit G is confined to the location of this depression.

Table 4.6: Overview of seismostratigraphic units

| Data Type | Unit | Horizon [Colour] | | Seismic Character | Expected Soil Type[1] | Age | Depositional Environment | Previous Studies[2] | |
		Top	Base					Jensen et al. (2002)	Bendixen et al. (2015, 2017)
SBP	A	H00 seafloor	H01 H05 H10	Acoustically transparent with occasional vague internal reflector near the base	CLAY to clayey medium SAND or sandy GYTTJA with shells and shell fragments and organic material	Holocene	Marine	H	PG III (6-1 ka BP)
	B	H01	H05 H10	Low to high amplitude horizontal and inclined stratified reflectors, locally chaotic	Interlaminated to interbedded CLAY and SILT with shells and shell fragments	Early Holocene	Deltaic	H	PG II (11.9 to 9.1 ka BP)
SBP 2D-UUHR	C	H05	H10	Acoustically semi-transparent to chaotic	Medium SAND with abundant shells and shell fragments	Early Holocene	Shallow marine (Spit or Barrier Island)	H	PG I (11.7 to 10.8 ka BP)
2D-UUHR	D	H10	H20	Dominantly low to medium amplitude parallel reflectors, becoming increasingly distorted in the southern part of the site. Three internal reflectors discriminate different acoustic facies: ■ H11 marks the base of channel features with infill characterised by parallel reflectors; ■ H12 marks the boundary between acoustically transparent facies above and parallel reflectors below; ■ H15 marks the boundary to generally more variable facies (chaotic, transparent or stratified) below.	CLAY with occasional laminae of SILT and/or SAND, locally sandy	Weichselian	Glaciomarine, glaciolacustrine to fluvial	LG I and LG II (16 to 13.5 ka BP)	LG I and LG II (16 to 12.6 ka BP)
	E	H10, H11, H20	H25	Acoustically semi-transparent to chaotic with locally steeply inclined internal reflectors	CLAY, locally with sand beds	Weichselian	Glaciomarine and/or glacial deposits	GL	WG II
	F	H20, H25	H30	Medium to high amplitude closely spaced parallel reflectors	CLAY with laminae or thin beds of SILT or SAND	Pleistocene	Glaciomarine	-	WG I
	G	H25 H30	H35	Acoustically semi-transparent to chaotic. Locally inclined discontinuous reflectors are present within semi-transparent character.	Poorly sorted gravelly and sandy CLAY, SAND TILL or CLAY TILL	Pleistocene	Glaciomarine and/or glacial till	-	-
	H	H20? H25 H30 H35	H50	Variable, either medium amplitude parallel reflectors, acoustically semi-transparent with occasional inclined lateral discontinuous internal reflectors or a chaotic seismic character	SAND, CLAY, CLAY TILL and/or SAND TILL	Pleistocene	Glacial, periglacial and/or glaciomarine	-	-
	I	H30 H35 H50	N/A	Low to medium amplitude low frequency parallel reflectors; Locally acoustically (semi-)transparent	Sandy MUDSTONE, LIMESTONE and glauconitic SANDSTONE	Jurassic to Cretaceous	Marine	BR	-

Notes:
1) Based on historic geotechnical data:
    Units A, B, C and D and I from GEUS (2020)
    Units E, F, G and H from Jensen (2002); Bendixen et al. (2015; 2017); Andrén et al. (2015a; 2015b)
2) The units were correlated to seismostratigraphic units and age dating provided in previous studies of the southern Kattegat (Figure 4.4 - Jensen et al., 2002; Bendixen et al., 2015, 2017), where: H = Holocene, PG = Postglacial, LG = Late Glacial, GL = Glacial, WG = Weichselian Glacial, BR = Bedrock

The interpreted horizons represent seismostratigraphic unit boundaries (Table 4.7), with the exception of Horizons H11, H12 and H15, which are interpreted as internal surfaces separating different seismic facies within Unit D.

Horizon H10 marks the deepest reflector interpreted in the SBP data and is also interpreted in the 2D-UUHR dataset. This horizon represents the base of the Holocene deposits (i.e. comprising Unit A, Unit B and Unit C). Horizon H10 is very irregular and truncates deeper strata within the pre-Quaternary depression. In the 2D-UUHR data, Horizon H10 is a medium to high-amplitude positive reflector.

Table 4.7: Depth range of the interpreted horizons in the HOWF site.

Data Type	Horizon	Description	Depth Range	
			MSL [m]	BSF [m]
SBP	H01	Top of Unit B	25 to 35	0 to 3
	H05	Top of Unit C	30 to 46	1 to 14
SBP 2D-UUHR	H10	Base Holocene	30 to 49	0 to 17
2D-UUHR	H11	Internal horizon in Unit D	30 to 62	0 to 31
	H12	Internal horizon in Unit D	31 to 82	0 to 30
	H15	Internal horizon in Unit D	32 to 95	1 to 63
	H20	Base of Unit D	32 to 104	1 to 72
	H25	Base of Unit E	40 to 154	9 to 122
	H30	Base of Unit F	43 to 148	14 to 113
	H35	Base of Unit G	59 to 198	27 to 166
	H50	Base of Unit H	66 to 142	40 to 111
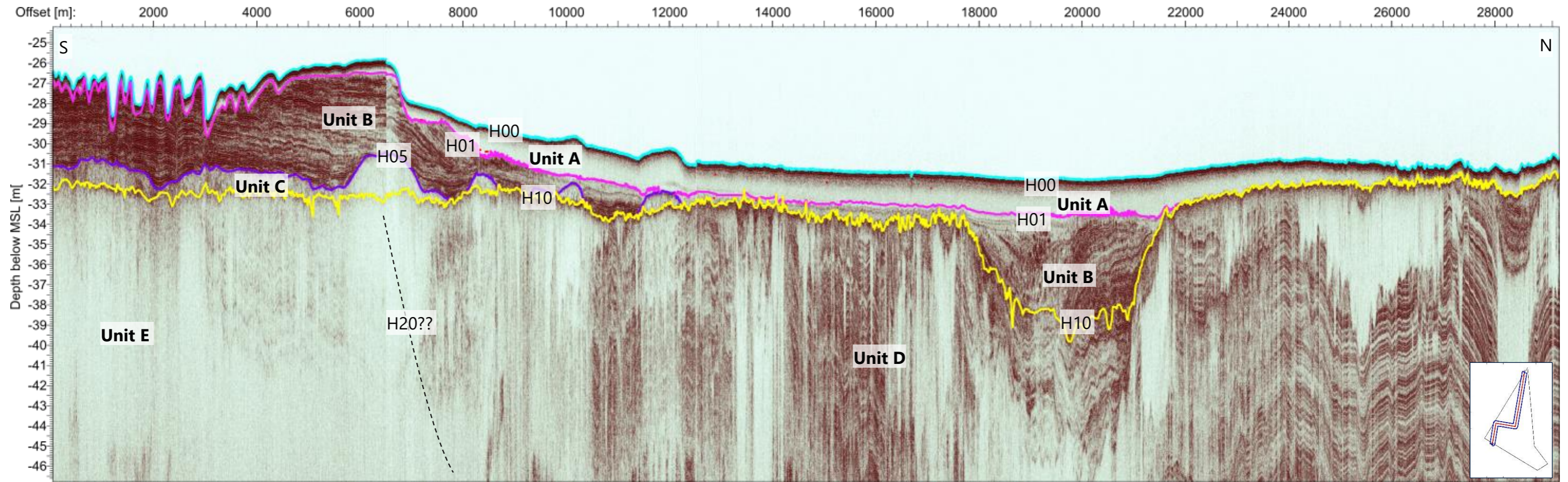
Figure 4.37: Overview of horizons and seismostratigraphic units interpreted in the SBP data (multiple lines).
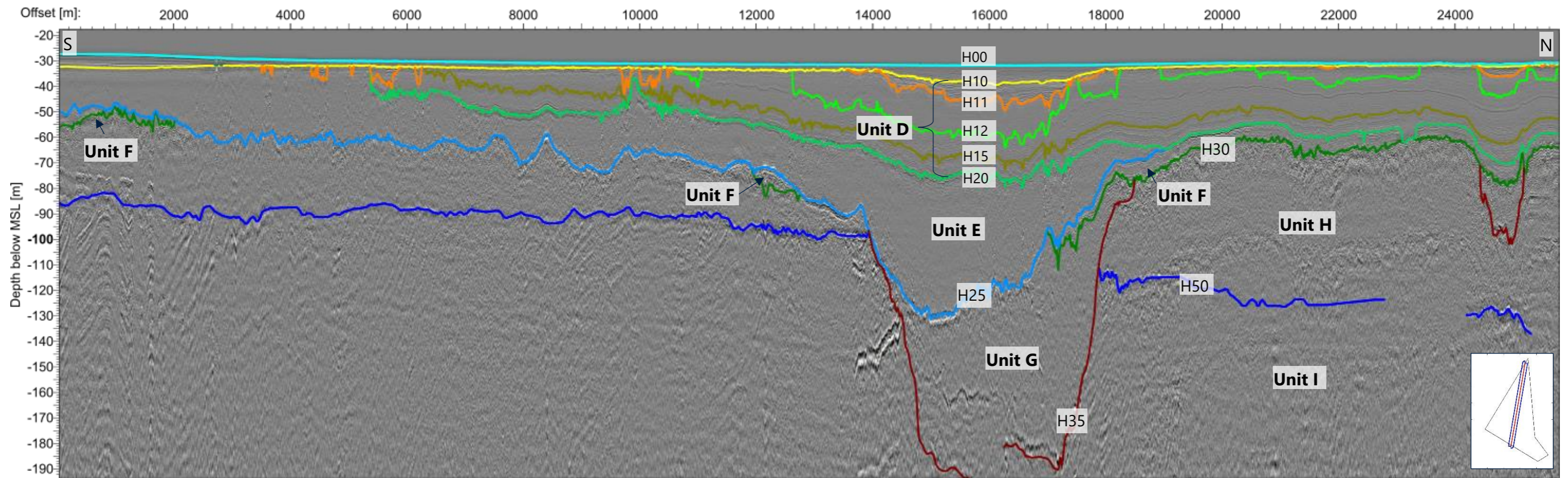
Figure 4.38: Line HAX2499P01. Overview of horizons and seismostratigraphic units interpreted in the 2D-UUHR data.

4.3.2 Seismostratigraphic Units

4.3.2.1 Unit A

Unit A, the uppermost interpreted unit (Figure 4.39; Figure 4.40), is present across the entire site, except for small areas within the eastern part of the site where erosional escarpments were observed on the seafloor (see Section 4.2.2.3). The unit generally forms a thin layer, which drapes older units (Figure 4.41). The maximum thickness is observed in the centre of the site, where it reaches approximately 3 m and decreases to less than 1 m towards the eastern and western margins of the site (Figure 4.39).

Internally the unit is acoustically transparent. Locally, vague internal reflector can be observed (Figure 4.40). Diffraction hyperbolas or enhanced amplitude reflections are present within this unit and are likely due to the presence of coarse material (i.e. gravel-sized shells, shell and rock fragments).

Where the unit overlies Unit B (mostly in the west; Figure 4.41), the base is regular and varies from flat to undulating. Where the unit overlies Unit D (mostly in the east), the base has an irregular, rugose character. In the eastern part of the site, the unit overlies Unit C.

In the western part of the site, Unit A is locally in erosional contact with the underlying Unit B (Figure 4.42), forming gullies of 1 m to 3 m deep, 80 m to 200 m wide with a west–east orientation (Figure 4.11). As the overlying Unit A is thin and drapes Horizon H01, these gullies can still be observed in the present seafloor morphology (Section 4.2.2.4).

In the western part of the site, the base of Unit A forms the eastern margin of a wide channel with a north–south orientation. Potentially these gullies and the channel were formed by the Dana River (Great Belt palaeo-river; Bendixen et al., 2015, 2017).

In the eastern part of the site, where the Holocene cover is generally thin, Unit A appears to fill in the depressional remnants of iceberg plough marks from the underlying Unit D (see Section 4.3.2.4; Figure 4.39).

Table 4.6 provides expected soil type for Unit A, which is based on historic geotechnical data (GEUS, 2020).

Unit A is interpreted to be deposited during the Holocene in a marine environment.

Figure 4.39: Thickness in metres of Unit A.
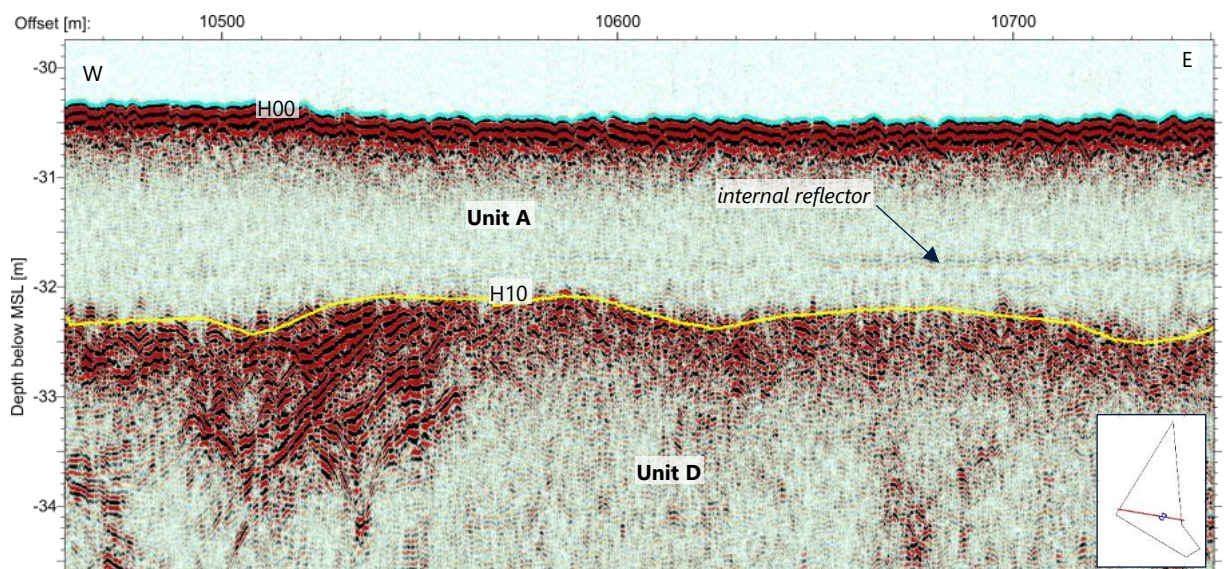
Figure 4.40: Line HAG2134P01. SBP data example showing the internal seismic character of Unit A.
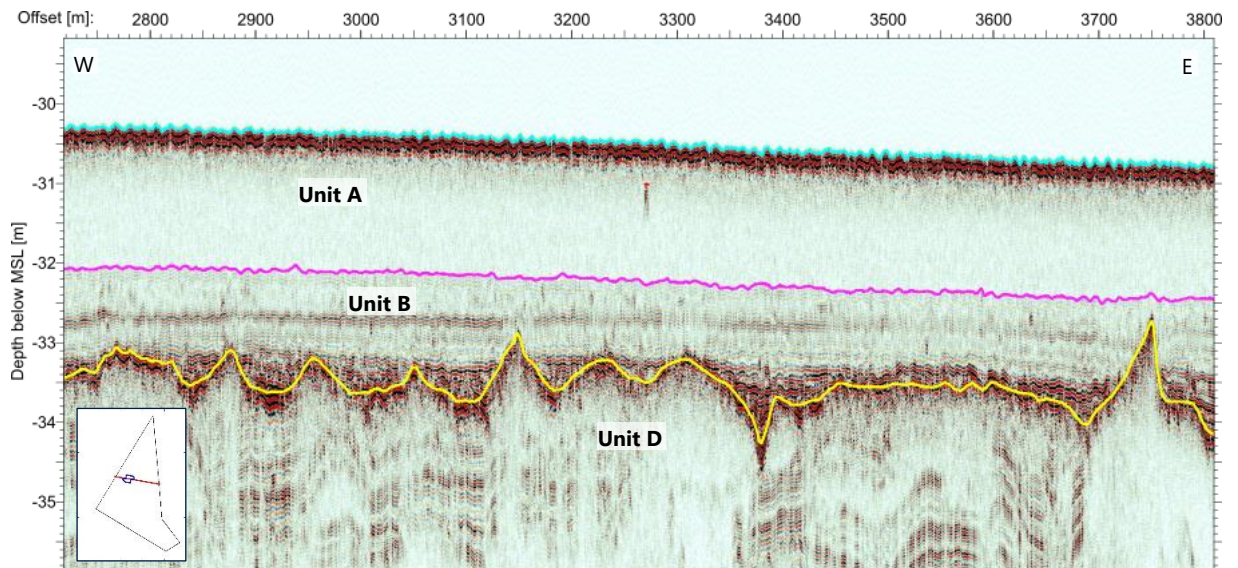
Figure 4.41: Line HAK1241P01. SBP data example showing the internal seismic character of Unit A and Unit B.
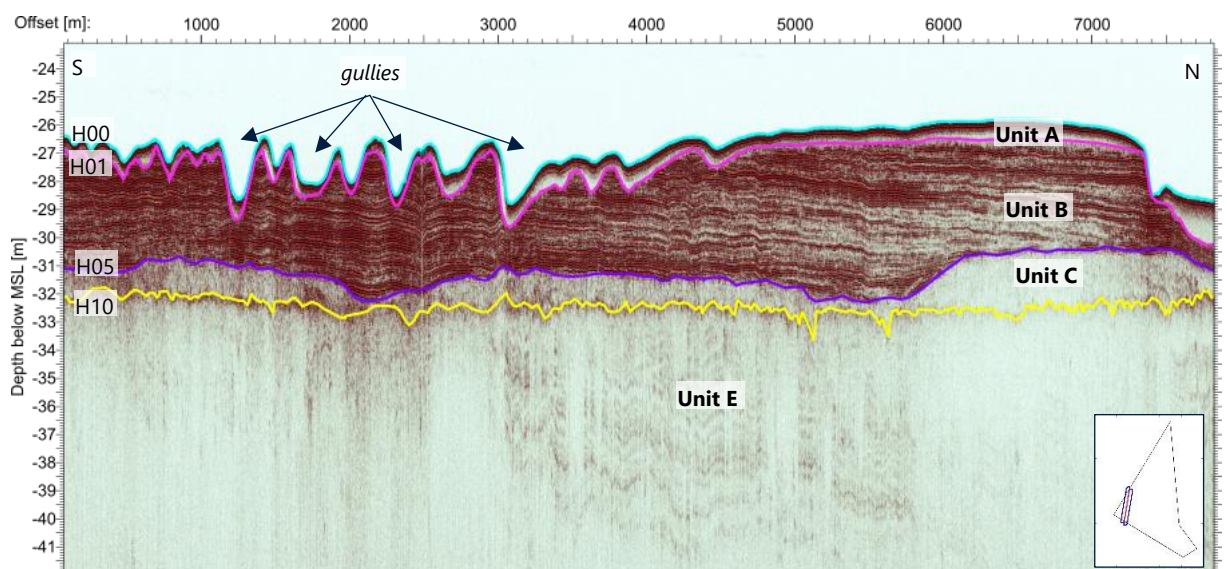
Figure 4.42: Line HAX2505P01. SBP data example of Unit B, Unit C and erosional gullies.

4.3.2.2   Unit B

Unit B is present in the central and western part of the site (Figure 4.43). In general, the unit is thin, on average approximately 1 m. It reaches locally greater thickness of approximately 6 m in the shallower south-western part of the site (Figure 4.44) and a maximum thickness of approximately 14 m in the large pre-Quaternary depression in the north-eastern part of the site (Figure 4.43: ; Figure 4.45).Figure 4.45: Line HAM1325R01. SBP data example of the Holocene infill of the pre-Quaternary depression in the north of the site.

Internally the unit is stratified, comprising of low to high-amplitude, parallel reflectors. Where Unit B is thickest in the south-western part of the site, the stratification has an eastward directed inclined orientation and high amplitudes (Figure 4.42; Figure 4.44). In the east where Unit B is thin, the stratification is sub-horizontal and is associated with low amplitudes (Figure 4.41). Locally, where Unit B overlies Unit C and becomes thinner, the low-amplitude stratification transitions into a more chaotic seismic character (Figure 4.46).

Within the large pre-Quaternary depression, the stratification in Unit B has a dominant westward orientation and shows abundant high-amplitude reflectors of variable lateral extent (Figure 4.45). They are interpreted as possible pockets of peat/organic clay. Acoustic blanking is observed in Unit B in the deepest parts of the large pre-Quaternary depression.

The character of the base of Unit B is either undulating (Horizon H05) or irregular (Horizon H10). Horizon H01 forms the top of this unit and marks a change in seismic character between acoustically transparent (Unit A) above and a stratified character (Unit B) below. At the south-western part of the site, with shallower water depth, the internal stratification of Unit B shows an angular unconformity with the overlying Unit A and at the large Quaternary depression an internal angular unconformity can be observed (Figure 4.44; Figure 4.45).

Table 4.6 provides expected soil type for Unit B.

Unit B is interpreted to be deposited in a deltaic environment, at the mouth of the Dana River System (Great Belt palaeo-river) through which the Ancylus Lake drained into the Kattegat (Figure 4.3; Bendixen et al., 2015, 2017).

Figure 4.43: Thickness in metres of Unit B.
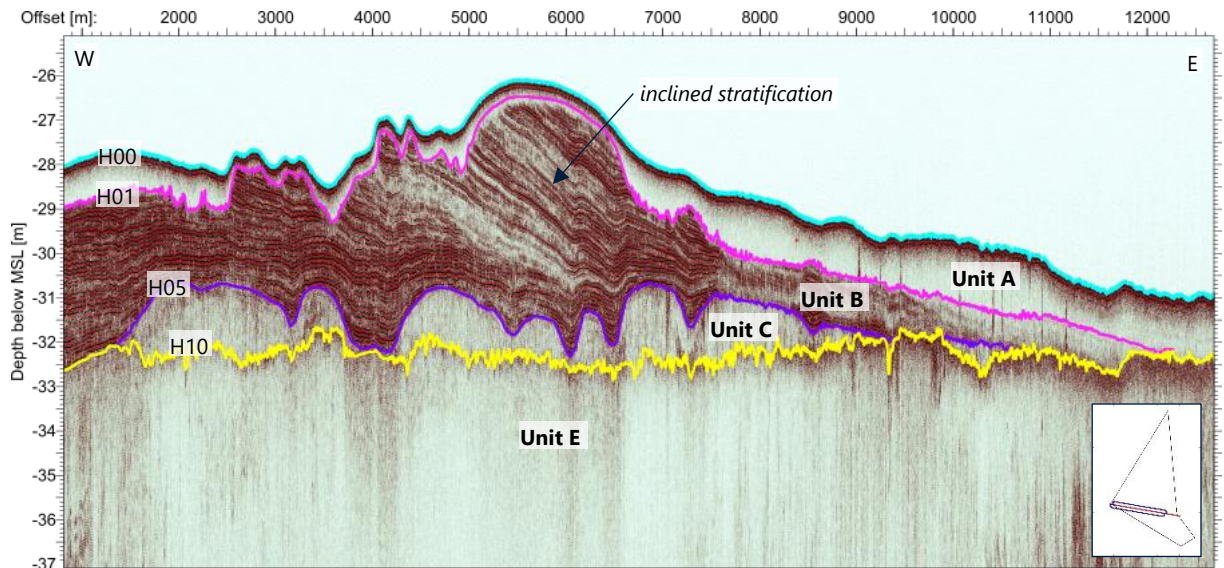
Figure 4.44: Line HAF6110P01. SBP data example showing the internal seismic character of Unit B and Unit C.
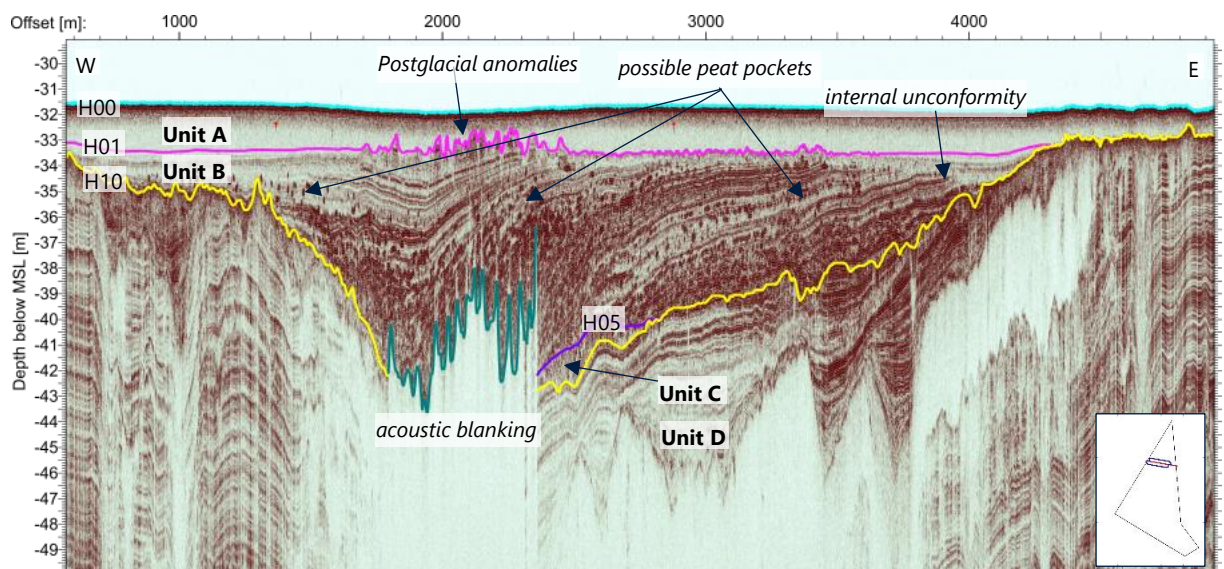
Figure 4.45: Line HAM1325R01. SBP data example of the Holocene infill of the pre-Quaternary depression in the north of the site.
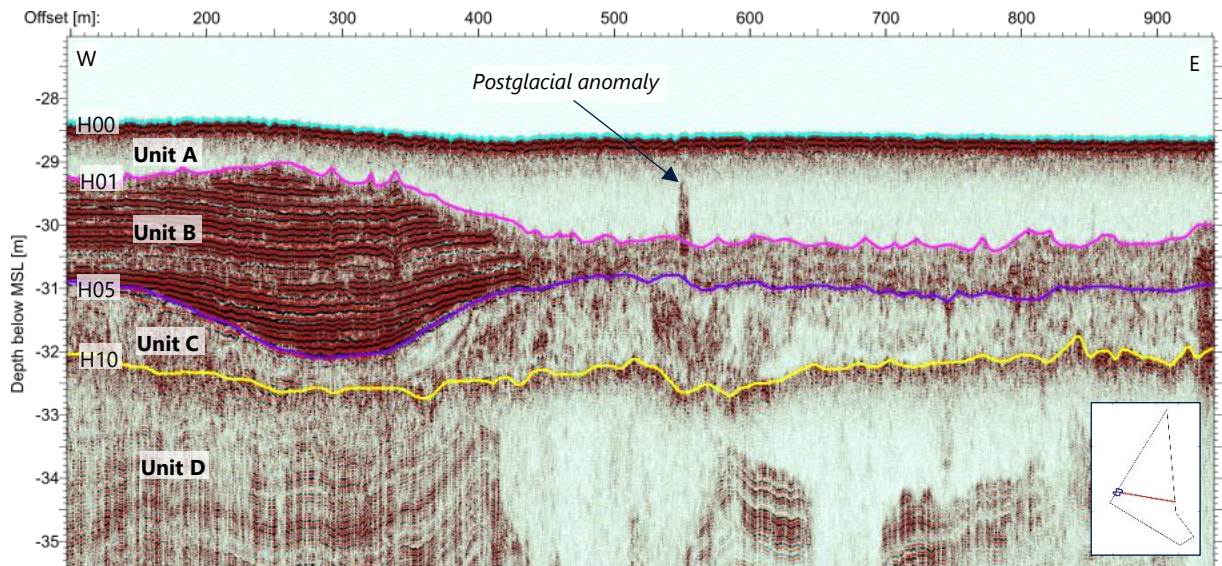
Figure 4.46: Line HAH1156P01. SBP data example of Unit B and Unit C showing a variable internal seismic character from chaotic to internal stratification.

4.3.2.3 Unit C

Unit C is present in the south-western part of the site, where it forms hummocks/ridges with approximately a north–south orientation (Figure 4.47). The unit is also present in the pre-Quaternary depression in the north of the site.

Internally this unit is variable. Its seismic character is often acoustically (semi-)transparent to chaotic (Figure 4.44). However, where Unit C increases in thicknesses it can also show stratification, with low-amplitude parallel reflectors (Figure 4.46) oriented in various directions. The base of Unit C (Horizon H10) has an irregular and erosional character.

Table 4.6 provides expected soil type for Unit C.

Unit C is interpreted to be deposited as coast-parallel spits or barrier islands during the marine transgression in the early Holocene.
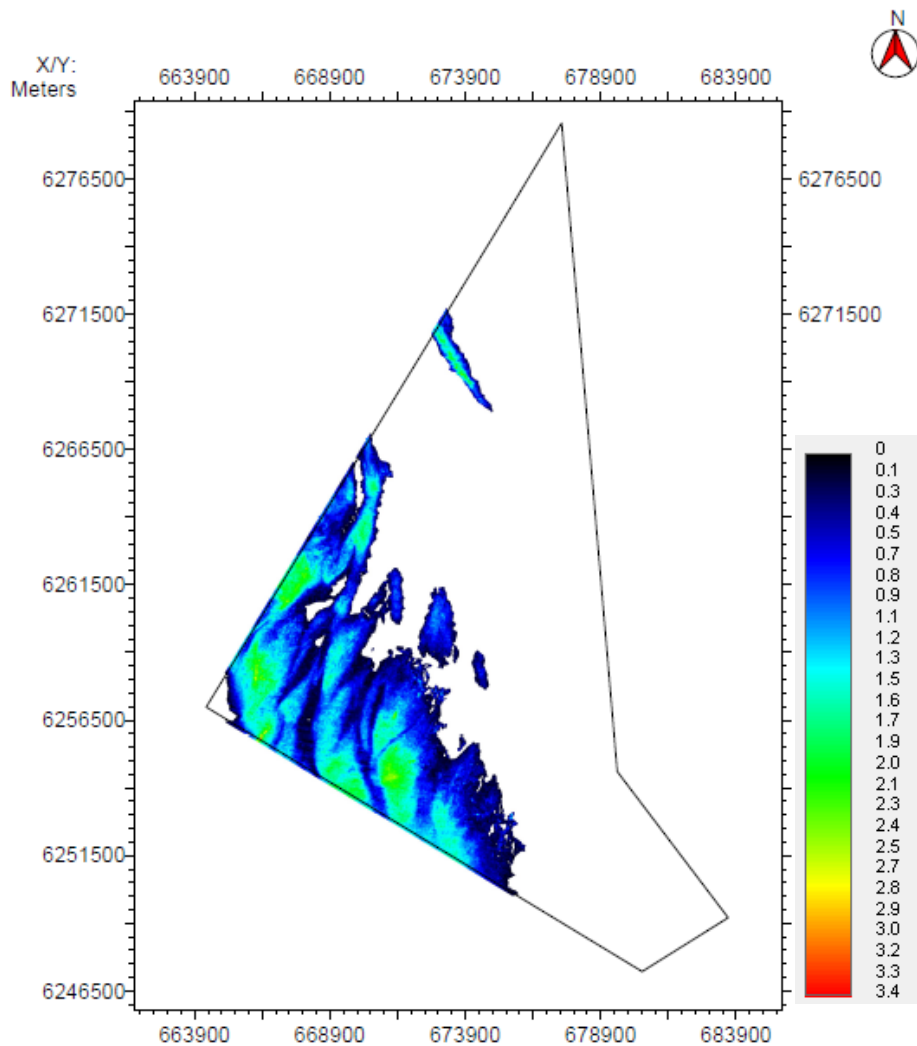
Figure 4.47: Thickness in metres of Unit C.

4.3.2.4 Unit D

Unit D (Figure 4.49) is absent in the south and south-western part of the site. The unit has a typical thickness of approximately 20 m to 30 m and reaches a maximum thickness of approximately 66 m in the large pre-Quaternary depression (Figure 4.48). It thins to less than 10 m in the south, where the underlying Unit E substantially increases in thickness.

The internal seismic character of Unit D is quite variable (Figure 4.49; Figure 4.50; Figure 4.51; Figure 4.52) and varies between low to high-amplitude parallel reflectors, chaotic and transparent. These changes in seismic character in Unit D are marked by several internal horizons (H11, H12 and H15).

The dominant seismic character of Unit D is low to high-amplitude parallel reflectors. These reflectors become increasingly distorted towards the southern part of the site. In the SBP data, the top of Unit D is characterised by parallel reflectors that show abundant acoustic blanking with very short lateral extent (metre scale).

Internal Horizon H11 is a negative reflector (Figure 4.52) marking the base ofchannels in the upper part of Unit D. The infill of these channels in the 2D-UUHR data is characterised by

high-amplitude parallel reflectors, which contrasts with the general seismic character of Unit D showing typically low to medium-amplitude reflectors. Internal channels at Horizon H11 are described in more detail in Section 4.3.3.5.

Internal Horizon H12 is a negative reflector (Figure 4.51) and denotes the base of channel-like features, whose infill has a transparent seismic character. These features can be observed in both the SBP and 2D-UUHR data. Occasionally, within these channel-like features some vague parallel reflectors can be observed in the 2D-UUHR data and patches of stratified reflectors in the SBP data. Evidence for mass transport deposits (MTDs) was observed in the upper part of Unit D, which are demarcated at the base by Horizon H12 (see Section 4.3.3.8).

Internal Horizon H15 is a flat to undulating high-amplitude positive reflector (Figure 4.49; Figure 4.50). Horizon H15 discriminates between the low to medium-amplitude parallel reflectors above and a more variable (chaotic, transparent, or parallel reflectors) seismic character below.

Internal Horizons H11 and H12 are present locally and are laterally limited. They denote bases of internal channels and MTDs, which are considered as geological features. They were mapped, and the boundaries are presented on the 'Geological Features Charts' . Horizon H15 is a laterally continuous surface, present across most of the site, except the southern part. Elevation and depth below seafloor maps are provided for the internal Horizon H15. Refer to Appendix B for all geological charts.

High-amplitude positive anomalies are common within Unit D. These are considered to be associated with coarse deposits (see Section 4.3.3.4).

Based on historic geotechnical data (GEUS, 2020), Unit D consists of CLAY with occasional laminae of SILT and/or SAND and can be locally sandy. The channel-fills related to Horizon H11 consist of medium coarse SAND interbedded with silty CLAY (GEUS, 2020).

Based on its seismic character, stratigraphic position and geotechnical properties, Unit D is interpreted as predominantly Late Glacial clays deposited in a glaciomarine and glaciolacustrine environment. Channel infills demarcated at the base by Horizon H11 are interpreted to be deposited in a fluvial environment and the channelling features demarcated by Horizon H12 are interpreted as mass-transport deposits within the Late Glacial deposits (see Section 4.3.3.8).
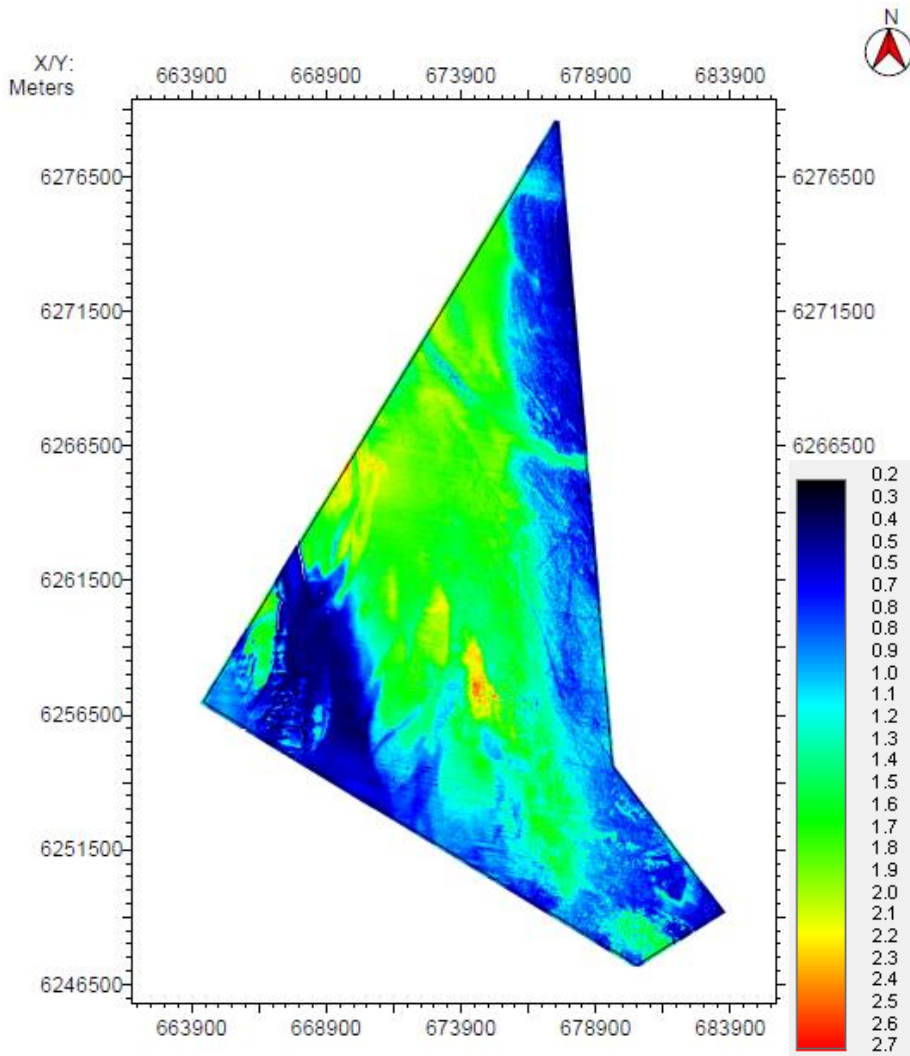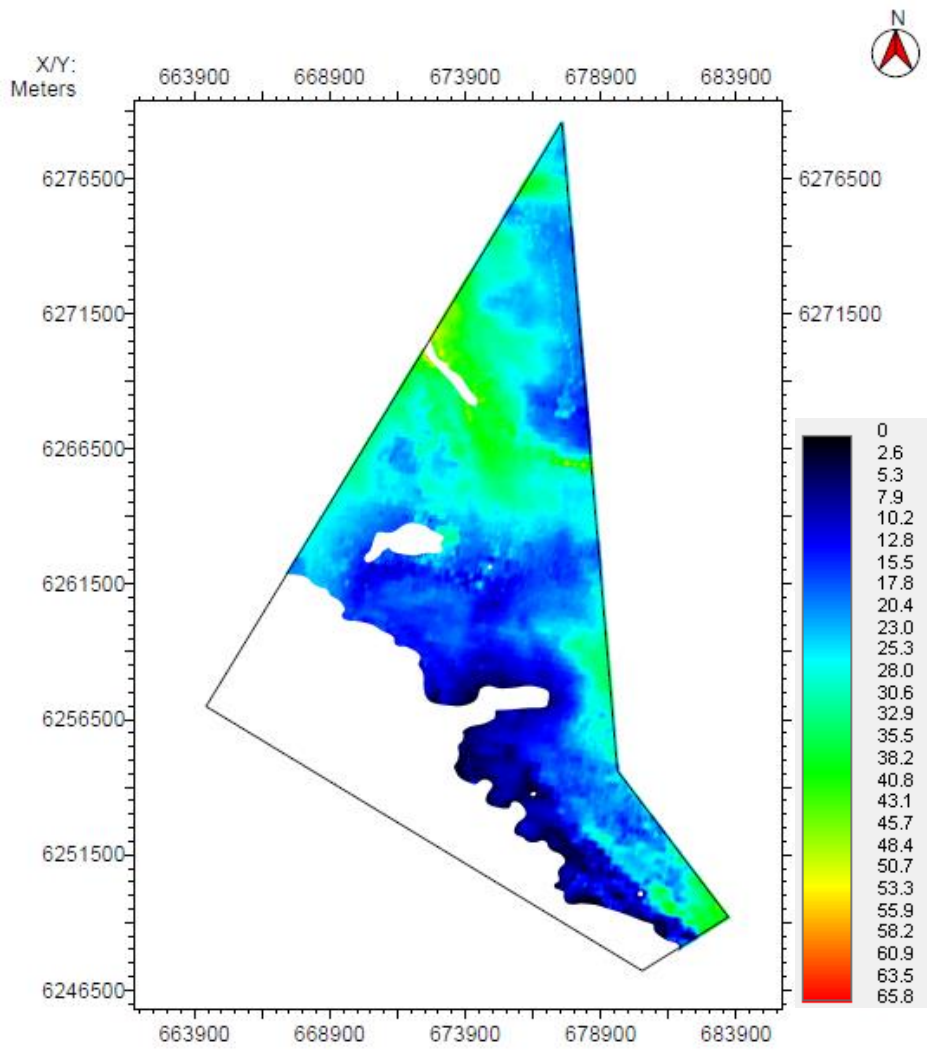
Figure 4.48: Thickness in metres of Unit D.
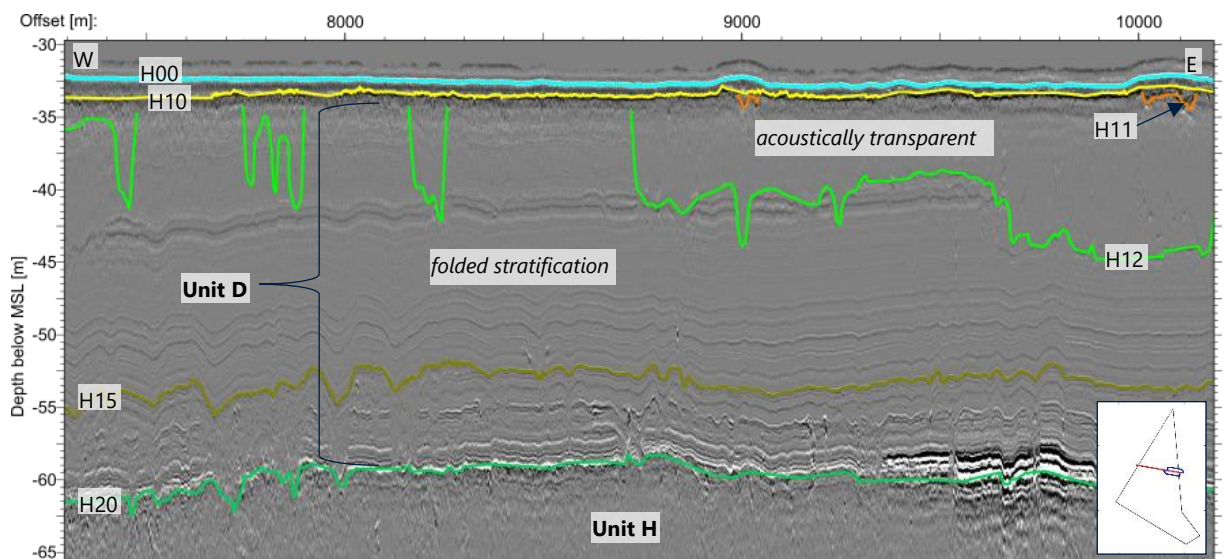
Figure 4.49: Line HAK2258R01. 2D-UUHR data example of the internal seismic character of Unit D.
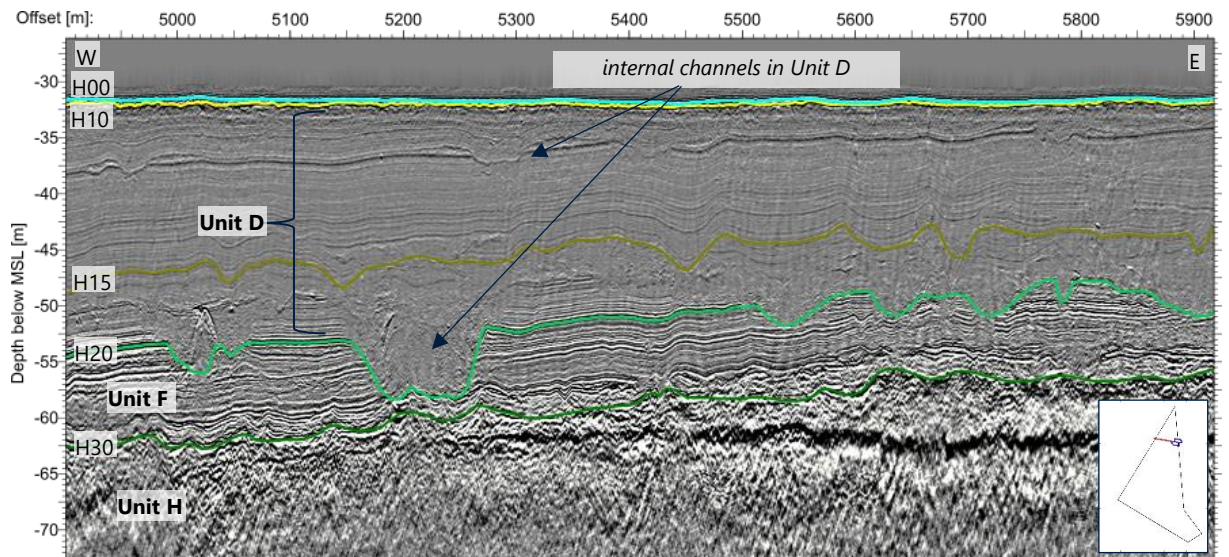
Figure 4.50: Line HAN2358P01. 2D-UUHR data example of the internal seismic character of Unit D with the internal Horizon H15.
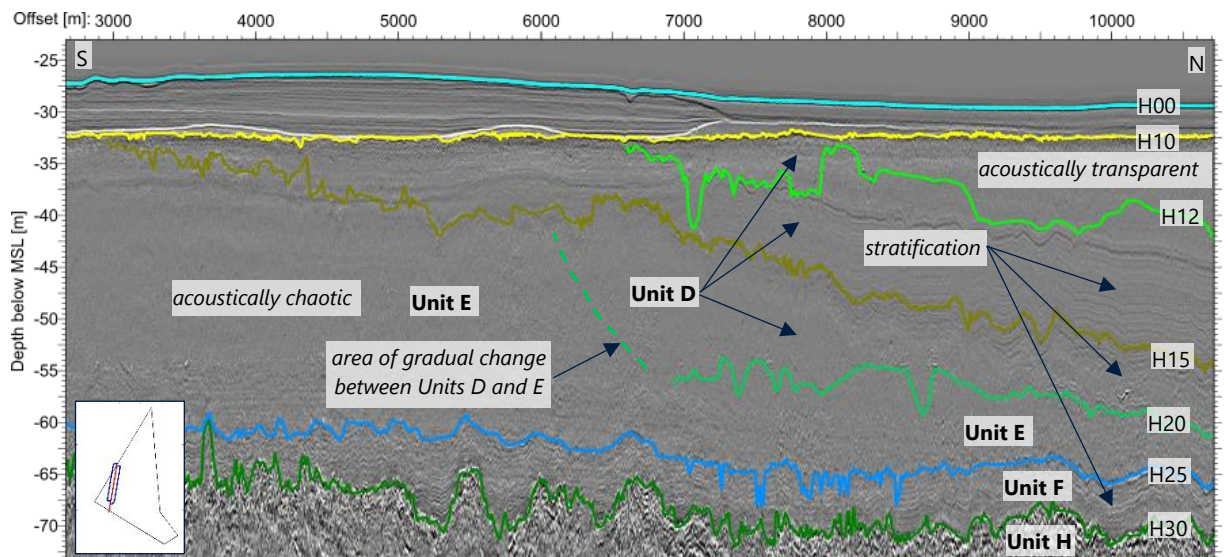
Figure 4.51: Line HAX2504P01. 2D-UUHR data example of the lateral variability of the seismic character of Unit D and Unit E.
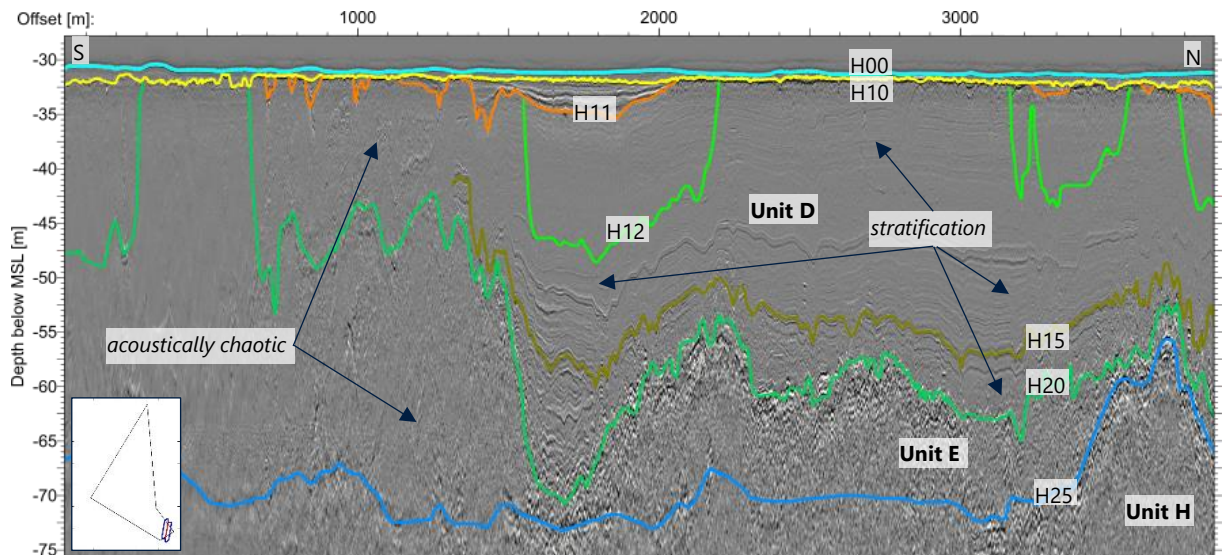
Figure 4.52: Line HAX2489P01. 2D-UUHR data example of the lateral variability of the seismic character of Unit D and Unit E.

4.3.2.5 Unit E

Unit E is present across a large part of the HOWF site, but is absent in the north and locally in the west of the site (Figure 4.53). The unit shows a typical thickness of 10 m to 20 m, and reaches a maximum thicknesses of approximately 62 m within the pre-Quaternary depression and approximately 40 m in the south. The unit is thinnest (< 10 m) in the western and eastern edge of the site.

The internal seismic character of Unit E is semi-transparent to chaotic (Figure 4.54). Locally, laterally limited steep internal reflectors can be present.

In the south-western part of the site, the top of the unit (Horizon H20) is fading out and it becomes difficult to properly differentiate this unit from the overlying unit.

Table 4.6 provides expected soil type for Unit E.

Unit E is interpreted as a unit of glaciotectonised deposits. In the south-west, where Unit E increases in thickness and is present directly below the Holocene (Horizon H10), the top of this unit likely represents glaciotectonised glaciomarine and glaciolacustrine deposits of Unit D. Where the base of Unit E (Horizon H25) cuts into the underlying Unit F, Unit E likely comprises glaciotectonised glaciomarine deposits of Unit F.
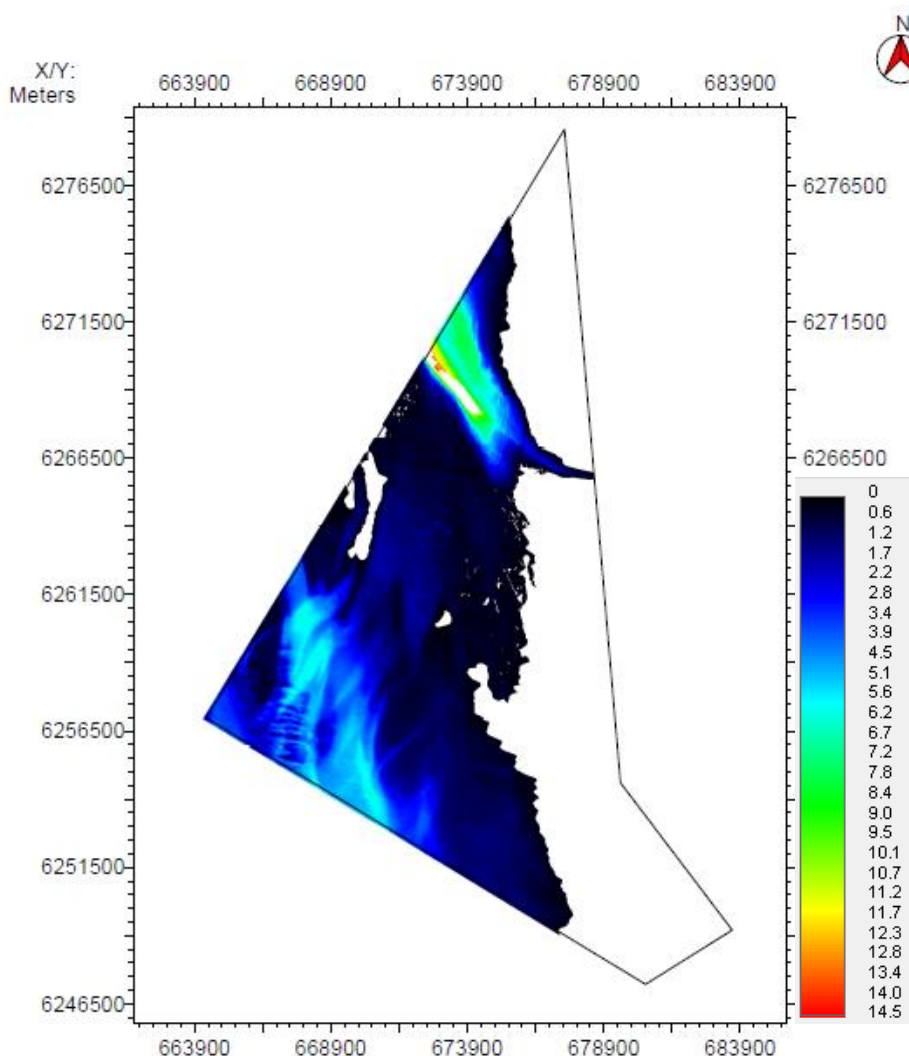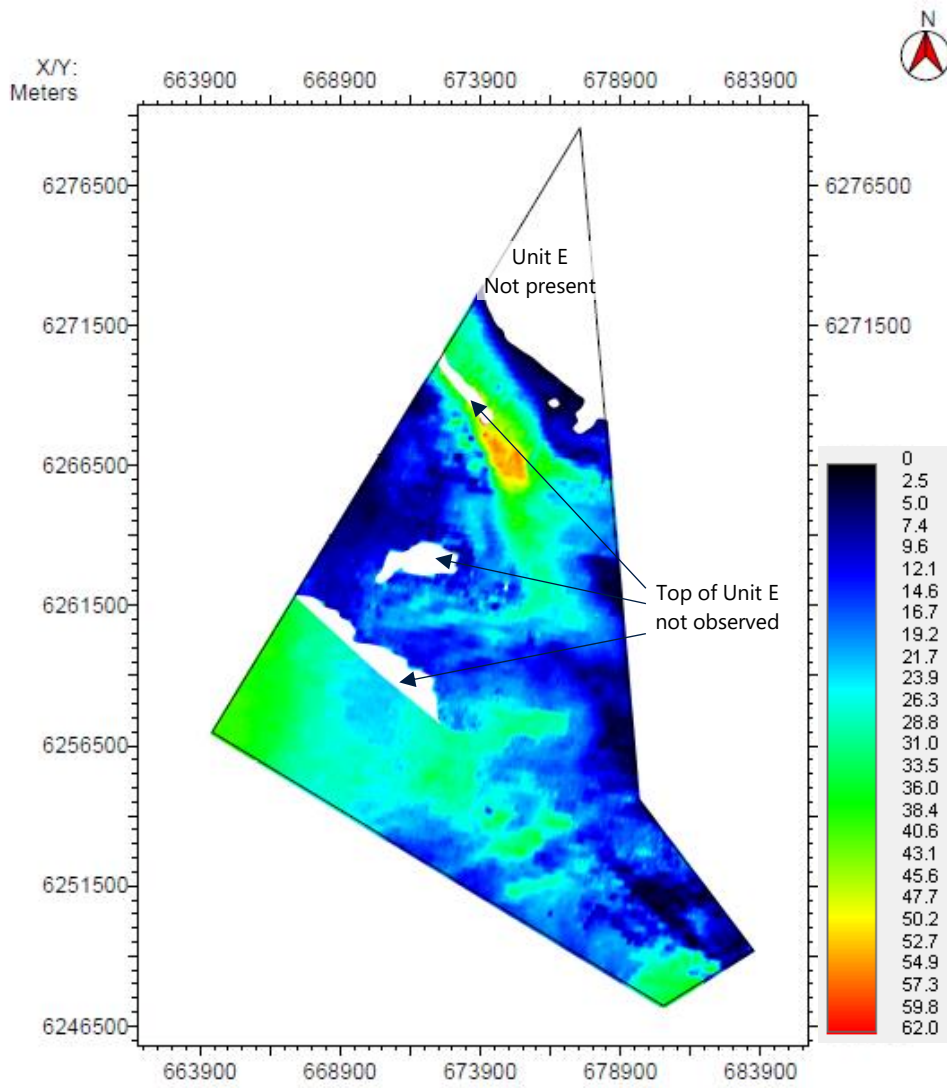
Figure 4.53: Thickness in metres of Unit E.
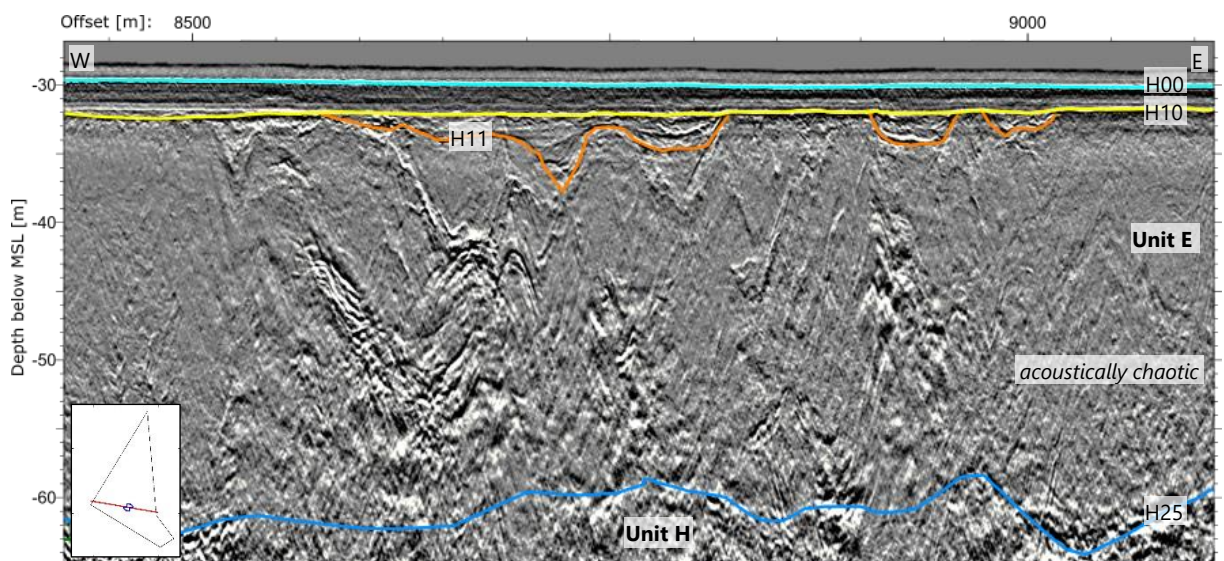
Figure 4.54: Line HAG2126P01. 2D-UUHR data example showing the internal seismic character of Unit E.

4.3.2.6   Unit F

Unit F (Figure 4.56) is present locally, in the north and in the western part of the site. The unit is typically less than 10 m thick, but locally reaches thicknesses up to 39 m in the eastern EW-oriented channel feature directed towards the large pre-Quaternary depression.

The internal seismic character of Unit F shows closely spaced medium to high amplitude parallel reflectors (Figure 4.56). This character is similar to the dominant seismic character of Unit D, but the distinction between Unit D and Unit F is made due to the presence of Unit E stratigraphically in between Unit D and Unit F. Unit F is overlain by Unit E (Horizon H25) in the centre and southern part of the site and by Unit D (Horizon H20) in the north.

Table 4.6 provides expected soil type for Unit F.

Unit F is interpreted as glaciomarine deposits due to its bedded seismic character and similarity to the bedded facies of the overlying Unit D.
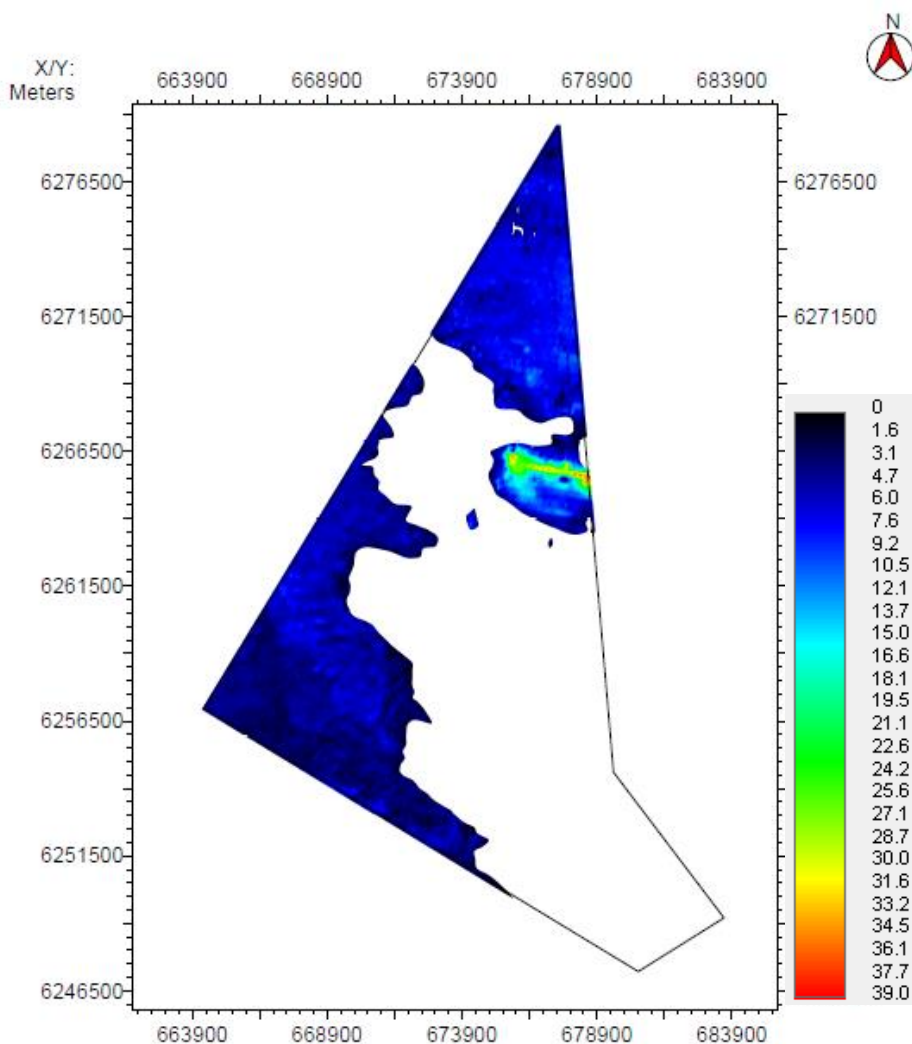
Figure 4.55: Thickness in metres of Unit F.
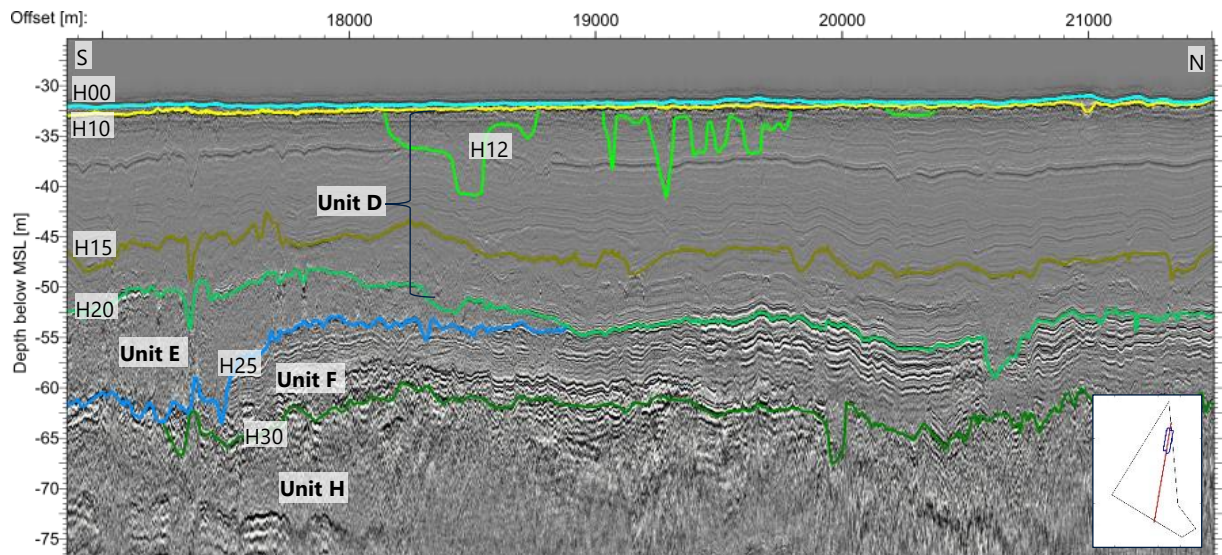
Figure 4.56: Line HAX2497P01. 2D-UUHR data example of Unit F underlying Unit D and Unit E.

4.3.2.7   Unit G

Unit G is mainly present in the area of the large pre-Quaternary depression and locally in other parts in the site (Figure 4.57). The unit reaches a maximum thickness of approximately 94 m in the deepest parts of the depression. In the shallower parts of the depression and in the other parts of the site, it shows a typical thickness of approximately 10 m. Locally within the large depression, Unit G is not observed due to acoustic blanking in the units above (See Section 4.3.3.2), but is likely still present (Figure 4.57)

The base of Unit G (Horizon H35) is an erosional surface cutting deeply into the underlying Unit H and Unit I (Figure 4.58). The internal seismic character of Unit G varies from acoustically semi-transparent with occasional inclined discontinuous internal reflectors where Unit G is thick to more chaotic where Unit G is thin.

Table 4.6 provides expected soil type for Unit G.

Unit G is interpreted to comprise a diamicton which fills the base of a valley. A similar valley was penetrated by an IODP borehole (Andrén, 2015a and 2015b), where similar fills were interpreted as debris flows deposits. Alternative interpretation is possible (e.g. glacial TILL).
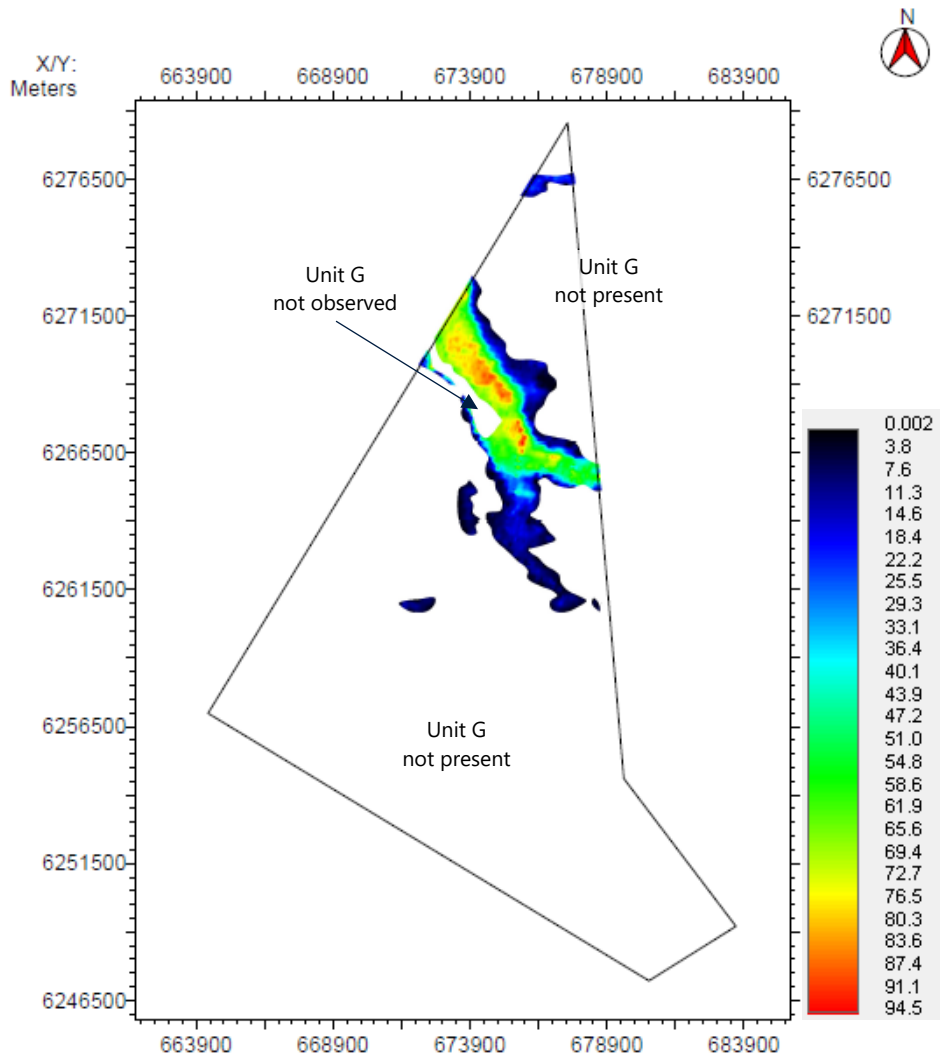
Figure 4.57: Thickness in metres of Unit G.
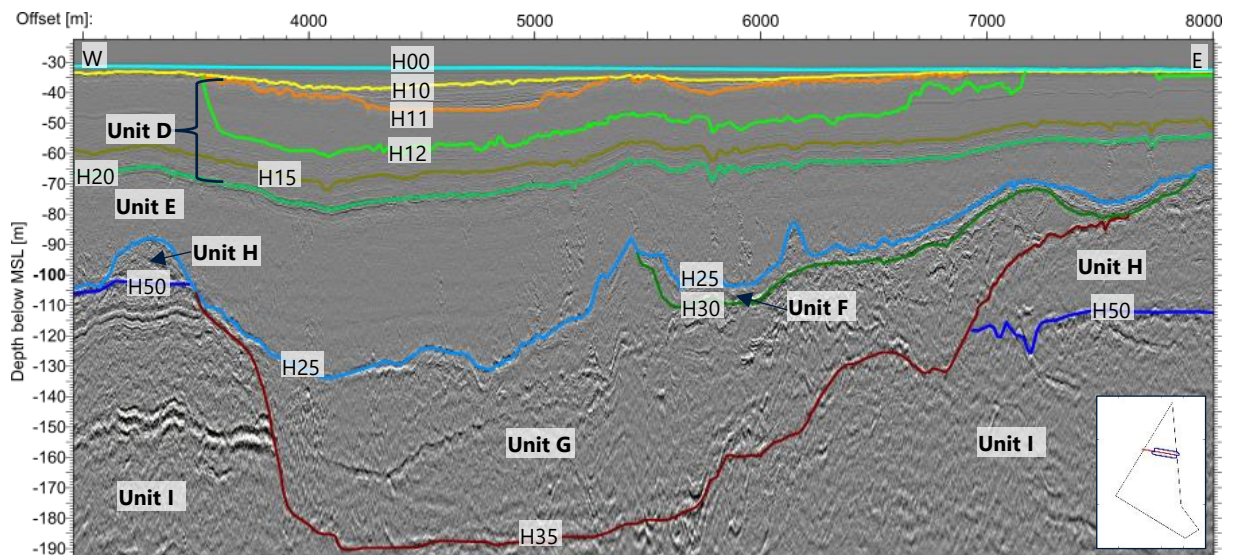
Figure 4.58: Line HAM2298P01. 2D-UUHR data example of Unit G with a variable internal seismic character.

4.3.2.8 Unit H

Unit H is present in the majority of the site, except the large pre-Quaternary depression. The unit shows typical thicknesses of 25 m to 35 m south of the depression and reaches a thickness beyond 80 m north of the depression (Figure 4.59).

The internal seismic character of Unit H (Figure 4.60; Figure 4.61) is very variable from medium-amplitude parallel reflectors (Figure 4.61), dominantly observed south of the large pre-Quaternary depression to acoustically transparent (Figure 4.60) and chaotic with short internal reflectors, observed north of the depression.

Horizon H50 is a low to medium positive amplitude reflector and marks an angular unconformity, where the underlying bedrock (Unit I) is clearly folded. This is most prominently visible south of the depression. North of the depression, Horizon H50 is often obscured by the first seafloor multiple. As a result, the depth at which Horizon H50 occurs is subject to uncertainty.

Table 4.6 provides expected soil type for Unit H.

Unit H is interpreted as early Pleistocene sediments deposited in glacial, periglacial and/or glaciomarine conditions.
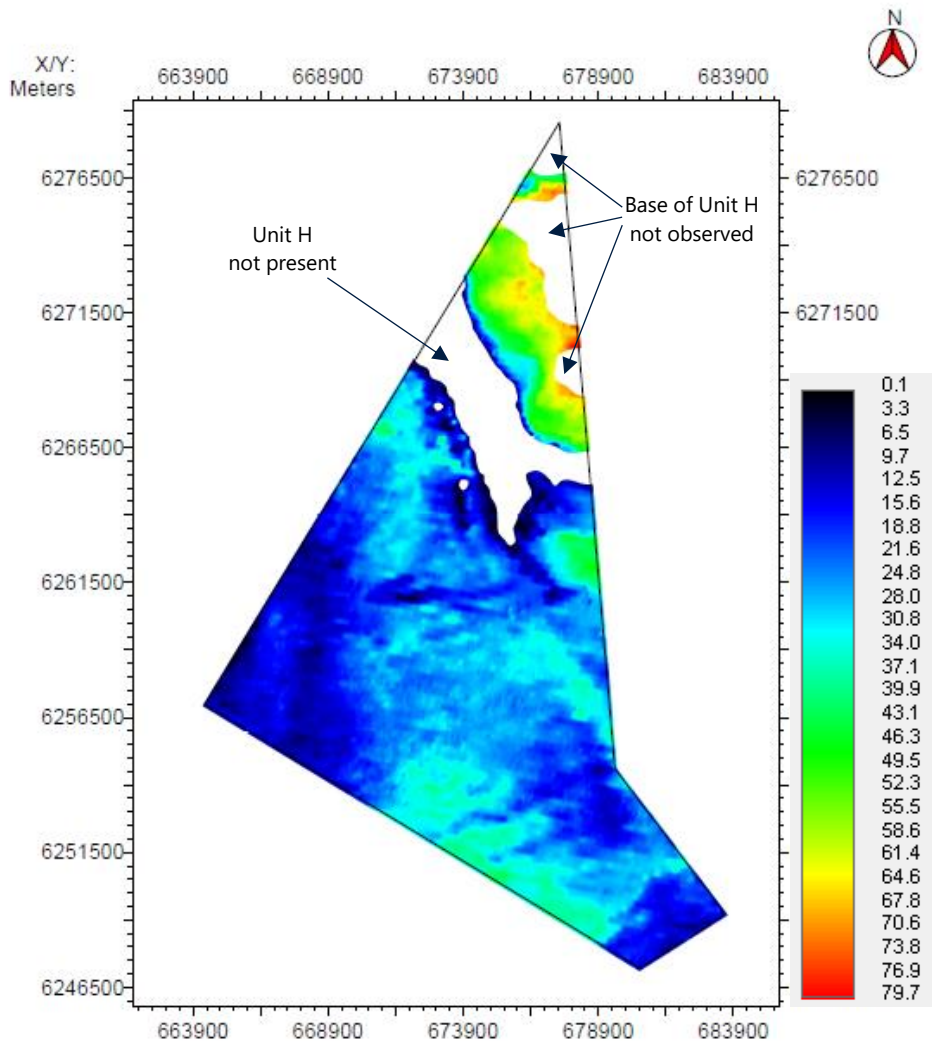
Figure 4.59: Thickness in metres of Unit H.
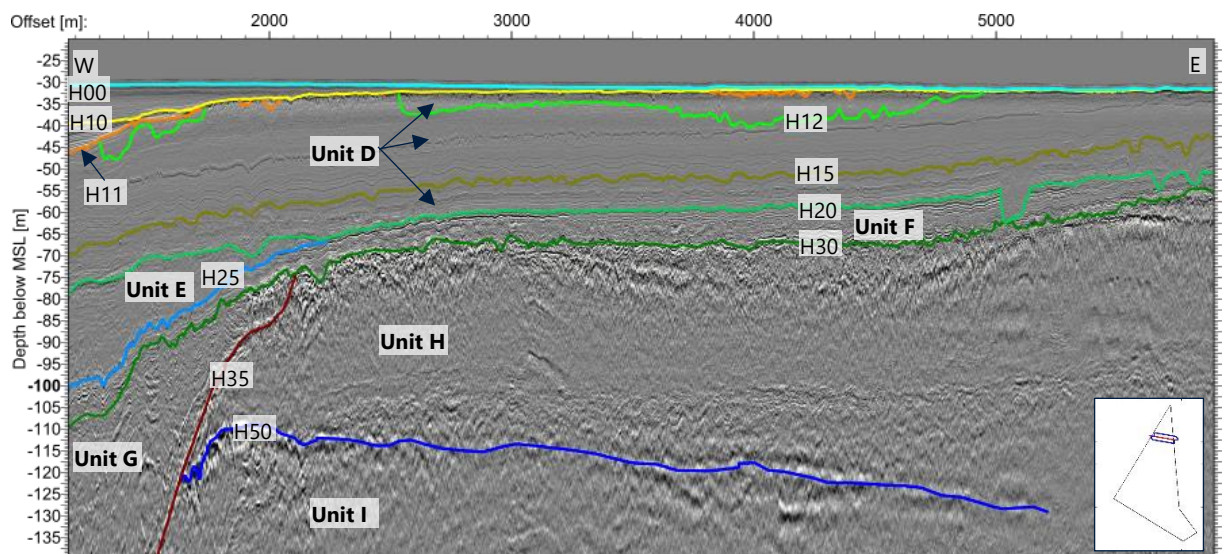
Figure 4.60: Line HAN6362P01. 2D-UUHR data example of Unit H.
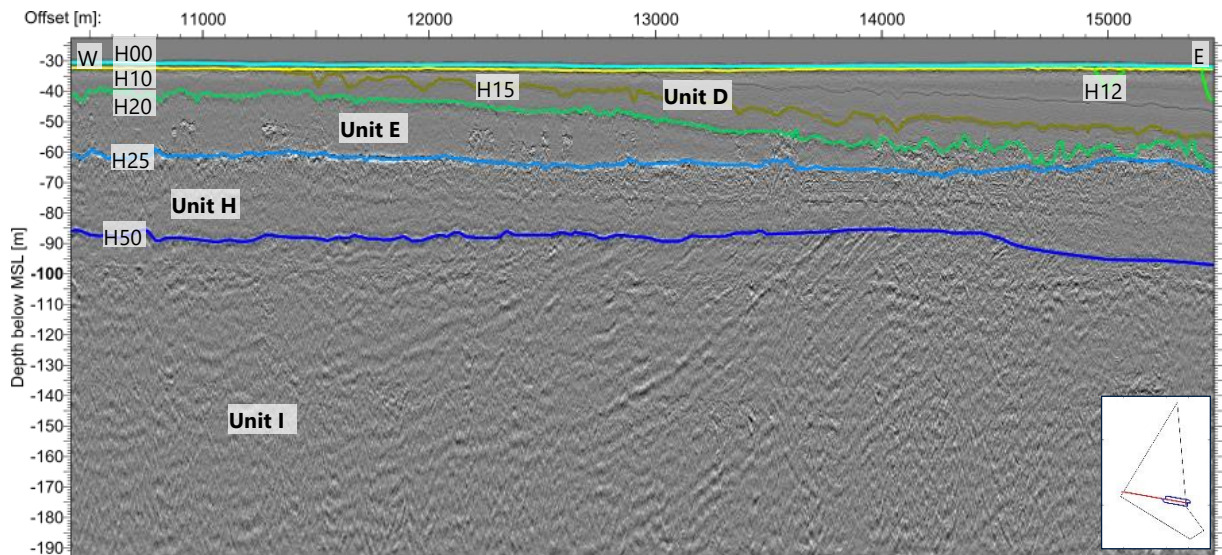
Figure 4.61: Line HAG2130R01. 2D-UUHR data example of Unit H and Unit I.

4.3.2.9   Unit I

Unit I is expected to be present over the entire site. Within the large pre-Quaternary depression and locally north of this depression the top of Unit I was not observed as it lies below the penetration depth of the 2D-UUHR data (Figure 4.62). Unit I is interpreted as pre-Quaternary bedrock.

The internal seismic character shows predominantly low to medium-amplitude, large wavelength parallel reflectors (Figure 4.63). Particularly north of the large depression, the seismic character of Unit I can be acoustically (semi-)transparent (Figure 4.61). Where Unit I shows parallel inclined (possibly folded) reflectors, the horizon marking the top of Unit I (Horizon H50) represents an angular unconformity with the overlying units. Due to the tectonic history of the general area, the presence of faults may be expected in Unit I. No faults were identified within Unit I in the 2D-UUHR data (see Section 4.3.3.6).

The bedrock consists of Jurassic sandy mudstone to Lower Cretaceous limestone and glauconitic sandstone, deposited in a marine environment (GEUS, 2020; Figure 4.2).
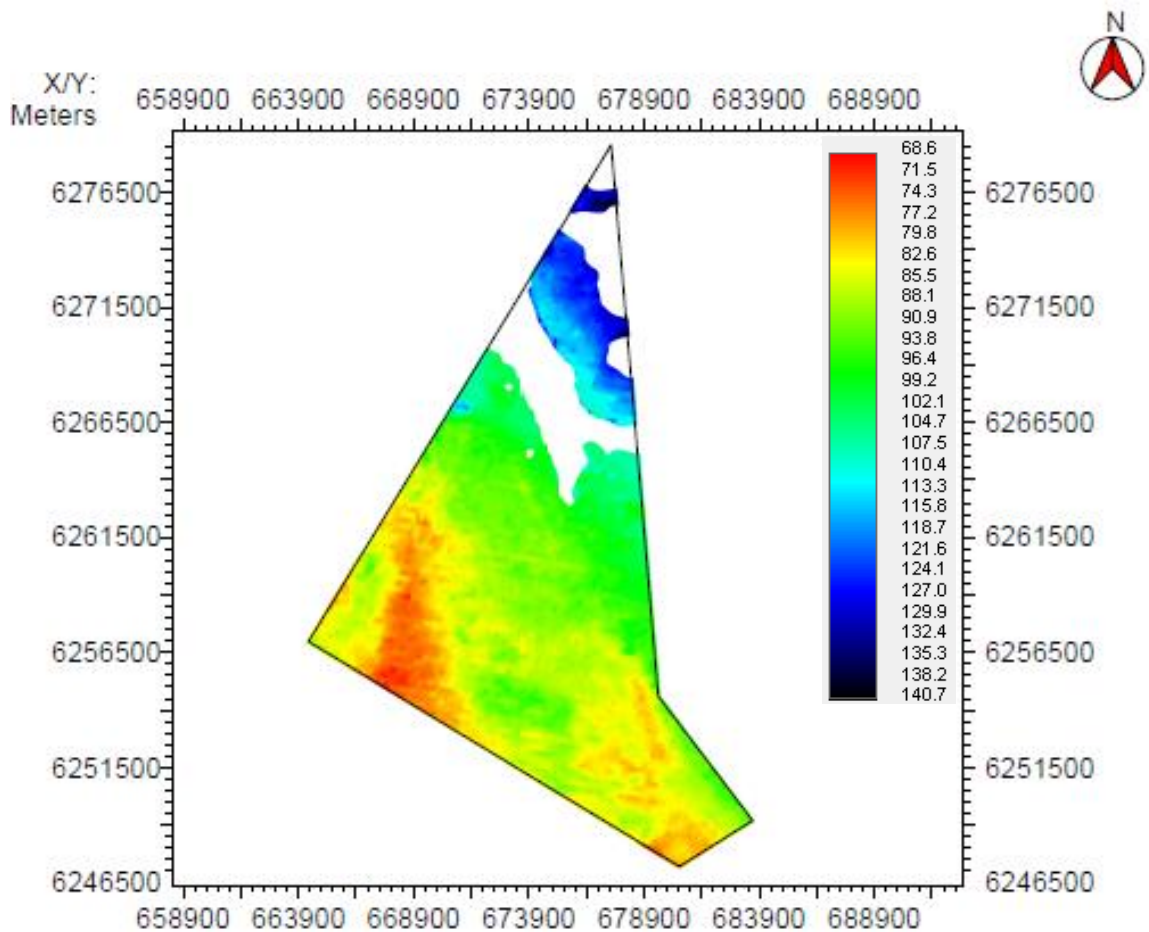
Figure 4.62: Depth to Horizon H50 (top bedrock) in metres BSF.
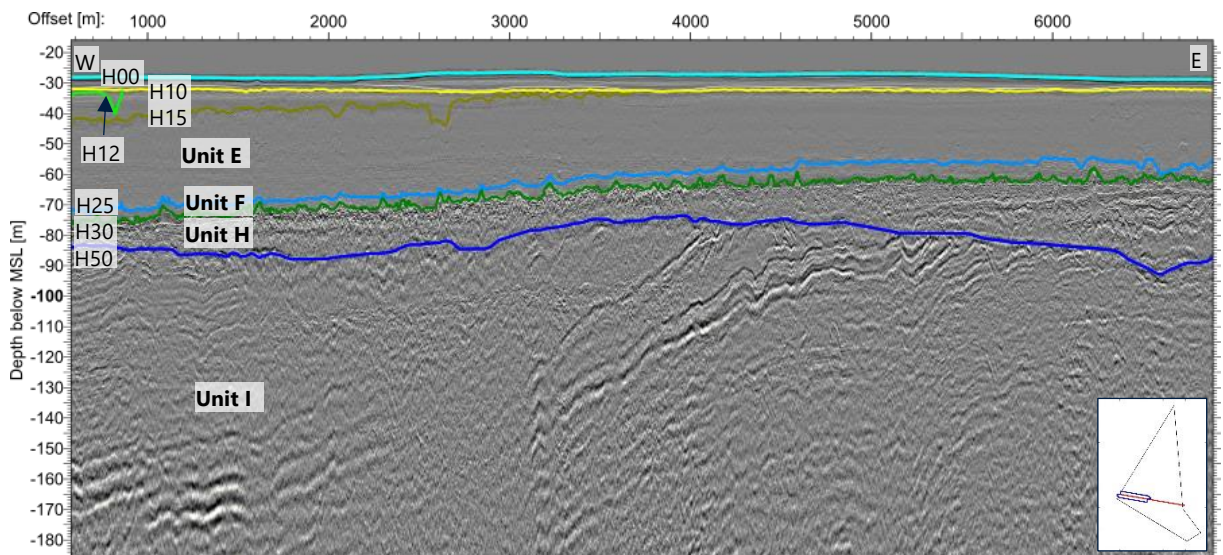
Figure 4.63: Line HAG2130R01. 2D-UUHR data example of Unit H and Unit I.

4.3.3 Geological Features

Section 4.3.3 should be read in conjunction with the geological features charts provided in Appendix B.

4.3.3.1　Local Enhanced Amplitude Anomalies

The local enhanced amplitude anomalies were observed in the SBP, 2D-UUHR and 3D-UHR seismic datasets. Details of the 3D-UHR data and interpretation is provided in report F172145-REP-UHR-001.

They appear as laterally limited amplitude enhancements, which extent vertically through the seismic records (Figure 4.64; Figure 4.65; Figure 4.66). Based on their stratigraphic position, the anomalies were differentiated in two types: Late Glacial anomalies (present below Unit C) and Postglacial anomalies (present within Units A, B, and locally continue in deeper units).

Late Glacial Anomalies

Late Glacial anomalies were only identified in the SBP data. They occur sporadically below Horizon H10, mainly in the northern and eastern part of the site. They appear as vertically stacked enhanced amplitude point reflections and/or diffraction hyperbolas (Figure 4.64) and occasional signal distortion. The exact origin of these features is unknown, but they may be related to local carbonate cementation or accumulation of shells and/or gravel.
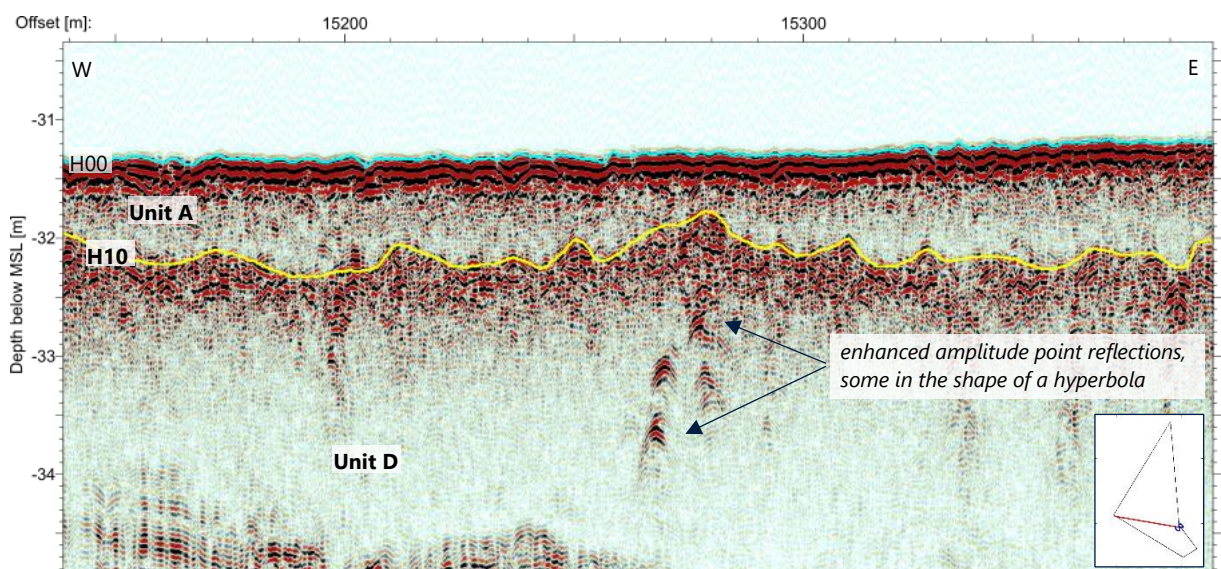
Figure 4.64: Line HAF1108P01. SBP data example showing Late Glacial anomalies in Unit D.

Postglacial Anomalies

Postglacial anomalies occur as enhanced amplitude parallel reflectors, with a varying spatial extent. Occasionally acoustic blanking and/or signal distortion is observed below these anomalies. The top of the anomalies is generally observed in Unit A and Unit B (Figure 4.65). Locally, these anomalies appear to extend below into Late Glacial units, e.g. Unit D (Figure 4.66). These anomalies are typically topped by a high-amplitude negative reflector in the 2D-UUHR data.

The anomalies are most abundant in the central part of the HOWF site, in the area of the pre-Quaternary depression and locally in the western limits of the site. The lateral extent of these anomalies along seismic lines ranges from a few metres to over 300 m. They may occur more

frequently than interpreted in the SBP and 2D-UUHR data as detection is limited by the line spacing.

Where the anomalies are close to the seafloor (Figure 4.65), they can sometimes be correlated with shallow seafloor depressions of 0.1 m to 0.2 m deep (see Section 4.2.2.1).
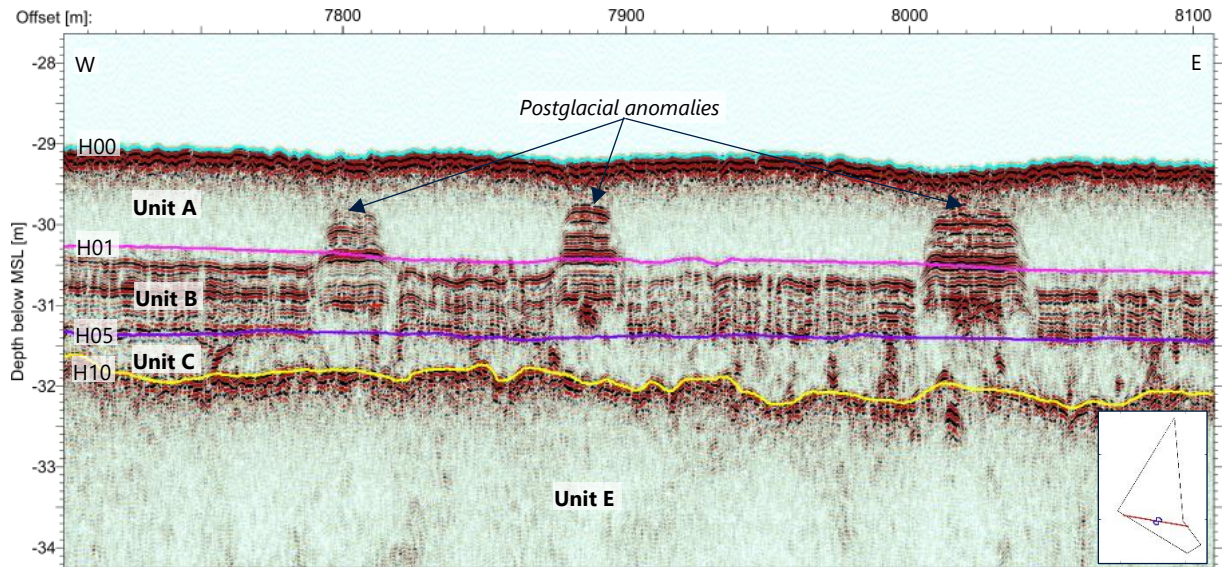
Figure 4.65: Line HAF1100P01. SBP data example of Postglacial anomalies in Unit A and Unit B.
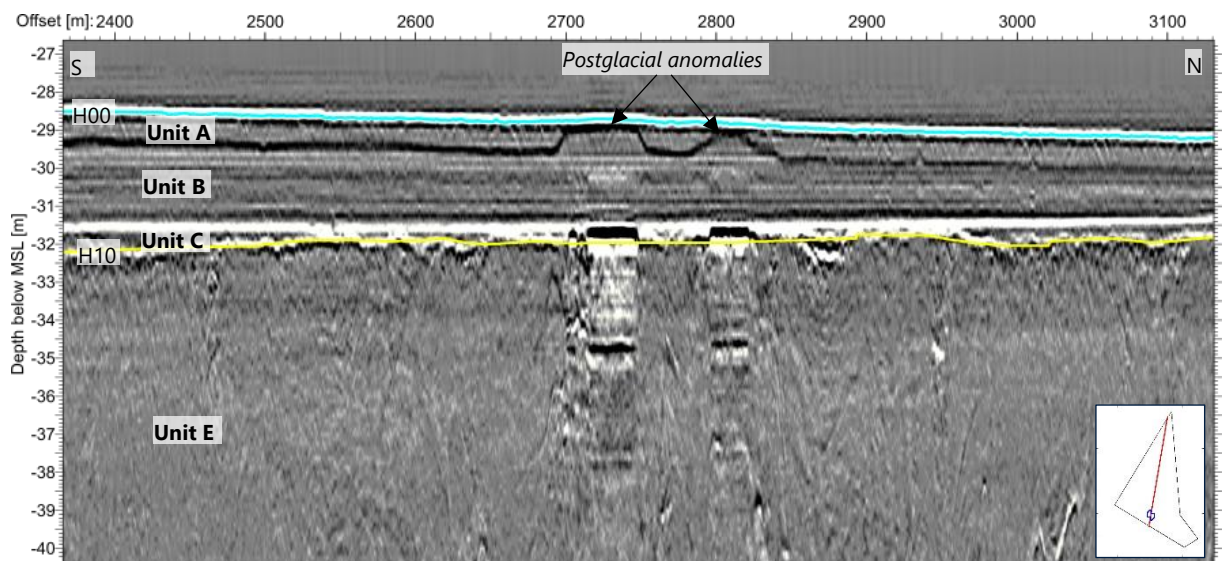
Figure 4.66: Line HAX2499P01. 2D-UUHR data example showing enhanced amplitude anomalies in Postglacial and Late Glacial sediments.

Correlation with Geotechnical Data and Interpretation

It is not likely that the seismic anomalies represent acquisition artefacts. These features are considered to have a geological origin. The exact origin of these features cannot be determined with confidence. Several explanations for these features are described below.
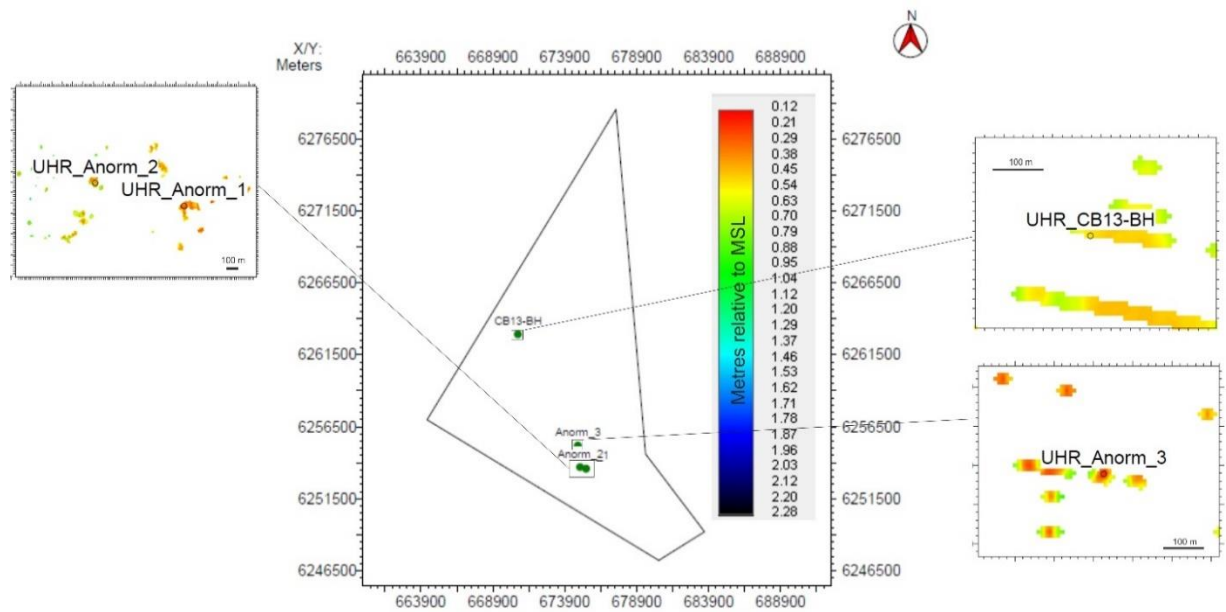
Figure 4.67: Overview map with the position of the four enhanced amplitude anomalies that were sampled.

Four (4) Postglacial anomalies were sampled for ground truthing (Gardline, 2021). Three geotechnical borehole locations are located in the south and one is located in the central-western part of the HOWF site (Figure 4.67). Representative data examples showing the geotechnical borehole locations projected on the SBP, 2D-UUHR and 3D-UHR seismic sections are presented in Figures 3.66 to 3.73.

The top of the anomalies, as observed in the seismic data, occurs in Unit A. Geotechnical boreholes penetrating these anomalies indicate that their tops occur within very low strength CLAY (Unit A). which is underlain by a bed of SAND varying in thickness between 0.1 m and 1.2 m. This sand bed is associated with Unit B or Unit C and its base is associated with Horizon H10 (Figure 4.68; Figure 4.69; Figure 4.70; Figure 4.72; Figure 4.74).

This SAND bed is slightly to highly calcareous and includes (frequent) shell fragments. It is locally silty, gravelly and may contain cobbles (described as 'cobbly' (Gardline, 2021)). At the Anorm_1, Anorm_2 and Anorm_3 geotechnical borehole locations, the top of the SAND bed corresponds to a local positive reflector in the 2D-UUHR data and 3D-UHR data (Figure 4.71; Figure 4.73).

Below the SAND bed, slightly to highly calcareous, low to medium strength CLAY with black organic staining or slight organic odour is present.

The geotechnical borehole data show that the soil conditions and properties vary over the vertical interval covered by the anomaly: i.e. the top of the anomaly may coincide with CLAY, whilst lower parts of the anomaly are associated with slightly to highly calcareous SAND. Cemented sand was not observed at the sampled locations.

Possible origins for these local enhanced amplitude anomalies are listed below:

- The Postglacial anomalies appear to be related to the SAND beds observed in Unit B and Unit C, and associated with Horizon H10 (Figure 4.68; Figure 4.70; Figure 4.72). Bendixen et al. (2015) and Jensen et al. (2002) reported that PG II (corresponding to Unit B in this report) comprises laminated SILT and CLAY. This deviates from the geotechnical properties of Unit B as observed at both the Anorm_2 and Anorm_3 borehole locations and the base of Unit B at Anorm_1: i.e. SAND. This may suggest that Unit B and Unit C are generally associated with SILT and CLAY and that local occurrences of SAND (e.g. very local sand bars) are present. This lateral change in soil conditions (and possible accumulation of gravel and cobbles within the sand bed) may be the cause for a relatively large acoustic contrast and hence a local enhanced amplitude anomaly. At the CB13-BH location, however, no (thick) SAND bed was observed at the level of the seismic anomaly (Figure 4.74).

- Acoustic blanking and signal distortion were observed below some of these anomalies. This suggests that (small amounts of) free gas may be present in sediment below the anomalies and that the anomalies themselves may reflect the approximate position of where the gas is trapped below or within the clayey sediments of Unit A. At these shallow depths, sealing capacity of normally consolidated soils is expected to be low and possibly insufficient to contain gas accumulations. The natural buoyancy of the free gas bubbles may be in equilibrium with capillary forces in pores within the fine-grained sediments of Unit A.

- The northern Kattegat is known for methane-derived authigenic carbonates (MDAC) or 'bubbling reefs' (Jensen et al., 1992). These features are associated with gas seeps and/or expulsion and are evidenced by the presence carbonate-cemented sandstone structures (e.g. mounds). Where they are associated with active gas seepage, they are often accompanied by a diverse marine ecosystem (Judd and Hovland, 2007). The geotechnical borehole data at the investigated anomalies do not indicate the presence of a carbonate-cemented sandstone. Within the sampled sands (Unit B, Unit C and Horizon H10), only (small) shell fragments were described (i.e. not a diverse marine ecosystem). From this it may be concluded that the targeted anomalies do not resemble fully developed MDAC features. In addition, these features are covered by recent sediment that may suggest that gas seepage activity has ceased in the past, effectively stopping authigenic carbonate formation. As such, these features may resemble an early stage form of an MDAC at the onset of carbonate cementation (as evidenced by varying carbonate contents in the sampled sands).

Only a limited number of local enhanced amplitude anomalies were sampled. The results of the acquired geotechnical data and integration with the seismic data result in various potential origins of these features. A definite, single origin for the sampled features could however not be deduced. These features could result from various processes. Therefore, the origins of the sampled features and the non-sampled features remain speculative without

FUGRO

further ground truth information (e.g. soil sampling and CPT testing, geochemical analysis, high resolution geological logging).
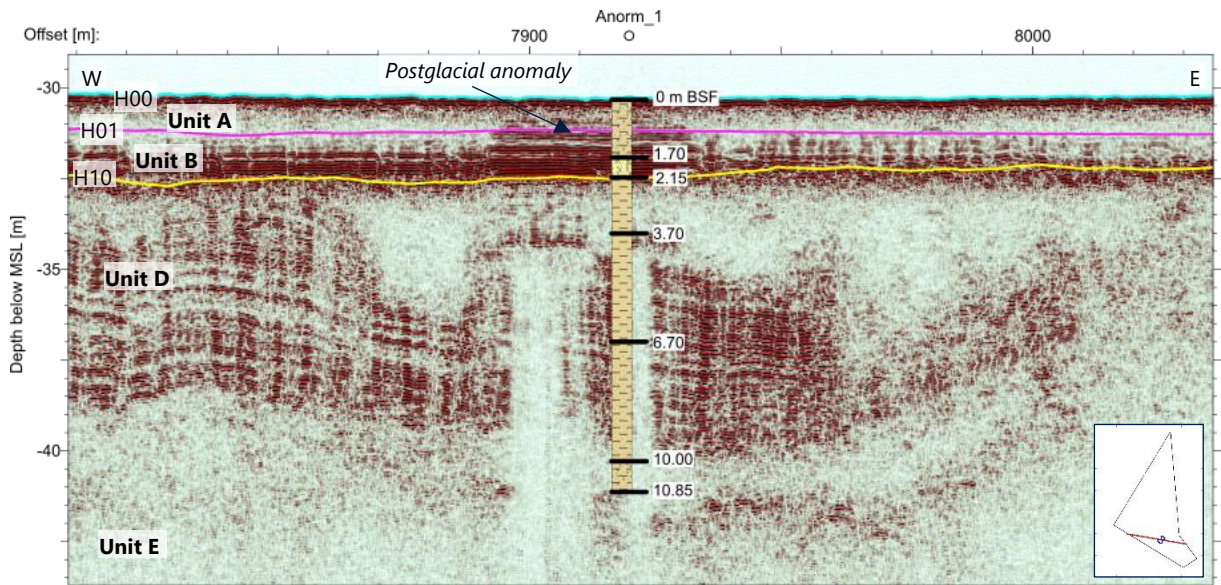
Figure 4.68: Line HAF1088P01. Borehole log of Anorm_1 projected on a SBP seismic line.
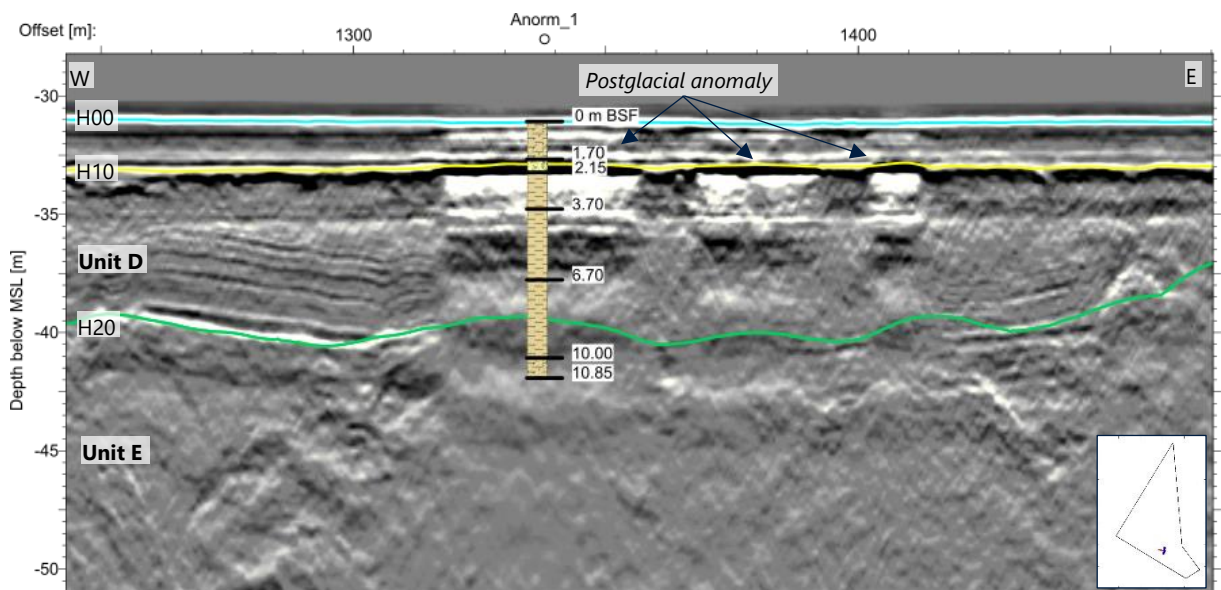
Figure 4.69: Inline 12410 in the OSS2 Site. Borehole log of Anorm_1 projected on a 3D-UHR seismic line.
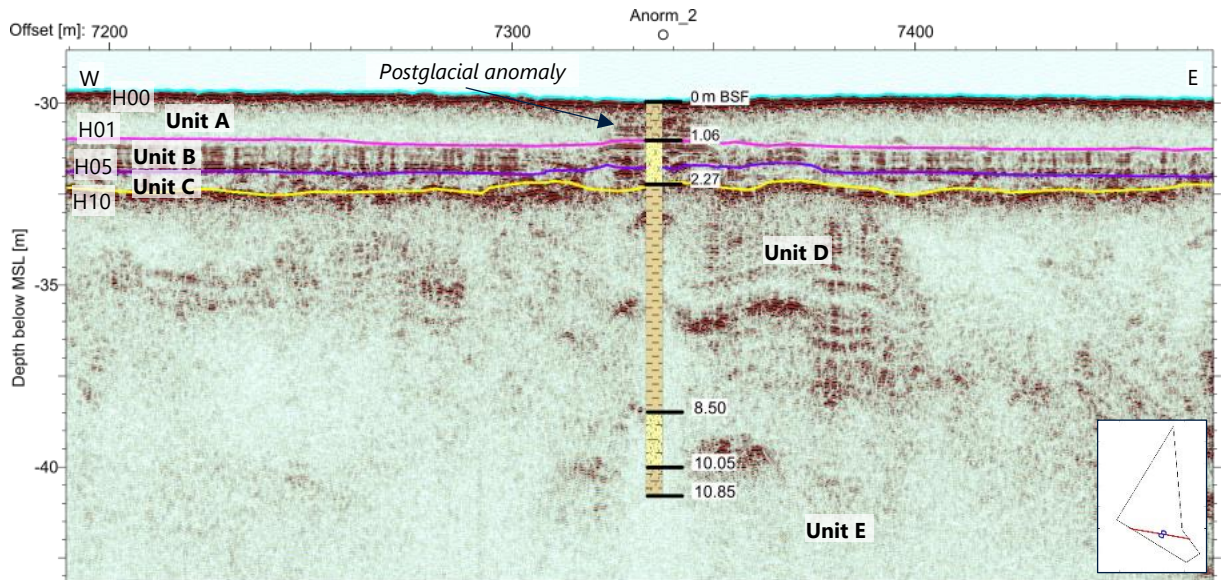
Figure 4.70: Line HAF1702P01. Borehole log of Anorm_2 projected on a SBP seismic line.
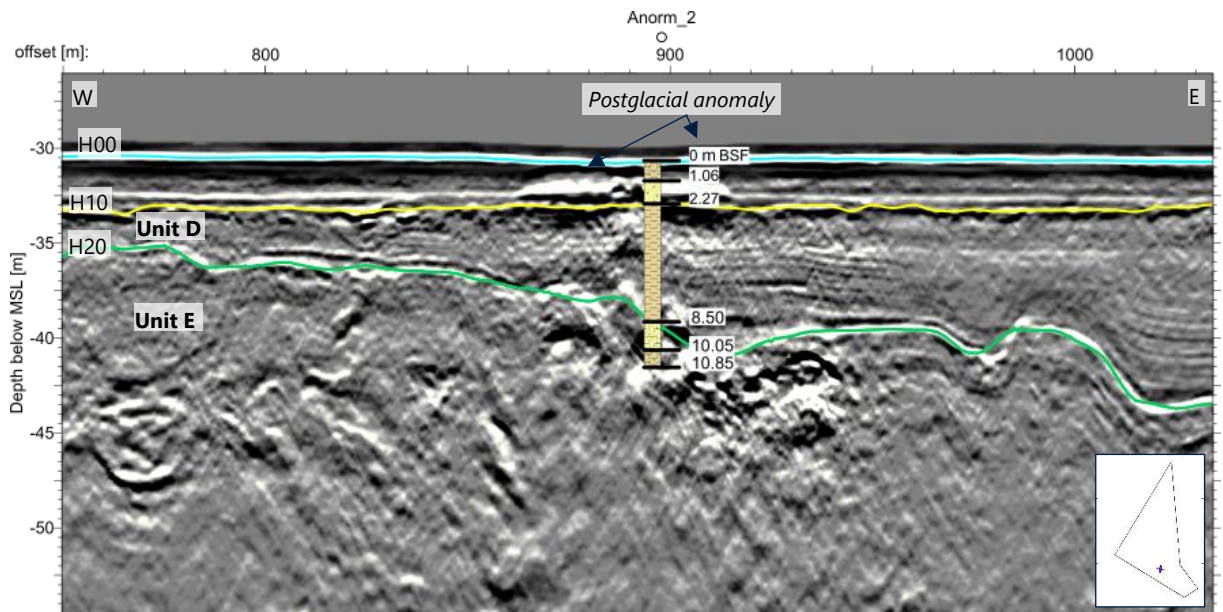
Figure 4.71: Inline 12370 in the OSS2 Site. Borehole log of Anorm_2 projected on a 3D-UHR seismic line.
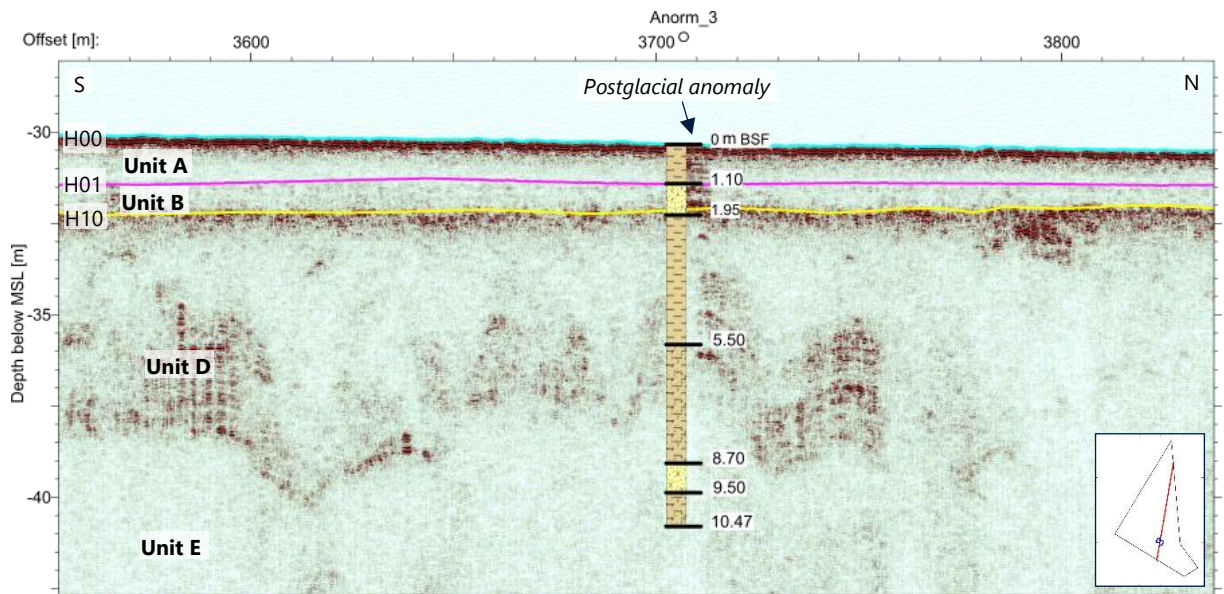
Figure 4.72: Line HAX2497P01. Borehole log of Anorm_3 projected on a SBP seismic line.
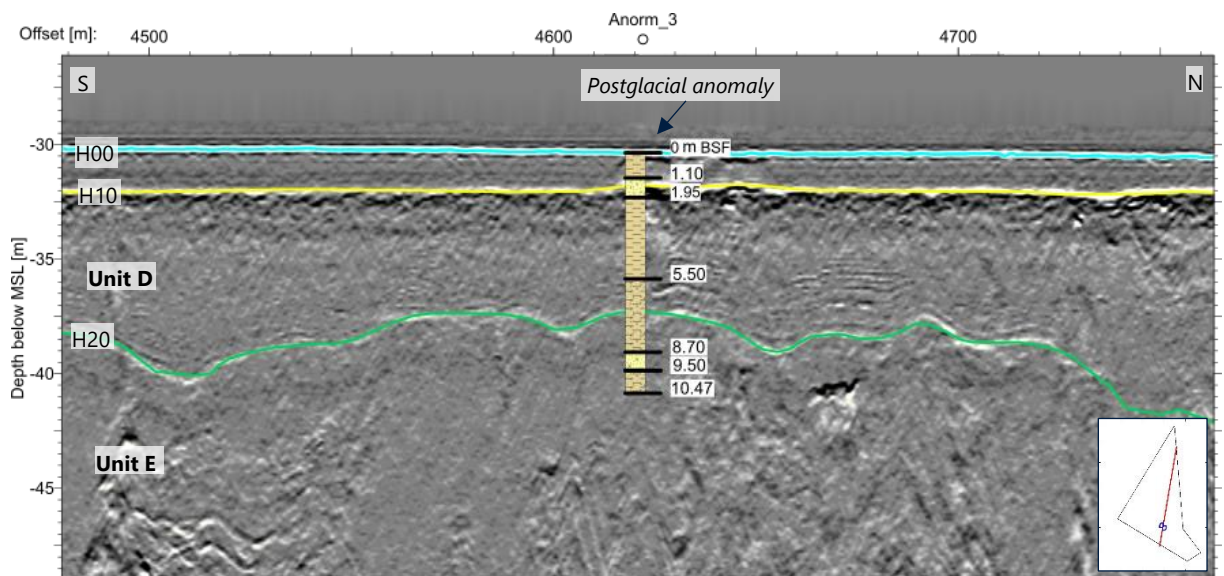
Figure 4.73: Line HAX2497P01. Borehole log of Anorm_3 projected on a 2D-UUHR seismic line.
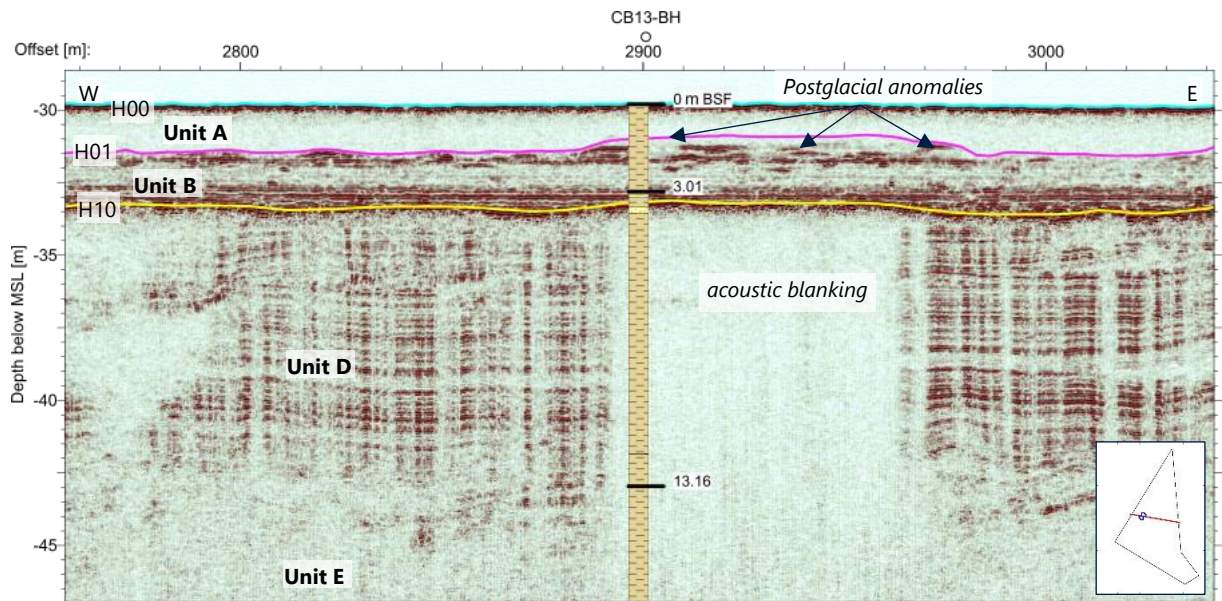
Figure 4.74: Line HAJ6222P01. Borehole log of CB13-BH projected on a SBP seismic line.
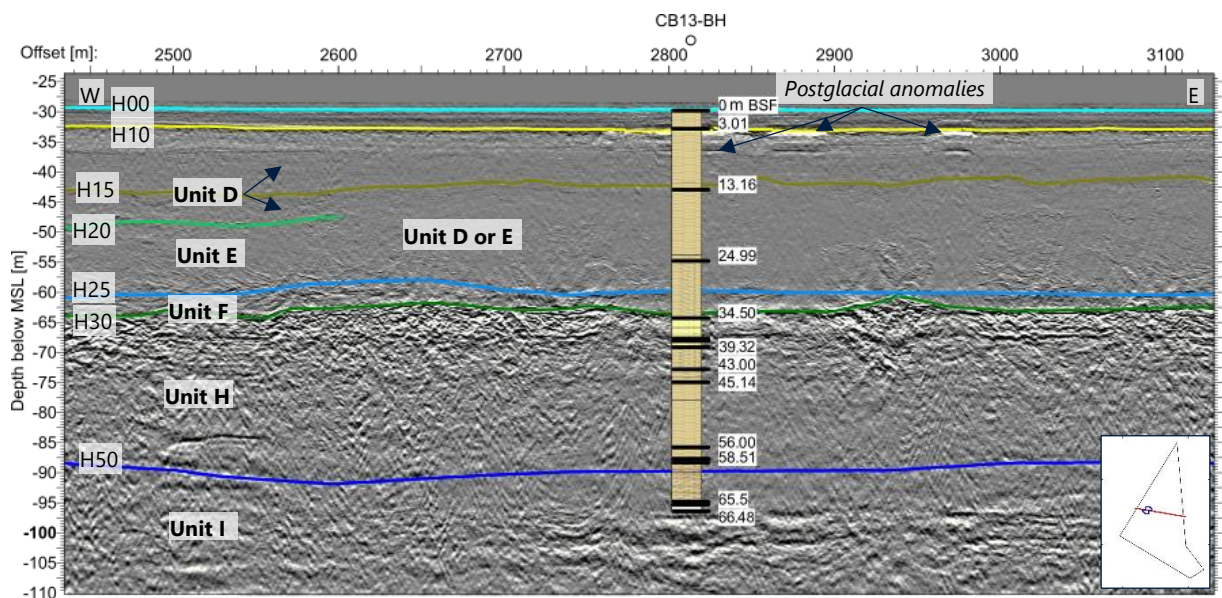
Figure 4.75: Line HAJ6222P01. Borehole log of CB13-BH projected on a 2D-UUHR seismic line.

4.3.3.2   Shallow Gas

Acoustic blanking was observed in the SBP data (Figure 4.76) and 2D-UUHR data (Figure 4.77). The main area of observed acoustic blanking is in the large pre-Quaternary depression. Occasionally acoustic blanking is also observed in other parts of the site, where it is associated with local enhanced amplitude anomalies and has a limited lateral extent (Figure 4.76).

The blanking often obscures visibility of layered (clayey) deposits (Unit D) suggesting that they may be associated with (small quantities) of gas in the soil.
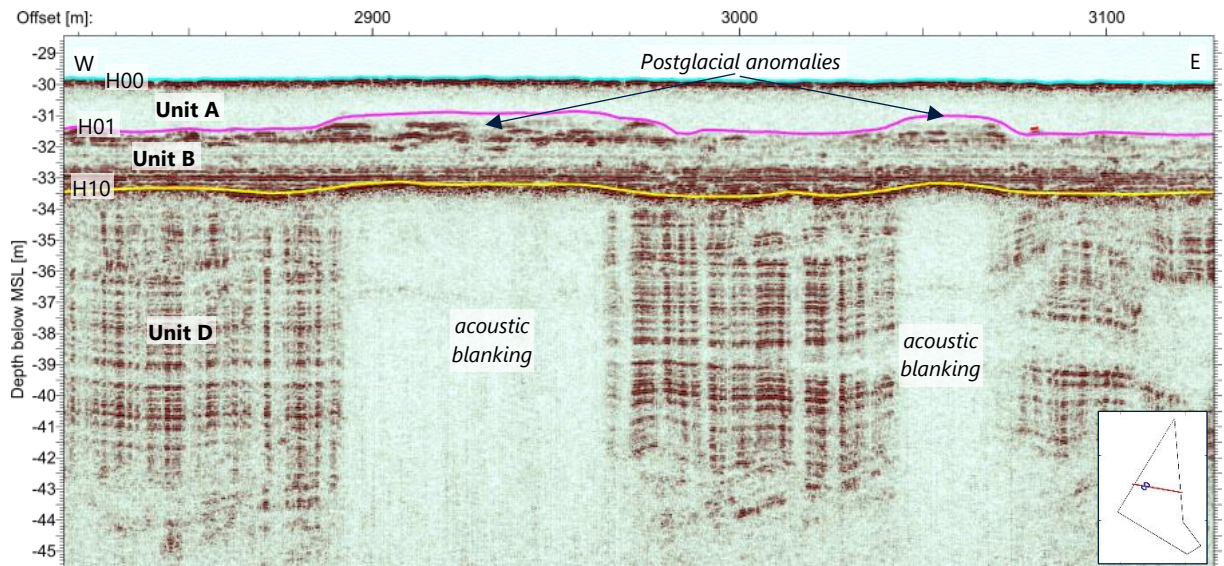
Figure 4.76: Line HAJ6222P01. SBP data example of acoustic blanking below Postglacial anomalies.
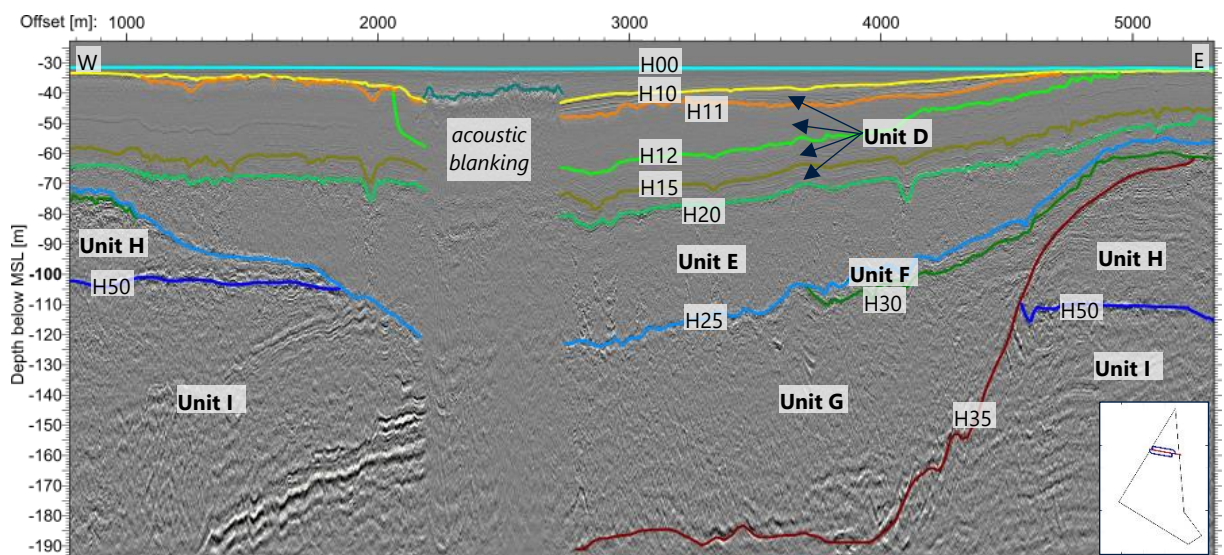
Figure 4.77: Line HAM2322P01. 2D-UUHR data example showing acoustic blanking in the pre-Quaternary depression.

4.3.3.3 Peat Pockets

High-amplitude reflectors, typically discontinuous and of limited extent, were observed in the SBP data (Figure 4.45) and 2D-UUHR data. In the 2D-UUHR data these seismic events show clear negative amplitudes (Figure 4.78). These negative amplitude events most likely represent small pockets of (reworked) peat or organic-rich clays.

The high amplitude reflectors are very abundant within Unit B in the large pre-Quaternary depression. They are also sporadically present within Unit B outside of the large pre-Quaternary depression.
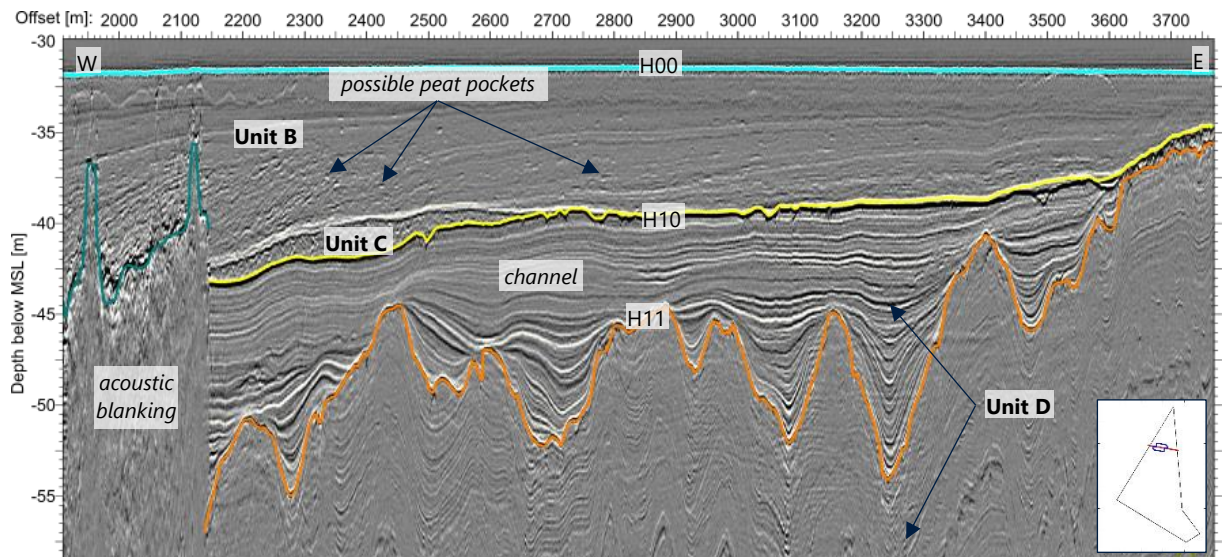
Figure 4.78: Line HAM2330R01. 2D-UUHR data example showing possible peat pockets within Unit B and a channel in Unit D.

4.3.3.4   Boulders, Cobbles and Gravel

Individual diffraction hyperbolas were observed in the SBP data (Figure 4.79) in all units within the penetration depth (i.e. Units A to D). They are most abundant in the central part of the site (Appendix B) and particularly within Unit A. Diffraction hyperbolas in the SBP data are interpreted as coarse material; possibly cobble to gravel-sized shells and rock fragments.

In the 2D-UUHR data positive amplitude point anomalies were observed (Figure 4.80). They are mostly identified in Unit D and are particularly abundant below Horizon H15. They also occur locally within Unit E and Unit H. They are most abundant in the centre and northern part of the site, which corresponds with the spatial distribution of Unit D.

The point anomalies observed in the 2D-UUHR data may indicate the presence of individual cobbles and boulders or small patches of coarse material (e.g. gravel). Point anomalies in Unit D may possibly represent ice-rafted debris.
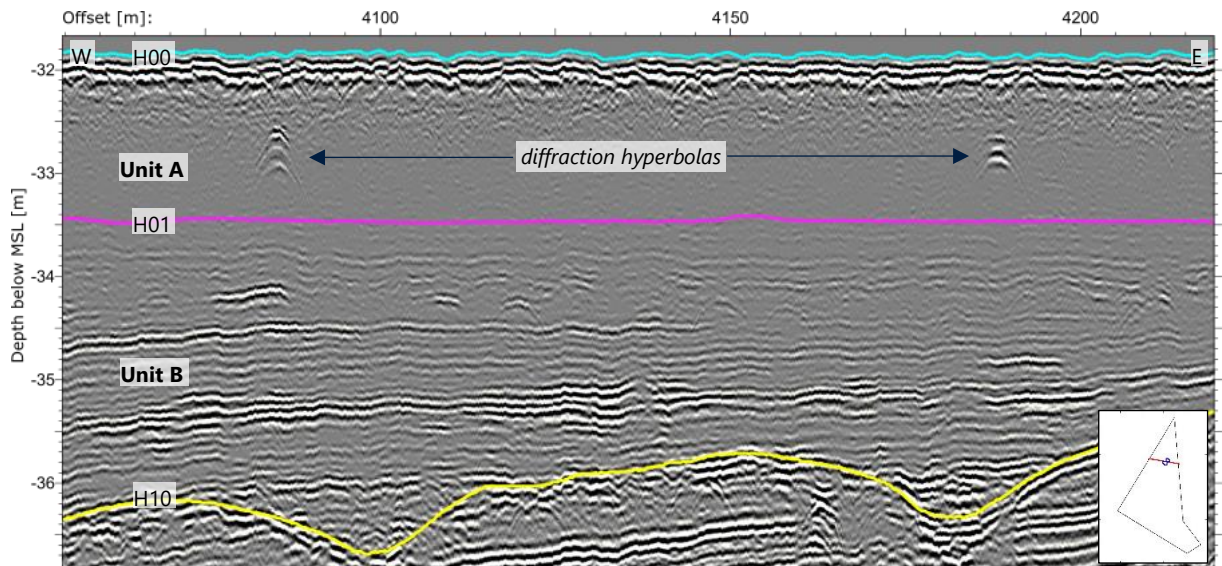
Figure 4.79: Line HAM1805P01. SBP data example showing diffraction hyperbolas.
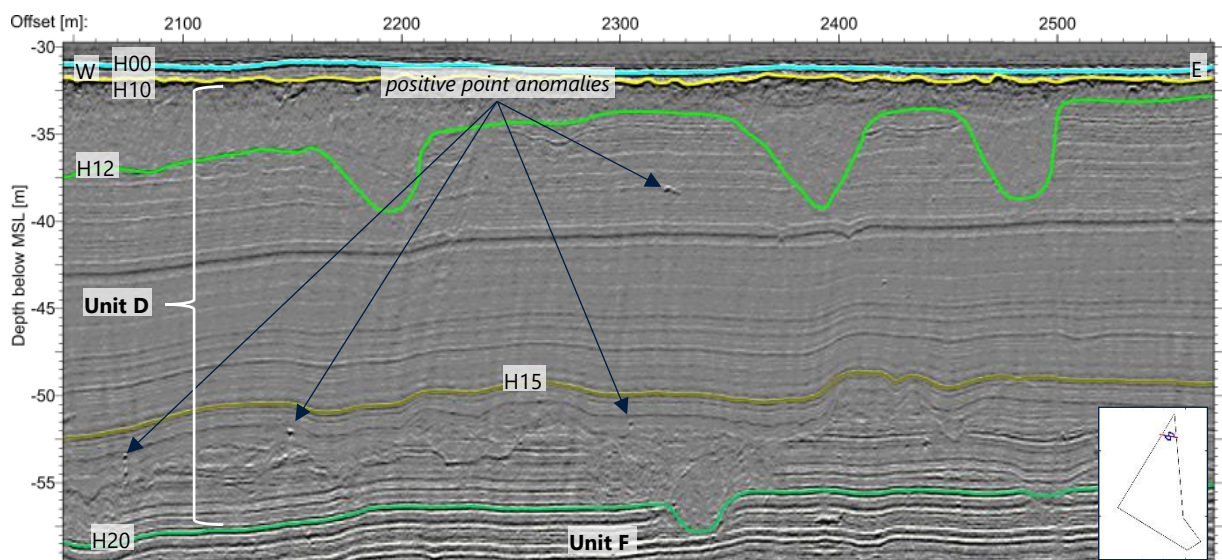
Figure 4.80: Line HAN2402P01. 2D-UUHR data example of positive point anomalies representing possible ice-rafted debris within Unit D.

4.3.3.5 Buried Channels

Buried channels were observed at various stratigraphic levels in Unit D. The dimension of these features is variable. They occur at the following seismostratigraphic levels within Unit D:

- Buried channels at Horizon H11;
- Internal buried channels within Unit D (i.e. not associated with an internal reflector);
- Buried channels at the base of Unit D (i.e. Horizon H20).

Horizon H11 represents the base of channels in the upper part of Unit D (Figure 4.78). Their infill is stratified, characterised by high-amplitude parallel reflectors, which contrast with the low to medium amplitude parallel reflectors of the underlying parts of Unit D.

These channels are present throughout the site except for the western part (Figure 4.81). They vary in orientation between north-west to south-east and north to south. The depth of

the channels varies from a few metres to up to 10 m, reaching a maximum depth more than 20 m, within the large pre-Quaternary depression. Their width varies from over 2 km within the depression to approximately 100 m where they form smaller channel bodies.

Due to their stratigraphic position (i.e. near the top of Unit D), the size and stratified internal seismic character indicating an alternation of sand and clay, these channels are interpreted to be of fluvial and/or tidal origin.

Erosional surfaces associated with smaller internal channels (gullies) are also present at varying stratigraphic levels within Unit D (Figure 4.50), predominantly observed north of the large pre-Quaternary depression. In the seismic data they show typical depths of 2 m to 5 m and widths of 10 m to 50 m.
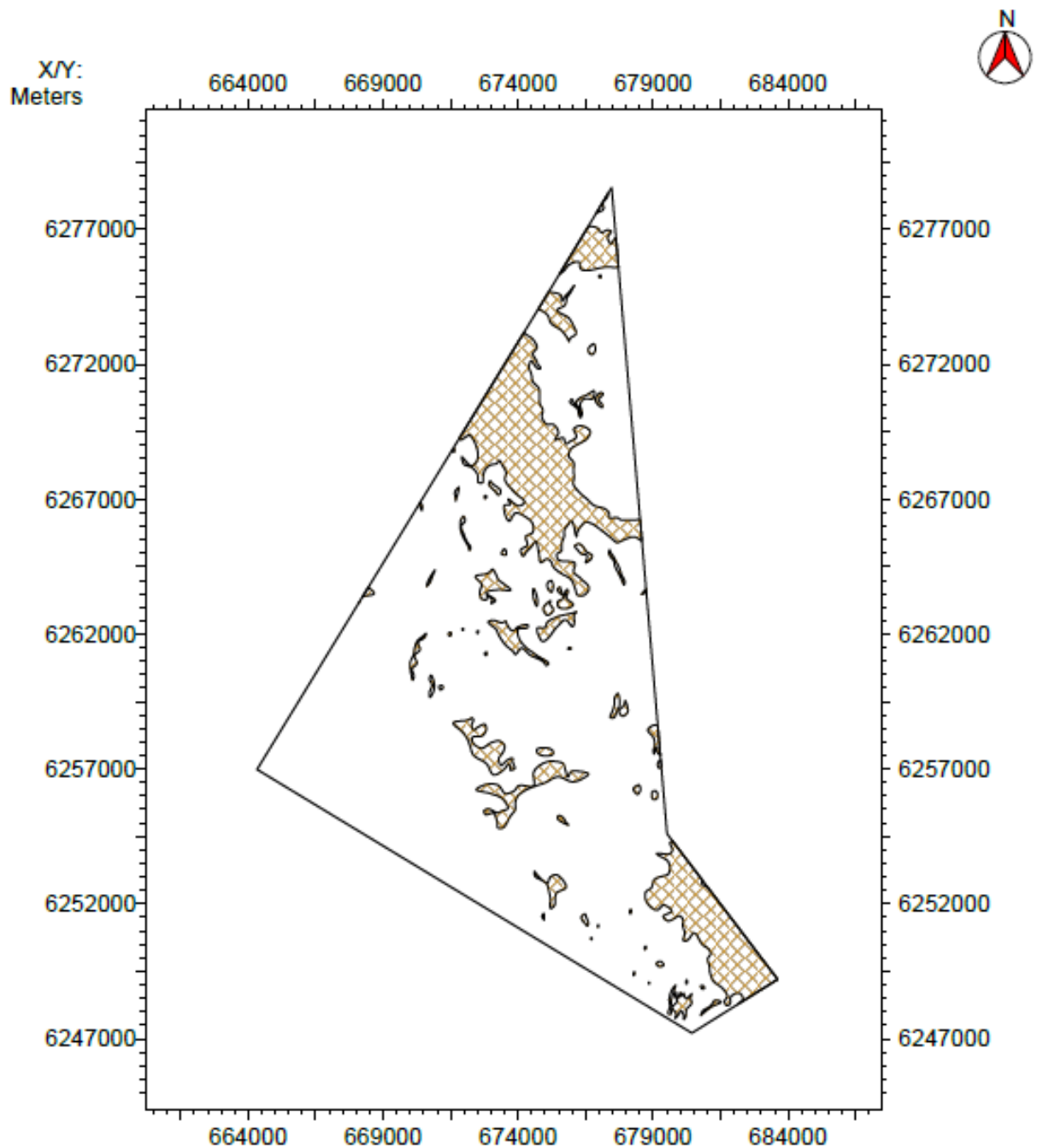
Figure 4.81: Distribution of Horizon H11 channels in the HOWF site.

4.3.3.6 Faults

Faults are expected to occur in the HOWF site associated with the Sorgenfrei–Tornquist (fault) Zone. The sub-surface architecture, changes in unit thickness and erosive contact between units within the pre-Quaternary depression may imply tectonic activity during the Quaternary.

Large faults were not identified in the seismic data. They may occur at deeper levels, beyond the penetration depth of the seismic data. Faults are likely to be present in the bedrock (Unit I).

Small-scale faulting was observed in Unit D, which is possibly related to mass transport deposits (see Section 4.3.3.8).

4.3.3.7 Glacial Deformation

The site has been affected by glacial processes during the Quaternary. In particular, evidence of the Weichselian ice movement can be expected at the site (GEUS, 2020). Ice sheet advance and retreat cycles may have deformed the Weichselian and older deposits resulting in folding or thrusting. They are present in the seismic data as undulating and steeply inclined, discontinuous reflectors, respectively (Figure 4.54).

Unit D is undeformed in the central and northern part of the HOWF site. In the southern part of the site, folded, undulating reflectors were observed throughout Unit D. The deformation of soil strata increases below internal Horizon H15 (Figure 4.82) and towards the south. Here, the acoustic character of Unit D changes from undulating reflectors to chaotic and Unit D cannot be distinguished from Unit E.

Towards the south, Unit E increases in thickness and the seismic character becomes more chaotic. This may be attributed to increased glacial deformation due to ice sheet advance south of the site (GEUS, 2020).
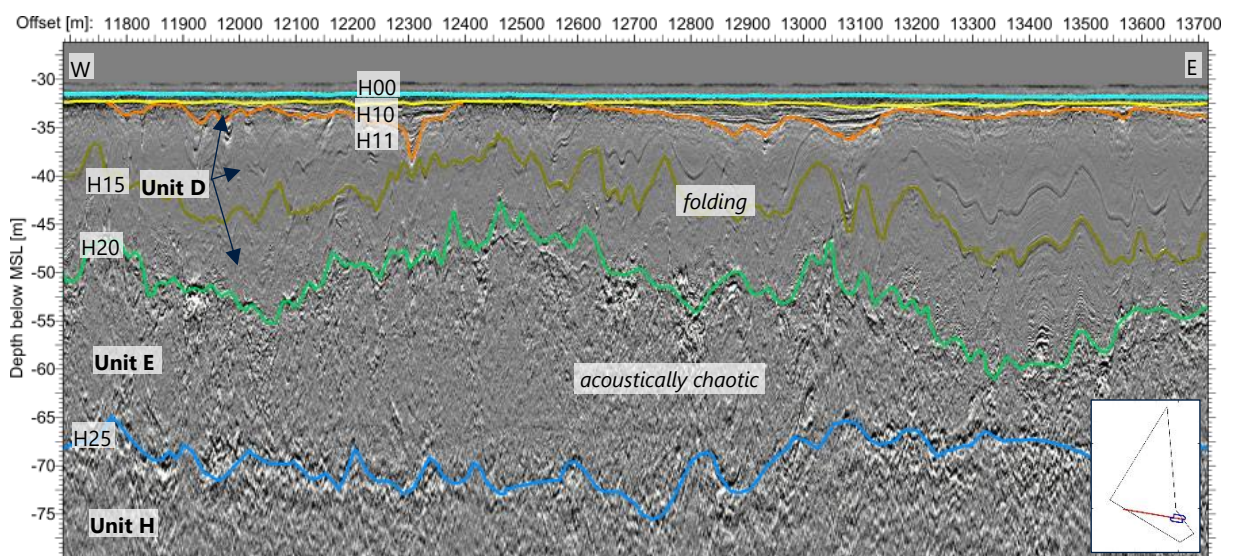
Figure 4.82: Line HAF2086P01. 2D-UUHR data example of slight glaciotectonic deformation in Unit D.

4.3.3.8 Mass Transport Deposits

Evidence for mass transport deposits (MTDs) was observed at multiple levels within Unit D. These MTDs are associated with different seismic characters, which may be a result of different types of past sediment failure. The different MTD levels are described below.

1. Channel-like features demarcated at the base by Horizon H12 occur near the upper part of Unit D. Horizon H12 is regionally present across the HOWF site, except in the central southern part (Figure 4.83). The seismic character of the channel infills is generally transparent facies, locally becoming more chaotic with the presence of sharp parallel

reflectors (Figure 4.49; Figure 4.51; Figure 4.52; Figure 4.80). Transparent seismic character was observed in these features in the SBP data, with the difference that in these data the character is more prone to show intervals with parallel reflectors (Figure 4.41). The typical thickness of these transparent intervals is approximately 5 m up to 10 m. In the pre-Quaternary depression, the transparent facies were observed to reach a thickness of up to 35 m.

2. In the proximity of the pre-Quaternary depression, Unit D also comprises intervals which display small faults separating (rotated) blocks of sediments with intact stratification (Figure 4.84). Here, Horizon H12 occurs either at the stratigraphic level at which these small faults terminate (i.e. decollement or glide plane) or slightly above (Figure 4.60). These faulted areas generally display normal fault movements, creating either horst and graben-like structures or rotated sediment blocks. The faulted units change laterally into undisturbed Unit D (i.e. parallel reflectors).

3. In the north of the site, the base of Unit D (Horizon H20) was found to incise into the underlying units (e.g. Unit F). Here, the unit has a chaotic seismic character, which is in contrast with the underlying Unit F which displays parallel reflectors (Figure 4.50). These incision features at the base of Unit D are typically 50 m to 400 m in width and approximately 5 m in depth.

The MTDs levels in Unit D show deviating seismic characters from the dominant character (i.e. parallel layered reflectors). They are likely the result of multiple large-scale sediment failures, triggered by fault movement along the Sorgenfrei–Tornquist Zone. Temporal variation in tectonic activity during the deposition of Unit D may have influenced the stratigraphic position of MTD occurrences in the unit.

Where faulted, Unit D may have been subject to (translational) failure, resulting in blocks of undeformed Unit D bounded by faults. In case the seismic character is chaotic or transparent, sediment deformation was likely higher and past sediment failure likely represented slumps. The geotechnical behaviour of these remobilised deposits may differ from the surrounding non-mobilised Unit D.
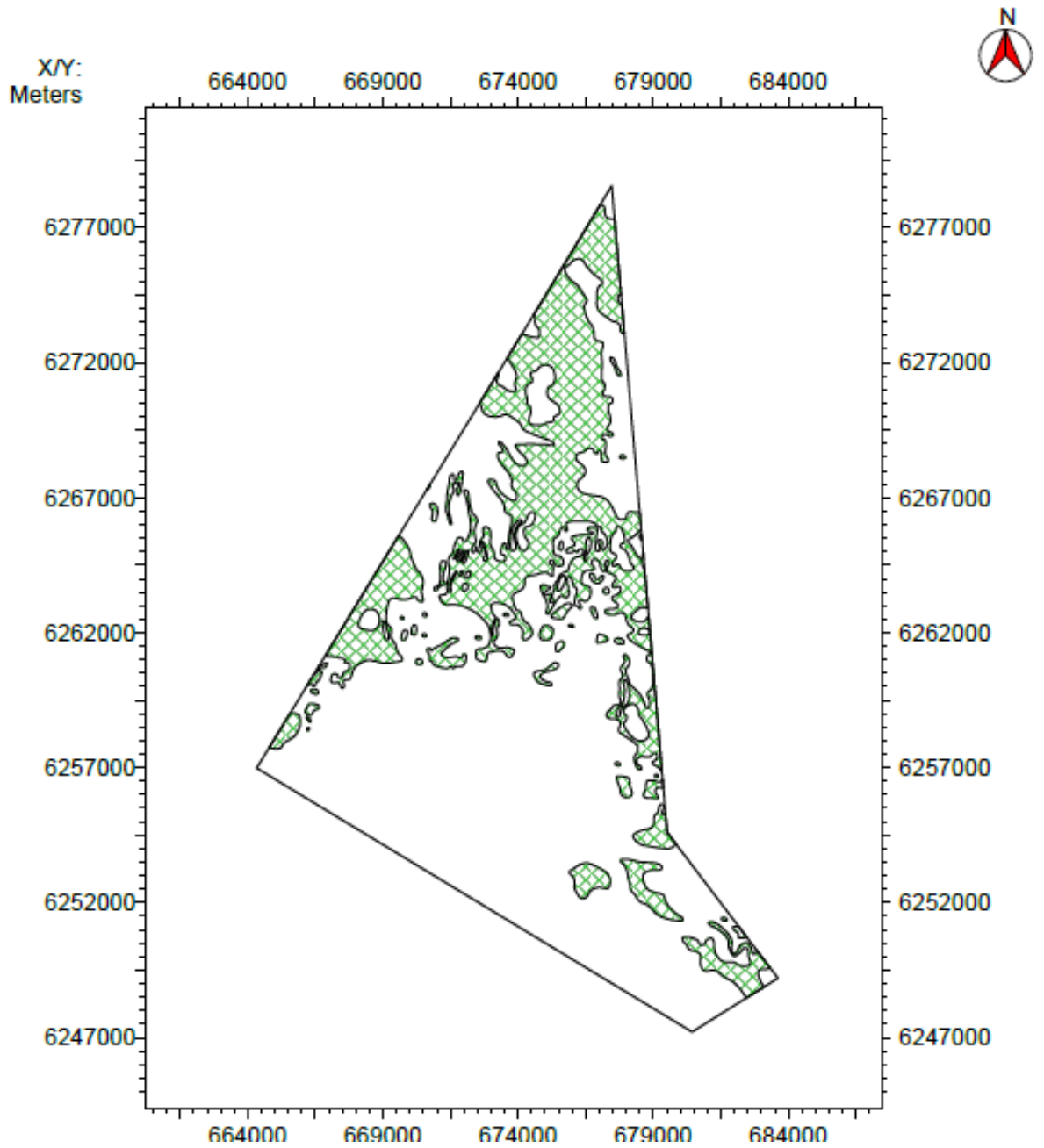
Figure 4.83: Distribution of Horizon H12 in the HOWF site.
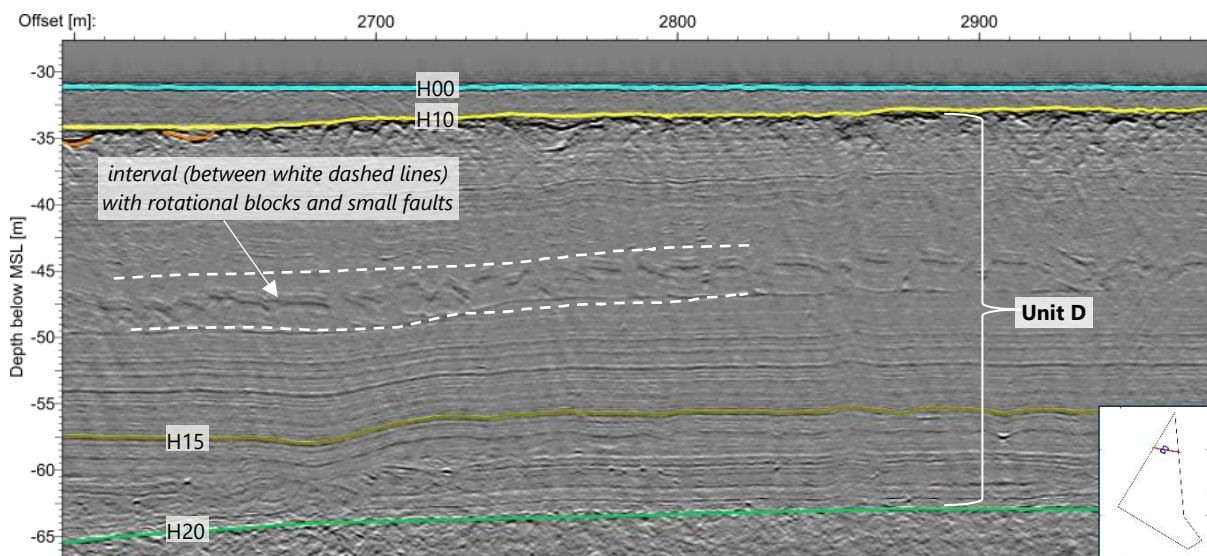
Figure 4.84: Line HAM2346P01. 2D-UUHR data example showing abundant faulting in Unit D.

4.3.3.9   Areas of Debris

Seventeen (17) small areas, 100 m to 200 m in diameter with clear irregular seafloor were observed in the SBP data (Figure 4.85). Just below the irregular seafloor, numerous diffraction hyperbolas were observed in Unit A.

These areas may have a man-made origin and could represent debris dropped on the seafloor. These areas correspond with the 'Area of Debris' as described in the seafloor morphology section of this report (Section 4.2.2.7).
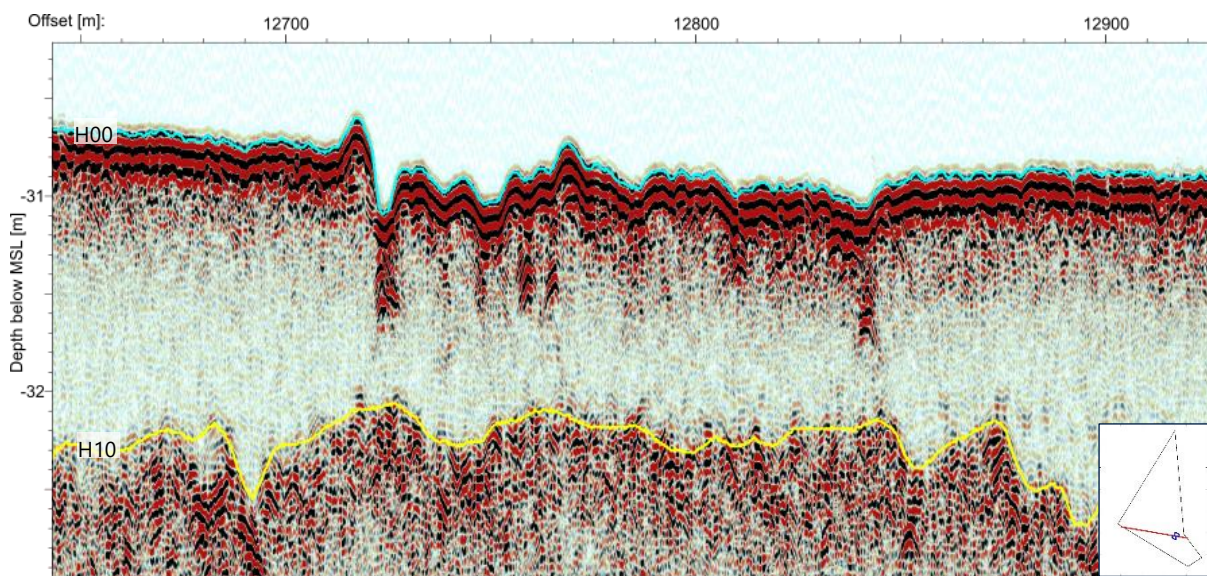
Figure 4.85: Line HAF1104P01. SBP data example of an area with seafloor disturbance and shallow diffraction hyperbolas in Unit A.

4.4   Archaeological Findings and Anomalies with Archaeological Potential

Fugro's expertise is limited with regard to identification of archaeological findings. Thus, only one object interpreted as potential wreck was classified as archaeological. It was observed in the central part of the HOWF site and surrounded by scattered debris items. Detailed

positions and measurements of the debris items are presented in Table 4.8. Refer to Figure 4.86 for SSS, MBES and MAG data examples of the potential wreck found within the HOWF site.

Table 4.8: Positions and measurements of potential archaeological findings within the HOWF site.

SSS_ID	Easting [m]	Northing [m]	Length [m]	Width [m]	Height [m]
HAJ_SSS_00023	672275.1	6262412.0	20.6	8.6	1.1
HAJ_SSS_00041	672273.3	6262406.9	1.1	0.4	0.3
HAJ_SSS_00042	672283.7	6262413.4	1.4	0.5	0.4
HAJ_SSS_00043	672265.1	6262401.5	2.1	0.4	0.1
HAJ_SSS_00044	672266.9	6262403.9	6.0	0.5	nmh*
HAJ_SSS_00045	672277.3	6262403.9	3.8	0.4	0.1
HAJ_SSS_00046	672268.9	6262422.5	4.1	0.4	0.2
HAJ_SSS_00047	672269.7	6262421.4	3.3	0.3	0.2
HAJ_SSS_00048	672270.8	6262420.7	2.3	0.3	0.1
HAJ_SSS_00049	672282.3	6262416.8	2.9	0.2	0.2
Notes: -all the numbers in the table were rounded to one decimal point *nmh = non-measurable height					

Fugro cannot exclude or confirm archaeological potential of the identified seafloor targets supplied in the GIS database as part of the final deliverables.
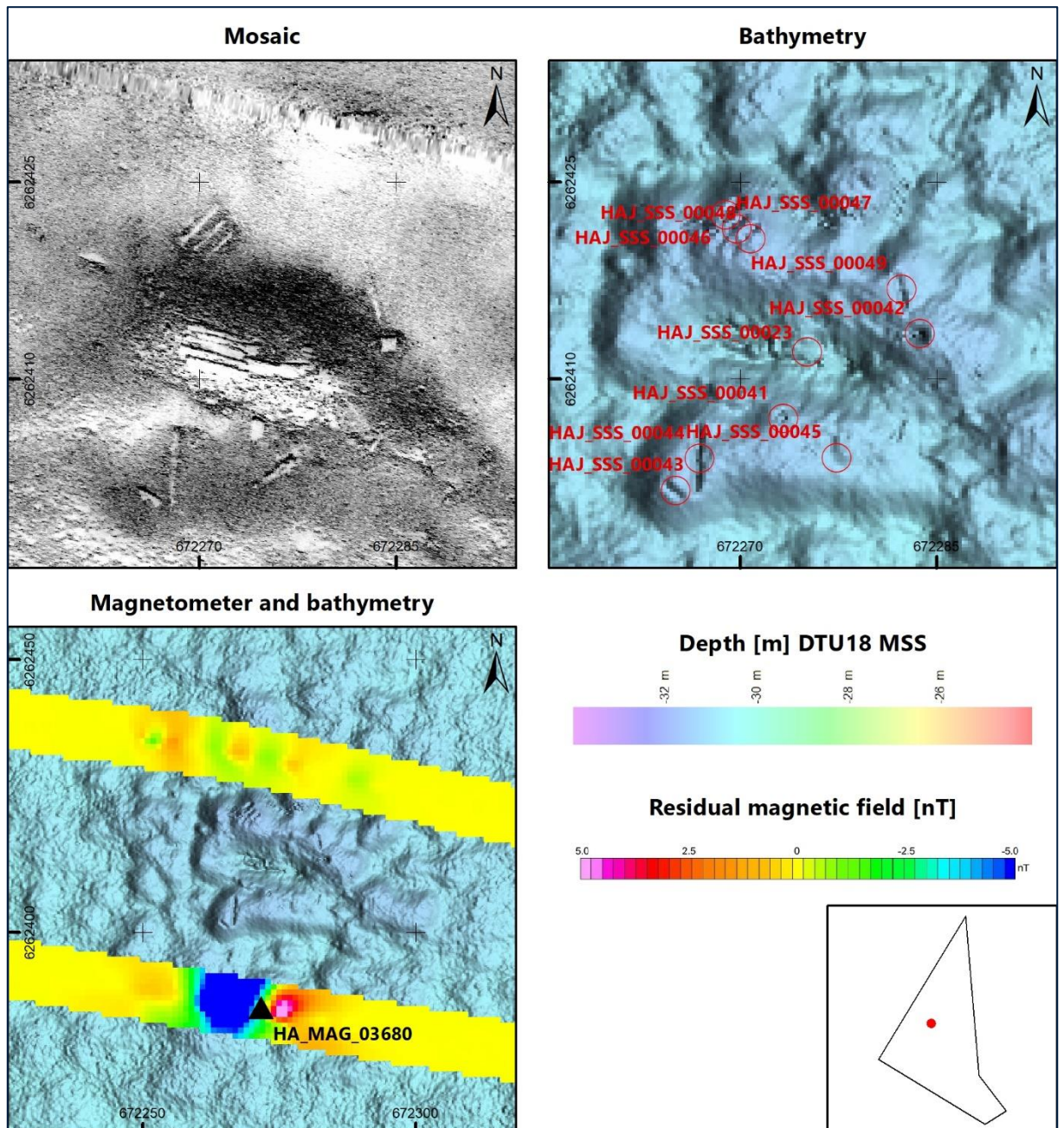
Figure 4.86: Potential wreck and surrounding debris observed in the HOWF site. Note: the scale of the 'magnetometer and bathymetry' panel is different than for 'mosaic' and 'bathymetry' panels.

5. Processing and Interpretation Methodology

5.1 Positioning and Navigation

All raw DGPS data were edited to remove erroneous fixes. No smoothing filters were applied to the position data during acquisition.

The antenna position was corrected to the vessel common reference point position (CRP) using measured offsets, during the acquisition of data. The position of the antenna during the analogue programme was corrected for layback of each towed instrument by applying the offset along the vessel track.

Real-time logging of navigation was done using Fugro's StarfixNG navigation system. Bathymetric sounding (water depth) data was logged in Kongsberg SIS software.

The processing of the acquired navigation data was carried out using Starfix VBAProc software.

The data were processed using offsets from the vessel datum for all sensors. Equipment offsets from the CRP position are presented in the Operations Reports (F172145-REP-OPS-001 and F172145-REP-OPS-002).

5.2 Multibeam Echosounder

5.2.1 Data Processing

Bathymetry data collected from the hull mounted dual head Kongsberg EM2040 multibeam echo sounder onboard the survey vessel were processed with CARIS Hydrographic Information Processing System and Sonar Information Processing System (HIPS and SIPS) software (Version 11.3). The CARIS HIPS and SIPS general workflow is presented in Table 5.1. Neighbouring blocks were systematically merged towards completion of data processing.

Table 5.1: CARIS HIPS and SIPS bathymetry processing workflow.

CARIS HIPS Work Step	Description
1. Raw MBES data	MBES raw data as logged by SIS, in combination with data input from StarfixNG
2. HIPS vessel file	Before data were converted into Caris HIPS, a so-called HIPS Vessel File (HVF) was defined. This HVF contains all relevant sensor definitions with information regarding offsets, correction values and system configurations. The HVF defines amongst others: ■ Offsets relative to the centre of gravity (COG); ■ Sound velocity information; ■ Dynamic MBES motion (heading, roll, heave, pitch); ■ Static corrections for gyro heading and error for roll, heave and yaw heading alignment of the multibeam system;

CARIS HIPS Work Step	Description
	■ Static TPU (total propagated uncertainty) settings including offsets and survey equipment standard deviations (based on technical specifications).
3. Data conversion to HIPS	The multibeam raw data exported from the online software was converted into HIPS format. Positioning information included in the raw data is based on geographical co-ordinates.
4. Quality control (navigation, attitude data)	Navigation and attitude data were checked for spikes. This is done manually or by using self-defined filters. Spikes were marked and flagged as 'not to be used for further calculation.' The resulting gaps were interpolated over time by calculating new values. Secondary (backup) systems for navigation and attitude data could be added to the HIPS and SIPS project if required.
5. Swath filter	Depth information of one survey line was filtered for spurious values and data not to be used. Filter settings for flagging data as rejected can include the following settings: ■ Min-max. accepted depth range; ■ Distance off nadir; The filters are applied according to the encountered morphology, weather conditions etc. The applied values may vary from area to area. Nevertheless, each line was checked separately, and the filter parameters were adapted if necessary.
6. Tide reduction	All depths were reduced to MSL using the DTU18 MSS model within Caris HIPS & SIPS. Navigation, motion and Starfix.G2+ GNSS elevation data were processed using Fugro Starfix.VBAProc. Ellipsoidal heights of the GNSS antennas were corrected for motions. The heights were reduced to the water line using draught and dimensional offset measurements. Waterline elevations are further reduced to the vertical datum (MSL) by means of DTU18 MSS model. A smooth tide curve was created to reduce MBES data to datum.
7. Sound velocity correction	Each trackline line was corrected for sound velocity.
8. Calculation of final position and depth for each beam (georeferenced bathymetry)	For each individual beam a position and a depth value were calculated with respect to vessel (gyro) heading, tide data (including dynamic draft) and sound velocity correction using time as correlation. In addition, the TVU and THU for each sounding was calculated.
9.TVU-THU filtering[1]	For TVU an IHO Special Order filter was run to remove erroneous soundings exceeded project requirements. For THU a filter was run to remove erroneous soundings exceeded project requirements (0.50 m).
10. Create work surface	The pre-checked data were used to calculate a CUBE (Combined Uncertainty and Bathymetric Estimator) surface.

CARIS HIPS Work Step	Description
11. Surface filter using CUBE	The CUBE algorithm creates a hypothesis for the depth value of a grid cell from the first depth value that falls into a cell. Every following depth value is checked against this hypothesis and according to a variety of settings selected to contribute to the existing hypothesis, to create a new, second hypothesis or to be rejected. A most probable surface is resulting from these calculations. This surface is then used as a base for a surface filter, for which a data window of acceptance around this surface has to be specified using certain parameters. The survey data is then checked against these conditions. Data outside the specified window of acceptance were rejected.
12. Create quality control surfaces	New base surfaces are calculated to check the result. Having undergone these procedures, the data is in a final state for delivery. Contour calculation was achieved by using Fugro Starfix Workbench.
13. Quality control	The data quality is mainly checked using the standard deviation, density (hit count), TVU/THU and visual bathymetry inspection. Local anomalies are removed manually or by a locally applied filter.
14. Data export	As a deliverable from HIPS a gridded dataset is produced and exported as ASCII files.

Note 1:

TVU and THU values were calculated using Caris HIPS&SIPS taking into account all contributing factors applicable for the vessels.

TVU and THU are defined as follows by the IHO Standards for Hydrographic Surveys (S-44), 6th Edition:

- Total horizontal uncertainty (THU): Component of total propagated uncertainty (TPU) calculated in the horizontal dimension. THU is a two-dimensional quantity with all contributing horizontal measurement uncertainties included. Total propagated uncertainty (TPU): Three dimensional uncertainty with all contributing measurement uncertainties included;
- Total vertical uncertainty (TVU): Component of total propagated uncertainty (TPU) calculated in the vertical dimension. TVU is a one-dimensional quantity with all contributing vertical measurement uncertainties included.;
- Uncertainty: Estimate characterising the range of values within which the true value of a measurement is expected to lie as defined within a particular confidence level. It is expressed as a positive value.

5.2.2 Data Interpretation

MBES gridded data was exported to GeoTiff format with 0.25 m resolution in order to complement interpretation of the seafloor sediments and morphology. Also, it was used in determining the position of the seafloor targets during the SSS data interpretation in SonarWiz.

For sediment and morphology classification the MBES GeoTiff was imported into ArcMap where SHP files delimiting identified features were created.

The manual mapping is a subjective process and serves only to highlight areas where morphological features are particularly well-developed.

5.3 Backscatter

5.3.1 Data Processing

Backscatter data collected by the MBES were processed by using Caris HIPS&SIPS (Version 11.3). Data were initially divided in blocks alike the bathymetry. All blocks were recombined into a single, site-wide 0.5 m backscatter surface.

Backscatter data is of high quality and was generated after finalisation of the bathymetry point cloud. Local backscatter anomalies associated with the nadir beams of the MBES could not be fully resolved during backscatter processing. The artefacts were amplified by the use of Dual Swath which significantly increases the amount of energy in the water column. The subtle presence of nadir is typically visible on the flat and featureless seabed (Figure 5.1).

Figure 5.1: HOWF site backscatter, highlighting subtle nadir striping on flat seafloor.

5.3.2 Data Interpretation

Backscatter data (grid cell size 0.5 m) was imported as raster into a GIS database and used for the seafloor sediments and substrate type classifications. Interpretation was carried out in ArcMap and the results are presented in GIS deliverables.

5.4 Side Scan Sonar

5.4.1 Data Processing

SSS data were recorded in digital formats (.jsf and .xtf) using Fugro Starfix GLog/GPlot in combination with EdgeTech Discover software.

The .xtf files were imported into Chesapeake SonarWiz software for quality control and subsequent data analysis and interpretation. Each line was checked on import for navigation artefacts and coverage and infills were planned as necessary. Following the Fugro standard procedures, gains were applied using EGN table to normalise the amplitude of a reflected signal across the range. The accuracy of the USBL positioning was carefully assessed throughout the survey by comparing targets observed on reciprocal lines.

A severe pycnocline (i.e. the combined effect of thermocline and halocline layers in the water column) affected the far-range areas of the SSS data. This occurred at various places within the individual survey blocks of the HOWF site. The affected segments were clipped and additional SSS infills were run to acquire good quality SSS data coverage in the affected areas. The plots presenting areas of 100% and ≥ 200% coverage were exported from SonarWiz and are included in the GIS deliverables.

For more details on SSS processing procedures refer to Operations Reports (F172145-REP-OPS-001 and F172145-REP-OPS-002).

5.4.2 Data Interpretation

Individual lines were checked on a line by line basis for sonar targets and other features in a waterfall display, which provides the highest resolution display of the data. Target picking started offshore as the survey proceeded and was continued later in the office.

A high-frequency dataset was used for the purpose of target picking. SSS targets of at least 1.0 m in any dimension were picked and rationalised against each other (i.e. the same target may be picked from two or more lines) and then checked against MBES data. If a target (e.g. a boulder) has recognisable relief on the DTM, its position can be adjusted to the more accurately georeferenced DTM. For the offshore part of the survey rationalisation took place in SonarWiz and the results were checked in ArcMap.

Finally, sidescan sonar targets were verified against database information (e.g. known wrecks and other seafloor features) and against the magnetometer data.

5.5 Magnetometer

5.5.1 Data Processing

The magnetometer data were acquired along the survey lines except for cross lines orientated in approximately north–south direction. Data quality was monitored throughout the survey and was deemed to be high.

In Fugro Starfix VBA Proc processing software, navigational data were merged with raw magnetometer data and exported as a single ASCII file per line. The position of the magnetometer was calculated by applying offset from the USBL beacon to the magnetometer sensor. In VBA Proc, USBL beacon positions were manually de-spiked, and after applying offsets to the magnetometer, the navigation was interpolated. Where an USBL gap exceeded 10 seconds, the magnetic data were not considered.

The required cut-off altitude value was 5 m. All the magnetic data with an altitude greater than 5 m were masked out from the calculation of the residual grid. Outliers (data spikes) in altimeter readings were removed manually. Resultant gaps of up to 30 fiducials were interpolated.

Generally, the data were free from noise and therefore within the specified noise levels (±1 nT). The noise level in the magnetic data was constantly monitored in order to achieve the required specifications. Sections of noisy data were flagged, analysed and infills were acquired where necessary. Several areas were found to be associated with strong geological background noise, occasionally exceeding 2 nT amplitude. These areas were observed particularly within the southern part of the site. An additional QC was conducted where the signal strength value dropped below 100: in none of the cases the magnetic field showed evidences of being distorted or affected.

Spikes in the magnetometer data were manually removed and magnetometer data were not interpolated but replaced by a dummy which was not displayed in the profile or plan view. High-frequency and low-amplitude noise was removed from the despiked magnetometer data by applying a B-spline filter.

Long-wavelength variations in the magnetic field were removed in order to isolate the shorter wavelengths which make up the residual magnetic field. After de-spiking and noise removal, as described above, the sequence of non-linear filters was applied to the magnetometer data.

5.5.2 Data Interpretation

Magnetometer data were processed and interpreted using Oasis montaj software. A set of linear filters was applied to the measured magnetic field in order to obtain a magnetic residual field representing any ferrous or magnetic objects on the seafloor or at shallow burial depth. For detailed description of magnetometer processing refer to Operations Reports (F172145-REP-OPS-001 (01) and F172145-REP-OPS-002 (01)).

The magnetometer target picking was performed using the Blakely test method on the analytical signal grid with a cut-off value of 1 nT/m. Duplicates from the automatically picked targets were removed and the remaining target was manually measured on the magnetic residual field. This was done to remove targets smaller than 5 nT peak-to-peak amplitude as well as to avoid targets being picked multiple times due to their complexity. Magnetometer target positions were moved either to the centre of the maximum inflection points (dipoles), the highest point of the residual peak-to-peak value (monopoles) or anomaly midpoints (complex anomalies).

5.6   Parametric Sub-Bottom Profiler

5.6.1   Data Processing

Vertical data resolution and ping rate were 0.3 m and >8 Hz as per the specification requirements. Ping rate was monitored with respect to vessel speed during real-time survey to avoid multiple effects in SBP data.

Positioning of the SBP data was checked to ensure that it remained within the project specification of +/- 1 m. Features present within the HOWF site were used to check the SBP positioning against the MBES and SSS data.

The SBP data were logged using SESWIN software recording files in .ses3 format. Vessel heave at the SBP transducer location was recorded and applied during the acquisition. The recorded .ses3 files were converted to .sgy format and processed in RadExPro. Processing steps applied offshore consisted of:

- Amplitude correction to compensate for spherical spreading and anelastic losses during the propagation of acoustic waves;
- Bandpass filtering to remove noise from the data (Butterworth filter 2500 Hz – 12500 Hz);
- Burst noise removal to remove exceptionally high amplitudes from the data.

Subsequently, the .sgy files were imported into IHS Kingdom software where navigation was checked for artefacts and data quality was assessed. Where extensive cavitation due to bad weather occurred, data was consulted with the Onboard Client Representative and infills were planned as required.

Processing of the SBP data continued in the office where the following processing was done:

- Tide and draft correction;
- Automatic seabed pick;
- Time–depth conversion;
- Correctly formatted text header inserted into .sgy files.

The result of automated seabed pick was injected into byte 61–64 in .sgy files and imported into IHS Kingdom as a horizon, where it was compared with seismic and MBES data. For the time–depth conversion a two-layer model was used, separating water column and subsurface, with sound velocities of 1470 m/s up to 1495 m/s for the water column (varying between lines) and 1500 m/s for the shallow soils, respectively.

5.6.2   Data Interpretation

The following strategy was applied for SBP data interpretation:

- Compiling historical geotechnical, geophysical and geological data from client-provided sources and Fugro database as well as from available literature;
- Interpretation of seismically distinct units and horizons in the time-domain, verified by available historical shallow geotechnical data and literature;

- Identification and interpretation of key geological features, which can be potential hazards (geohazards) for offshore infrastructure;
- Time–depth conversion of horizons and features by the utility of a two-layer velocity model, identical to the velocity model applied to the SBP data;
- Creation of polygons based on the interpreted horizons to define areas where soil units and horizons were not observed and areas where soil units and horizons were not present;
- Gridding (and contouring) of soil unit boundaries/horizons in metres BSF and in metres below MSL; isochore unit thicknesses in metres.

The following needs to be considered for the SBP data:

- The quality of the SBP data was deemed to be very high with a typical penetration depth of over 20 m BSF;
- The line spacing for the SBP data was 62.5 m. Potential features smaller than this distance may not have been detected where present in between seismic lines;
- Gridding of horizons was performed within IHS Kingdom Suite 2018. All gridding was done with the 'flex gridding' algorithm and parameters were kept the same among all SBP horizons. The cell size was set to 5 m by 5 m. Polygons were used to limit the extent of the produced grids. The search distance was set to 60 m, to make sure there were no gaps in the grids due to line spacing variations. Minimum curvature was applied, and smoothness was set to halfway (6).

5.7 Multichannel 2D-UUHR Seismic

5.7.1 Data Processing

Detailed description of the processing flow applied to the 2D-UUHR seismic data collected during the survey is presented in the seismic processing report (F172145-REP-PROC-001 (01)).

5.7.2 Data Interpretation

The following strategy was applied for 2D-UUHR data interpretation:

- Compiling historical geotechnical, geophysical and geological data from client-provided sources and Fugro database as well as from available literature;
- Interpretation of seismically distinct units and horizons in the time-domain, verified by available historical shallow geotechnical data and literature;
- Identification and interpretation of key geological features, which can be potential hazards (geohazards) for offshore infrastructure;
- Time–depth conversion of horizons and features using the same velocity model as applied to the seismic data;
- Polygons were created based on the interpreted horizons to define areas where soil units and horizons were not observed and areas where soil units and horizons were not present;

- Gridding (and contouring) of soil unit boundaries/horizons in metres BSF and in metres below MSL; isochore unit thicknesses in metres.

The following needs to be considered for the 2D-UUHR data:

- The quality of the 2D-UUHR data was good with a typical penetration depth of 150 m BSF;
- The line spacing for the 2D-UUHR data is 250 m. Potential features smaller than this distance may not be detected where present in between seismic lines;
- Gridding of horizons was performed within IHS Kingdom Suite 2018. All gridding was done with the 'flex gridding' algorithm and parameters were kept the same among all 2D-UUHR horizons. The cell size was 5 m by 5 m. Polygons were used to limit the extent of the produced grids. The search distance was set to 150 m, to make sure there were no gaps in the grids due to line spacing variations. Minimum curvature was applied, and smoothness was set to halfway (6).

5.8   Grab Samples

Grab samples were collected at the agreed locations within the HWOF site. Each sample was weighed, as per specification, with a minimum of 3 kg of sediment collected per grab.

Initial visual analysis was recorded, and high-resolution photographic images were taken of each sample. The grab samples were sealed and stored in separate boxes to maintain the integrity of each sample and for safety during transit. Samples were offloaded during a port call at the soonest opportunity and transported to the onshore geotechnical lab for further, in-depth analysis.

All the grab samples were analysed in the laboratory. The results of the organic matter content and particle size distribution tests are supplied as part of the final deliverables.

Based on the results of the laboratory testing, the grab samples were classified following the Danish standard (Larsen et al., 1995). For the purpose of seafloor sediment classification GEUS terminology was required (Leth, J.O. (ed.) et al., 2014: Danmarks digitale havbundssedimentkort 1:250.000). In order to link grab sample analysis with the seafloor sediments interpretation, the correlation was established between the two terminologies (Table 5.2).

Table 5.2: Correlation between the Danish standard and GEUS terminologies.

Danish Standard	GEUS
Gravelly clayey silty SAND	Gravel and coarse sand
Clayey and silty SAND	Sand
Very sandy CLAY and SILT	Muddy sand
	Mud and sandy mud
Very clayey very silty SAND	Quaternary clay and silt

Based on the grab sample content analysis, muddy sand and mud and sandy mud represent the same class according to the Danish standard. However, the distinction between these two classes was made following the difference in backscatter intensity observed in the acquired data, where mud and sandy mud are characterised by higher reflectivity than muddy sand.

5.9 Data Quality

5.9.1 Multibeam Echosounder

Multibeam echosounder data quality overall was well within desired specification for the entire HOWF survey area.

The spatial accuracy achieved for MBES sensor for the present survey are resolution 0.25m and 1m. Standard deviation (2 sigma) was <0.2. THU was <0.5m and TVU are depth dependent values and the results were satisfying IHO special order 44. Block based MBES QC reports were supplied to the OCR and are presented in the operations reports.

5.9.2 Side Scan Sonar

The SSS data quality was monitored throughout the survey and was of high quality throughout the HOWF survey area. The technical requirements of the survey with regards to resolution and range were met throughout the survey. Severe pycnocline (combined effect of thermocline and halocline events) affected the far range areas of SSS data at various places within the individual blocks of HOWF survey area. The affected segments were clipped and additional infills were run to acquire good quality SSS data coverage of the complete HOWF survey blocks. Overall 200% SSS data coverage including nadir was achieved as per approved exceptions in TQ-013, TQ-022 and Field Memo 01. All TQ documents and the Field Memo are presented in the operations reports.

The spatial accuracy achieved for SSS sensor aided by USBL positioning was between +/- 1.2 m to 0.4 m. SSS samples per channel was 4096. Minimum detected target dimension was 0.5 m length, 0.2 m width and 0.1 m height within various survey blocks.

5.9.3 Magnetometer

The magnetometer data quality was monitored throughout the survey and was deemed to be high quality. Noisy data sections were flagged by the offline team and further confirmed by Fugro QHD processors. Infills were planned and acquired where necessary. OCR also reviewed the data quality and noise interference in the magnetometer data. Several areas of strong background geological noise were observed within the site.

The overall magnetometer data quality was good. The noise interference level in the magnetometer data was generally lower than 2.0 nT. Sparker noise was removed by applying narrow linear filter to the raw magnetic field acquired along the 2DUHR survey lines.

As single magnetometer was being used during the survey, the coverage was assessed along each line within specified survey blocks of HOWF survey area. Furthermore, additional

magnetometer lines, including infills and reruns acquired for other sensors, i.e. SSS, SBP, 2DUHR, also have been processed to provide more coverage if the magnetometer data quality was devoid of any major noise interference.

The single magnetometer was towed at a consistent altitude of less than 5.0 m (mostly 3 m) above the seafloor, throughout the survey. Any areas where the altitude was outside of this permitted range were removed from the magnetometer gridded dataset and infills were planned wherever necessary. Final magnetometer coverage was assessed by Fugro QHD and checked by FNLM. All infill requirements were planned accordingly and passed onto the vessels.

5.9.4   Parametric Sub-Bottom Profiler

SBP data quality was monitored throughout the survey and generally deemed to be high. The technical requirements of the survey with regards to resolution, penetration and trigger rate were met throughout the survey. Penetration varied across the survey area depending on the geology, however in general a minimum penetration of 10 m below seafloor was achieved as per technical requirements (Energinet, 2020) with a maximum observed penetration of approximately 25 m. Occasionally hyperbolae related to either gravel, cobbles or small boulders were discerned. Vertical data resolution and ping rate were 0.3 m at the minimum and 8.8 Hz (pulse per seconds) respectively as per the specification requirements (Energinet, 2020). Ping rate was monitored with respect to vessel speed during real-time survey to avoid multiple effect in SBP data.

Positioning of the SBP data was checked to ensure that it remained within the project specification of +/- 1 m. Vertical and horizontal resolution of the Innomar sensor as derived from the survey results were 0.05 m and 1.36 m, respectively. Features present within the survey site were used to check the SBP positioning against the MBES and SSS data.

Although data quality of sub-bottom profiler was generally good for the entire survey, some lines exhibited vertical noise and cavitation caused by marginal weather conditions. During the 2DUHR survey, the electrical/sparker noise was visible. These noise artefacts were reduced using burst noise removal during processing. Interpretability is not affected by this noise as it is only apparent as vertical artefacts in the data that are dissimilar to real reflectors. Areas of cavitation in sub-bottom profiler data were assessed with collaboration of OCR. Reruns were attempted as and when required.

5.9.5   2D-UUHR

2D-UUHR (MCS) data quality was monitored throughout the survey and generally deemed to be high. The technical requirements of the survey with regards to resolution were met throughout the survey for the entire HOWF area. Penetration was achieved to at least 100 m below seafloor. The penetration is particularly good at the Pre-Quaternary depression. Vertical resolution better than 0.3 m was achieved with fundamental frequencies between 1 and 3 kHz as per technical requirements (Energinet, 2020).

Positioning of the 2D-UUHR data (MCS) was checked to ensure that it remained within the project specification of +/- 7 m for 95% of the line (Energinet, 2020). Infills / reruns were run for the sections of the lines / complete lines as and when required to adhere with the required survey specification and deemed data quality. OCR was involved for respective data acceptance of the survey blocks.

The raw SEG-D data was assessed and QCd as per standard Fugro Procedure. After merging the navigation, the raw SEG D data underwent a series of sequential processing flows onboard such as de-noise, linear noise attenuation, applying preliminary statics, de-ghosting, de-multiple, velocity picking, applying final statics, zero phase data adjustments and migration. The final migrated brute stacks were then checked for any data gaps with reference to the proposed line plan.

Although data quality of 2D-UUHR (MCS) data was generally good for the entire survey blocks, some lines had vertical noise and cavitation caused by marginal weather condition acquisitions. This noise was reduced during further processing.

Some lines had noise at bottom of the stacks, which was caused by overlapping of the shots due to high vessel speed. These shots were muted during processing.

Further details including additional data examples are included in the Fugro Operations Reports complied during the project. Refer to reports F172145-REP-OPS-001 (Fugro Pioneer) and F172145-REP-OPS-002 (Fugro Frontier).

6. References

Andersen, S. (1998) Israndslinier i Norden. Nordic Council of Ministers.

Andrén, T., Jorgensen, B.B., Cotterill, C. and Green, S. (2015a). IODP Expedition 347: *Baltic Sea basin paleoenvironment and biosphere*. Scientific Drilling, 20, 1-12.

Andrén, T., Jorgensen, B.B., Cotterill, C., Green, S. and the Expedition 347 Scientists (2015b). Expedition 347 Summary, Proceedings of the Integrated Ocean Drilling Program, Volume 347.

Bendixen, C., Jensen, J.B., Boldreel, L.O., Clausen, O.R., Bennike, O., Seidenkrantz, M.-S., Nyberg, J., and Hübscher, C. (2015). *The Holocene Great Belt connection to the southern Kattegat, Scandinavia: Ancylus Lake drainage and Early Littorina Sea transgression*. Boreas 46(1), 53-68. https://doi.org/10.1111/bor.12154

Bendixen, C., Boldreel, L.O., Jensen, J.B., Bennike, O., Hübscher, C., and Clausen, O.R. (2017). *Early Holocene estuary development of the Hesselø Bay area, southern Kattegat, Denmark and its implication for Ancylus Lake drainage*. Geo-Marine Letters 37, 579-591. https://doi.org/10.1007/s00367-017-0513-7

Danish Råstofbekendtgørelsen (BEK no. 1680 of 17/12/2018, Phase IB) - Template Survey Geodatabase (TSG): Requirements to TSG

Energinet. (2020). Geophysical survey, Hesselø offshore wind farm – Scope of Services – Enclosure 1 - Technical requirements, Document No. 20/03856-4, dated 01 July 2020.

Erlström, M., and Sivhed, U. (2001). *Intra-cratonic dextral transtension and inversion of the southern Kattegat on the southwest margin of Baltica – Seismostratigraphy and structural development*. Sverige Geologiska Undersökning. Research Paper C 832.

Gardline, (2021). Preliminary borehole logs (PDF format) of four (4) locations within the HOWF site. Provided by Energinet to Fugro on 10 June 2021.

GEUS. (2020). *General geology of southern Kattegat; the Hesselø wind farm area; Desk Study*. GEUS Rapport 2020/53.

Houmark-Nielsen, M., and Kjær, K.H. (2003). *Southwest Scandinavia, 40–15 kyr BP: palaeogeography and environmental change*. Journal of Quaternary Science 18(8), 169-186. https://doi.org/10.1002/jqs.802

Jensen, P., Aagaard, I., Burke Jr., R.A., Dando, P.R., Jorgensen, N.O., Kuijpers, A., Laier, T., O'Hara, S.C.M. and Schmaljohann, R. (1992). *'Bubbling reefs' in the Kattegat: Submarine landscapes of carbonate-cemented rocks support a diverse ecosystem at methane seeps*. Marine Ecology Progress Series, V. 83, P. 103-112.

Jensen, J.B., Petersen, K.S., Konradi, P., Kuijpers, A., Bennike, O., Lemke, W., and Endler, R. (2002). *Neotectonics, sea-level changes and biological evolution in the Fennoscandian Border*

Zone of the southern Kattegat Sea. Boreas 31(2), 133-150. https://doi.org/10.1111/j.1502-3885.2002.tb01062.x

Judd, A and Hovland, M., (2007). *Seabed Fluid Flow: The impact on geology, biology and the marine environment*, Cambridge University Press, pp. 475.

Larsen, G., Frederiksen, J., Villumsen, A., Fredericia, J., Graversen, P., Foged, N., Knudsen, B. and Baumann, J., (1995). *A guide to engineering geological soil description*, Danish Geotechnical Society – Bulletin, Revision 1., pp 129.

Larsen, N.K., Knudsen, K.L., Krohn, C.F., Kronborg, C., Murray, A.S., and Nielsen, O.B. (2009). *Late Quaternary ice sheet, lake and sea history of southwest Scandinavia – a synthesis*. Boreas 38(4), 732-761. https://doi.org/10.1111/j.1502-3885.2009.00101.x

Leth, J.O. (ed.) et al., (2014). Danmarks digitale havbundssedimentkort 1:250.000

Appendices

Appendix A

Guidelines on Use of Report

This report (the "Report") was prepared as part of the services (the "Services") provided by Fugro for its client (the "Client") and in accordance with the terms of the relevant contract between the two parties (the Contract") and to the extent to which Fugro relied on Client or third party information as was set out in the Contract.

Fugro's obligations and liabilities to the Client or any other party in respect of this Report are limited to the extent and for the time period set out in the Contract (or in the absence of any express provision in the Contract as implied by the law of the Contract) and Fugro provides no other representation or warranty whether express or implied, in relation to the use of this Report, for any purpose. Furthermore, Fugro has no obligation to update or revise this Report based on any future changes in conditions or information which emerge following issue of this Report unless expressly required by the provisions of the Contract.

This Report was formed and released by Fugro exclusively for the Client and any other party expressly identified in the Contract, and any use and/or reliance on the Report or the Services for purposes not expressly stated in the Contract, will be at the Client's sole risk. Any other party seeking to rely on this Report does so wholly at its own and sole risk and Fugro accepts no liability whatsoever for any such use and/or reliance."

Appendix B

Charts

Charts (detailed below) have been presented as a separate PDF file.

Chart Type	Chart Name
OVERVIEW CHART	SN2020_031_Hesselo_OWF_01_NU_25k_OVERVIEW_North
OVERVIEW CHART	SN2020_031_Hesselo_OWF_02_NU_25k_OVERVIEW_South
CRP TRACKS AND GRAB SAMPLE LOCATION CHART	SN2020_031_Hesselo_OWF_03_NU_25k_CRP_GRAB_North
CRP TRACKS AND GRAB SAMPLE LOCATION CHART	SN2020_031_Hesselo_OWF_04_NU_25k_CRP_GRAB_South
SHADED RELIEF BATHYMETRY CHART	SN2020_031_Hesselo_OWF_05_NU_25k_SHR_BTY_North
SHADED RELIEF BATHYMETRY CHART	SN2020_031_Hesselo_OWF_06_NU_25k_SHR_BTY_South
BACKSCATTER MOSAIC CHART	SN2020_031_Hesselo_OWF_07_NU_25k_BKS_North
BACKSCATTER MOSAIC CHART	SN2020_031_Hesselo_OWF_08_NU_25k_BKS_South
SEAFLOOR CLASSIFICATION - MORPHOLOGY CHART	SN2020_031_Hesselo_OWF_09_NU_25k_SBC_MORPHOLOGY_North
SEAFLOOR CLASSIFICATION - MORPHOLOGY CHART	SN2020_031_Hesselo_OWF_10_NU_25k_SBC_MORPHOLOGY_South
SEAFLOOR CLASSIFICATION - SUBSTRATE TYPE CHART	SN2020_031_Hesselo_OWF_11_NU_25k_SBC_SUBSTRATE_North
SEAFLOOR CLASSIFICATION - SUBSTRATE TYPE CHART	SN2020_031_Hesselo_OWF_12_NU_25k_SBC_SUBSTRATE_South
SEAFLOOR CLASSIFICATION - GEOLOGY CHART	SN2020_031_Hesselo_OWF_13_NU_25k_SBC_GEOLOGY_North
SEAFLOOR CLASSIFICATION - GEOLOGY CHART	SN2020_031_Hesselo_OWF_14_NU_25k_SBC_GEOLOGY_South
SEABED OBJECTS CHART	SN2020_031_Hesselo_OWF_15_NU_25k_SBO_North
SEABED OBJECTS CHART	SN2020_031_Hesselo_OWF_16_NU_25k_SBO_South
SEABED FEATURES CHART	SN2020_031_Hesselo_OWF_17_NU_25k_SBF_North
SEABED FEATURES CHART	SN2020_031_Hesselo_OWF_18_NU_25k_SBF_South
DEPTH TO HORIZON H01 (METRES BSF) - TOP OF UNIT B	SN2020_031_Hesselo_OWF_19_NU_25k_SBG_DEPTH_BSF_H01_North
DEPTH TO HORIZON H01 (METRES BSF) - TOP OF UNIT B	SN2020_031_Hesselo_OWF_20_NU_25k_SBG_DEPTH_BSF_H01_South
DEPTH TO HORIZON H05 (METRES BSF) - TOP OF UNIT C	SN2020_031_Hesselo_OWF_21_NU_25k_SBG_DEPTH_BSF_H05_North
DEPTH TO HORIZON H05 (METRES BSF) - TOP OF UNIT C	SN2020_031_Hesselo_OWF_22_NU_25k_SBG_DEPTH_BSF_H05_South
DEPTH TO HORIZON H10 (METRES BSF) - BASE HOLOCENE	SN2020_031_Hesselo_OWF_23_NU_25k_SBG_DEPTH_BSF_H10_North
DEPTH TO HORIZON H10 (METRES BSF) - BASE HOLOCENE	SN2020_031_Hesselo_OWF_24_NU_25k_SBG_DEPTH_BSF_H10_South
DEPTH TO HORIZON H01 (METRES MSL) - TOP OF UNIT B	SN2020_031_Hesselo_OWF_25_NU_25k_SBG_DEPTH_MSL_H01_North

Chart Type	Chart Name
DEPTH TO HORIZON H01 (METRES MSL) - TOP OF UNIT B	SN2020_031_Hesselo_OWF_26_NU_25k_SBG_DEPTH_MSL_H01_South
DEPTH TO HORIZON H05 (METRES MSL) - TOP OF UNIT C	SN2020_031_Hesselo_OWF_27_NU_25k_SBG_DEPTH_MSL_H05_North
DEPTH TO HORIZON H05 (METRES MSL) - TOP OF UNIT C	SN2020_031_Hesselo_OWF_28_NU_25k_SBG_DEPTH_MSL_H05_South
DEPTH TO HORIZON H10 (METRES MSL) - BASE HOLOCENE	SN2020_031_Hesselo_OWF_29_NU_25k_SBG_DEPTH_MSL_H10_North
DEPTH TO HORIZON H10 (METRES MSL) - BASE HOLOCENE	SN2020_031_Hesselo_OWF_30_NU_25k_SBG_DEPTH_MSL_H10_South
DEPTH TO HORIZON H15 (METRES BSF) - INTERNAL HORIZON IN UNIT D	SN2020_031_Hesselo_OWF_31_NU_25k_SBG_DEPTH_BSF_H15_North
DEPTH TO HORIZON H15 (METRES BSF) - INTERNAL HORIZON IN UNIT D	SN2020_031_Hesselo_OWF_32_NU_25k_SBG_DEPTH_BSF_H15_South
DEPTH TO HORIZON H20 (METRES BSF) - BASE OF UNIT D	SN2020_031_Hesselo_OWF_33_NU_25k_SBG_DEPTH_BSF_H20_North
DEPTH TO HORIZON H20 (METRES BSF) - BASE OF UNIT D	SN2020_031_Hesselo_OWF_34_NU_25k_SBG_DEPTH_BSF_H20_South
DEPTH TO HORIZON H25 (METRES BSF) - BASE OF UNIT E	SN2020_031_Hesselo_OWF_35_NU_25k_SBG_DEPTH_BSF_H25_North
DEPTH TO HORIZON H25 (METRES BSF) - BASE OF UNIT E	SN2020_031_Hesselo_OWF_36_NU_25k_SBG_DEPTH_BSF_H25_South
DEPTH TO HORIZON H30 (METRES BSF) - BASE OF UNIT F	SN2020_031_Hesselo_OWF_37_NU_25k_SBG_DEPTH_BSF_H30_North
DEPTH TO HORIZON H30 (METRES BSF) - BASE OF UNIT F	SN2020_031_Hesselo_OWF_38_NU_25k_SBG_DEPTH_BSF_H30_South
DEPTH TO HORIZON H35 (METRES BSF) - BASE OF UNIT G	SN2020_031_Hesselo_OWF_39_NU_25k_SBG_DEPTH_BSF_H35_North
DEPTH TO HORIZON H35 (METRES BSF) - BASE OF UNIT G	SN2020_031_Hesselo_OWF_40_NU_25k_SBG_DEPTH_BSF_H35_South
DEPTH TO HORIZON H50 (METRES BSF) - BASE OF UNIT H	SN2020_031_Hesselo_OWF_41_NU_25k_SBG_DEPTH_BSF_H50_North
DEPTH TO HORIZON H50 (METRES BSF) - BASE OF UNIT H	SN2020_031_Hesselo_OWF_42_NU_25k_SBG_DEPTH_BSF_H50_South
DEPTH TO HORIZON H15 (METRES MSL) - INTERNAL HORIZON IN UNIT D	SN2020_031_Hesselo_OWF_43_NU_25k_SBG_DEPTH_MSL_H15_North
DEPTH TO HORIZON H15 (METRES MSL) - INTERNAL HORIZON IN UNIT D	SN2020_031_Hesselo_OWF_44_NU_25k_SBG_DEPTH_MSL_H15_South
DEPTH TO HORIZON H20 (METRES MSL) - BASE OF UNIT D	SN2020_031_Hesselo_OWF_45_NU_25k_SBG_DEPTH_MSL_H20_North
DEPTH TO HORIZON H20 (METRES MSL) - BASE OF UNIT D	SN2020_031_Hesselo_OWF_46_NU_25k_SBG_DEPTH_MSL_H20_South
DEPTH TO HORIZON H25 (METRES MSL) - BASE OF UNIT E	SN2020_031_Hesselo_OWF_47_NU_25k_SBG_DEPTH_MSL_H25_North

Chart Type	Chart Name
DEPTH TO HORIZON H25 (METRES MSL) - BASE OF UNIT E	SN2020_031_Hesselo_OWF_48_NU_25k_SBG_DEPTH_MSL_H25_South
DEPTH TO HORIZON H30 (METRES MSL) - BASE OF UNIT F	SN2020_031_Hesselo_OWF_49_NU_25k_SBG_DEPTH_MSL_H30_North
DEPTH TO HORIZON H30 (METRES MSL) - BASE OF UNIT F	SN2020_031_Hesselo_OWF_50_NU_25k_SBG_DEPTH_MSL_H30_South
DEPTH TO HORIZON H35 (METRES MSL) - BASE OF UNIT G	SN2020_031_Hesselo_OWF_51_NU_25k_SBG_DEPTH_MSL_H35_North
DEPTH TO HORIZON H35 (METRES MSL) - BASE OF UNIT G	SN2020_031_Hesselo_OWF_52_NU_25k_SBG_DEPTH_MSL_H35_South
DEPTH TO HORIZON H50 (METRES MSL) - BASE OF UNIT H	SN2020_031_Hesselo_OWF_53_NU_25k_SBG_DEPTH_MSL_H50_North
DEPTH TO HORIZON H50 (METRES MSL) - BASE OF UNIT H	SN2020_031_Hesselo_OWF_54_NU_25k_SBG_DEPTH_MSL_H50_South
THICKNESS UNIT A (METRES)	SN2020_031_Hesselo_OWF_55_NU_25k_SBG_THICKNESS_UNIT_A_North
THICKNESS UNIT A (METRES)	SN2020_031_Hesselo_OWF_56_NU_25k_SBG_THICKNESS_UNIT_A_South
THICKNESS UNIT B (METRES)	SN2020_031_Hesselo_OWF_57_NU_25k_SBG_THICKNESS_UNIT_B_North
THICKNESS UNIT B (METRES)	SN2020_031_Hesselo_OWF_58_NU_25k_SBG_THICKNESS_UNIT_B_South
THICKNESS UNIT C (METRES)	SN2020_031_Hesselo_OWF_59_NU_25k_SBG_THICKNESS_UNIT_C_North
THICKNESS UNIT C (METRES)	SN2020_031_Hesselo_OWF_60_NU_25k_SBG_THICKNESS_UNIT_C_South
THICKNESS UNIT D (METRES)	SN2020_031_Hesselo_OWF_61_NU_25k_SBG_THICKNESS_UNIT_D_North
THICKNESS UNIT D (METRES)	SN2020_031_Hesselo_OWF_62_NU_25k_SBG_THICKNESS_UNIT_D_South
THICKNESS UNIT E (METRES)	SN2020_031_Hesselo_OWF_63_NU_25k_SBG_THICKNESS_UNIT_E_North
THICKNESS UNIT E (METRES)	SN2020_031_Hesselo_OWF_64_NU_25k_SBG_THICKNESS_UNIT_E_South
THICKNESS UNIT F (METRES)	SN2020_031_Hesselo_OWF_65_NU_25k_SBG_THICKNESS_UNIT_F_North
THICKNESS UNIT F (METRES)	SN2020_031_Hesselo_OWF_66_NU_25k_SBG_THICKNESS_UNIT_F_South
THICKNESS UNIT G (METRES)	SN2020_031_Hesselo_OWF_67_NU_25k_SBG_THICKNESS_UNIT_G_North
THICKNESS UNIT G (METRES)	SN2020_031_Hesselo_OWF_68_NU_25k_SBG_THICKNESS_UNIT_G_South
THICKNESS UNIT H (METRES)	SN2020_031_Hesselo_OWF_69_NU_25k_SBG_THICKNESS_UNIT_H_North
THICKNESS UNIT H (METRES)	SN2020_031_Hesselo_OWF_70_NU_25k_SBG_THICKNESS_UNIT_H_South
GEOLOGICAL FEATURES CHART	SN2020_031_Hesselo_OWF_71_NU_25k_GEOF_North
GEOLOGICAL FEATURES CHART	SN2020_031_Hesselo_OWF_72_NU_25k_GEOF_South
Seabed Geology Cross-Section Profile	SN2020_031_Hesselo_OWF_73_PR_25k_SBP_2DUUHR_01
Seabed Geology Cross-Section Profile	SN2020_031_Hesselo_OWF_74_PR_25k_SBP_2DUUHR_02
Seabed Geology Cross-Section Profile	SN2020_031_Hesselo_OWF_75_PR_25k_SBP_2DUUHR_03
Seabed Geology Cross-Section Profile	SN2020_031_Hesselo_OWF_76_PR_25k_SBP_2DUUHR_04
Seabed Geology Cross-Section Profile	SN2020_031_Hesselo_OWF_77_PR_25k_SBP_2DUUHR_05
Seabed Geology Cross-Section Profile	SN2020_031_Hesselo_OWF_78_PR_25k_SBP_2DUUHR_06
Seabed Geology Cross-Section Profile	SN2020_031_Hesselo_OWF_79_PR_25k_SBP_2DUUHR_07
Seabed Geology Cross-Section Profile	SN2020_031_Hesselo_OWF_80_PR_25k_SBP_2DUUHR_08

Appendix C

2D UHR Processing Report

fugro

2D-UUHR Processing Report

Energinet Denmark Hesselø Geophysical Survey | *Denmark, Inner Danish Sea, Kattegat*

F172145-REP-PROC-001 01 | 21 January 2021

Complete

Energinet Eltransmission A/S

ENERGINET

Document Control

Document Information

Project Title	Hesselø Offshore Wind Farm, 2D Seismic Survey
Document Title	2D-UUHR Processing Report
Fugro Project No.	F172145
Fugro Document No.	F172145-REP-PROC-001
Issue Number	01
Issue Status	Complete

Client Information

Client	Energinet Eltransmission A/S
Client Address	Tonne Kjærsvej 65, DK-7000 Fredericia, Denmark
Client Contact	Nicky Hein Witt
Client Document No.	N/A

Revision History

Issue	Date	Status	Comments on Content	Prepared By	Checked By	Approved By
01	21 Jan 2021	Complete		GS	AE	PB

Project Team

Initials	Name	Role
MT	Maria Theander	Global Product Owner – Seismic Processing Marine Site Characterisation
PB	Patrick Burn	Operations Supervisor - Seismic Processing Marine Site Characterisation
GS	Graeme Scott	Inhouse Seismic Processing Geophysicist
IW	Iain Walby	Onboard Seismic Processing Geophysicist – Pioneer
ML	Mark Lee	Onboard Seismic Processing Geophysicist – Pioneer
MS	Moumita Sasmal	Onboard Seismic Processing Geophysicist – Frontier
NB	Nikolai Blokhin	Onboard Seismic Processing Geophysicist – Frontier

Contents

Appendices

Figures

FUGRO

Tables

Abbreviations

2D-UUHR	Two Dimensional Ultra Ultra High Resolution
CDP	Common Depth-point
CMP	Common Mid-Point
DGPS	Differential Global Positioning System
FTP	File Transfer Protocol
F-K	Frequency - wave number
F-X	Frequency - space domain
GPS	Global Positioning System
LNA	Linear Noise Attenuation
MLSS	Multi-Level Stacked Sparker
MSL	Mean Sea Level
NMO	Normal Move Out
PoSTM	Post-Stack Time Migration
QC	Quality Control
SFT	Secure File Transfer
SRME	Surface Related Multiple Elimination
TWTT	Two-Way Travel Time
UTM	Universal Transverse Mercator
WB_ZO	Water Bottom Zero Offset Time
X-T	Space – Time Domain
.csv	Comma Separated Values

FUGRO

1. Introduction

Energinet Eltransmission A/S (Energinet) is developing a new offshore wind farm in the inner Danish Sea, Kattegat, the Hesselø Offshore Windfarm (HOWF). The project area is located between Denmark and Sweden approximately 30km North of Sjælland.

The seismic processing report aims to detail the step by step processes used to get the best imaging of the seismic data. The techniques involved aim to reduce the noise in the datasets, improve signal to noise ratios, and improve upon the acquisition brute bandwidth of the data.

1.1 Scope of Work

Fugro acquired 2D Ultra Ultra High Resolution (2D-UUHR) seismic data at the Hesselø offshore wind farm, utilising two vessels; the Fugro Frontier and Fugro Pioneer. The data were QC'd offshore and processed onshore, using Fugro *Uniseis* software.

The aim of this survey was to acquire and provide high quality and high resolution data of the work locations. The data from the survey will assist the client to determine the water depth, seabed sediment types, seabed features, and obstructions identifying any hazards in the shallow section (seabed risk assessment).

In general data was of high quality. Lines were assessed onboard between the QC and client to determine if a client concession could be issued for lines that were technically out of spec.

Other requirements of the 2D-UUHR were imaging a minimum target depth of 100m below the seabed and achieving a vertical resolution of 0.3m in the very shallow section.
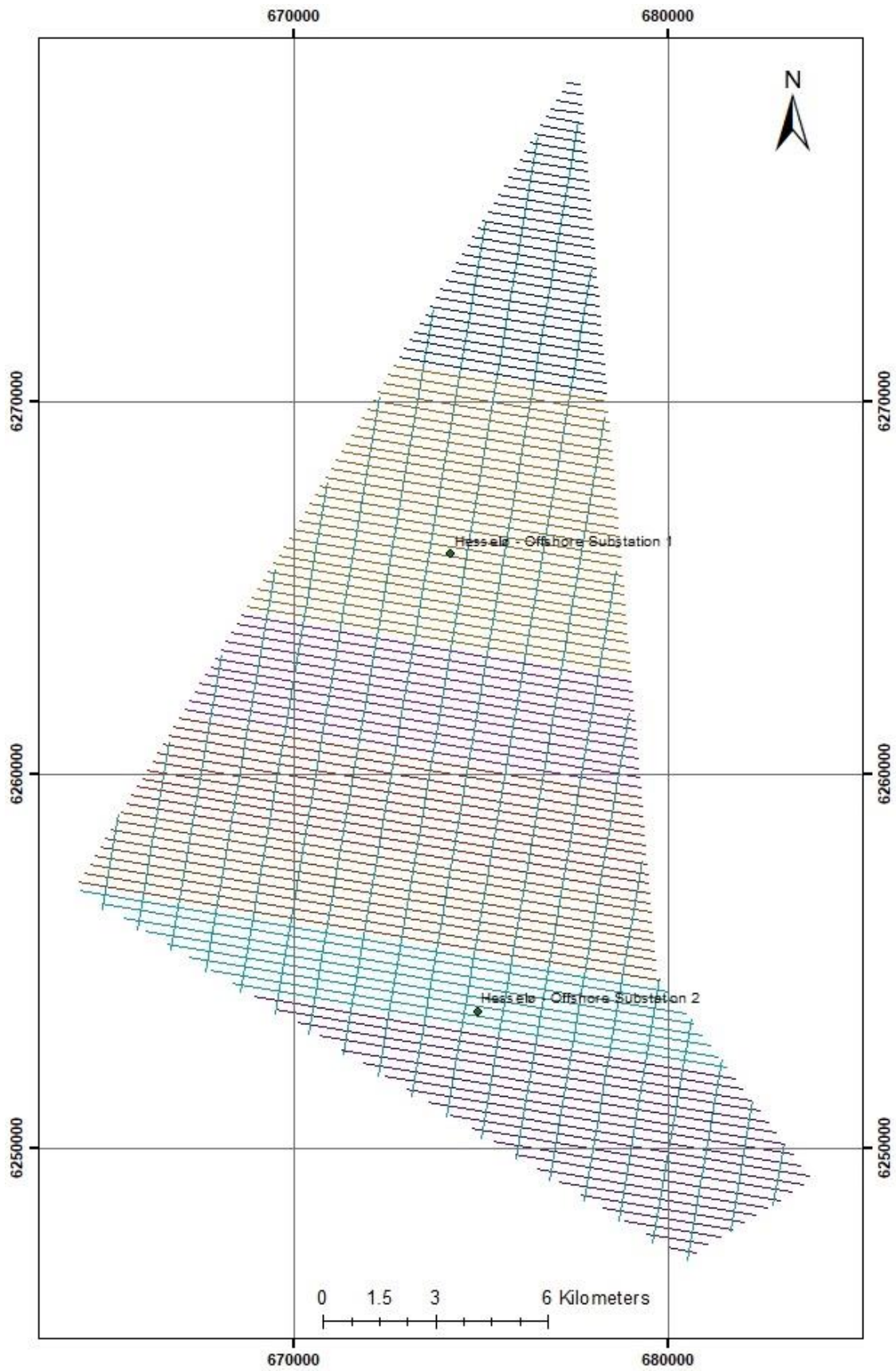
Figure 1.1: Hesselø 2D-UUHR Line Plan

1.2　　Acquisition Configuration

Table 1.1: 2D-UUHR Acquisition parameters

Acquisition	
Source	
Type	Multi-Level Stacked Sparker (MLSS)
Power	900 Joules (300 / 300 / 300)
Shot Interval	0.5 m
Depth	0.52 m, 0.67 m, 1.12 m
Streamer	
Model	GeoEel gel filled hybrid
Groups	48 (24 / 24)
Group Interval	1 m / 2 m
Active Length	72 m
Near Offset	~5 m
Recording System	
Model	TTS
Sample interval	0.125 ms
Record length	219.875 ms
Format	SEG-D

FUGRO

2. Processing 2D-UUHR

2.1 2D-UUHR Processing Summary

The agreed processing flow was applied to all the lines as follows:

- Reformat from SEG-D
- Apply recording delay correction static: 0 ms (No delay on TTS recording system)
- Apply low-cut filter: 20Hz / 18 dB/Oct
- Apply T^2 spherical divergence
- Merge seismic with source & receiver navigation, update offsets, assign 2D geometry
- Pick zero offset seabed – assign hyperbolic seabed time per channel
- Edit out bad shots / channels identified from offshore QC
- Shot domain swell noise attenuation
- Channel domain swell noise attenuation
- Receiver domain swell noise attenuation
- Linear noise attenuation
- Temporary statics application (to aid QC – statics reassessed after final velocities)
- Source Deghosting
- Receiver Deghosting
- 2D SRME
- Velocity analysis in Pegasus: 250 m pick intervals
- Sort to CMP domain
- NMO using picked velocity
- Final statics application
- Outer trace final mute
- Stack using 1/N trace normalisation – 48 fold max
- Zero phase filter application using data derived wavelet (positive seabed)
- Post stack pre migration processing
- Post stack Kirchhoff time migration
- Post stack surface wave noise attenuation
- Time variant bandpass filter
- Inverse Amplitude Q compensation
- Apply source and receiver datum correction
- Apply tidal static correction
- Cosmetic seabed mute
- Output to SEG-Y

2.2 Reformatting and Navigation Merge

For each sequence, raw field data in SEG-D format was reformatted into *Uniseis* internal processing format. As part of the reformatting process a bulk shift is applied to the data to compensate for the delay in the recording system. The TTS recoding system has zero start of data delay, so the resulting trace data had the original acquired 219.875 ms record length and a sample rate of 0.125 ms. A de-bias low-cut filter of 20 Hz / 18 dB/Octave was applied to the data in order to remove low frequency noise and instrument DC bias prior to processing. A spherical divergence correction (time squared) was applied to the data to aid in QC and further processing.

A QC of the data was conducted on the vessel so that any missing shots, bad channels and noisy records that may have an adverse effect on data quality could be identified.

Geometry was assigned in order to give each trace a CMP number and source / receiver positions were merged into the seismic dataset in order to get accurate offsets and locations for the data prior to velocity picking. Correct CMP locations enabled trends from nearby lines to be used in order to help with consistency and accuracy of velocity picks.

Finally, at this stage, near trace gathers were used to interactively pick a zero offset water bottom time (near trace seabed time with normal moveout applied) for use in later processing.
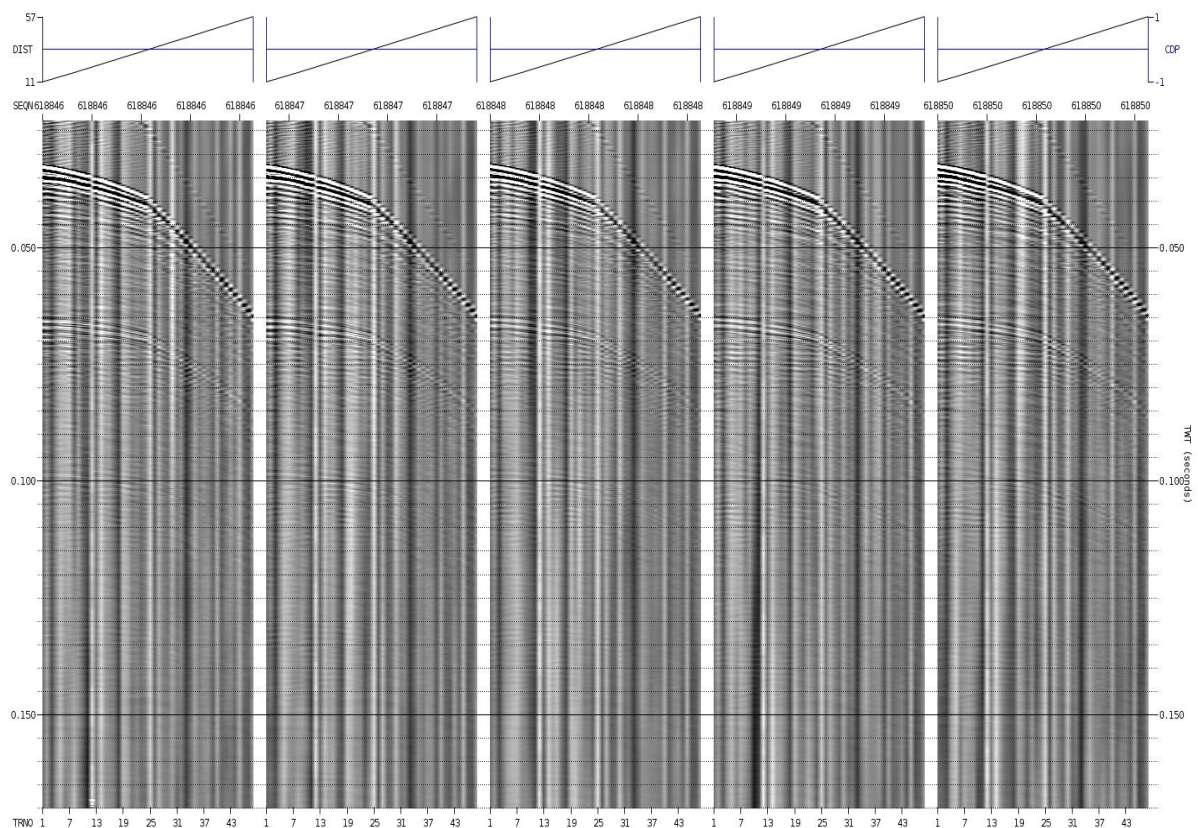
Figure 2.1: Reformat: Raw shots
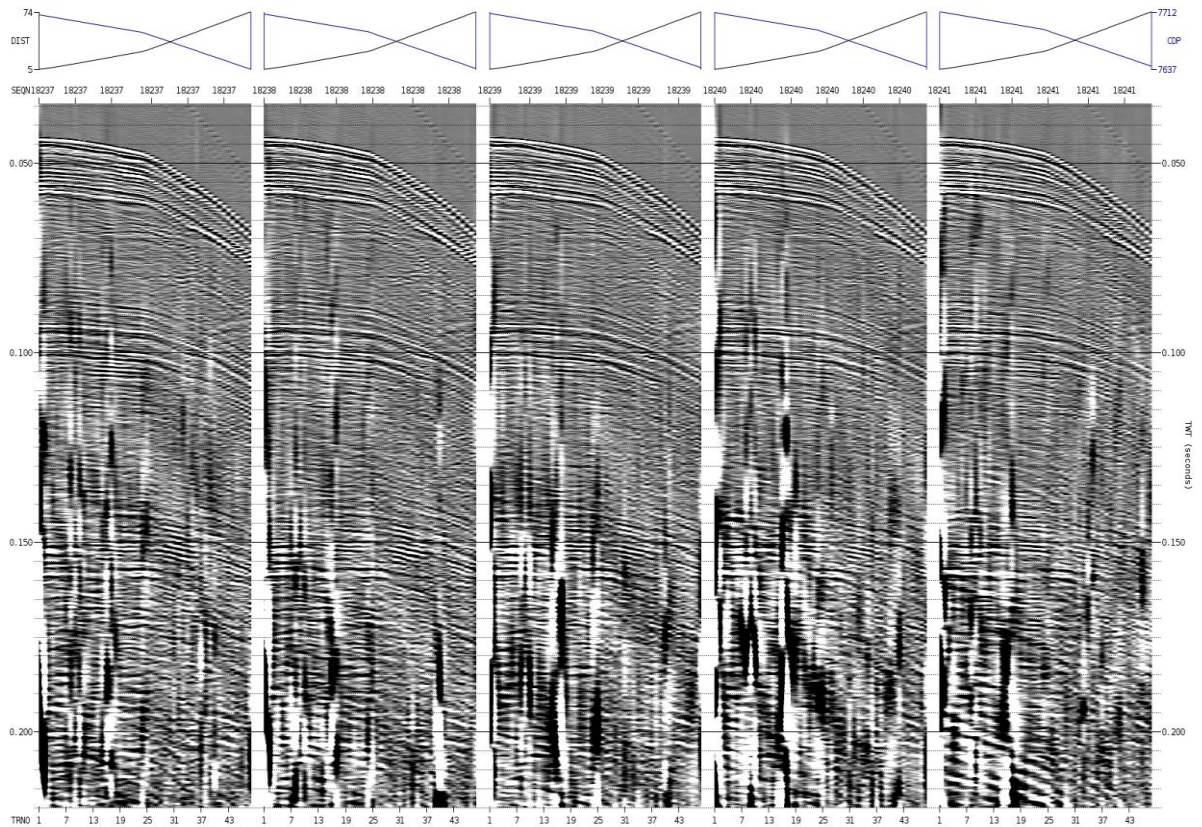
Figure 2.2: Reformat: Low cut and geometrical spreading

2.3 Swell Noise Attenuation

Swell noise was effectively attenuated using the *Uniseis 'SWNA'* and *'TFDN'* tools. The *'TFDN'* algorithm makes use of the fact that, unlike an impulsive source such as a shot, the amplitude of the swell noise will not decay with time since it is being continuously generated during recording. The process decomposes the trace data into signal and noise components, down-weighting or removing the noise to leave a clean trace.

An initial pass of de-swell (TFDN) was applied to frequencies up to 100Hz in the shot domain. Dip attenuation (SWNA) was then applied to attenuate any non-physical dips up to 100Hz below 1000 m/s apparent velocity. This was followed by a second pass of TFDN / SWNA performed in the channel domain up to 100 Hz, and a third pass of TFDN / SWNA in the receiver domain up to 150Hz.

Higher values than 150 Hz were tested, but these did not show any improvement in swell noise attenuation, as it is predominantly a lot lower frequency than this. The maximum value of 150Hz was based on no improvement to the denoise routine, only an increase in CPU runtime if we went any larger.
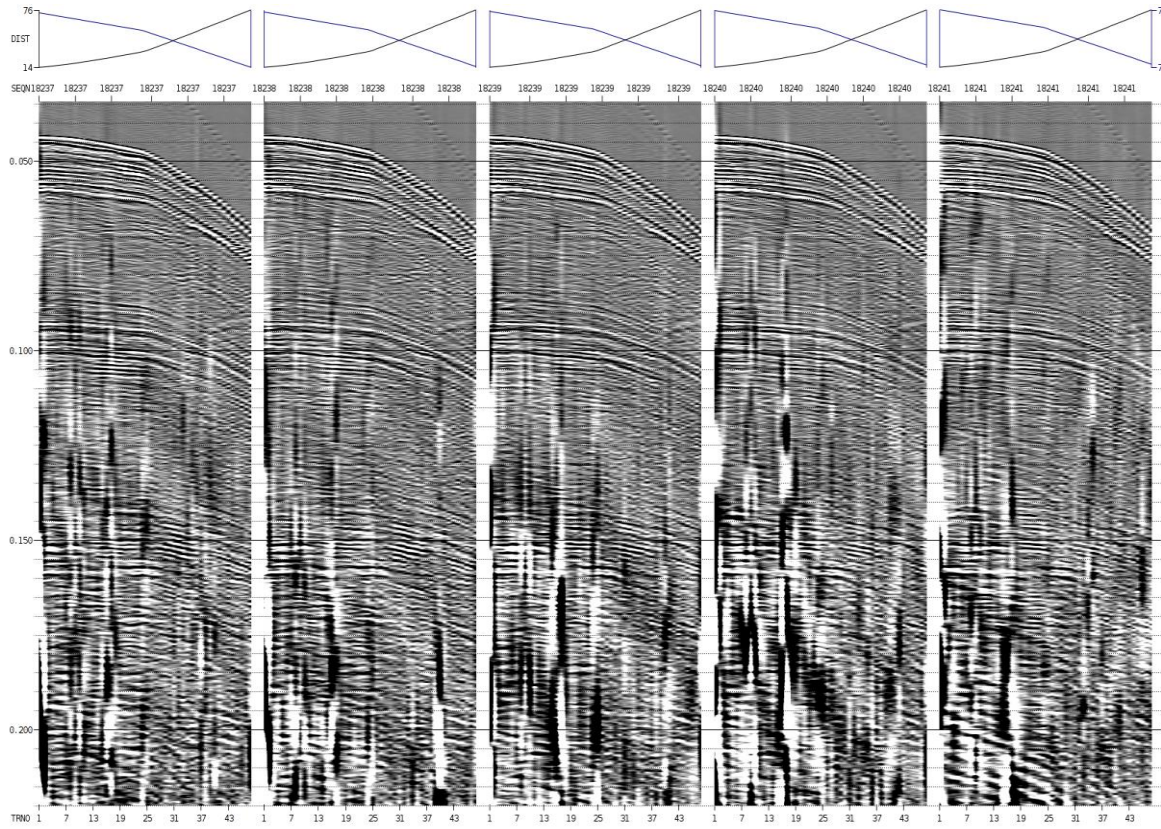
Figure 2.3: Denoise: Input shots
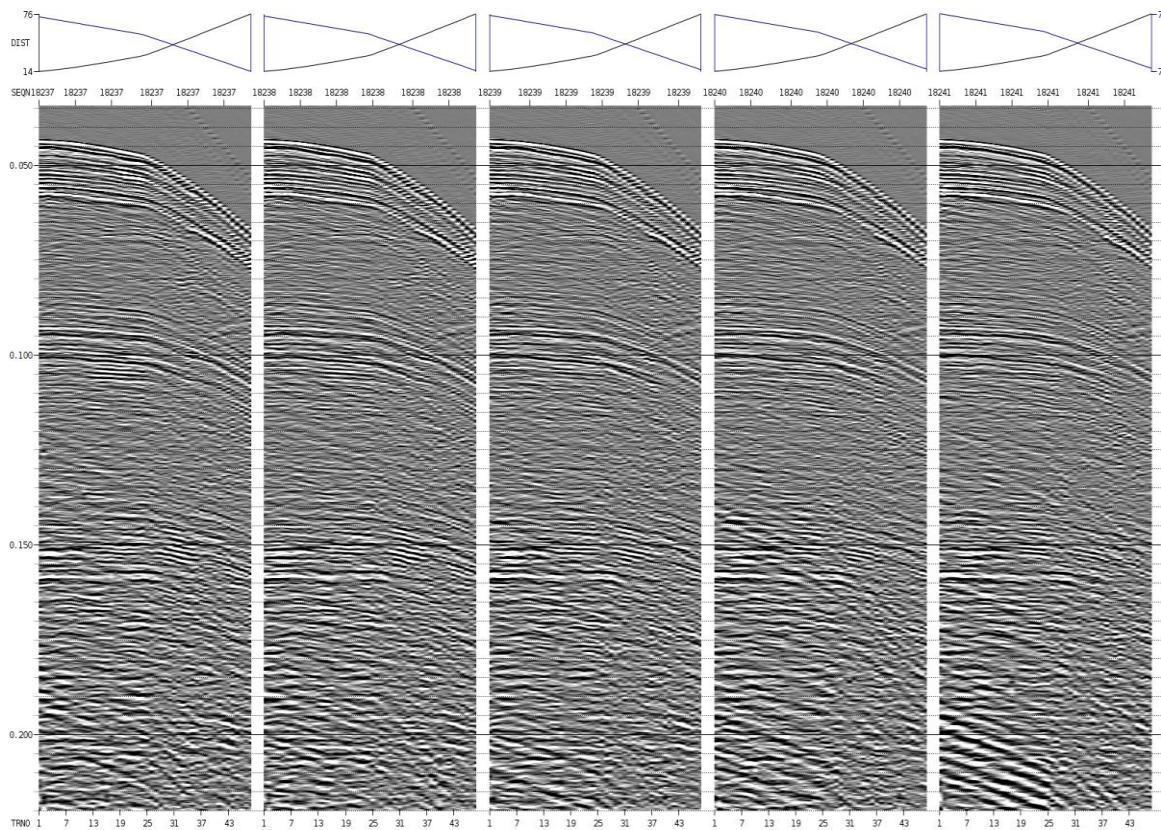
Figure 2.4: Denoise: Output shots
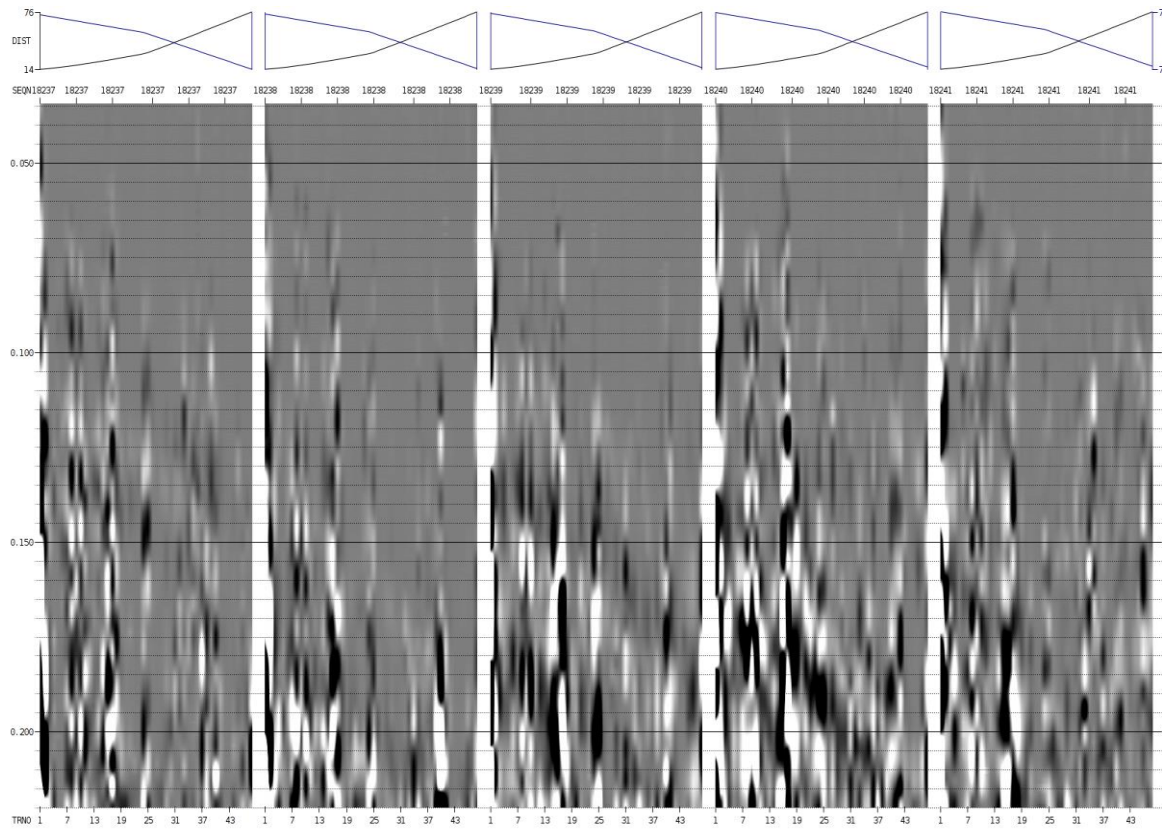
Figure 2.5: Denoise: Difference
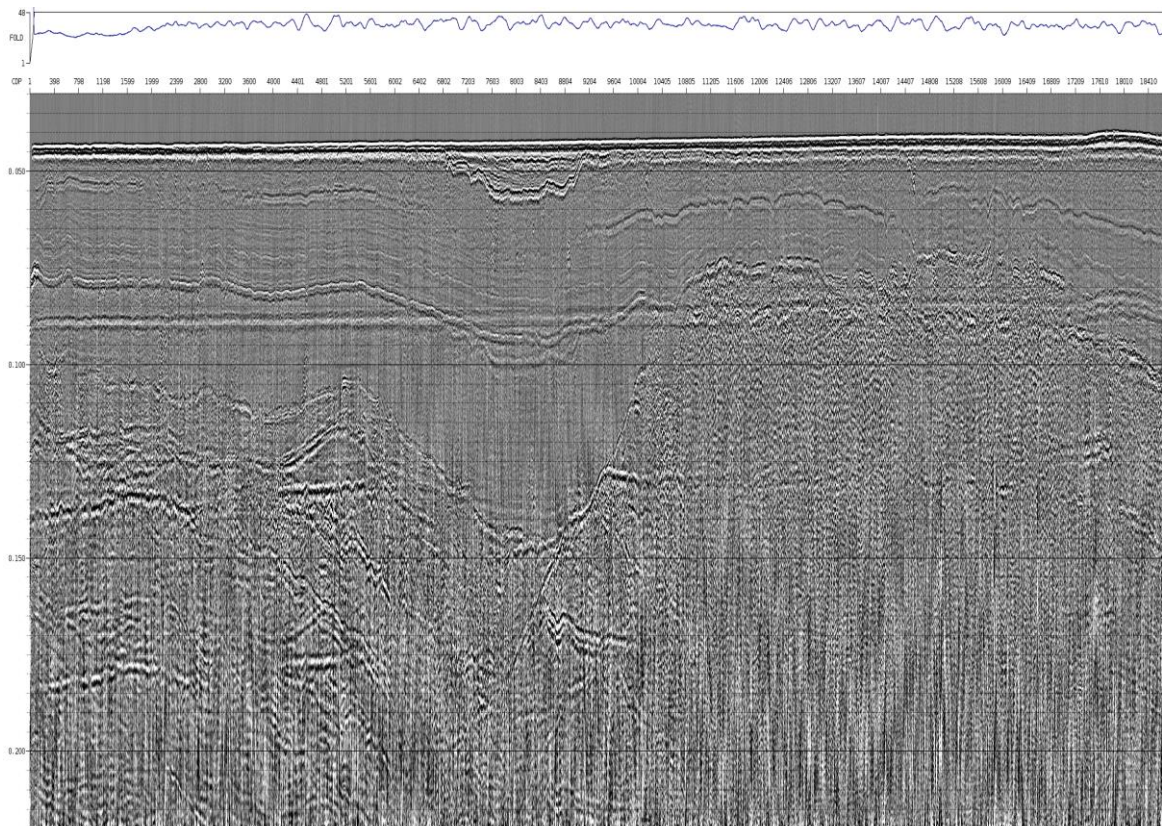
Figure 2.6: Denoise: Input stack
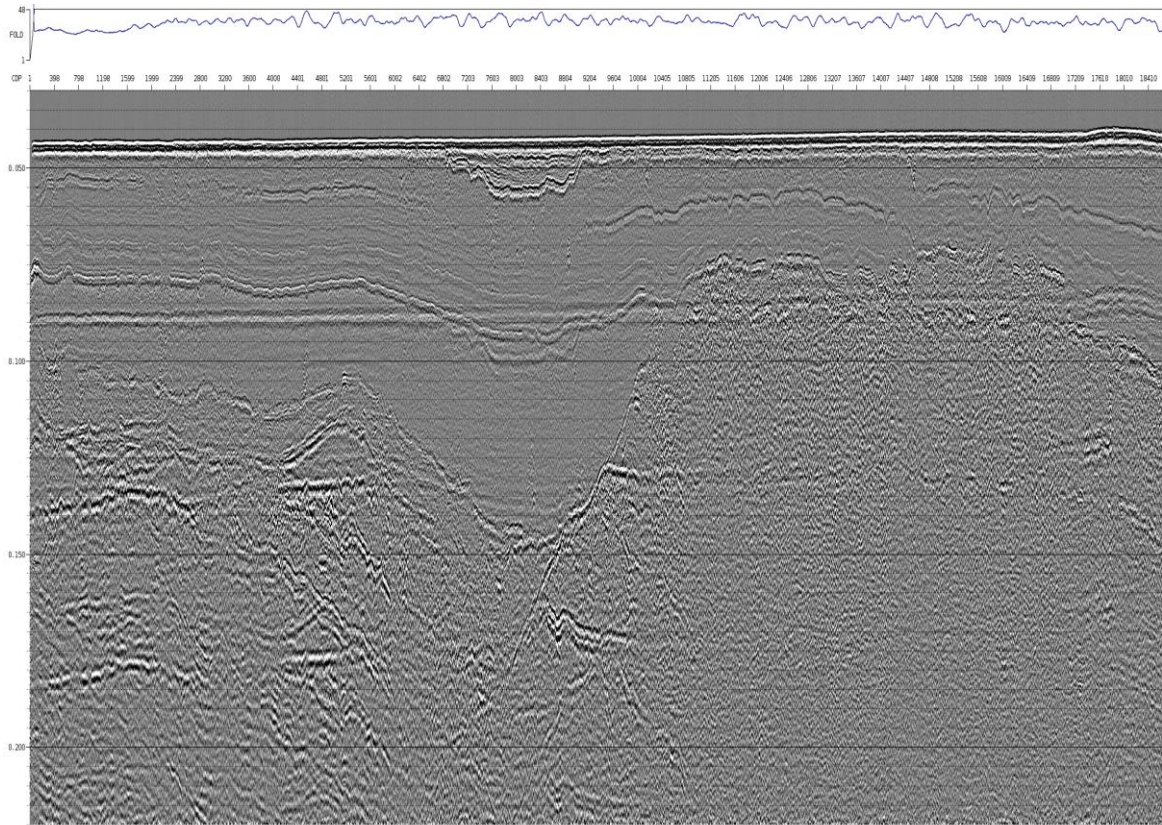
Figure 2.7: Denoise: Output stack
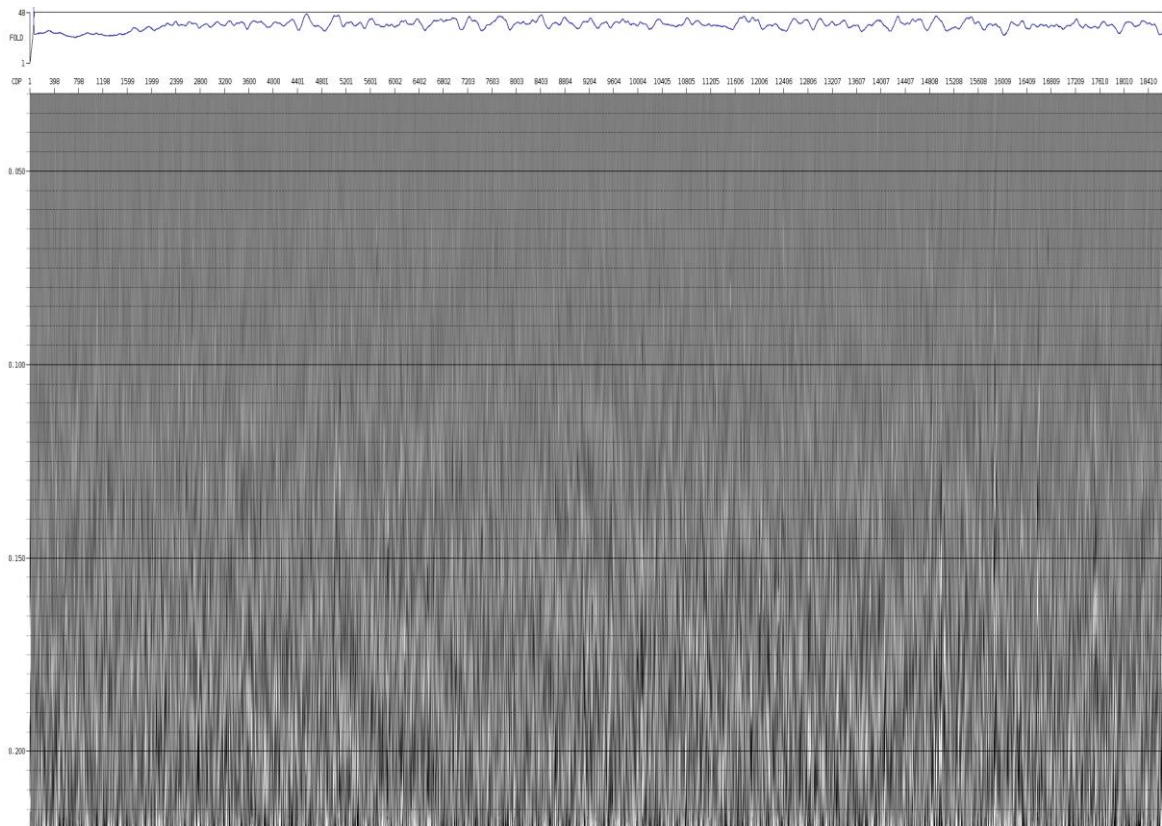
Figure 2.8: Denoise: Difference

2.4   Linear Noise Attenuation

Linear noise was observed on most lines in this survey. A Tau-P linear transform was applied to the data to effectively attenuate this noise. An NMO-correction was applied first using a brute velocity then data with dip greater than 30 ms at maximum offset was muted from the full Tau-P transform. Values of ±25 ms transform range began to show hints of primary removal, and ±35 ms was less effective at linear noise attenuation.
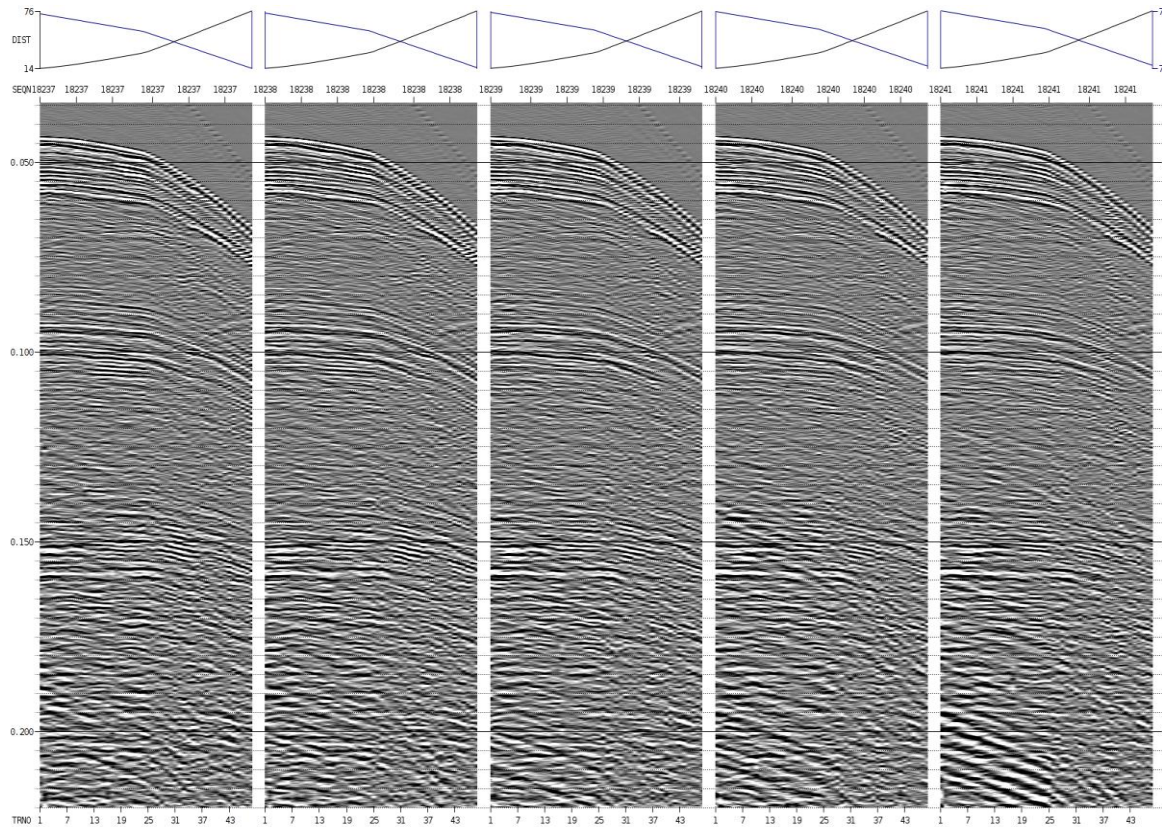
Figure 2.9: LNA: Input shots
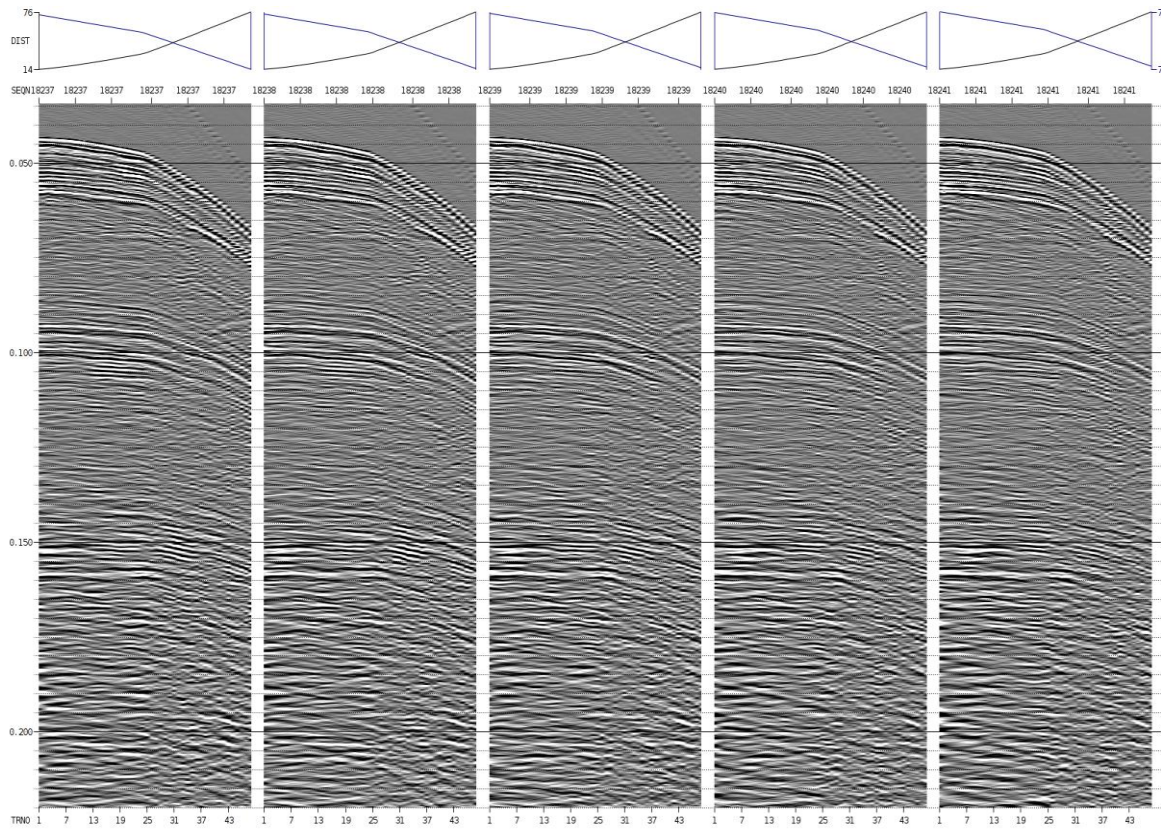
Figure 2.10: LNA: Output shots
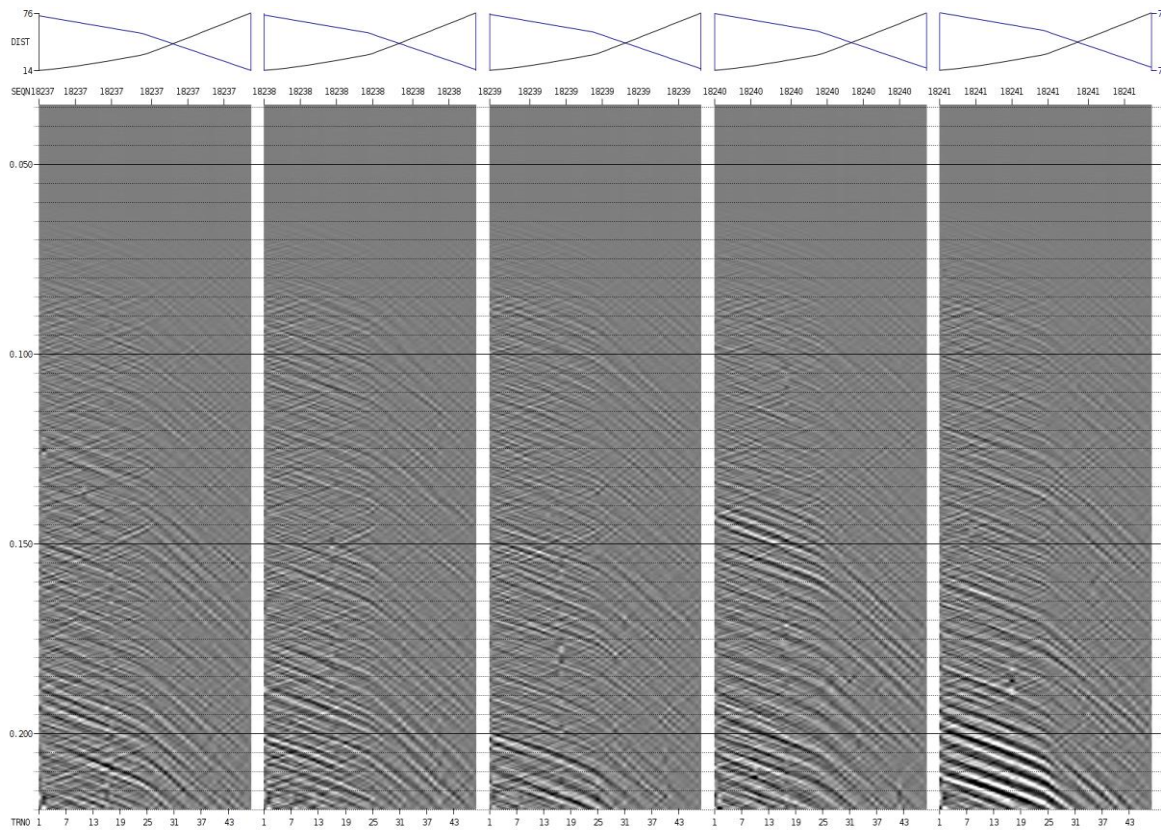
Figure 2.11: LNA: Difference

2.5   Preliminary Shot Statics

Due to the fine sampling rate, shot statics were a large factor in the resolution of the shallow section of the data. It was important at this stage, once data was relatively free of low frequency swell noise, to apply some preliminary shot statics to aid the QC of some of these further processes. It is particularly useful to have shot statics applied prior to deghosting as it is difficult with this resolution of data to identify what the process is doing if shot statics are still predominant.

To achieve this, a provisional shot statics computation was ran using the *Uniseis* module *'NEPTUNE'*. This is ran on NMO corrected CMPs, creating a pilot trace for each CMP using a weighted mix of local stacked traces. Cross-correlations of the pilot trace with the traces in its respective CMP gather are used to assess the static, and this is ran in multiple iterations. With each iteration, the static computed is applied and the pilot trace is correspondingly updated. This run focused solely on the shot static which is a short period effect that locally damages the stack. 5 iterations were chosen, as there was a slight uplift from 3 iterations. Any more than 5 iterations were where the static had already converged to the accepted value and would only unnecessarily increase the runtime.

Later in the processing, once the data is deghosted and velocities are picked, we rerun this computation and add in a component to correct for the streamer depth static using the module *'PASTA'*.
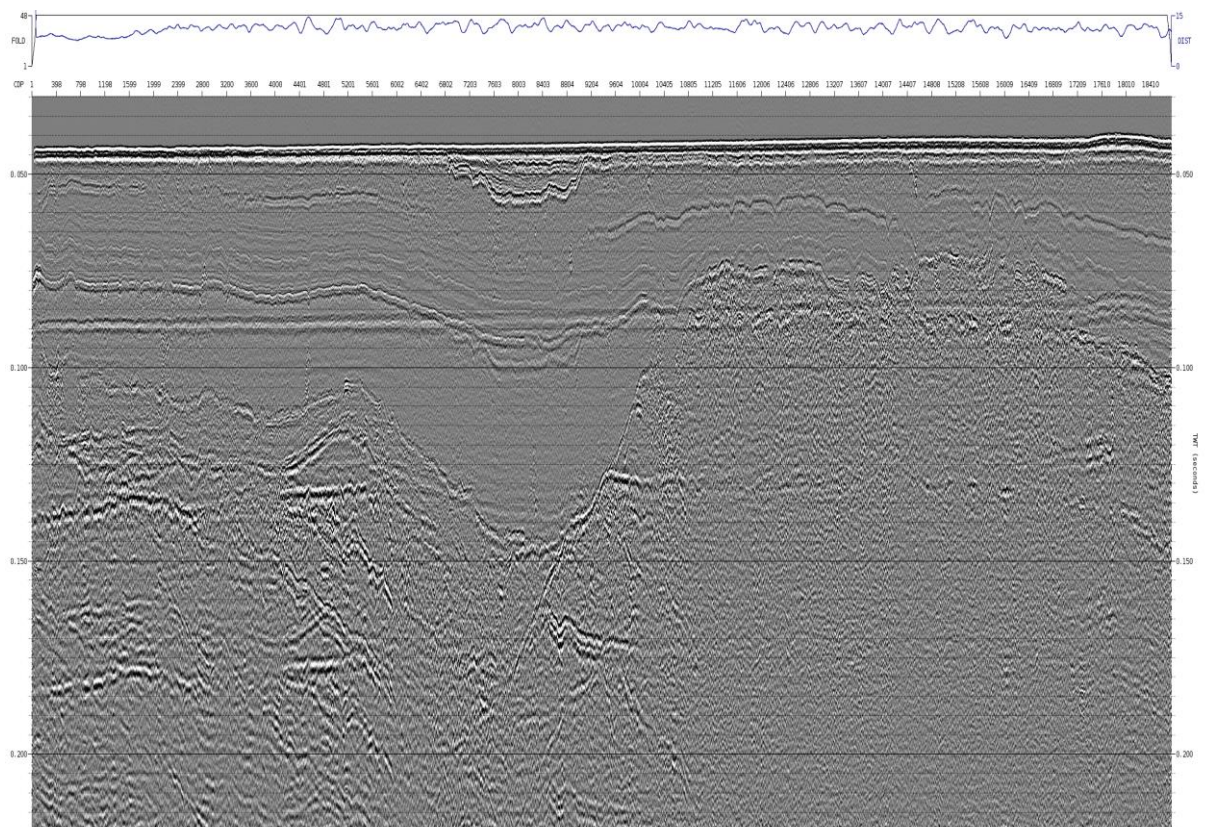
Figure 2.12: Preliminary shot statics: Input stack
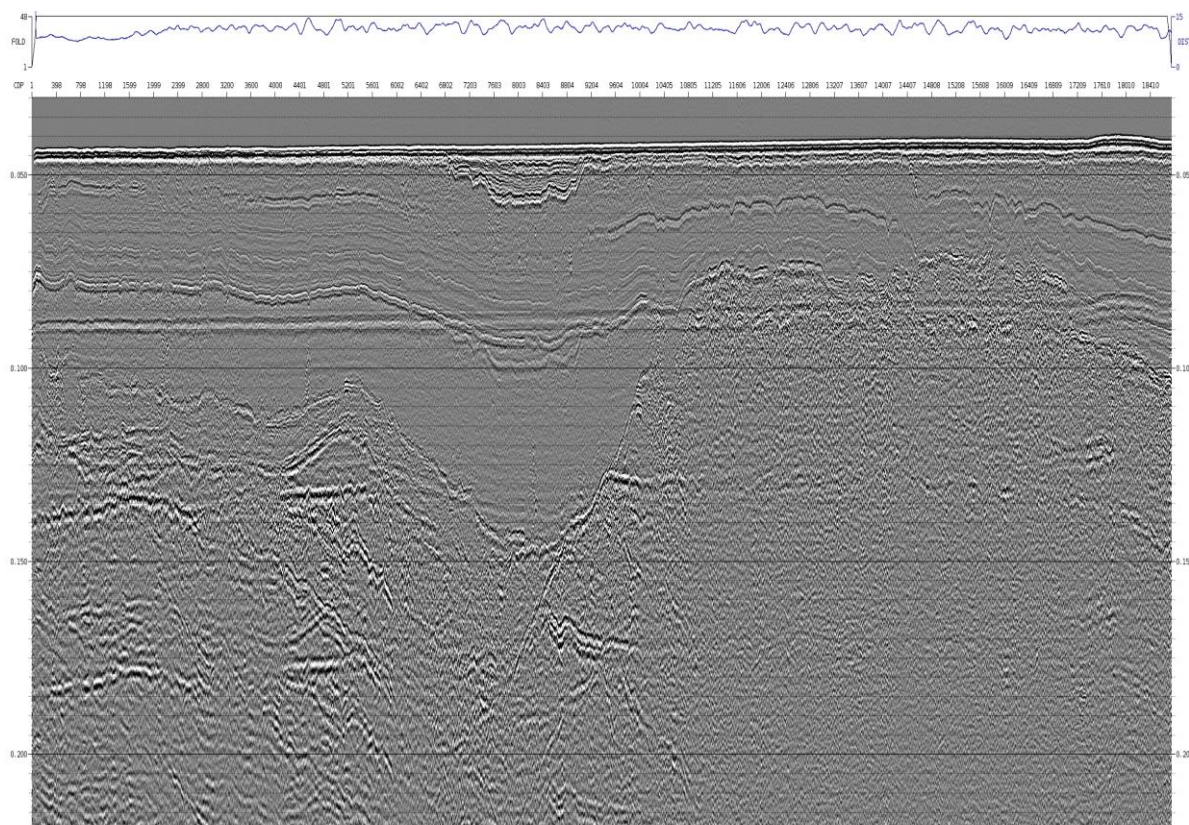
Figure 2.13: Preliminary shot statics: Output stack

2.6 Source and Receiver Deghosting

The high acoustic impedance contrast between the water column and the sea surface causes the latter to act as a near perfect reflector of acoustic energy. Consequently, some of the acoustic energy from a seismic source reflects at this interface before being recorded at the receivers and this is referred to as (source/receiver) ghost, thereby limiting the wavefield spectral band.

To attenuate source, receiver and combined source / receiver ghosts, the *Uniseis 'DEGHOST'* module was applied. *'DEGHOST'* attempts to separate the primary energy from the secondary ghosted wavefield. The primary upcoming wavefield should be more representative of the subsurface reflectivity required for interpretation & well-log matching. Reflections should become shorter, less complex wavelets and be more representative of their characteristic reflectivity in magnitude and polarity. The consequence of this is that we improve the resolution and achieve a broader spectrum. Various tests showed the standard reflection coefficient of -1 for the source and receiver deghosting worked well to attenuate the ghost. A 0.5m wave height allowance for the frequency dependent scattering model was applied to the source deghosting (none for receiver side), and this helped to reduce ringing from the deghosting process.
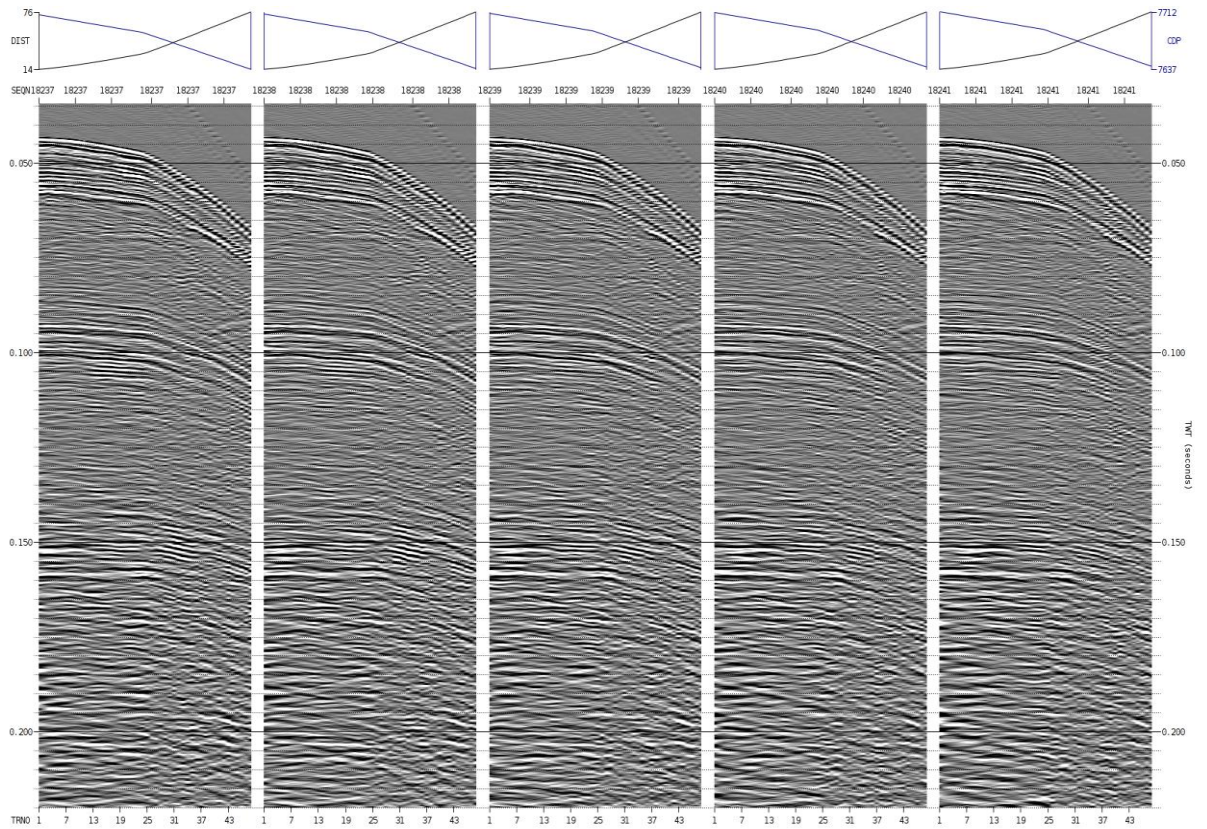
Figure 2.14: Deghost: Input shots
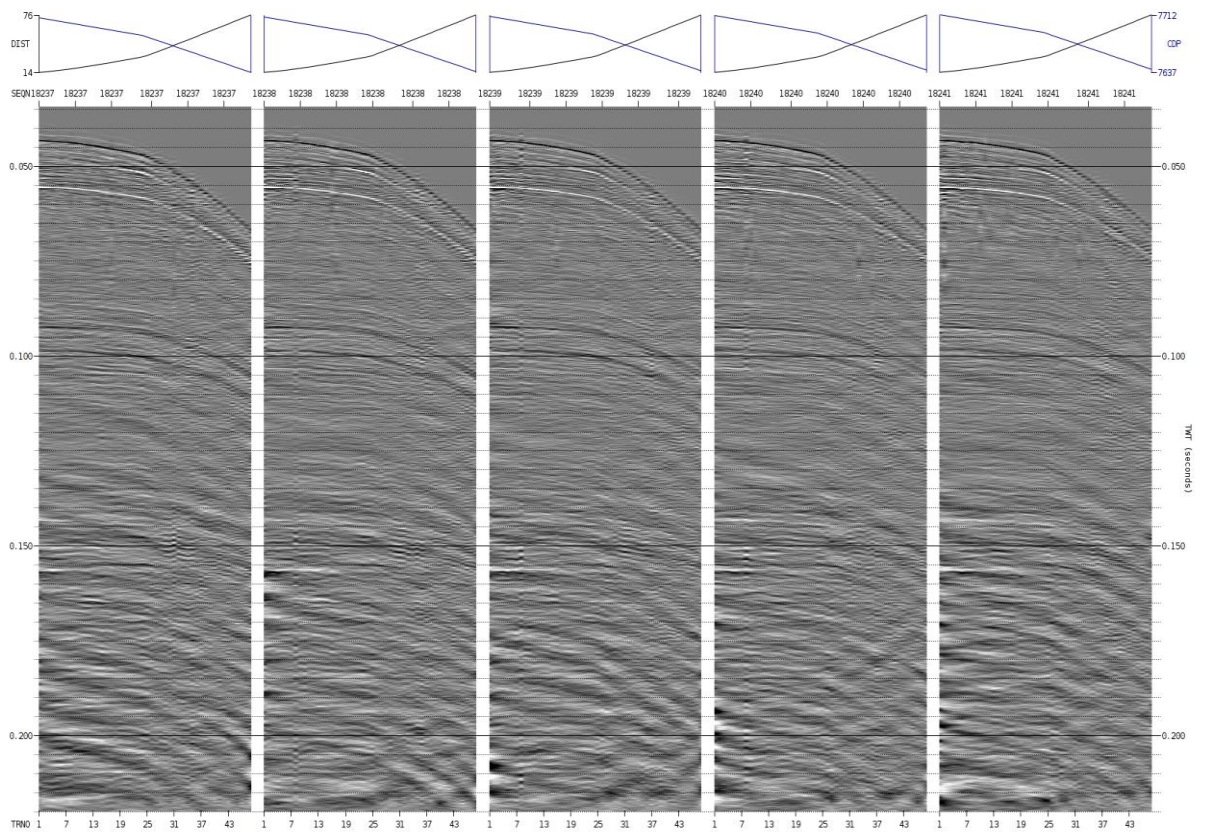
Figure 2.15: Deghost: Source & receiver deghost shots
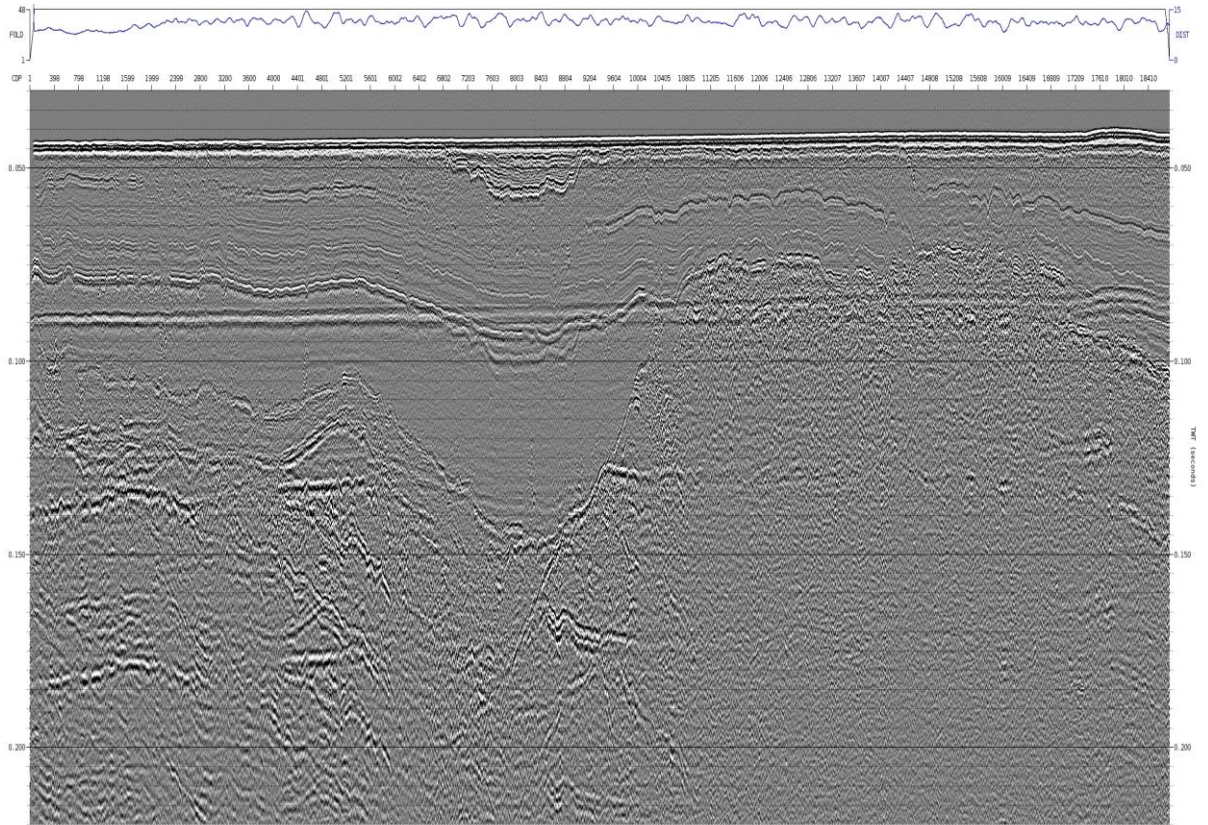
Figure 2.16: Deghost: Input stack
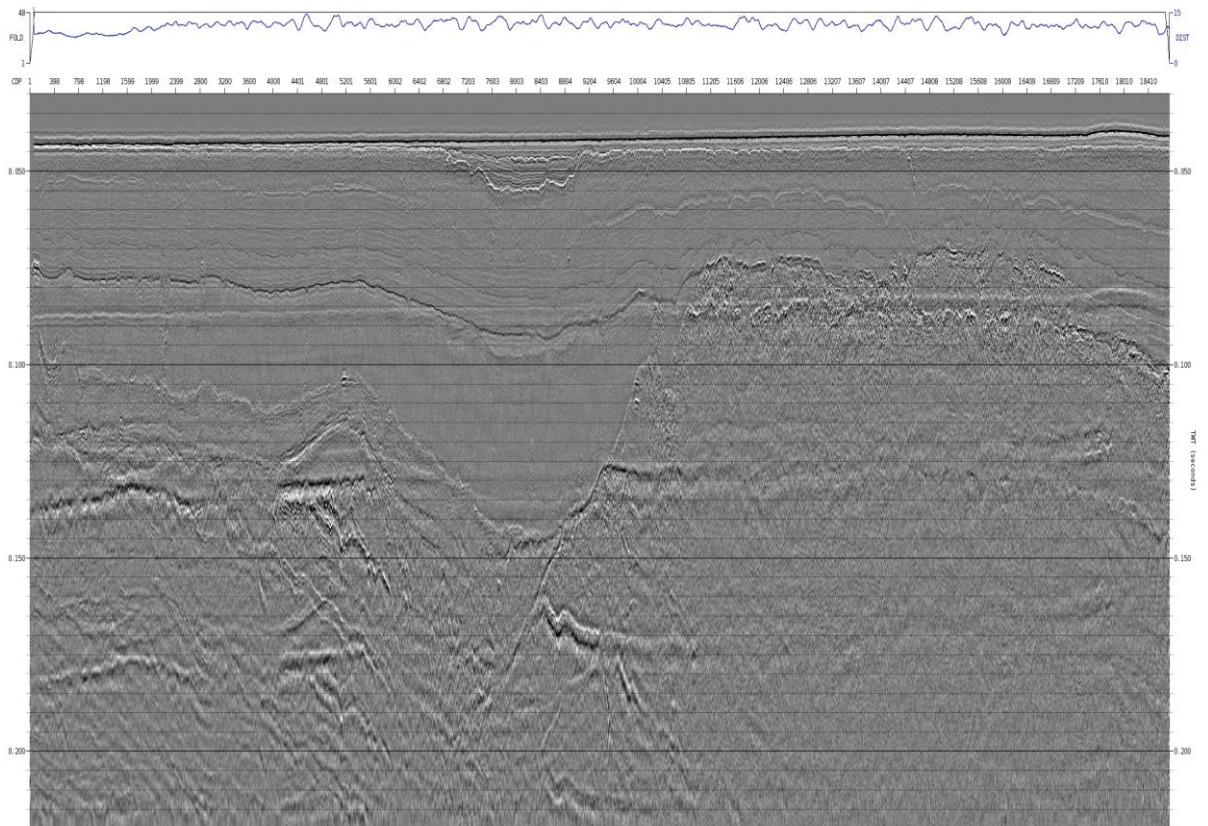
Figure 2.17: Deghost: Source & receiver deghost stack

2.7   Surface Related Multiple Elimination (SRME)

There was significant multiple energy within the data, mainly associated with the water bottom. To attenuate multiple energy, SRME (Surface Related Multiple Elimination) was carried out. SRME uses the geometry of shot recording to estimate all possible multiples that can be generated by the surface. Before evaluating the multiple model, the recorded data was extrapolated to zero offset and a mute was applied to the input shot records to remove direct arrival and guided wave energy. The predicted multiple energy was removed from the input gathers with a double adaptive matching algorithm, the first done in the common channel domain and the second in the shot domain. The adaption in the common offset domain was computed over 211 neighbouring shots, with a filter length of 15ms and an operator of 50ms which was longer than the seabed reflection time. Less traces than 211 can cause the SRME to be too harsh (with a small SP interval of 0.5 m this is just over 100 m), and conversely a higher number of traces can often lead to a degraded model where there is steeply dipping and variable multiple. Before adaptive subtraction, the modelled multiples were muted above the first seafloor multiple. SRME was found to be effective in attenuating multiple energy whilst preserving primary events.

FUGRO
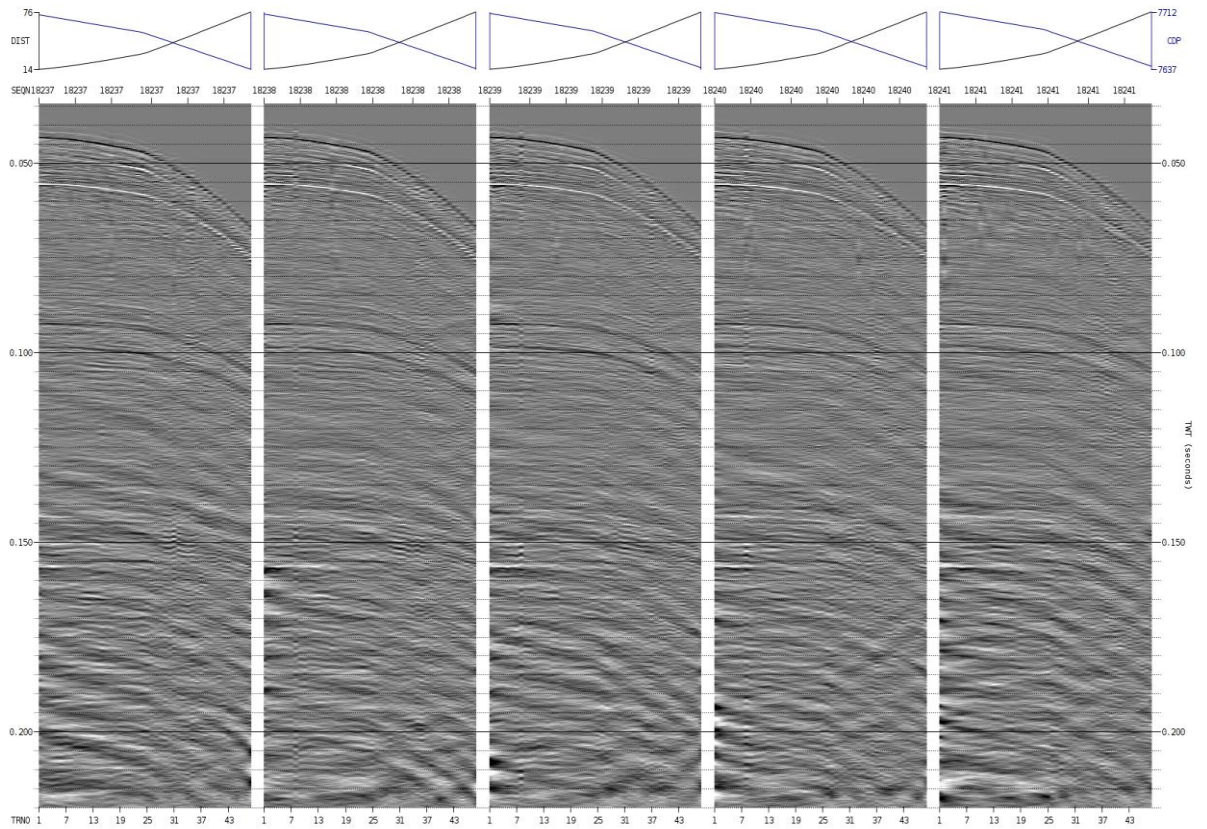
Figure 2.18: SRME: Input shots
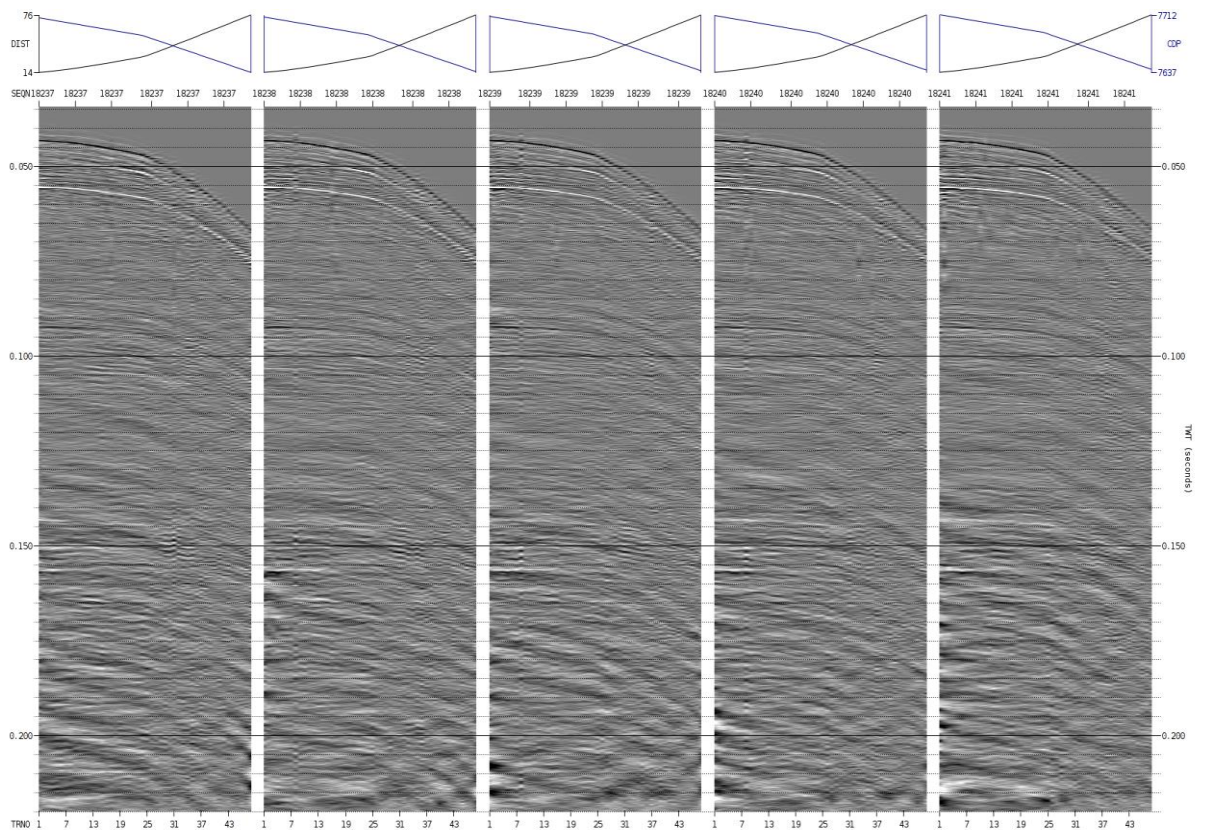
Figure 2.19: SRME: Output shots
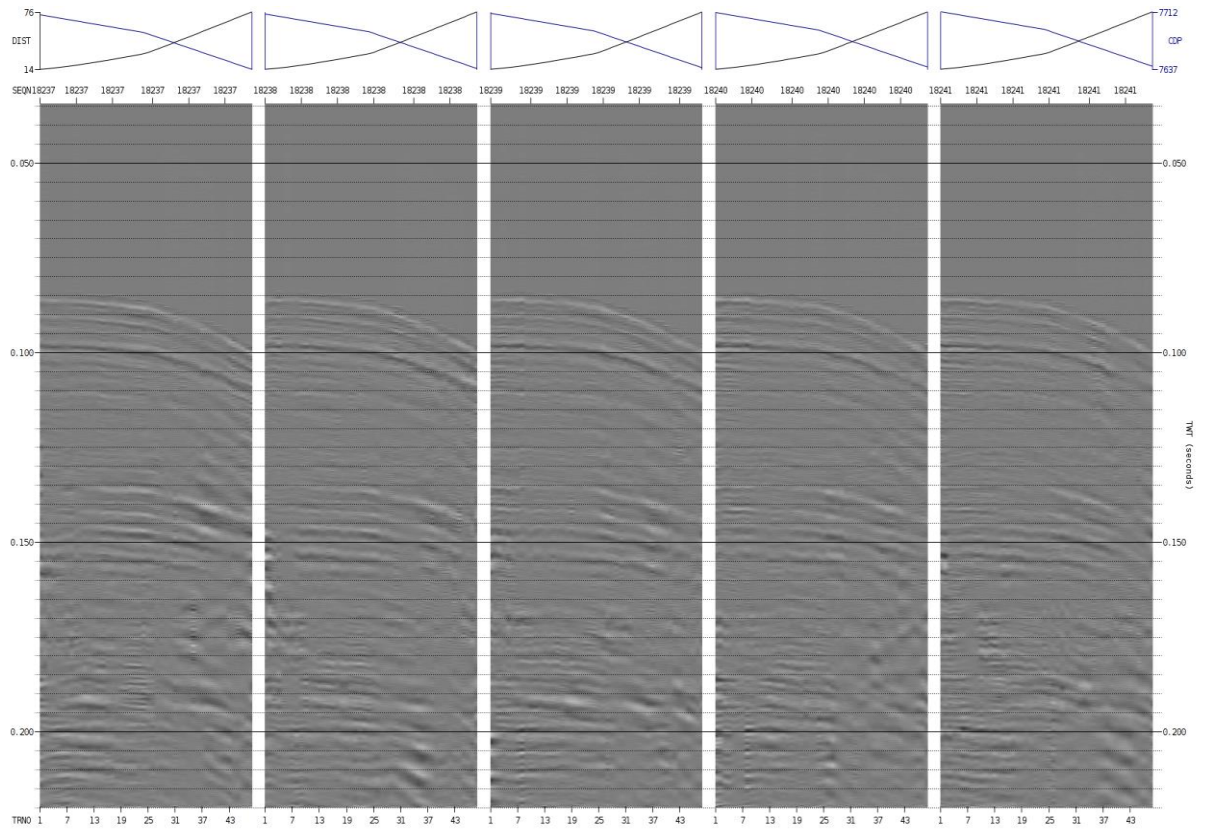
Figure 2.20: SRME: Difference
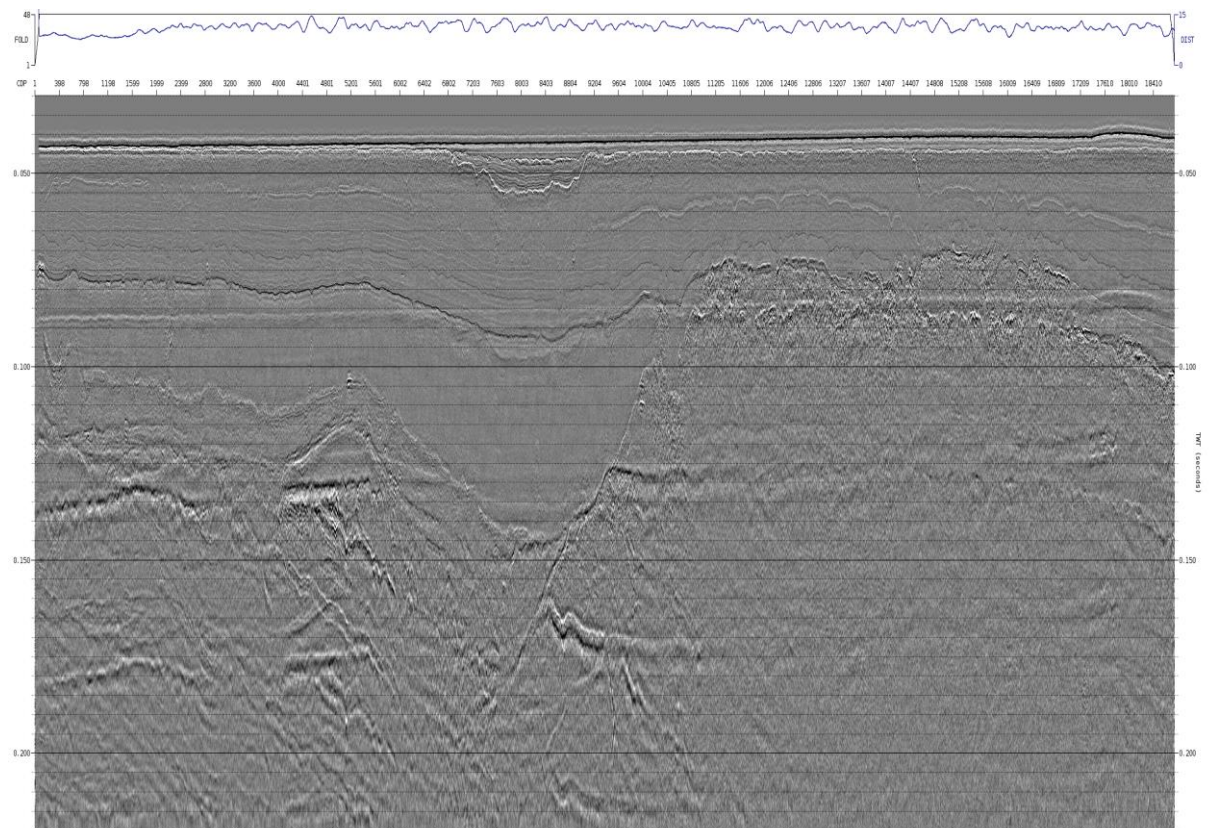
Figure 2.21: SRME: Input stack
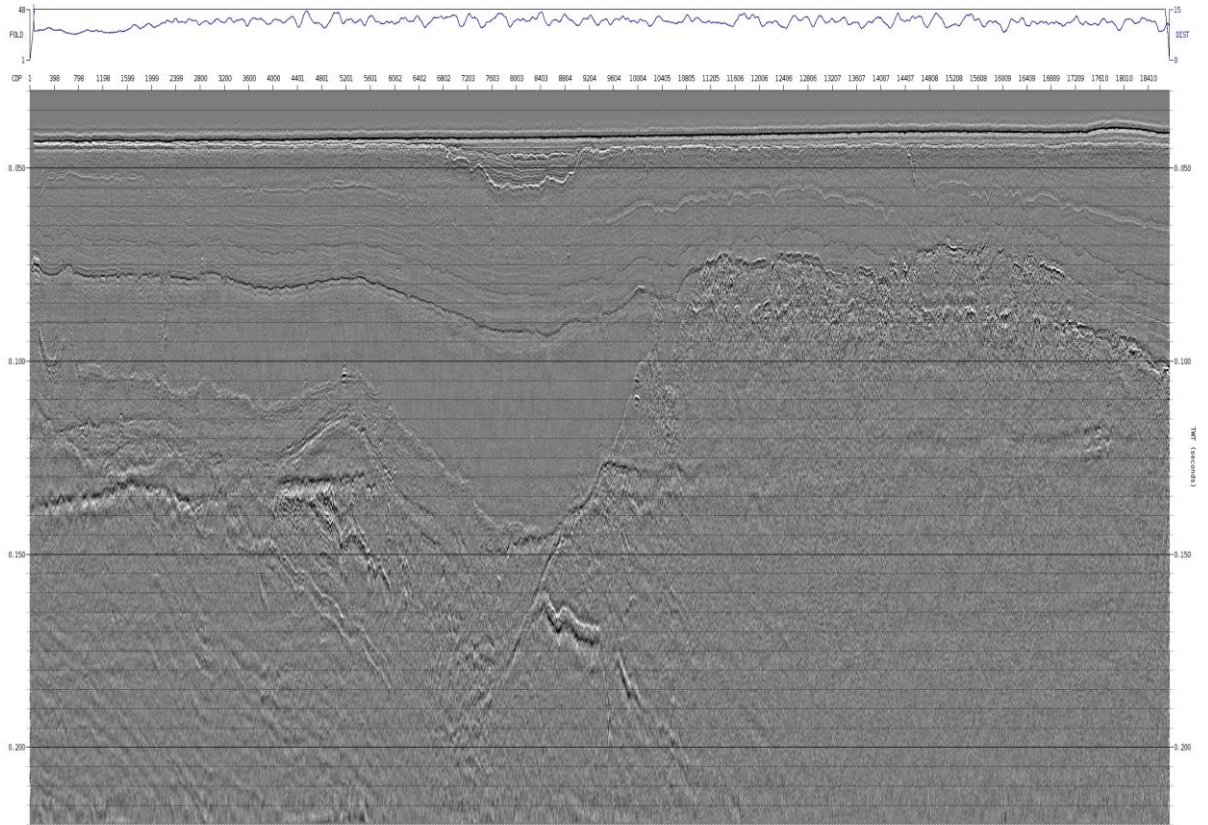
Figure 2.22: SRME: Output stack
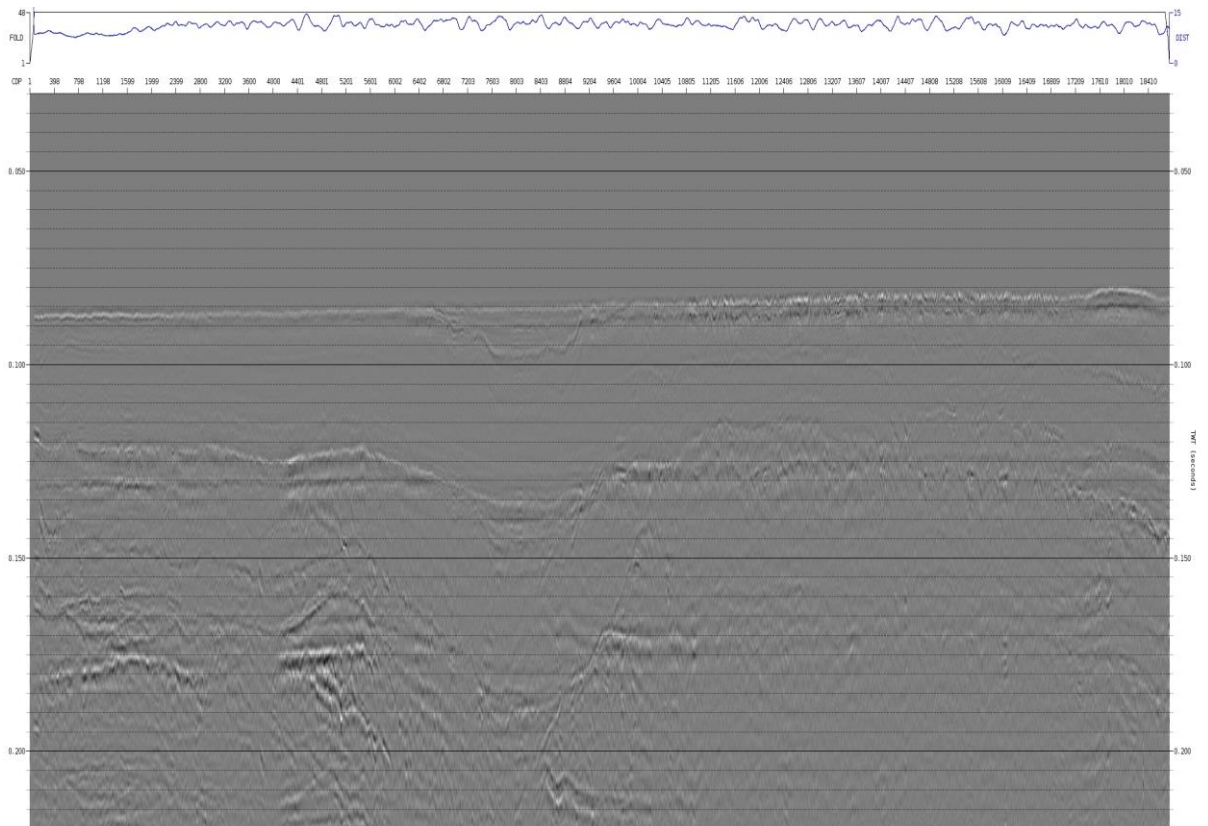
Figure 2.23: SRME: Difference

2.8   Velocity Analysis

A high-resolution velocity analysis using 2nd order NMO correction was conducted for each line using the interactive velocity analysis software *Pegasus*. The analysis was performed at 250 m intervals with each location being compared to and constrained by neighbouring locations. This ensured that consistency was maintained between adjacent lines and velocity locations. Examples below show the displays generated by *Pegasus* for the purposes of velocity analysis. This image shows the semblance, NMO corrected gather, constant velocity stacks and real time stack.
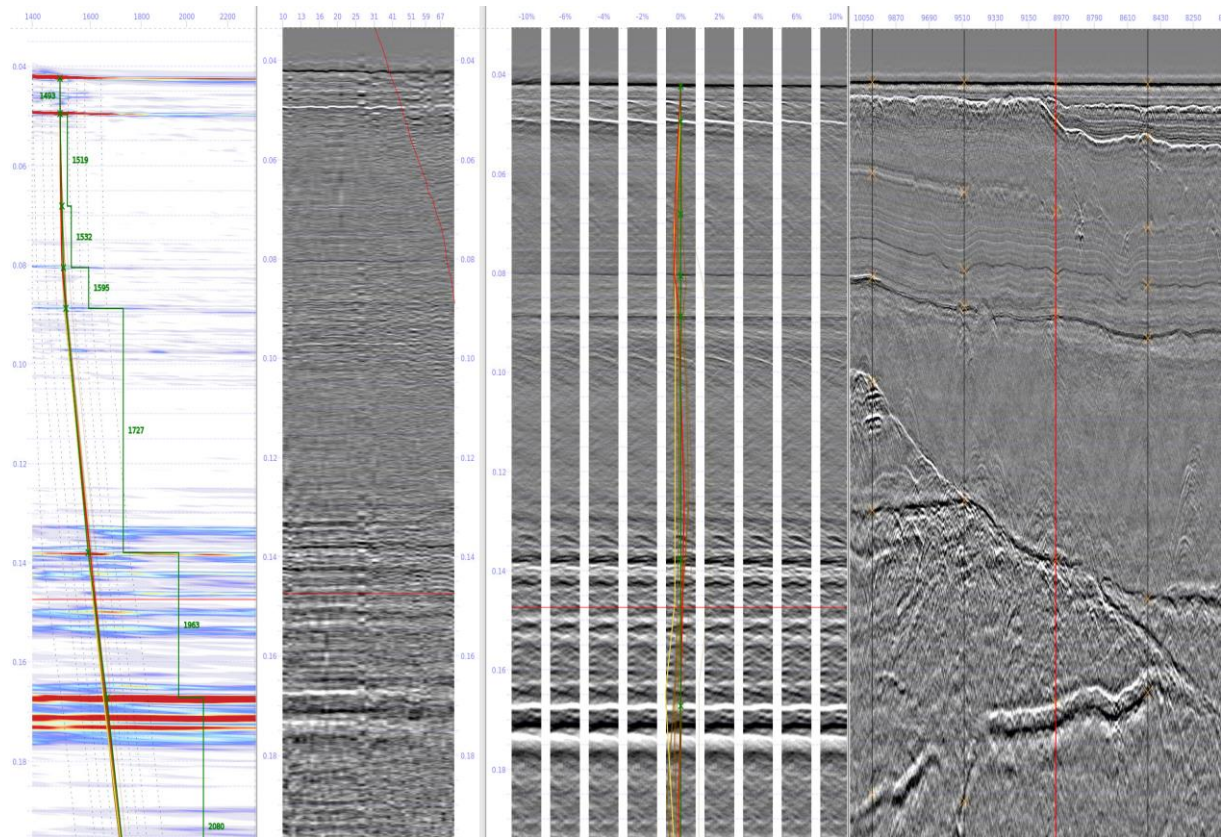
Figure 2.24: Pegasus 2D velocity picking example on HAK2278P01

2.9   Final Statics

Similar to Section 2.5 on preliminary shot statics, we now recompute the shot statics using the same *'NEPTUNE'* process, but now the data has a significantly attenuated ghost along with picked velocities. This allowed for a slightly improved shot static computation. Again 5 iterations were used to converge the static to an acceptable value; 3 being too little, and any more iterations being unnecessary.

Once this was calculated and applied to the shots, an additional pass of *'PASTA'* was applied to NMO corrected CMPs to correct for residual streamer depth statics. This is achieved in a similar manner, by cross correlating the traces in the CMP with a pilot trace which is a weighted trace mix of the stack. We achieve a better result by isolating the shot statics independently first with *'NEPTUNE'* rather that attempting to correct for both at the same time.
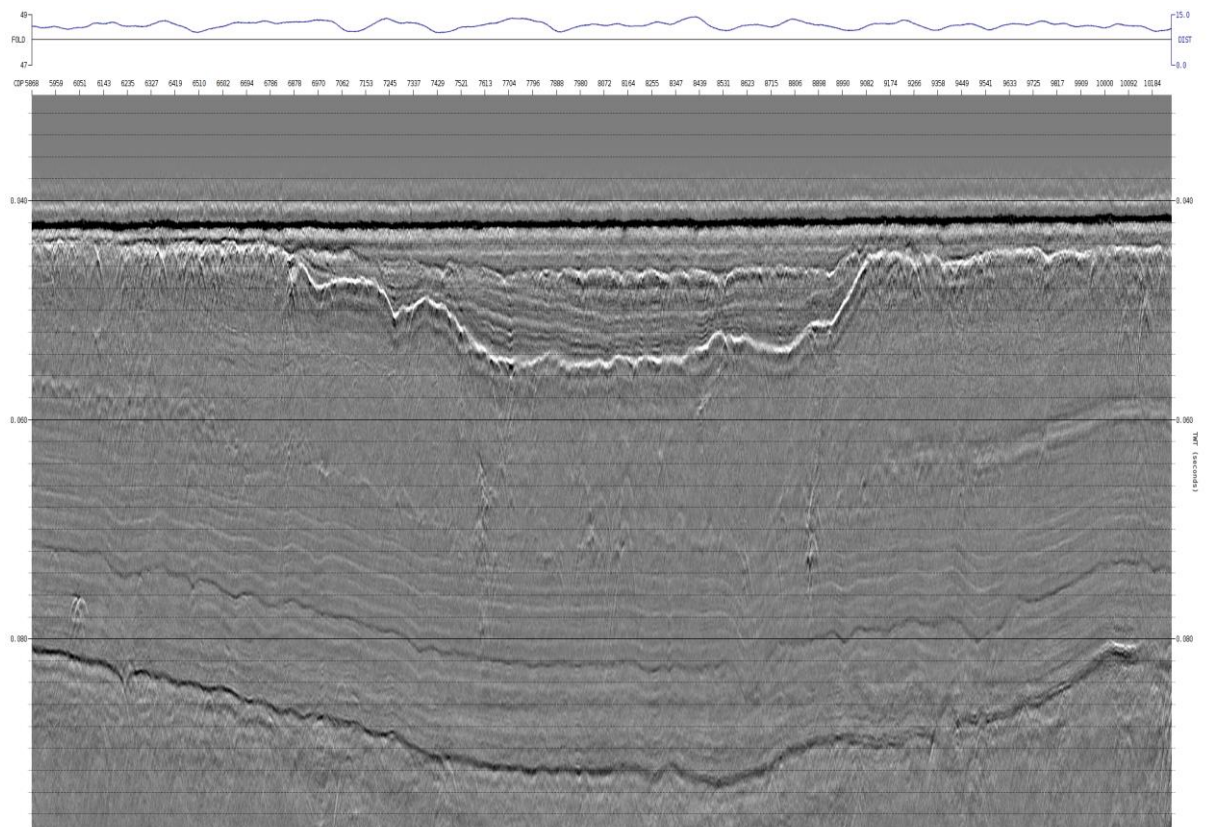
Figure 2.25: Stack without shot statics
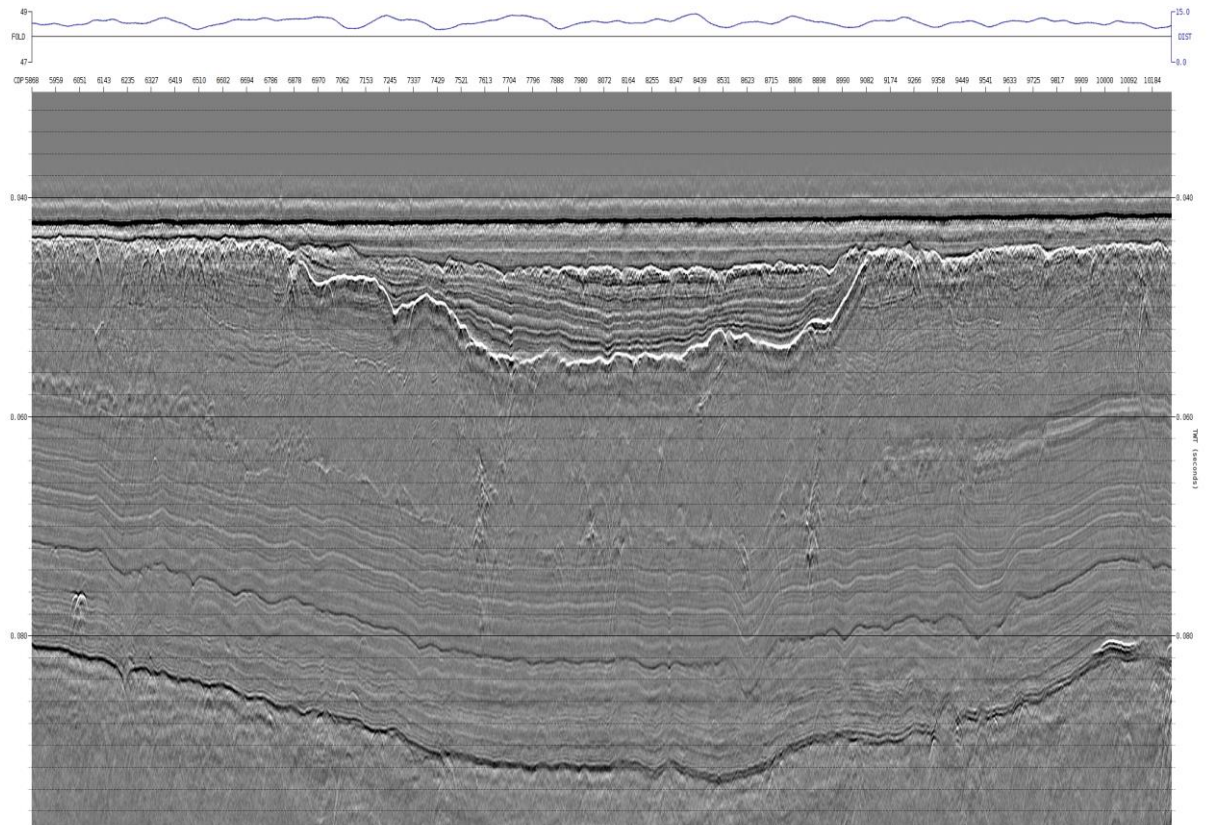
Figure 2.26: Stack with final shot statics

2.10   Final Mute & Stack

The data were now ready to be stacked. An outer trace mute was applied to remove NMO stretch on the far offsets. After various testing of tight and more open mutes than the QC mute so far, a slightly tighter mute was used at the seabed as an improvement was shown in the top 10ms by doing this during testing. A more open mute was shown to introduce stretch in the shallow regions, a consequence of the rather shallow conditions. Trace normalization of 1 / N was used when stacking. See below for an example of the gathers with the tighter final mute overlaid.

Table 2.1: Final mute parameters

Time [ms]	Offset [m]
Seabed - 5 ms	27
Seabed + 5 ms	28
Seabed + 15 ms	33
Seabed + 80 ms	Full offset range
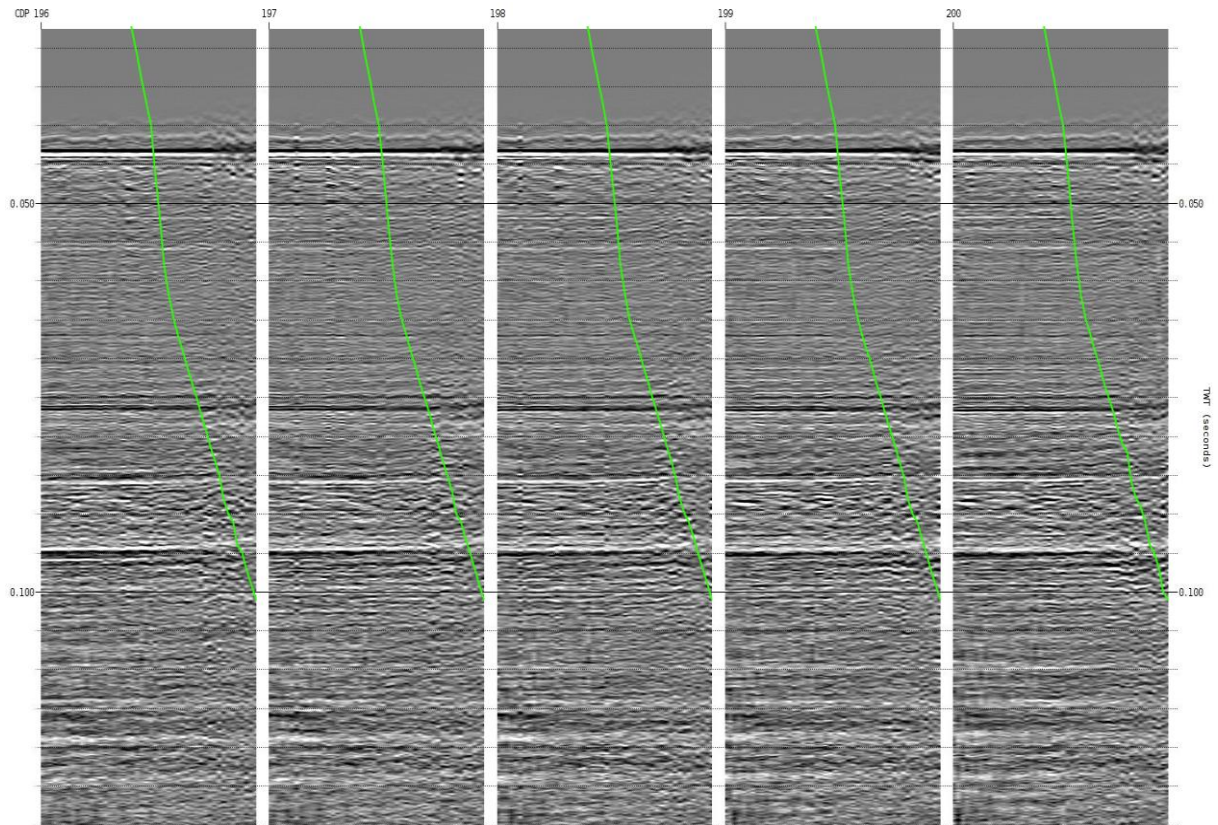
Figure 2.27: CMP gathers with final tighter stacking mute overlaid

2.11 Zero Phase

A zero-phase filter was designed using a data derived source signature wavelet, itself obtained by super stacking the stack. The water bottom was flattened, and traces shifted to 30 ms prior to the CMPs being super stacked. The onset of the super stacked wavelet was then shifted to 0 ms and the filter calculated. See below for an example of the zero-phase filter applied to the stack.
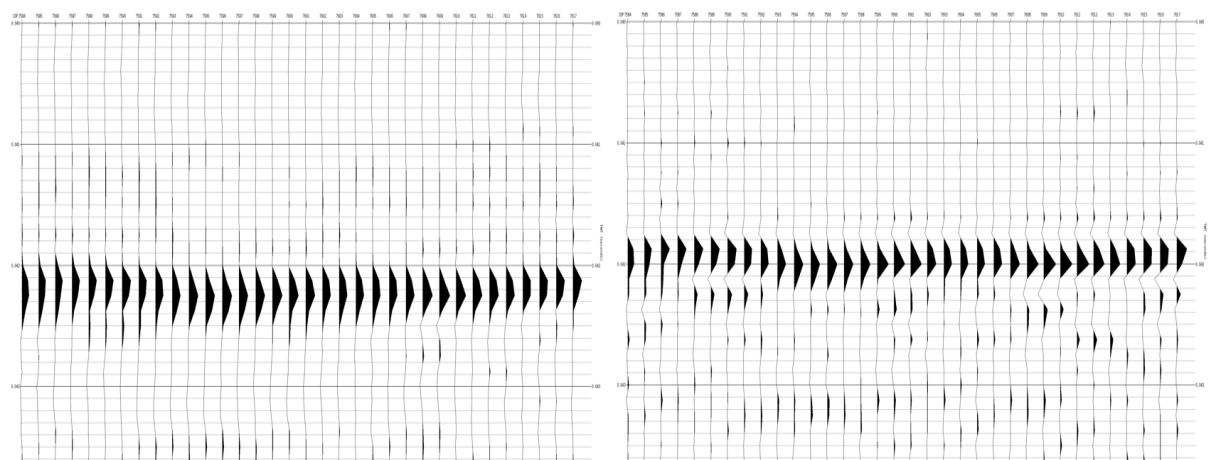
Figure 2.28: Zero Phase: Zoomed seabed before and after

2.12   Post Stack Processing Step One

The low frequency noise, mainly boosted by the deghosting process, was attenuated at this stage using the *Uniseis 'SWELL'* module. This decomposed each seismic trace into signal and noise components by filtering the data with a user specified Butterworth filter, which in this case was over the range 0 - 80 Hz only.

A post stack deconvolution followed this to remove further multiple, hitting the remnant second seabed bounce rather effectively. Much like the common channel deconvolution this was again a very mild application with averaging of the deconvolution operator over a very large 2001 traces/CDPs, computed with a gap 4ms shorter than the seabed, and operator 10ms longer than the seabed.
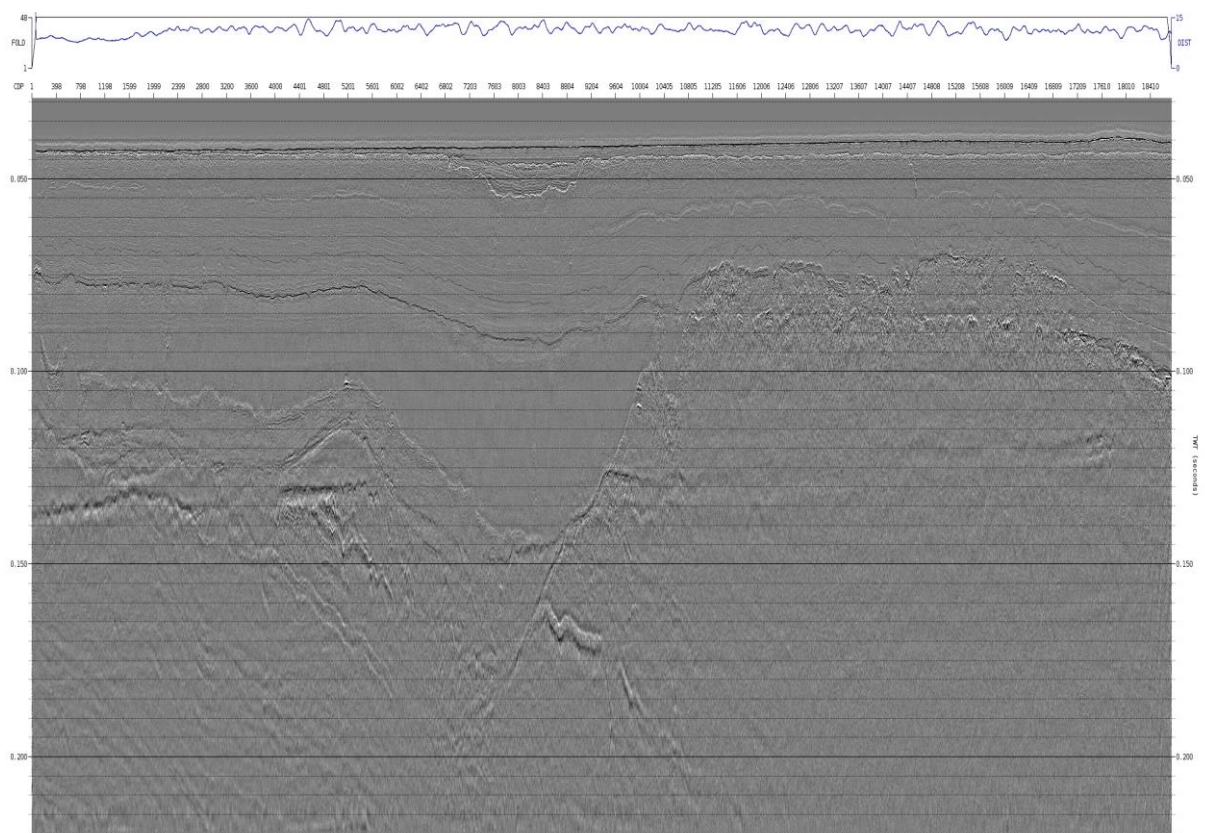
Figure 2.29: Stack before first post stack processing 1
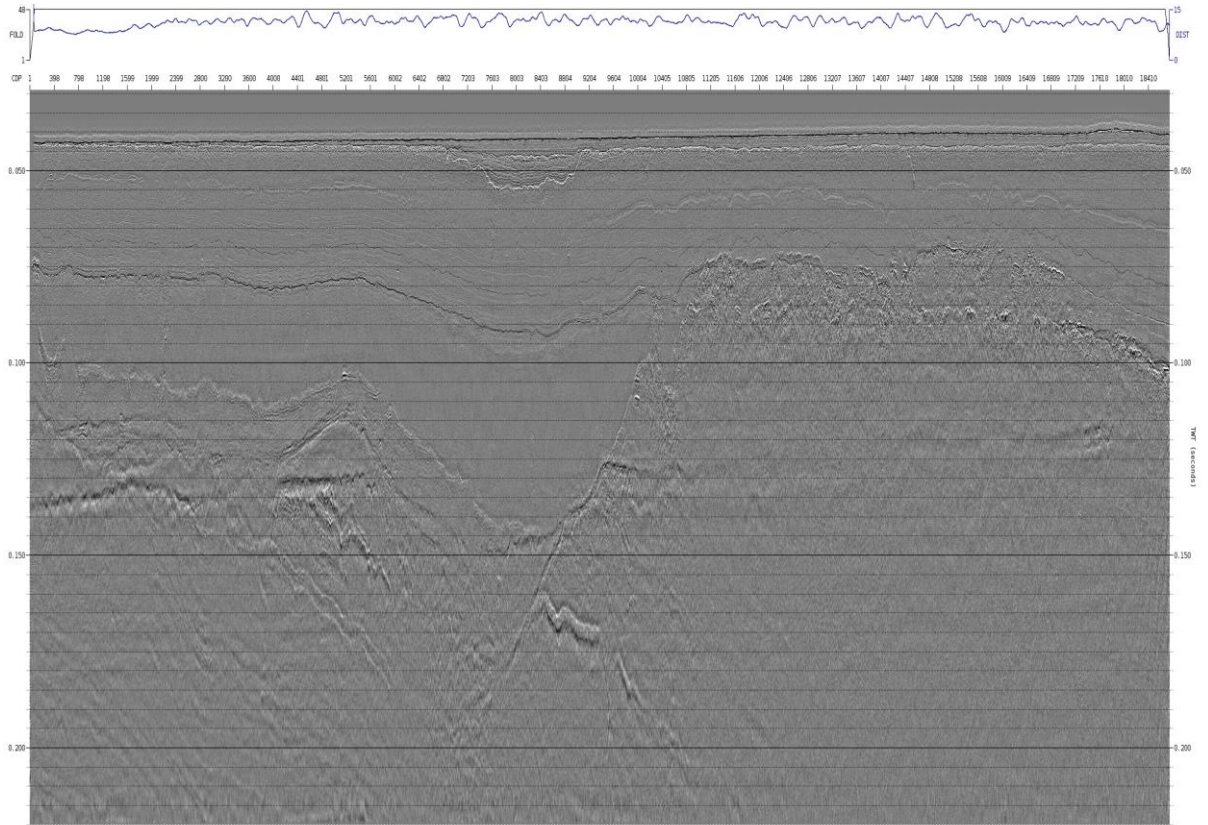
Figure 2.30: Stack after first post stack processing 1

Figure 2.31: Difference

2.13 Post Stack Kirchhoff Time Migration (PoSTM)

As velocity control was good, 2D Post-Stack Kirchhoff Time Migration was performed using 100% of the picked velocity. A migration aperture of radius 80 m was used. Anti-aliasing of 50% was applied by pre-filtering the data within the migration scan depending upon the local migration operator dip. Anti-aliasing protection prevents any undesirable data being included, so aperture muting is unnecessary. No anti-aliasing gave a slightly noisier result, and 80-100% anti-aliasing began to slightly attenuate higher frequency dipping structure in the shallow region, therefore 50% was used as is standard on much of the UUHR data.
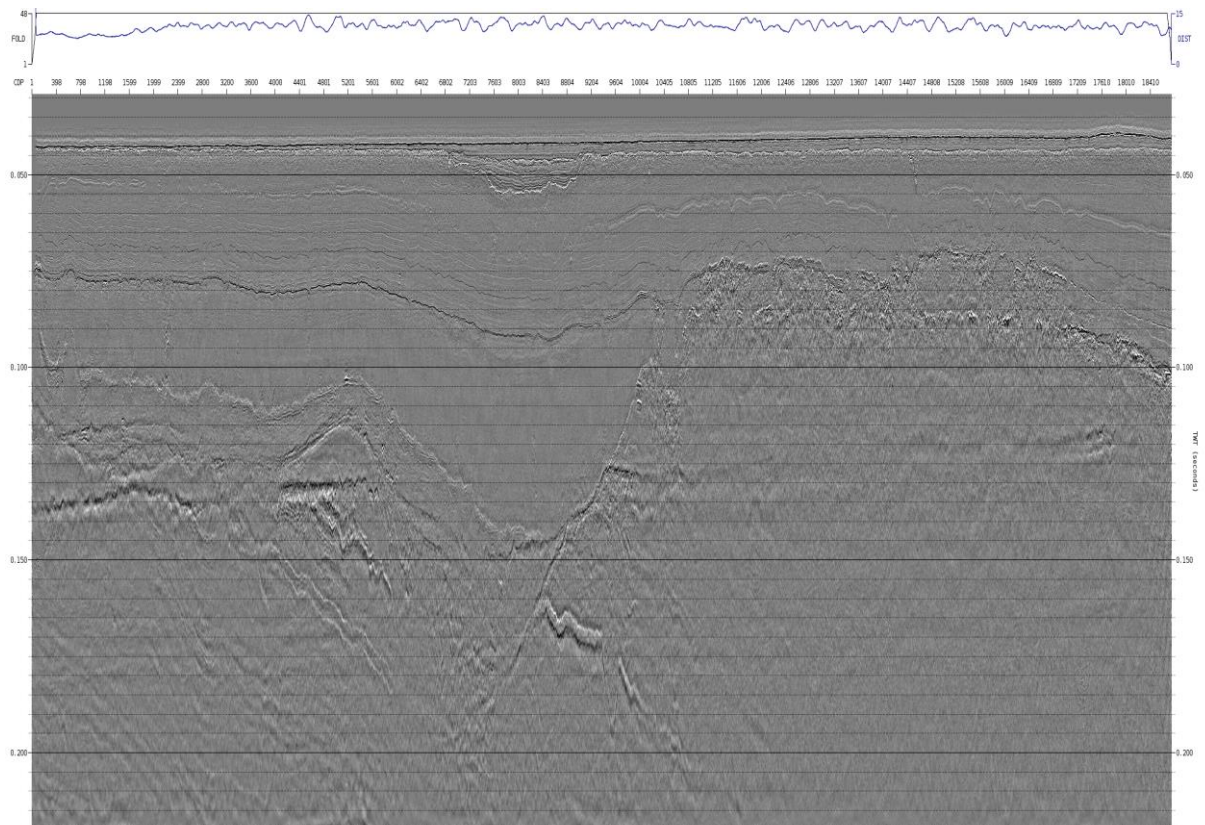
Figure 2.32: PoSTM stack

2.14   Post Stack Processing Step Two

After migration, the final processing steps were to filter the stack before being output as a final product. Various filters were tested with the aim of enhancing signal, preserving resolution and reducing noise. The following set of processes was arrived at:

- Gain of 6 dB/Sec
- Surface wave noise attenuation up to 80 Hz
- Time varying bandpass filter – ref. Table 2.2
- Q compensation from seabed, amplitude only: Q = 100
- Apply source / receiver static shift
- Apply tidal static shift
- Cosmetic mute above seabed

Table 2.2: 2D-UUHR Time varying bandpass filter

Start Time	Low Cut [Hz]	Slope [dB Oct]	High Cut [Hz]	Slope [dB Oct]
Seabed +20ms	80	18	3300	32
Linear taper between				
Seabed + 80ms	60	18	2600	32
Linear taper between				
Seabed + 160ms	40	18	900	32
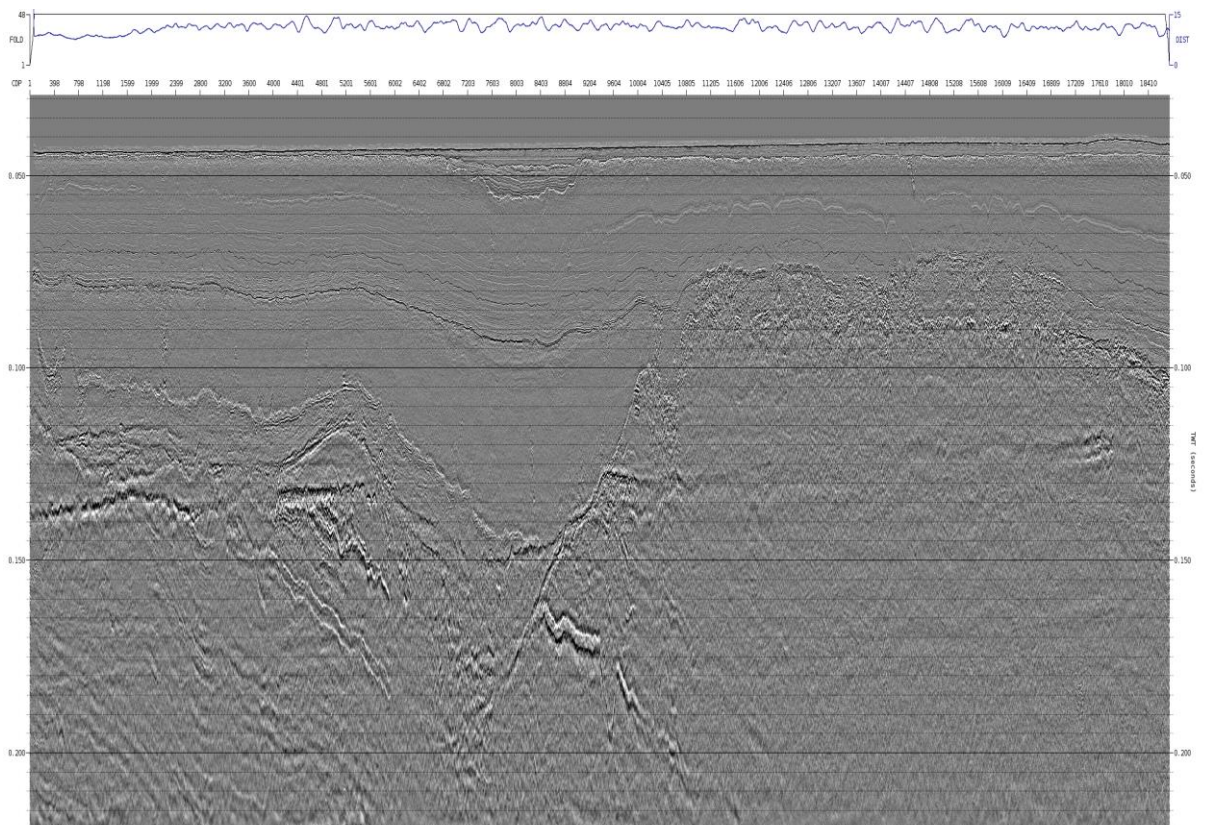
Figure 2.33: Final stack after post stack processing 2

Figure 2.34: Final spectral comparison: Brute (black) vs final migrated time (red)

2.15   Output to SEG-Y

The final stacks were output in SEG-Y format with the CMP positions from the standard UKOOA format P1/90 files. These files were electronically transferred internally to the geophysicists for interpretation via *Fugro Shares*. An example of the approved EBCDIC header is displayed below.

```
C01 CLIENT: ENERGINET   RECORDED BY: FUGRO
C02 LINE: HAM6306R01    PROJECT: HESSELO 2DUUHR
C03 AREA: HESSELO       SITE SURVEY: WINDFARM 2DUUHR
C04 RECORDING PARAMETERS ==========================================
C05 VESSEL: FUGRO FRONTIER                   DATE: 19.10.20
C06 FORMAT: SEGY REV1
C07 REC LENGTH: 219.875 MS        SAMPLE RATE: 0.125 MS
C08 FILTERS LOW CUT: N/A          HIGH CUT: N/A
C09 SOURCE: MULTI-LEVEL SPARKER   SOURCE DEPTH: 0.5 M
C10 VOLUME: N/A    LEVEL: 900 J   SP INTERVAL: 0.5 M
C11 CABLE TYPE: TELEDYNE HYBRID   CABLE DEPTH: 1.4 M  LENGTH: 72M
C12 NUM CHANNELS: 48              GP INTERVAL: 1 / 2 M
C13 NAVIGATION PRIMARY: STARFIX NG
C14 PROCESSING BY: FUGRO          DATE: 19.10.20
C15 PROCESSING SYSTEM: UNISEIS
C16 PROCESSING SEQUENCE ==========================================
C17
C18 1)TRANSCRIPTION TO 219.875 MS AT 0.125 MS NO. CHANNELS: 48
C19 2)MERGE SRC/REC NAV 3)APPLY 2D GEOMETRY 4)EDIT BAD TRACES
C20 5)SHOT DENOISE 6)CHANNEL DENOISE 7)RECEIVER DENOISE 8)LNA
C21 9)PRELIMINARY RESIDUALS 10)SRC AND REC DEGHOSTING 11)2D SRME
C22 12)250M VELOCITY PICKS 13)REMNANT DEMULTIPLE 14)FINAL RESIDUALS
C23 15)SORT TO CMP 16)NMO 17)MUTE 18)STACK 19)ZERO PHASE
C24 20)POST STACK MIGRATION 21)TVF 18)Q COMPENSATION
C25 22)FINAL ZERO SEA LEVEL STATIC 23)OUTPUT TO SEGY
C26
C27
C28 TRACE HEADER BYTE INFORMATION ==================================
C29 HEADER,BYTE,FORMAT
C30 SHOT,17,4I              COORD_SCALAR,71,72
C31 CHANNEL,21,4I
C32 SRC_X,73,4I REC_X,81,4I
C33 SRC_Y,77,4I REC_Y,85,4I
C34 DATA INFORMATION ==============================================
C35 LINE: HAM6306R01         DATA TYPE: FINAL MIGRATED TIME STACK
C36 CDP SORT
C37 SP 26975 TO 10594
C38 POLARITY ======================================================
C39 INCREASE IN ACOUSTIC IMPEDANCE = POSITIVE NUMBER
C40
```

Figure 2.35: 2D-UUHR: Final migrated time stack approved EBCDIC example

FUGRO

2.16   Depth Conversion

Data deliverables were also requested in depth. This was done using the *Uniseis 'DTCONV'* tool. The RMS stacking velocities were first converted to intervals with a DIX transformation, and then smoothed, prior to depth conversion.

2.17   Additional Analysis

Comparisons were made with the sub bottom profiler and the UUHR data during acquisition. This further supported the initial suggestions that the UUHR data was of very good quality – imaging much of the fine structure visible in the SBP
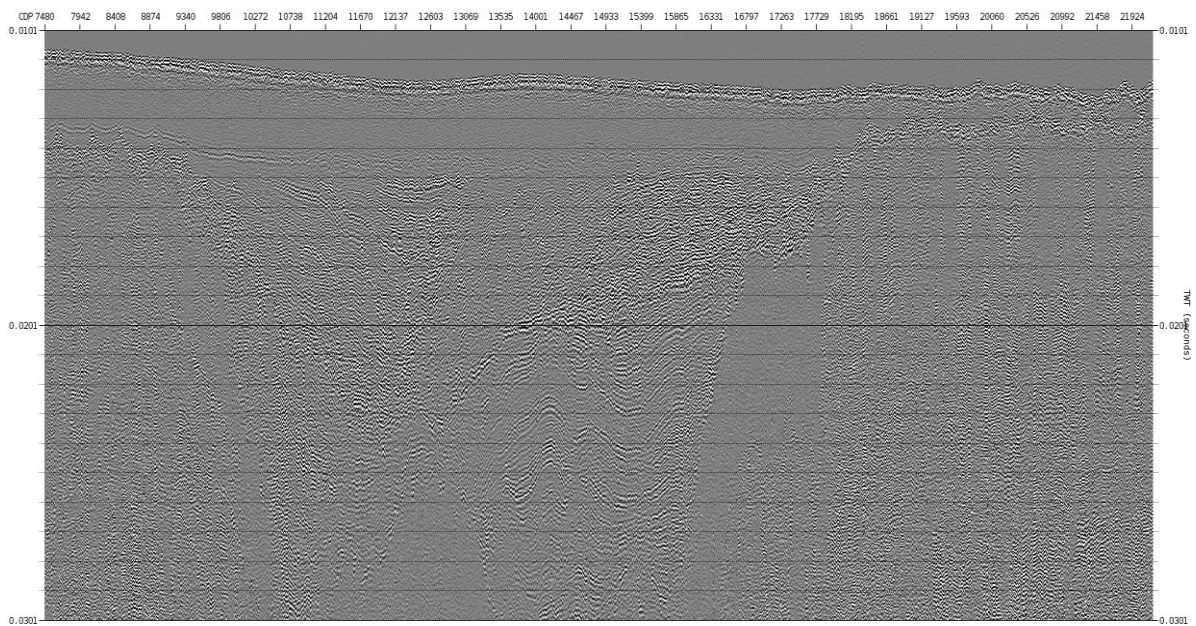
Figure 2.36: SBP Line
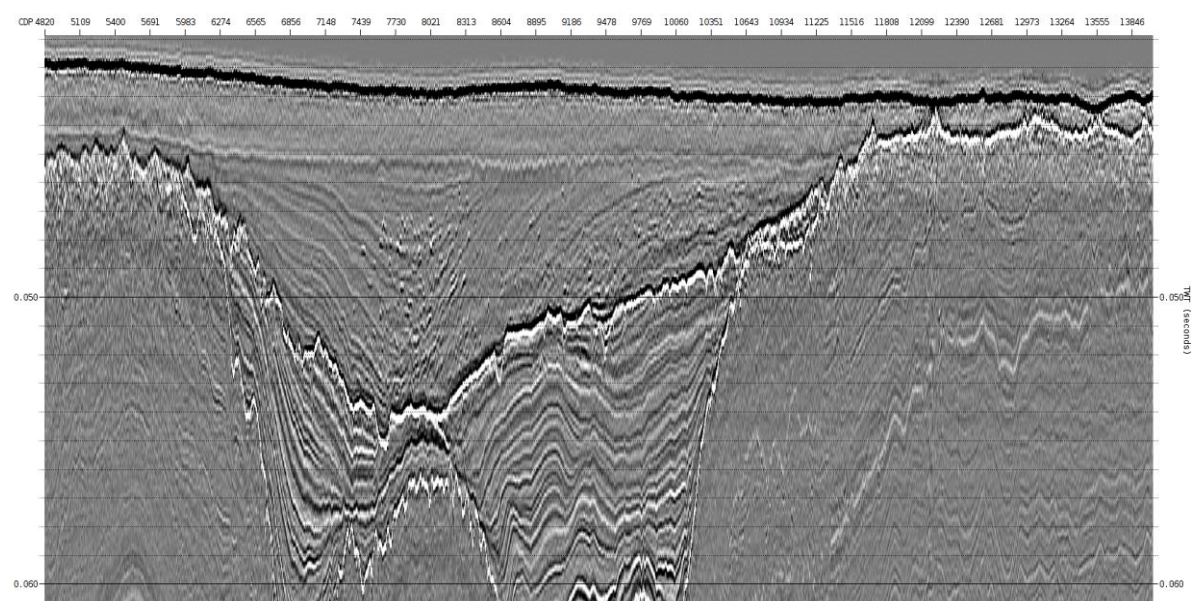
Figure 2.37: 2D UUHR Line

Appendix A

Line Listings

A.1   2D-UUHR Lines Frontier

Table A.1: 2D-UUHR Frontier - Accepted lines processed

Line Name	Sequence	First SP	Last SP	Length [km]
HAN6446P01	078	10602	15474	2.44
HAN6418P01	079	17769	10593	3.59
HAN6390P01	080	10601	20079	4.74
HAN6362P01	081	22372	10595	5.89
HAM6334P01	082	10601	24679	7.04
HAM6306R01	084	26975	10594	8.19
HAK6278P01	085	10601	29282	9.34
HAK6250P01	086	31578	10595	10.49
HAJ6222P01	087	10601	33889	11.64
HAJ6194P01	088	36181	10594	12.79
HAH6166P01	089	10601	38494	13.95
HAG6138R01	091	40784	10593	15.10
HAF6110P01	092	10601	43365	16.38
HAF2094P01	093	40423	10595	14.91
HAF6082P01	094	10601	38231	13.82
HAK2294P01	113	27961	10595	8.68
HAK2262P01	118	30592	10595	10.00
HAK2274P01	119	10601	29614	9.51
HAK2266P01	120	30262	10592	9.84
HAK2278P01	121	10601	29288	9.34
HAK2286P01	123	10601	28627	9.01
HAK2254P01	124	31249	10594	10.33
HAK2282P01	125	10601	28954	9.18
HAK2270R01	136	29934	10594	9.67
HAK2290P01	137	10601	28500	8.95
HAK2246P01	138	31907	10392	10.76
HAK2242P01	139	10601	32454	10.93
HAJ2226P01	140	33551	10392	11.58
HAJ2238P01	141	10602	31726	10.56
HAJ2230P01	142	33222	10396	11.41
HAJ2234P01	143	10601	33102	11.25
HAJ2218P01	144	10601	34418	11.91
HAJ2210P01	145	34866	10392	12.24
HAJ2214P01	146	10601	34746	12.07
HAJ2198P01	147	35852	10392	12.73
HAJ2202P01	150	10602	35731	12.56
HAH2182P01	151	37167	10394	13.39
HAH2186P01	152	10601	37045	13.22
HAH2170P01	153	38154	10394	13.88
HAH2178P01	154	10601	37703	13.55
HAH2162P01	155	38811	10393	14.21
HAH2174P01	156	10627	38031	13.70

Line Name	Sequence	First SP	Last SP	Length [km]
HAH2154P01	157	39469	10395	14.54
HAH2158P01	158	10601	39343	14.37
HAG2142P01	159	40455	10396	15.03
HAG2134P01	161	40986	10259	15.36
HAH2150R01	162	10734	40138	14.70
HAG2146P01	164	10601	40334	14.87
HAG2114P01	165	42959	10397	16.28
HAG2126P01	166	10601	41978	15.69
HAF2106P01	167	42620	10394	16.11
HAG2122P01	168	10690	42309	15.81
HAG2118P01	169	10601	42635	16.02
HAF2098P01	170	41155	10395	15.38
HAF2102P01	171	10601	42094	15.75
HAF2086P01	172	38958	10394	14.28
HAF2090P01	173	10601	39897	14.65
HAH6166J01	174	10601	12413	0.91
HAH2182J02	175	12215	10393	0.91
HAH2190R01	176	36510	10392	13.06
HAJ2206R01	177	10601	35403	12.40
HAJ2238J01	178	13186	10394	1.40
HAJ2218J01	179	23529	10396	6.57
HAJ2230J01	180	10601	32857	11.13
HAK2270J01	181	19372	10395	4.49
HAK2258R01	184	10601	31125	10.26
HAG2134J01	185	12441	10395	1.02
HAF2106J01	186	12352	10395	0.98
HAG2122J01	187	12227	10394	0.92
HAG2130R01	188	10601	41653	15.53
	70 Lines		**Total Frontier**	**763.16 km**

FUGRO

A.2   2D-UUHR Lines Pioneer

Table A.2: 2D-UUHR Pioneer - Accepted lines processed

Line Name	Sequence	First SP	Last SP	Length [km]
HAE6026P01	001	10364	22836	6.24
HAE6054R01	002	10001	32206	11.10
HAE2078P01	003	10001	36600	13.30
HAE2050P01	004	10001	31475	10.74
HAE2070P01	007	10001	35133	12.57
HAE2058P01	008	10001	32939	11.47
HAE2018P01	012	10001	19384	4.69
HAE2038P01	013	10001	28514	9.26
HAE2022R01	014	10265	21212	5.47
HAE2042P01	015	10001	30010	10.01
HAE2030P01	016	10001	24861	7.43
HAE2066R01	017	10001	34404	12.20
HAE2034P01	018	10001	26687	8.34
HAX2488P01	019	10001	13843	1.92
HAE2014P01	020	10001	17562	3.78
HAE2006P01	021	10001	13910	1.96
HAE2010P01	022	10001	15736	2.87
HAE2002P01	023	10001	12083	1.04
HAX2489P01	024	10001	17624	3.81
HAX2492P01	025	10001	23943	6.97
HAX2490P01	026	10001	21394	5.70
HAX2491P01	027	10001	22657	6.33
HAE2022J01	028	10001	12999	1.50
HAE2074R01	029	10001	35931	12.97
HAE2070J01	030	10001	13858	1.93
HAE2046R01	031	10001	30740	10.37
HAE2062R01	032	10001	33672	11.84
HAX2498P01	033	10001	63430	26.72
HAX2499P01	034	10001	61474	25.74
HAX2497P01	035	10001	56538	23.27
HAX2500P01	036	10001	56089	23.04
HAX2496P01	037	10001	49938	19.97
HAX2502P01	038	10001	44022	17.01
HAX2501P01	039	10081	49837	19.88
HAM2354P01	040	10001	22135	6.07
HAX2495P01	041	10001	42449	16.22
HAX2493P01	042	10001	28962	9.48
HAX2494P01	043	10001	35855	12.93
HAX2506P01	044	10001	20759	5.38
HAX2507P01	045	10002	15702	2.85
HAX2504P01	046	10001	32435	11.22
HAX2505P01	047	10001	26569	8.28

Line Name	Sequence	First SP	Last SP	Length [km]
HAX2503R01	049	10001	38203	14.10
HAM2298P01	050	10001	26740	8.37
HAM2334P01	051	10001	23779	6.89
HAM2302P01	052	10001	26410	8.21
HAM2318P01	053	10001	25094	7.55
HAM2306P01	054	10001	26082	8.04
HAM2322P01	055	10001	24768	7.38
HAM2310P01	056	10001	25751	7.88
HAM2326P01	057	10001	24437	7.22
HAM2314P01	058	10001	25423	7.71
HAM2350P01	059	10001	22464	6.23
HAM2346P01	061	10001	22795	6.40
HAM2330R01	062	10001	24109	7.05
HAM2342P01	063	10001	23123	6.56
HAM2338P01	064	10001	23451	6.73
HAN2378P01	065	10001	20162	5.08
HAN2358P01	066	10028	21807	5.89
HAN2382P01	067	10001	19832	4.92
HAN2362P01	068	10001	21477	5.74
HAN2366P01	070	10001	21149	5.57
HAN2390P01	071	10001	19175	4.59
HAN2370P01	072	10001	20821	5.41
HAN2386R01	073	10001	19505	4.75
HAN2374P01	074	10001	20490	5.25
HAN2410P01	075	10304	17534	3.62
HAN2394P01	076	10001	18848	4.42
HAN2414P01	077	10001	17203	3.60
HAN2398P01	078	10001	18517	4.26
HAN2418P01	079	10121	16874	3.38
HAN2402P01	080	10001	18190	4.10
HAN2422R01	081	10001	16545	3.27
HAN2406P01	082	10001	17862	3.93
HAN2442P01	083	10001	14903	2.45
HAN2426P01	084	10001	16216	3.11
HAN2446P01	085	10001	14573	2.29
HAN2430P01	086	10083	15888	2.90
HAN2450P01	087	10001	14245	2.12
HAN2434P01	088	10001	15561	2.78
HAN2454P01	089	10001	13916	1.96
HAN2438P01	090	10001	15229	2.61
HAN2474P01	091	10001	12271	1.14
HAN2458P01	092	10001	13586	1.79
HAN2478P01	093	10001	11943	0.97
HAN2462P01	094	10040	13258	1.61

Line Name	Sequence	First SP	Last SP	Length [km]
HAN2486P01	095	10001	11284	0.64
HAN2466P01	096	10001	12928	1.46
HAN2482P01	097	10001	11617	0.81
HAN2470P01	098	10007	12599	1.30
	90 Lines		**Total Pioneer**	**647.88 km**

Appendix B

Internal Deliverables

B.1   Internal 2D-UUHR Deliverables

- Offshore
    – Seg-Y   : Raw navigation merged shot gathers
    – Seg-Y   : Brute stacks
    – PDF   : End of line QC

- Onshore
    – Seg-Y   : Migrated time stacks
    – Seg-Y   : Migrated stacks converted to depth
    – ASCII   : 2D picked 250m RMS velocities
    – Seg-Y   : 2D smooth depth conversion velocities
    – Png   : Migrated time stacks

Appendix D
Digital Deliverables

fUGRO

Deliverable Type	Sensor	Deliverable ID	Deliverable Content	Format
Interim Deliverable 1	MBES	ID1_001	Fugro Point file (0.25m)	XYZ
Interim Deliverable 1	ALL	ID1_002	TSG Database	GDB
Interim Deliverable 1	Grabs	ID1_003	Grab sample classification	XLSX
Interim Deliverable 1	Grabs	ID1_004	Grab sample laboratory analysis, overview table and result tables	XLSX/PDF
Interim Deliverable 2	MBES	ID2_001	Fugro Point file (0.25m)	XYZ
Interim Deliverable 2	ALL	ID2_002	TSG Database	GDB
Interim Deliverable 2	SSS	ID2_003	Data (HF/LF)	XTF
Interim Deliverable 2	MAG	ID2_004	Processed data	CSV
Interim Deliverable 2	SBP	ID2_005	Elevation Grids	XYZ
Interim Deliverable 2	SBP	ID2_006	Isochore (layer thickness) Grids	XYZ
Interim Deliverable 2	SSS	ID2_007	SonarWiz Projects	N/A (folder structure)
Final Deliverable	ALL	FD_001	Electronic database of deliverables	XLSX
Final Deliverable	ALL	FD_002	TSG Database	GDB
Final Deliverable	MBES	FD_003	Fugro Point file (0.25m)	XYZ
Final Deliverable	MBES	FD_004	Fugro Point file (1m)	XYZ
Final Deliverable	MBES	FD_005	Fugro Point file (5m)	XYZ
Final Deliverable	MBES	FD_006	TVU (1.0m)	XYZ
Final Deliverable	MBES	FD_007	THU (1.0m)	XYZ
Final Deliverable	MBES	FD_008	MBES Soundings data	XYZ
Final Deliverable	SVP	FD_009	SVP Profiles	XLSX
Final Deliverable	SSS	FD_010	Data (HF)	XTF
Final Deliverable	SSS	FD_011	Data (LF)	XTF
Final Deliverable	SSS	FD_012	SSS Navigation Files	CSV
Final Deliverable	MAG	FD_013	Processed data	CSV
Final Deliverable	SBP	FD_014	Processed data	SEGY

Deliverable Type	Sensor	Deliverable ID	Deliverable Content	Format
Final Deliverable	SBP	FD_015	Processed Recordings	PDF
Final Deliverable	SBP	FD_016	Digitised Horizons	CSV
Final Deliverable	SBP	FD_017	Elevation Grids	XYZ
Final Deliverable	SBP	FD_018	Depth below Seabed (BSB) Grids	XYZ
Final Deliverable	SBP	FD_019	Isochore (layer thickness) Grids	XYZ
Final Deliverable	2DUHR	FD_020	Processed data	SEGY
Final Deliverable	2DUHR	FD_021	Processed Recordings	PNG
Final Deliverable	2DUHR	FD_022	Digitised Horizons	CSV
Final Deliverable	2DUHR	FD_023	Elevation Grids	XYZ
Final Deliverable	2DUHR	FD_024	Depth below Seabed (BSB) Grids	XYZ
Final Deliverable	2DUHR	FD_025	Isochore (layer thickness) Grids	XYZ
Final Deliverable	SBP/2DUHR	FD_026	Kingdom Project (v2018)	ZIP (folder structure)
Final Deliverable	Grabs	FD_027	Grab sample classification	XLSX
Final Deliverable	Grabs	FD_028	Grab sample laboratory analysis, overview table and result tables	XLSX/PDF
Final Deliverable	Targets	FD_029	Target Catalogues	XLSX
Extra Deliverable	Velocities	N/A	2D UHR Velocities	SEGY